Communauté
UNIVERSITÉ Grenoble Alpes

THÈSE

Pour obtenir le grade de

DOCTEUR DE LA COMMUNAUTÉ UNIVERSITÉ GRENOBLE ALPES

Spécialité : **Physique Théorique**

Arrêté ministériel : 25 Mai 2016

Présentée par

Jordan BERNIGAUD SAMATAN

Thèse dirigée par **Björn HERRMANN**

Préparée au sein du **Laboratoire d'Annecy-le-Vieux de Physique Théorique** et de l'**École doctorale de physique de Grenoble**

Phénomenologie de la violation de saveur dans les modèles supersymmétriques

Thèse soutenue publiquement le **26/09/2019**,
devant le jury composé de :

Stefan ANTUSCH
Professeur, Université de Bâles - Bâles, Rapporteur
Geneviève BELANGER
Directrice de recherche, LAPTh - Annecy, Présidente
Michele FRIGERIO
Chargé de recherche, L2C - Montpellier, Examinateur
Joachim KOPP
Professeur, Université Johannes Gutenberg - Mayence, Examinateur
Ana Margarida TEIXEIRA
Chargée de recherche, LPC - Clermont-Ferrand, Rapporteure

Phenomenology of flavour violation in supersymmetric models

Jordan Bernigaud Samatan

Univ. Grenoble Alpes, Univ. Savoie Mont Blanc, CNRS, LAPTh,
9 Chemin de Bellevue, F-74000 Annecy, France.

Ph.D supervisor:

Dr. Björn Herrmann, LAPTh - Annecy

Presented on September the 26th, 2019.

Evaluation committee:

Prof. Stefan Antusch, University of Basel - Basel (Referee)
Dr. Geneviève Bélanger, LAPTh - Annecy (President)
Dr. Michele Frigerio, L2C - Montpellier
Prof. Joachim Kopp, University of Johannes Gutenberg - Mayence
Dr. Ana M. Teixeira, LPC - Clermont-Ferrand (Referee)

Abstract

Despite the lack of experimental evidence, Supersymmetry remains an attractive candidate for physics beyond the standard model of particle physics. Simple and viable supersymmetric extensions, such as the Minimal Supersymmetric Standard Model, adresses, among other shortcomings of the standard model, the electroweak hierarchy problem, the gauge coupling unification and provide attractive dark matter candidates.

One of the general characteristics of such extensions is that they may present a non-trivial flavour structure, which can lead to sizable contributions to flavour violating processes which are precisely measured and can be used to constrain the parameter space of new physics. The purpose of this manuscript is to discuss aspects of the extended flavour structure within supersymmetric models.

The manuscript will first introduce the Standard Model of particle physics and its supersymmetric extensions before exposing three research projects.

The first one will treat the problematic of the reconstruction of the squark flavour structure. Here, we have employed different strategies relying on inference statistical methods together with machine learning algorithms and assuming that a squark-like state is to be observed at colliders. Being a first step in this direction, improvement and complementary study will need to be proposed in case of the actual observation of a squark-like state but the obtained results are appealing.

As a second step, we shall discuss constraints and experimental signatures of $SU(5)$ Grand Unified Theories including flavour symmetries. In this framework, we will focus on A_4 family symmetry inspired models. This analysis is based on a numerical scan of the parameter space, including experimental flavour constraints as well as dark matter relic density. The results show, as it has already been pointed out before, that the lepton sector is much more constraining that the hadronic one. Additionally, interesting features arise in case of a simultaneous scan over the flavour violating parameters, and suggest that the allowed ranges for these parameters are larger than in the case of a single parameter study because of correlation effects.

Finally, the last chapter will be dedicated to leptoquark extensions of the standard model. These models, not necessary supersymmetric, have received considerable attention over the past few years, mainly due to the potential observation of lepton non universality at the Large Hadron Collider. We will discuss such extensions in the context of discrete flavour symmetries, useful tool for constraining the leptoquark patterns to a very predictive form. Finally, a model independent scan will be exposed, where we have obtained a list of potential symmetry candidates able to reproduce very specific leptoquark patterns alongside to the standard model fermionic mixing structure.

Résumé

Malgré l'absence de signatures expérimentales, les extensions supersymétriques du modèle standard de la physique des particules sont encore considérées parmi les plus attractives. La supersymétrie permet entre autres de résoudre le problème de la hiérarchie électrofaible, favorise l'unification des couplages de jauge nécessaire à une construction réaliste d'une théorie de grande unification, et propose des candidats viable à la matière noire.

Une des caractéristiques générale des extensions supersymétriques est de présenter une structure de saveur nouvelle, pouvant entraîner de larges contributions dans les observables de violation de la saveur. L'étude de certaines de ces structures et de leurs conséquences expérimentales est l'objet de ce manuscrit.

Ce manuscrit débutera avec une introduction générale au modèle standard de la physique des particules et de ses extensions supersymétriques avant de présenter trois projets de recherche.

Dans le premier travail exposé, nous aborderons des approches permettant d'identifier la structure de saveur dans le secteur des squarks (partenaire supersymétrique des quarks). Ces analyses, pionnières pour la problématique, reposent sur l'observation hypothétique d'un squark et utilisent des méthodes d'inférence statistique et de "machine learning". Bien qu'il ne s'agisse que d'une première approche, les résultats sont encourageants et la méthode pourrait être développée en cas d'observation réelle d'un état semblable à un squark aux collisionneurs.

Nous discuterons ensuite de contraintes et conséquences expérimentales présentes dans des modèles de grande unification du type $SU(5)$ avec symétrie de saveur. Dans ce contexte, nous discuterons de modèles inspirés par le groupe A_4. Cette analyse propose une exploration de l'espace des paramètres de ce type de modèles en incluant les contraintes expérimentales de saveur ainsi que la densité relique de matière noire. Les résultats confirment que le secteur leptonique est bien plus contraignant que le secteur hadronique. En addition, plusieurs particularités émergent lors d'une exploration simultanée de l'ensemble des paramètres conduisant à un espace autorisé par les contraintes plus important que dans le cas d'étude ne variant qu'un paramètre à la fois.

Finalement, le dernier chapitre de ce manuscrit sera dédié à la discussion d'extensions du modèle standard incluant des leptoquarks. Ces extensions, non nécessairement supersymétriques, ont reçu un regain d'attention ces dernières années, en particulier suite à des mesures qui suggéreraient l'existence de structure non universelle de saveur leptonique. Nous discuterons de ces extensions dans le contexte des symmetries discrètes de saveur qui peuvent conduire à des structures de couplages très prédictives. Enfin, une méthode indépendante de modèles sera proposée pour obtenir une liste de groupes candidats à la reproduction de ces structures de couplages et du mélange fermionique du Modèle Standard de façon simultanée.

Résumé détaillé du manuscrit

Ce manuscrit présente le travail et la recherche bibliographique éffectués pendant ces trois années de thèse. Au travers de la lecture de ce manuscrit, j'esquisse également le chemin et les évolutions scientifiques que j'ai traversés. La thématique générale concerne la physique de la saveur au delà du modèle standard. En particulier, nous discuterons des nouvelles structures de saveur émergent dans les modèles Supersymétriques.

Dans un premier temps, il s'agira d'établir les bases théoriques et le contexte des différents projets de recherche que j'ai menés. Tout cheminement se doit de commencer quelque part, ici j'ai choisi d'introduire dans le premier chapitre le Modèle Standard de la physique des particules. Nous aborderons lors de cette introduction quelques points clefs du modèle standard. Premièrement, nous dresserons le contenu en particules du Modèle Standard ainsi que de leurs propriétés sous les différents groupes de symmétries. Puis, nous parlerons plus particulièrement du méchanisme de Higgs qui nous permet de briser la symmétrie électrofaible et de générer des termes de masse pour les différentes particules. Un point d'attention particulier sera de détailler la structure de la saveur du modèle standard, dictée par la matrice de Cabibbo-Kobayashi-Maskawa (CKM). Cette première illustration de structure de saveur s'averera fort utile car des calculs similaires de changement de base seront abordés que ce soit en Supersymétrie ou dans le dernier chapitre, sur les leptoquarks, afin d'extraire du modèle les informations sur les nouvelles sources de violation de la saveur. Finalement, ce chapitre se concluera par la discussions de quelques questions non résolues par le Modèle Standard, encourageant la recherche de nouveaux modèles.

Le second chapitre sera quand à lui dédié à l'introduction de quelques notions des théories Supersymétriques. Nous aborderons les notions d'algèbre de Supersymétrie et des représentations de celle-ci. En particulier, nous introduirons le formalisme du super-espace et des super-champs, particulièrement éfficace afin de construire des Lagrangiens Supersymétriques. Nous discuterons également de quelques autres points, tel que la brisure de la Supersymmétrie, ingrédient indispensable dans la construction de théories Supersymétriques phénoménologiquement viables.

Enfin, nous rentrerons dans le coeur du sujet en présentant la plus simple des extensions Supersymétriques viables du modèle standard : Le Modèle Standard Supersymétrique Minimal (MSSM). Ce chapitre sera l'occasion de discuter de l'application concrète du formalisme introduit lors des deux premiers chapitres ainsi qu'un premier contact avec la phénoménologie de la violation de saveur en Supersymétrie. En particulier, nous introduirons la violation de saveur dans le secteur des squarks, partenaires supersymétriques des quarks. Nous définirons la base Super-CKM, particulièrement utile pour mesurer les nouvelles sources de violation de la saveur en Supersymétrie. Nous concluerons ce chapitre en discutant de conséquences phénoménologiques et des contraintes importantes issues de diverses expériences pour les modèles supersymétriques, ce qui cloturera l'introduction générale à la problématique.

Le quatrième chapitre sera dédié au premier projet auquel j'ai participé durant mon doctorat et sera basé sur une publication. Après avoir abordé la question de la nouvelle structure de saveur dans le chapitre précédent, ce projet traite de méthodes pouvant être utilisées pour déterminer, ou du moins accéder à des informations sur la structure de la saveur des théories supersymétriques. Nous nous concentrerons, à titre d'exemple, sur le secteur des squarks et cherchons à déterminer, étant donné une situation expérimental hypothétique, le contenu en saveur "top" du plus léger des squarks en utilisant un ensemble aussi minimal que possible d'observables et d'hypothèses. Pour ce faire, nous employons deux méthodes indépendantes mais potentiellement complémentaires : une basée sur une inférence statistique à l'aide d'une "likelihood" et l'autre faisant appel à un classifieur

employant une analyse multivariée. Si la méthode d'inférence directe a le mérite de donner accés à la valeur explicite du contenu en top du squark, le nombre d'hypothèses nécéssaires à son application éfficace augmente. En particulier, une connaissance à priori relativement précise du secteur des gauginos est nécéssaire au bon fonctionnement de la méthode. D'un autre côté, le classifieur obtient des résultats intéréssants même s'il ne donne pas accés directement au contenu en top, mais permet de classer le squark dans certaines catégories de contenu en top. Ces méthodes ont été utilisées dans le contexte d'un scan simplifié ainsi que dans une étude assez générale du MSSM avec violation non minimale de saveur.

Finalement, une des questions découlant de ces premières rélexions était pour moi si le contexte de violation non minimale de saveur était motivé d'un point de vue théorique. C'est donc assez naturellement, que je me suis tourné vers des modèles supersymétriques avec grande unification et symétries de saveur. Ces modèles permettent notament de résoudre le problème de la saveur dans le modèle standard en répondant à ces différentes questions : Pourquoi les fermions existent-ils en trois générations ? Pourquoi y a-t-il une telle structure hiérarchique des masses ? Et pourquoi les matrices de mélange du secteur fermionique ont ces formes là ? Le cinquième chapitre introduit ces modèles en présentant le paradigme des symétries de saveur et un groupe de jauge, $SU(5)$, utilisé dans des modèles simples de grande unification. Un aspect intéréssant de ces modèles est que de nouvelles sources de violation de saveur sont prédites. De plus, les secteurs leptonique et hadronique sont intimement connectés du à l'unification $SU(5)$. Ce court chapitre bibliographique aura pour objet de préparer le lecteur à la discussion du chapitre six, qui sera une étude phénoménologique de ce type de modèle.

Ce sixième chapitre, basé sur une publication éffectuée notamment lors de mon échange de deux mois avec l'Université de Southampton, se propose d'étudier des conséquences et aspects typiques des modèles de grande unification $SU(5)$ avec symétrie de saveur A_4, notamment du point de vue de la violation de saveur. Pour ce faire, nous partons de deux points de références, n'introduisant pas de violation de saveur nouvelle. Puis nous introduisons de façon simultanée de nouveaux paramètres violant la saveur de façon non minimale. A l'aide d'outils numériques, nous calculons ensuite les contraintes de saveur données par diverses expériences pour contraindre l'espace des paramètres du modèle. Un point intéréssant de cette analyse est que les paramètres sont variés simultanément, à la différence d'études précédentes, perméttant de mettre en évidence des relations de corrélation. Nous détaillons également plus en avant l'impact de chaque contraintes sur chaque paramètres.

Le septième et dernier chapitre, basé également sur une publication, présentera un autre type d'extension du modèle standard. Nous quitterons le contexte de la supersymétrie pour nous intérésser aux modèles de type leptoquarks. Ces modèles ont reçu un regain d'attention ces dernières années notamment à la suite de mesures suggérant la non-universalité du secteur leptonique. Nous aborderons ces modèles dans le contexte des symmétries discrètes de saveur. L'idée sous-jacente est d'imposer les symmétries résiduelles de saveur des termes de masse des différents secteurs fermioniques pour contraindre les couplages des leptoquarks à une forme très prédictive. De plus, comme les couplages des leptoquarks et les termes de masse sont dans ce cas sensibles à la même symmétrie résiduelle de saveur, nous cherchons à déterminer quelles symmétries sont susceptibles de reproduire ces couplages prédictifs et simultanément les matrices de mélanges (CKM et PMNS) du modèle standard. Pour ce faire, nous déduisons à partir des générateurs de la symmétrie résiduelle de saveur dans la base de masse, quelles sont les transformations associées dans la base de la saveur. Puis, à l'aide des expréssions explicites des générateurs nous pouvons fermer l'algèbre et reconstruire le groupe de saveur originel. En sondant l'espace des possibilités nous trouvons un grand nombre de groupes pouvant générer les couplages en question avec le mélange fermionique.

Le manuscrit se concluera briévement sur la discussion de possibles améliorations et projets futurs s'inscrivant dans l'ensemble de ces travaux.

Remerciements

Le mérite personnel, Ô grande vertue parmis les vertues, louangée par notre société méritocratique, est une farce. Dans mon cas, si j'ai réussi à en arriver là, ce n'est pas majoritairement basé sur mes compétences personelles. L'origine sociale et la chance ont à mon opinion beaucoup plus de poids dans la réussite que des qualités individuelles.

Un autre point crucial réside dans l'accompagnement dont j'ai pu bénéficier. Il s'agit d'un exercice de justice et de réalisme que de reconnaitre et remercier explicitement les différentes personnes qui nous soutiennent. Casser le mythe du mérite personnel pour plus de réalisme me semble être une raison suffisante pour faire de long remerciements !

Et il me semble tout naturel de démarrer la séance par remercier mon directeur de thèse, Björn Herrmann. Ses conseils precieux, sa patience et ses grandes qualités humaines m'ont soutenu et guidé pendant l'intégralité de ces trois ans; et au delà grâce à son soutient pour mes candidatures aux postdocs. Je le remercie également pour la confiance qu'il m'a accordé, d'abord en m'acceptant comme doctorant, puis en me laissant une grande autonomie dans les choix de projets et directions scientifiques entreprises ensemble. Je pense que ce dernier point m'a permis de réellement m'épanouir dans mon métier ces trois dernières années.

J'en profite également pour remercier Geneviève, ma marraine de thèse, qui a été très attentive à mon évolution et a su me faire part d'un grand nombre de conseils.

Je remercie également l'ensemble du LAPTh, son directeur, Luc Frappat et l'équipe administrative composée de Dominique, Virginie et Véronique qui m'ont sortis, avec amabilité, gentillesse et professionalisme, de nombreux tracas.

Je souhaite également adresser des remerciements tout particuliers à Paul Sorba. Pendant plus d'un an, il a pris sur lui de m'enseigner avec pédagogie la théorie des groupes, élément qu'aujourd'hui je juge fondamental. Ce faisant, il a modifié mes trajectoires et envies scientifiques en m'apportant une lecture plus profonde sur les modèles de physique des particules.

Il me semble impensable de ne pas préciser au combien le stress peut avoir des effets néfaste sur une personne. C'est dans ces moments là qu'une équipe de choc de doctorants et autre amis du labo ont pu m'aérer le cerveau au travers de nombreuses activités telles que boire de la bière, s'amuser, aller dans les bars pour boire de la bière, faire moulte jeux de société, consommer de la bière, faire un escape game et discuter autour d'une bière. Parmis ces gens je pourrais citer pelle-mêle: Florian, Dimitri, Marc, Victor, Iuri, Alix, Loïc, Laura, Alessandro et bien d'autres.

Un merci tout particulier à Carole pour m'avoir supporté et soutenu pendant certaines périodes difficile et pour me rendre très heureux, me faire rire et me faire rêver du futur.

Je souhaite également remercier ma famille, qui m'a toujours soutenu dans ce projet de longue haleine: depuis mes dix ans je veux faire de la recherche en physique. Ce long choix d'étude, dont on a peine à percevoir les difficultées à cet âge là, est semé de nombreuses péripéties. Heureusement qu'ils étaient tous là pour moi : Mon père, ma mère et mon petit frère.

Je souhaite également remercier quelques amis en particulier : Choucas, Elise, Guillaume, Pierre et Thomas. Ce sont des personnes exceptionnelles et je suis fier de les compter parmis mes proches.

Et finalement, en dernier pour insister, je souhaite remercier du fond du coeur Méril, doctorant au LAPTh, avec qui nous avons démarré ensemble cette aventure. Je loue chez Méril ses incroyables valeures humaines qu'il met sans modération au service des autres, ainsi que ses grandes compétences de physicien dont Méril m'a gentiment fait profiter au travers de très nombreuses discussions (désolé de t'avoir volé autant de temps !). Encore un grand merci cher co-bureau, et bon courage pour ta dernière année !

J'oublie probablement beaucoup de monde dans ces remerciements, et je présente mes excuses pour toute offense commise par cet oubli. Mais la petite page autorisée pour cet exercice n'est clairement pas suffisante ! Peut-être devrais-je y dédier un manuscrit tout entier ?

Je dédie ce manuscrit à tous ceux qui prennent le temps de le lire

Contents

1 The Standard Model of particle physics **1**
- 1.1 Overview . . . 1
- 1.2 Fermions in the standard model . . . 2
- 1.3 Gauge sector and interaction with fermions . . . 4
- 1.4 The Higgs mechanism and particle mass terms . . . 6
- 1.5 Limitations and open questions . . . 10

2 Supersymmetry **13**
- 2.1 Motivation for supersymmetry . . . 13
- 2.2 Supersymmetry Algebra . . . 14
- 2.3 Superspace and superfields . . . 16
- 2.4 Building SUSY invariant Lagrangians . . . 20
- 2.5 A word on R-symmetry and R-parity . . . 24
- 2.6 Explicit breaking of Supersymmetry . . . 24

3 The MSSM **27**
- 3.1 Lagrangian of the MSSM . . . 27
- 3.2 The MSSM spectrum . . . 30
- 3.3 Flavour mixing . . . 33

4 Accessing the squark flavour structure **37**
- 4.1 Objectives and setup . . . 37
- 4.2 Observables related to flavour violation at LHC . . . 39
- 4.3 Likelihood inference in a simplified model . . . 42
- 4.4 Multivariate analysis in a simplified model . . . 44
- 4.5 Application to the MSSM with mixed top-charm squarks . . . 46
- 4.6 Perspectives of the method . . . 49

5 Flavoured SUSY SU(5) GUT models **51**
- 5.1 Flavour symmetries . . . 51
- 5.2 SU(5): the simplest GUT model . . . 55
- 5.3 SUSY SU(5) meeting flavour symmetry . . . 59

6 Phenomenology of A_4 inspired GUT models **61**
- 6.1 Context of the study . . . 61
- 6.2 Model review . . . 62
- 6.3 Method and numerical setup . . . 65
- 6.4 Results and Discussion . . . 70
- 6.5 Conclusion and further projects . . . 80

7 Leptoquarks and flavour symmetries **83**
- 7.1 Introduction . . . 83
- 7.2 Residual Flavour Symmetries with Leptoquarks . . . 85
- 7.3 Closing Finite Groups: the Bottom-Up Approach . . . 94
- 7.4 Scanning Fully-Reduced Matrices in SE1 . . . 99
- 7.5 Scanning Partially-Reduced Matrices in SE2 . . . 103
- 7.6 Summary and Outlook . . . 109

Conclusion **111**

A Pocket formulae for two component notation **113**

B SPheno, SU(5) and the super-CKM basis **115**

Bibliographie **117**

Chapter 1

The Standard Model of particle physics

1.1 Overview

The standard model (SM) of particle physics has been established as the theory of fundamental particle interactions. Developed since the middle of the twentieth century, it is the product of a great theoretical and experimental effort [1–9]. Successful in describing three of the four fundamental interactions in Nature, it has lead to numerous predictions of bound states, mass relations, decay rates, and so on, which have been confirmed by a large number of experiments. In 2012, the Higgs boson, the last building block of the standard model, was discovered at the Large Hadron Collider (LHC) by ATLAS and CMS [10, 11]. This experimental achievement was one of the biggest successes of the SM.

The SM is a quantum field theory, a mathematical formalism which allows to take into account both quantum and special relativistic effects, with dynamics described by the semi-simple gauge group $G_{SM} = SU(3)_C \times SU(2)_L \times U(1)_Y$. The C, L and Y subscripts indicate the different interactions described by the subgroups. C stands for "colour", and $SU(3)_C$ describes the strong interaction called quantum chromodynamics (QCD) which is responsible for bound quark states such as the proton or the neutron. L stands for "left" and Y for "weak hypercharge". $SU(2)_L \times U(1)_Y$, later broken to $U(1)_{em}$ (electromagnetic interaction) through the Higgs mechanism, describes successfully the weak and electromagnetic interactions. The electric charge Q is then the result of a combination of the charges Y and T^3 (third generator of $SU(2)_L$) according to the following relation

$$Q = T^3 + \frac{Y}{2}. \tag{1.1}$$

This relation comes from the breaking pattern of the electroweak symmetry to the residual electromagnetic one. In addition to the invariance under the local G_{SM}, the theory must be invariant under the global special relativity group which is the Poincaré group.

Despite its numerous successes, the SM does not accommodate various observations. We can dress a non-exhaustive list of the SM shortcomings, distinguishing between experimental hints of new physics and more theoretically driven ones.

As a first example of experimental hints for new physics, cosmology suggests the presence of dark matter in order to explain the observed galaxy rotation curves, the structure formation in the Universe as well as the Cosmological Microwave Background (CMB) measurements [12]. The SM neither explains the asymmetry between matter and anti-matter [13] nor the value of the cosmological constant [14]. Furthermore, the discovery of neutrino oscillations [16], that implies that neutrinos have masses, was also a deviation from SM predictions. Additionally recent measurements from the LHCb and Belle collaborations [17–20] might hint towards lepton flavour non universality which will require physics beyond the standard model (BSM). From theoretical considerations, one can be worried about the electroweak naturalness argument: The Higgs boson mass, not protected by any symmetry, will receive large contributions from new physics. Among the several problems one can think about the strong CP problem, being an other naturalness issue [15].

Because of these limitations, the SM must be considered as an effective theory of nature and not as the ultimate theory, if such a theory exists. But taking into account the many successes of the SM at low energy, it is quite natural to think that the physics beyond the standard model under consideration has to give back the SM once we integrate out the new heavy degrees of freedom [1].

The main purpose of this first chapter is to discuss basic SM features and to settle notations we will use for the rest of the manuscript. Because staying in the SM can still lead to a lot of technical work, we do not aim at discussing all details. Many very good books and reviews on the SM can be found. The following ones [21–23] are part of the most known and can suit both a student or a more aware reader.

1.2 Fermions in the standard model

Fermions are spinor representations of the Poincaré group and thus obey Fermi-Dirac statistics. This leads to an antisymmetric wave function and so the fermions, denoted by ψ, are anti-commuting objects and obey the Dirac equation

$$(\not{p} - m)\psi = 0, \tag{1.2}$$

where $\not{p} = \gamma^\mu p_\mu$ and γ^μ are the Dirac matrices. The Lagrangian for a free propagating massive fermion is thus given by

$$\mathcal{L}_f = \bar{\psi}(i\not{\partial} - m)\psi. \tag{1.3}$$

where $\bar{\psi} = \psi^\dagger\gamma^0$. So far, we have been using Dirac spinors which have four components. Dirac spinors can be decomposed into two Weyl spinors, with two components each. Chirality projectors are used to project out the left or the right handed part of the Dirac spinor and they are defined as following:

$$P_L = \frac{1-\gamma^5}{2} \quad \text{and} \quad P_R = \frac{1+\gamma^5}{2}, \tag{1.4}$$

with $\gamma^5 = i\gamma^0\gamma^1\gamma^2\gamma^3$. We will denote with a subscript L, R the different projections of the Dirac fermions and we get $P_L\psi = \xi_L$, where ξ_L is a left handed Weyl spinor (and similar for P_R and ξ_R). Since it is quite useful to work in the two component notation, especially when we will introduce Supersymmetry in the next stages of the manuscript, let us discuss it in more detail (see [24] and Appendix A for complements).

The Lorentz group is isomorphic to a product of two $SU(2)$, i.e. $SO(1,3) \sim SU(2) \times SU(2)$. Indeed, the Lorentz algebra is defined as the following

$$[M^{\mu\nu}, M^{\rho\sigma}] = -i(\eta^{\mu\rho}M^{\nu\sigma} - \eta^{\mu\sigma}M^{\nu\rho} - \eta^{\nu\rho}M^{\mu\sigma} + \eta^{\nu\sigma}M^{\mu\rho}). \tag{1.5}$$

where the $M^{\mu\nu}$ are the Lorentz generators. In fact, $M^{\mu\nu}$ is composed of the three boost generators and the three space rotation generators (K^i, J^i) such as :

$$\mathbf{K} = \{M^{01}, M^{02}, M^{03}\}, \tag{1.6a}$$
$$\mathbf{J} = \{M^{23}, M^{31}, M^{12}\}. \tag{1.6b}$$

We can define two operators from the K^i and J^i:

$$N_i^+ = \frac{1}{2}(J_i + iK_i), \tag{1.7a}$$
$$N_i^- = \frac{1}{2}(J_i - iK_i). \tag{1.7b}$$

[1] Note that BSM extensions with light degrees of freedom (d.o.f) are possible, but we will not consider them in this manuscript.

One can show, using commutation relations of K^i and J^i, that these new operators satisfy the following commutation relations:

$$[N_i^+, N_j^+] = \epsilon_{ijk} N_k^+, \tag{1.8a}$$
$$[N_i^-, N_j^-] = \epsilon_{ijk} N_k^-, \tag{1.8b}$$
$$[N_i^+, N_j^-] = 0. \tag{1.8c}$$

The $N_{i,j}^{\pm}$ describe the algebra of an $SU(2) \times SU(2)$ group and it is thus natural to express irreducible representations as states transforming under these $SU(2)$. The representations are the following

$$(0,0) \rightarrow \text{Scalar}, \tag{1.9a}$$
$$(1/2,0) \rightarrow \text{Left handed spinor}\ , \tag{1.9b}$$
$$(0,1/2) \rightarrow \text{Right handed spinor}\ , \tag{1.9c}$$
$$(1/2,1/2) \rightarrow \text{Vector}. \tag{1.9d}$$

A Dirac fermion is made of a left and a right handed Weyl spinor : $\psi_D = (1/2,0) + (0,1/2)$. We can thus write the Dirac four-component spinor in terms of two two-component Weyl spinors

$$\psi_D = \begin{pmatrix} \xi_L \\ \xi_R \end{pmatrix}. \tag{1.10}$$

In the chiral representation, the Dirac matrices can be expressed in the following way:

$$\gamma^0 = \begin{pmatrix} 0 & 1 \\ 1 & 0 \end{pmatrix}, \quad \gamma^i = \begin{pmatrix} 0 & \sigma^i \\ -\sigma^i & 0 \end{pmatrix}, \tag{1.11}$$

where σ^i are the Pauli matrices. Therefore, in the two component notation, one can write down the kinetic term for the Lagrangian of a free Dirac fermion,

$$\mathcal{L}_D = i\bar{\xi_L}\sigma^\mu \partial_\mu \xi_L + i\bar{\xi_R}\bar{\sigma}^\mu \partial_\mu \xi_R, \tag{1.12}$$

where $\sigma^\mu = (1, \sigma^i)$ and $\bar{\sigma}^\mu = (1, -\sigma^i)$. From Eq. (1.12) we understand that, in the absence of a mass term, the Dirac Lagrangian describes the free propagation of two Weyl fermions. The mass term can be written as

$$\mathcal{L}_{D_m} = \bar{\xi_L} m \xi_R + \text{h.c.}\ . \tag{1.13}$$

Finally, a free massive Dirac fermion is equivalent to two Weyl fermions interacting through the mass term.

We close the digression here, moving on to the actual fermions present in the SM but this discussion needs to be kept in mind.

There are two classes of fermions in the standard model, the leptons and the quarks. While the leptons are colourless objects, and thus are not sensitive to QCD, the quarks are charged under $SU(3)_C$. Let us have a more detailed look at these two classes.

1.2.1 Leptons

There are three generations of leptons, which differ only by their masses, and we usually use the term flavour to distinguish these families. The three leptonic flavours are the electronic (e), the muonic (μ) and the tauic (τ). For each of the three generations there is one electrically charged and one neutral lepton called neutrino (ν). The leptons are charged under $SU(2)_L \times U(1)_Y$ and therefore interact with B boson (spawned by $U(1)_Y$) and weak gauge bosons. To describe the weak interactions of a charged lepton and the associated neutrino with a $W^\pm$, we gather them into a doublet of $SU(2)_L$. Thus, the eigenvalue of T^3 is then $-1/2$ for the charged lepton and $1/2$ for

the neutrinos. According to Eq. (1.1) and to the electric charge of the charged lepton ($Q = -1$), the weak hypercharge of the doublet must be $Y = -1$. For the right handed spinors, since they are not charged under $SU(2)_L$, the T^3 value is 0. Following again Eq. (1.1), we obtain the weak hypercharge assignment of the right handed spinors: $Y_{\ell_R} = -2$ and $Y_{\nu_{\ell R}} = 0$.

As a consequence, the right handed neutrinos are not charged under G_{SM}. Therefore, by choice, no right handed neutrinos is included in the SM leading to massless neutrinos. However, since neutrino oscillations have been observed [16], we know that neutrinos are massive, and we face here one of the limitations of the standard model about the nature and the mass of neutrinos.

1.2.2 Quarks

The quarks also exist in three generations, and for each of the generations there is one down-type and one up-type quark. As per the leptons sector, one can put the left handed quarks into doublets of $SU(2)_L$ which contains one up-type and one down-type quark. The three up-type quarks are labeled as (u, c, t) and the down-type ones are (d, s, b). Since the electric charge is different from the lepton sector, all right-handed quarks are charged under $U(1)_Y$ and can interact with the SM gauge bosons. Therefore, it is quite natural to include them in the SM, leading to massive quarks. In addition to the electroweak (EW) interactions, quarks are charged under $SU(3)_C$. Belonging to the fundamental representation **3** of the group, there are three colour indices r, b, g for "red", "blue" and "green".

1.2.3 Summary table

As a summary, we present the list and charge assignments for all the SM fermions in Table 1.1. As it can be seen, all families are just duplicates from one other and therefore exhibit the same quantum numbers as their cousins. However, the different states distinguish by their mass, as we shall see later. For the $SU(2)_L$ doublets, there are two different eigenstates with respectively T^3 values of $-1/2$ and $1/2$. This is the case for left-handed charged leptons and neutrinos or for the left-handed down and up quarks.

	Y	T^3	$SU(3)$	Q
e_L, μ_L, τ_L	-1	$-1/2$	**1**	-1
e_R, μ_R, τ_R	-2	0	**1**	-1
$\nu_{eL}, \nu_{\mu L}, \nu_{\tau L}$	-1	$1/2$	**1**	0
u_L, c_L, t_L	$1/3$	$1/2$	**3**	$2/3$
u_R, c_R, t_R	$4/3$	0	**3**	$2/3$
d_L, s_L, b_L	$1/3$	$-1/2$	**3**	$-1/3$
d_R, s_R, b_R	$-2/3$	0	**3**	$-1/3$

Table 1.1 – Fermions charges in the SM.

Remark: So far we have been discussing mass terms for fermions without being concerned about gauge invariance. But, having a look at Eq. (1.13) and Table 1.1, it is clear that the fermion mass terms are not $SU(2)_L \times U(1)_Y$ invariant. This question will be addressed later, when we will introduce the Higgs mechanism.

1.3 Gauge sector and interaction with fermions

In the previous chapter we introduced the fermionic content of the SM. We now wish to include dynamics. As we will see, enforcing gauge invariance under G_{SM} will naturally introduce gauge bosons and describe the dynamics of the particles. These theories are called Yang-Mills theories and are the basic theories for dynamics in particle physics.

As a first example, let us consider the following Lagrangian for a single massive Dirac fermion of charge Q under an $U(1)$ symmetry

$$\mathcal{L} = i\bar{\psi}\gamma^\mu\partial_\mu\psi - \bar{\psi}m\psi. \tag{1.14}$$

This is obviously globally invariant under a $U(1)$ group, where ψ transforms according to

$$\psi \to \mathcal{U}(\alpha)\psi = e^{i\alpha Q}\psi, \tag{1.15}$$

where Q is the generator of the $U(1)$ symmetry and simply reads as the identity. "Gauging" the symmetry, i.e. promoting $U(1)$ to a *local* symmetry, means that the parameter α is now dependent of the coordinates. The mass term is still invariant but the problem appears in the kinetic part since $[\mathcal{U}(\alpha(x)), \partial_\mu] \neq 0$. Therefore, one can introduce a *covariant* derivative D_μ which needs to involve normal derivatives. It can be shown (for example chapter 15 of [21]) that the form of D_μ is

$$D_\mu = \partial_\mu + ieA_\mu, \tag{1.16}$$

where e is an arbitrary constant and A_μ is a four vector object living in the adjoint representation of the group. Imposing $[\mathcal{U}(\alpha(x)), D_\mu] = 0$ leads to the transformation rule for A_μ

$$A_\mu \to A_\mu - \frac{1}{e}\partial_\mu\alpha(x). \tag{1.17}$$

Therefore, promoting ∂_μ to D_μ gives invariant kinetics terms for fermions. Starting from this new object of mass dimension equal to one, we can build more gauge invariant terms. For instance, $F_{\mu\nu} = \frac{1}{ie}[D_\mu, D_\nu]$ is gauge invariant. This antisymmetric object is called the field strength tensor and can be written as

$$F_{\mu\nu} = \partial_\mu A_\nu - \partial_\nu A_\mu. \tag{1.18}$$

In the Lagrangian, all terms must be Lorentz invariant. Thus, one can build the kinetic term for the gauge boson out of the field strength tensor in the following way:

$$\mathcal{L}_{gauge,kin} = -\frac{1}{4}F^{\mu\nu}F_{\mu\nu}. \tag{1.19}$$

The procedure can be repeated for a non-abelian group with generators T^a. In that case the covariant derivative becomes slightly different,

$$D_\mu = \partial_\mu - igA^a_\mu T^a, \tag{1.20}$$

and this modification leads to different expressions for the field strength tensor and infinitesimal transformations for A_μ,

$$A^a_\mu \to A^a_\mu + \frac{1}{g}\partial_\mu\alpha^a + f^{abc}A^b_\mu\alpha^c, \tag{1.21}$$

$$F^a_{\mu\nu} = \partial_\mu A_\nu{}^a - \partial_\nu A^a_\mu + gf^{abc}A^b_\mu A^c_\nu, \tag{1.22}$$

with f^{abc} being the structure constant of the group. As a final comment, we can note that the inclusion of the covariant derivative leads automatically to interactions of the gauge bosons with fermions. As an example, we can go back to the Lagrangian of Eq. (1.14). Using the covariant derivative for the $U(1)$ symmetry, we end with the following Lagrangian

$$\mathcal{L} = \bar{\psi}(i\gamma^\mu\partial_\mu - m)\psi - eA_\mu\bar{\psi}\gamma^\mu\psi, \tag{1.23}$$

which indeed describes successfully the QED interactions.

In the case of QCD interactions, the non-abelian group $SU(3)$, proposed in 1973 [25], has been adopted. One of the main difference between QCD and QED is that, because of the presence

on non-vanishing structure constant, the gauge bosons (gluons) can interact with each others.

There are still several questions we must address now: How can we generate mass for the bosons, since we know that $W^{\pm}$ and Z are massive bosons? How do we go from $SU(2)_L \times U(1)_Y$ to $U(1)_{em}$? And finally, how can we get a mass term for fermions that are charged under G_{SM} in the manner we described in Table 1.1? These question will be addressed all at the same time by the use of the Higgs mechanism and this will be the subject of the next section.

1.4 The Higgs mechanism and particle mass terms

The Higgs mechanism has been introduced in 1964 simultaneously by Peter Higgs, François Englert and Robert Brout [26, 27] [2], and so the complete name should be the Englert-Brout-Higgs mechanism. However, it is now commonly called the Higgs mechanism. It is an essential concept for the Standard Model which allows to introduce mass terms for particles in a gauge invariant way.

It is interesting to notice that the Higgs mechanism is not the only way of providing such mass terms. A very serious candidate has been the so called *Technicolor* [28] which provides a dynamical way to break electroweak symmetry by introducing a confining force that leads to fermion condensates. However, these models are under many constraints because of current LHC data, specifically on the Higgs boson and electroweak precision tests. However, it is still possible to accommodate technicolor with experiments. Still, we will discuss here the Higgs mechanism as it appears to be the favored explanation.

Without going into details, we explain here the basics of the Higgs mechanism, leaving aside the study of the Higgs boson interactions. The Higgs mechanism is also present for physics beyond the standard model when a new symmetry is implemented which needs to be broken below a certain scale. For instance, a Grand Unified Theory (GUT) model, where the SM is embedded in a large group, will be broken to recover the SM gauge group using the Higgs mechanism. For this chapter, we will focus on the electroweak symmetry breaking illustration.

We want to break $SU(2)_L \times U(1)_Y$ to $U(1)_{em}$ in a way that reproduces Eq. (1.1), the generator of $U(1)_{em}$ is $Q = T_3 + \frac{Y}{2}$. The idea is to find a vector ϕ_0 in $SU(2)_L \times U(1)_Y$ that is only invariant under $U(1)_{em}$

$$e^{iQ}\phi_0 = \phi_0 \quad \Longleftrightarrow \quad Q\phi_0 = 0. \tag{1.24}$$

First, we start from the simplest non trivial representation under $SU(2) \times U(1)$, meaning a doublet of $SU(2)$ with a non-zero Y hypercharge. We will see that this choice of representation is sufficient to break the electroweak group to the electromagnetism one. Since we will follow a parsimony principle, there will be no need to go beyond this scope.

An explicit representation of Q, for the doublet representation with an hypercharge of Y, is

$$Q = \begin{pmatrix} 1/2 + Y/2 & 0 \\ 0 & -1/2 + Y/2 \end{pmatrix}. \tag{1.25}$$

To satisfy Eq. (1.24), Q must have a least a zero eigenvalue. We can thus pick $Y = 1$ and therefore

$$\phi_0 = \begin{pmatrix} 0 \\ 1 \end{pmatrix}_{Y=1}. \tag{1.26}$$

In order to spontaneously break $SU(2) \times U(1)_Y$ to $U(1)_{em}$, we can introduce a doublet H, the Higgs field, which can acquire a vacuum expectation value (vev) along the ϕ_0 direction. The scalar potential of the Higgs field is given by

$$V(H) = -\mu^2 H^\dagger H + \lambda (H^\dagger H)^2, \tag{1.27}$$

[2] Actually, many publication sketching or developing the idea of this mechanism were released around that time

according to the $SU(2)_L \times U(1)_Y$ symmetry. The minimum of this potential is reached for $|H|^2 = v^2 = \mu^2/(2\lambda)$.

Once H acquires its vev, the system will be in a minimum of energy. However, because of quantum fluctuations, we need to develop the Higgs field around its minimum:

$$H = \begin{pmatrix} 0 \\ v \end{pmatrix} + \begin{pmatrix} \phi_1(x) + i\phi_2(x) \\ \phi_3(x) + i\phi_4(x) \end{pmatrix}, \tag{1.28}$$

where the ϕ_i are real scalar fields. If the symmetry was not local, all of these four degrees of freedom would have been physical. But this is not the case here. Indeed, we can perform a gauge transformation with a specific gauge choice that will get rid of the unphysical degrees of freedom. This is called the unitary gauge. Let us consider the transformation of H under the following $SU(2)_L \times U(1)_Y$ infinitesimal transformation

$$\begin{aligned} H \to H' &= \Big(1 - i\alpha_i(x)T^i - i\beta(x)Y/2\Big)\left(\begin{pmatrix} 0 \\ v \end{pmatrix} + \begin{pmatrix} \phi_1(x) + i\phi_2(x) \\ \phi_3(x) + i\phi_4(x) \end{pmatrix}\right) \\ &= \begin{pmatrix} 0 \\ v \end{pmatrix} + \begin{pmatrix} \alpha_2(x) + i\alpha_1(x) \\ i(\beta(x)/2 - \alpha_3(x)) \end{pmatrix} + \begin{pmatrix} \eta_1(x) + i\eta_2(x) \\ h(x) + i\eta_3(x) \end{pmatrix}, \end{aligned} \tag{1.29}$$

where T^i are the $SU(2)_L$ generators and $Y/2 = \mathbb{1}/2$ is the generator of $U(1)_{Y=1}$.

From above, we see that by a proper gauge choice we can remove all the η_i but the h field will remains. This remaining physical degree of freedom h is the Higgs boson. Generically, when breaking spontaneously a gauge group G with N_G generators to a subgroup H with N_H generators, one ends with $N_G - N_H$ massive gauge boson, N_H massless gauge bosons and N_H physical scalar fields. In the case of $SU(2) \times U(1)$ (four generators) broken to $U(1)$ (one generator), we are left with three massive gauge bosons $W^{\pm}, Z$, one massless gauge boson A and one real scalar field h. We will now discuss both boson and fermion masses coming from the Higgs mechanism.

1.4.1 Boson mass terms

We can now investigate the spectrum of the gauge bosons. First we have to write down the Lagrangian part involving the Higgs field together with the gauge bosons, meaning the gauge invariant kinetic part of the Higgs field:

$$\mathcal{L}_{kin} = (D^\mu H)^\dagger (D_\mu H). \tag{1.30}$$

We can now develop the Higgs field around its minimum. Imposing the unitary gauge and leaving out the terms involving h and derivatives (interaction and kinetic terms of the Higgs boson) we obtain the mass term for the electroweak gauge bosons

$$\mathcal{L}_m = \left[\left(-ig_2 W_a^\mu T^a - i\frac{g_1}{2} B^\mu Y \right) \begin{pmatrix} 0 \\ v \end{pmatrix} \right]^\dagger \left[\left(-ig_2 W_{a\mu} T^a - i\frac{g_1}{2} B_\mu \right) \begin{pmatrix} 0 \\ v \end{pmatrix} \right]. \tag{1.31}$$

Since $U(1)_{em}$ will be the remaining symmetry of the Lagrangian, it is quite natural to express the gauge bosons as eigenstates of the generator Q. $T^{1,2}$ are not but $T^\pm = T^1 \pm iT^2$ are indeed charge eigenstates as $[Q, T^\pm] = \pm T^\pm$. It is also quite natural to express the combination of T^3 and Y as Q and $Q_\perp = T^3 - Y/2$. In this basis, the previous term becomes

$$\mathcal{L}_m = \left[\left(-ig_2 W^{\pm\mu} T^\pm - \frac{i}{2}\sqrt{g_1^2 + g_2^2} A^\mu Q - \frac{i}{2}\sqrt{g_1^2 + g_2^2} Z^\mu Q_\perp \right) \begin{pmatrix} 0 \\ v \end{pmatrix} \right]^\dagger \tag{1.32}$$

$$\times \left[\left(-ig_2 W_\mu^\pm T^\pm - \frac{i}{2}\sqrt{g_1^2 + g_2^2} A_\mu Q - \frac{i}{2}\sqrt{g_1^2 + g_2^2} Z_\mu Q_\perp \right) \begin{pmatrix} 0 \\ v \end{pmatrix} \right], \tag{1.33}$$

where

$$A^\mu = \frac{1}{\sqrt{g_1^2+g_2^2}}(g_1 B^\mu + g_2 W_3^\mu), \quad Z^\mu = \frac{1}{\sqrt{g_1^2+g_2^2}}(-g_1 B^\mu + g_2 W_3^\mu), \\ \text{and} \quad W^{\mu\pm} = W_1^\mu \mp i W_2^\mu. \tag{1.34}$$

Because of Eq. (1.24), Q acting on the vacuum will vanish and A^μ will not acquire a mass term. Therefore it will be the massless photon spawned by the remaining electromagnetic symmetry.

Performing the matrix multiplication with $T^a = \sigma^a/2$ (σ^a are the Pauli matrices) leads to a mass term for the three remaining gauge bosons

$$\mathcal{L}_m = v^2 \left[\frac{g_2^2}{4} W_\mu^+ W^{-\mu} + \frac{(g_1^2+g_2^2)}{4} (Z_\mu)^2 \right]. \tag{1.35}$$

The mass relations are thus given by

$$M_W = v g_2/2, \quad M_Z = \frac{v}{2}\sqrt{g_1^2+g_2^2}. \tag{1.36}$$

1.4.2 Fermion mass terms

The remaining question concerns fermion masses. Introducing a scalar doublet of $SU(2)_L$ with hypercharge $Y = 1$ leads to additional terms which couple the Higgs field to the SM fermions. This part of the Lagrangian is called the Yukawa sector, and it is determined by the Yukawa couplings y_i which are 3×3 matrices

$$\mathcal{L}_y = y_u^{ij} \epsilon^{ab} \bar{Q}^i_{La} H_b^\dagger u_R^j + y_d^{ij} \bar{Q}^i_L H d_R^j + y_e^{ij} \bar{L}^i_L H e_R^j + \text{h.c.}, \tag{1.37}$$

where L_L and Q_L stand for the leptons and quarks $SU(2)_L$ doublets, u_R, d_R and e_R stand for the up quarks, down quarks and charged leptons right-handed singlets and $i, j = 1, 2, 3$ are generation indices. ϵ^{ab} is the Levi Civita tensor. We can note that these terms are indeed $SU(2)_L \times U(1)_Y$ invariant. When the Higgs field acquires its vev, we can develop the terms and we will end with the following Lagrangian

$$\mathcal{L}_{m_f} = m_u^{ij} \bar{u}^i_L u_R^j + m_d^{ij} \bar{d}^i_L d_R^j + m_e^{ij} \bar{e}^i_L e_R^j + \text{h.c.}, \tag{1.38}$$

with $m_f = v y_f$, which are precisely the fermion mass terms.

1.4.3 Physical basis and CKM matrix

As Eq. (1.38) introduces potentially non diagonal mass matrices, it is usual to move to the physical state basis. One can move to the physical mass eigenstates by performing the following transformations using unitary matrices V_f

$$u'_L = V_{u_L} u_L, \quad u'_R = V_{u_R} u_R, \quad d'_L = V_{d_L} d_L, \quad d'_R = V_{d_R} d_R, \quad e'_L = V_{e_L} e_L, \quad e'_R = V_{e_L} e_R, \tag{1.39}$$

and

$$V_{f_L}^\dagger m_f V_{f_R} = \text{diag}(m_{f_1}, m_{f_2}, m_{f_3}), \tag{1.40}$$

where the primed states correspond to the flavour eigenstates (the mass matrices are generic hermitian matrices) and the unprimed ones correspond to the mass eigenstates (the mass matrices are diagonal).

When we perform the rotations in the different sectors, the unitary matrices cancel each other except in the charged current. Indeed, the charged current associated with $W^\pm$ involves either an up-type quark with its associated down type quark or a charged lepton with its associated neutrino. As there are no right-handed neutrinos, no physical misalignment between neutrinos and leptons is left in the interaction. However the situation is different for the quark sector. Since we cannot

diagonalize simultaneously the down and up sector, V_{u_L} and V_{u_R} are a priori different. Writing down the charged weak current for the quarks in the physical basis introduces a mixing matrix

$$\mathcal{L} \subset \bar{u}_i V_{\text{CKM}}^{ij} \gamma^\mu P_L d_j W_\mu^+, \tag{1.41}$$

where

$$V_{\text{CKM}} = V_{u_L}^\dagger V_{d_L} \tag{1.42}$$

is the Cabibbo-Kobayashi-Maskawa matrix and has been introduced in 1973 [29] to generalize Cabibbo mixing angle [30] to an additional flavour. Because of this term, flavour violation can occur in the standard model from charged weak currents and thus, in addition to the six quarks masses, this matrix presents the additional physical degrees of freedom coming from the Yukawa terms.

A general 3×3 unitary matrix has nine free parameters and one of the usual parametrization is to use three rotation angles and six phases. Since we are now in the physical basis, the Lagrangian, apart from the weak current, is invariant under an $U(1)^6$ quark flavour symmetry. In addition, the full standard model including the weak current, is invariant under an $U(1)_B$ symmetry, where B stands for the baryon number. Because the weak charged current breaks $U(1)^6 \to U(1)_B$ we can remove five phases from the CKM matrix by performing five phase redefinitions. Finally, there will be three mixing angles and one phase in the CKM matrix [31].

One can double check this statement by counting the physical degrees of freedom coming from the Yukawa matrices. Indeed, switching off the Yukawa terms restore a $U(3)^3$ flavour symmetry for the quarks. Introducing the Yukawa couplings break the flavour symmetry to $U(1)_B$. There are 18 modulus and 18 phases in the quark Yukawa terms and in the breaking of $U(3)^3 \to U(1)_B$ we break 26 generators. $SO(3)$ being a maximal subgroup of $U(3)$ we can remove nine real parameters and, by counting remaining parameters, 17 phases. Out of the nine remaining real parameters, six are quark masses and three are angles, and we are also left with one phase, which matches what we derived previously.

There are two conventional ways to parametrize the CKM matrix. The first one is called the standard parametrization

$$V_{\text{CKM}} = \begin{pmatrix} c_{12}c_{13} & s_{12}c_{13} & s_{13}e^{-i\delta} \\ -s_{12}c_{23} - c_{12}s_{23}s_{13}e^{i\delta} & c_{12}c_{23} - s_{12}s_{13}s_{23}e^{i\delta} & s_{23}c_{13} \\ -s_{12}s_{23} - c_{12}c_{23}s_{13}e^{i\delta} & c_{12}s_{23} - s_{12}s_{13}c_{23}e^{i\delta} & c_{23}c_{13} \end{pmatrix} \tag{1.43}$$

where s_{ij} and c_{ij} are the sine and cosine of the three rotation angles θ_{ij} and δ is a Charge Parity (CP) violating phase. Another popular parametrization is the so called Wolfenstein parametrization [32] which is an approximation by developing the sines and cosines of the standard parametrization

$$V_{\text{CKM}} = \begin{pmatrix} 1 - \lambda^2/2 & \lambda & A\lambda^3(\rho - i\eta) \\ -\lambda & 1 - \lambda^2/2 & A\lambda^2 \\ A\lambda^3(1 - \rho - i\eta) & -A\lambda^2 & 1 \end{pmatrix} + O(\lambda^4), \tag{1.44}$$

where $\lambda \sim s_{12} \sim 0.22$ (value of the cosine of the Cabibbo angle).

Before concluding this section, let us briefly comment on neutrino masses. One can generate a mass term for the neutrinos through the introduction of a new Yukawa coupling by adding sterile right-handed neutrinos. However, despite the difficulty associated with introducing non interacting fields, this extension gives rise to a new naturalness issue. Indeed, the neutrino Yukawa coefficients must have extremely small values because of the tiny neutrino masses. To avoid this issue, it is possible to consider neutrinos as Majorana particles since they do not carry electric charge. This has led to various type of models called "see-saw" models. The basic principle of these models is to introduce very heavy neutrinos which, once integrated out, generate naturally small values for the neutrino Yukawa terms. In the case where neutrinos are massive, and we know it should be the case, a misalignement occurs in the lepton sector. In this case, in the same way we introduced the

CKM matrix, one needs to define the so called Pontecorvo-Maki-Nakagawa-Sakata (PMNS) matrix [33]. In the context of pure Dirac field, the PMNS matrix can take the exact same form as Eq. (1.43). However, in case of Majorana neutrinos, new phases appear.

1.5 Limitations and open questions

As mentioned in the introduction, the standard model cannot explain everything we see in Nature. In this section we will briefly introduce some of the shortcomings of the SM and present motivations for why one should search for physics beyond the Standard Model.

1.5.1 Dark matter and matter-antimatter asymmetry

There are several connections between particle physics and cosmology. As a first example one can think about the asymmetry between matter and antimatter. We observe that most of the universe is made of matter. This hints towards a different behavior of particles with respect to anti-particles. Actually, in order to explain this asymmetry, one would need additional sources of CP violation [34]. Indeed, the amount of CP violation in the standard model only comes from the CP phase of the CKM matrix presented in paragraph 1.4.3, and this is not enough in order to generate the observed asymmetry. One way out can be to consider additional sources of flavour violation which may increase the amount CP violation or extended neutrino sector. In that case, there are various models explaining the asymmetry by the Leptogenesis [35] or Baryogenesis [36] mechanisms.

Another strong motivation for BSM physics is dark matter. So far, there was no direct experimental detection of dark matter but many cosmological observations suggest its existence. The first experimental hint was the observation of galactic rotation curves by Zwicky who postulated the presence of an non-luminous mass present in the galaxies [37]. Since then, the problem is under investigation. Additionally, the dark matter is also needed to explain large structure formation in the universe [38]. Several models of modified gravity have tried to address the question but the simplest ones are in trouble especially since the observation of gravitational waves and the measurement of their speed (compatible with general relativity [39]). So, the most popular explanation at the moment is to postulate the existence of a new particle, beyond the scope of the Standard Model.

1.5.2 The electroweak hierarchy problem

The electroweak hierarchy problem occurs when introducing new physics at a high scale and can be summarized by saying that the observed value for the Higgs boson mass is very small compared to high scale quantities such as the Planck mass. Indeed, adding new particles in the game at a specific scale Λ generates corrections to the Higgs mass of order Λ^2. One can wonder: If the standard model is not to be considered as an effective field theory, do we actually face a hierarchy problem? The answer is indeed no. But the standard model needs to be considered as an effective field theory, even if we leave aside the problem of gravity. The reason why the SM is ill defined at very high scales is because of the presence of a Landau pole for the $U(1)_Y$ coupling. When running the hypercharge gauge coupling to very high scales, its value blows up, breaking pertubativity.

The conclusion is that something must happen before. Thus, new physics needs to be considered at high scales, above the electroweak scale, and so the electroweak hierarchy problem is indeed a serious issue of the SM. To illustrate the origin of large corrections to the Higgs mass, one can consider a toy model involving a fermion ψ and a scalar field ϕ described by the following Lagrangian

$$\mathcal{L} = \partial^\mu \phi^\dagger \partial_\mu \phi + i\bar{\psi}\partial\!\!\!/\psi - \frac{1}{2}m^2\phi^\dagger\phi - M\bar{\psi}\psi - y\phi\bar{\psi}\psi + \text{h.c.} \tag{1.45}$$

In the case where $M \gg m$, one can derive an effective field theory for ϕ which will be matched with the full theory at a given scale $\mu = M$. One needs to compute the fermion loop contribution to the propagator of the scalar field in the full theory in order to match the effective scalar propagator at

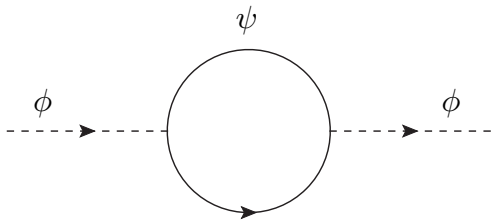

Figure 1.1 – Fermion loop contribution to the scalar propagator in the full theory. The diagram is to be matched to the effective scalar propagator at low energy.

low energy. The diagram is shown in Fig. 1.1. Neglecting the incoming momenta of the scalar field, the amplitude for the fermion contribution is given by

$$\mathcal{M} = (-1)y^2 \int \frac{d^4q}{(2\pi)^4} \mathrm{Tr}\left[\frac{\not{q} + M}{q^2 - M^2}\frac{\not{q} + M}{q^2 - M^2}\right]. \tag{1.46}$$

Following [40, 41] for notation and results on the loop integrals, we end with the following expression for the loop contribution:

$$\mathcal{M} = -\frac{i}{(4\pi)^2} 4y^2 \Big[A_0(M^2) + 2M^2 B_0(0, M^2, M^2)\Big]. \tag{1.47}$$

where B_0 and A_0 are Passarino-Veltman scalar integrals [42]. The expressions for the scalar integrals in dimensional regularization are

$$\begin{aligned} A_0(M^2) &= M^2\left[\Delta - \ln\left(\frac{M^2}{\mu^2}\right) + 1 + O(\epsilon)\right] \\ B_0(0, M^2, M^2) &= \Delta - \ln\left(\frac{M^2}{\mu^2}\right) \end{aligned} \tag{1.48a}$$

with $\Delta = \frac{1}{\epsilon} - \gamma_E + \ln(4\pi)$ (γ_E is the Euler-Mascheroni constant) and μ being the running scale.

After renormalization, where Δ is reabsorbed in a redefinition of the Lagrangian terms [3], the finite fermionic contribution to the scalar mass at scale $\mu = M$, where the matching occurs, will be therefore given by

$$\delta^{\psi}_{m^2} = \frac{4y^2}{(4\pi)^2} M^2, \tag{1.49}$$

as $B_0|_{\mu=M} = 0$ and $A_0|_{\mu=M} = M^2$. One can do the same exercise for the correction to the fermion mass in the case where $m \gg M$, but the result will be slightly different. Indeed, switching off the mass term of the fermion will restore the chiral symmetry $\psi \to e^{i\gamma^5}\psi$, meaning that any term breaking this chiral symmetry must be proportional to the fermion mass itself. The conclusion is that scalar fields, for which the mass term is not protected by any symmetries, will receive huge mass contributions from new physics degree of freedoms while the fermions will not. Since we already stated that new physics must happen above the electroweak scale, it means that the Higgs boson mass should be much larger than the observed value of 125 GeV. This is the so called electroweak hierarchy problem.

There has been a lot of investigation for making this parameter natural. For example, relaxion mechanisms [43] use a dynamical way to push the Higgs mass to the correct value. But most of the models are using additional symmetries such as the composite Higgs models, which state that the Higgs is a composite particle from pseudo Nambu-Goldstone bosons (PNGB) which originate from the breaking of a new symmetry [44].

In this manuscript, we will adopt the Supersymmetry framework which turns out to be one of the favoured extensions of the SM which makes the Higgs mass technically natural.

[3] The absorption of divergences is scheme dependent. There are different ways to absorb the infinities but we do not aim at discussing this in detail.

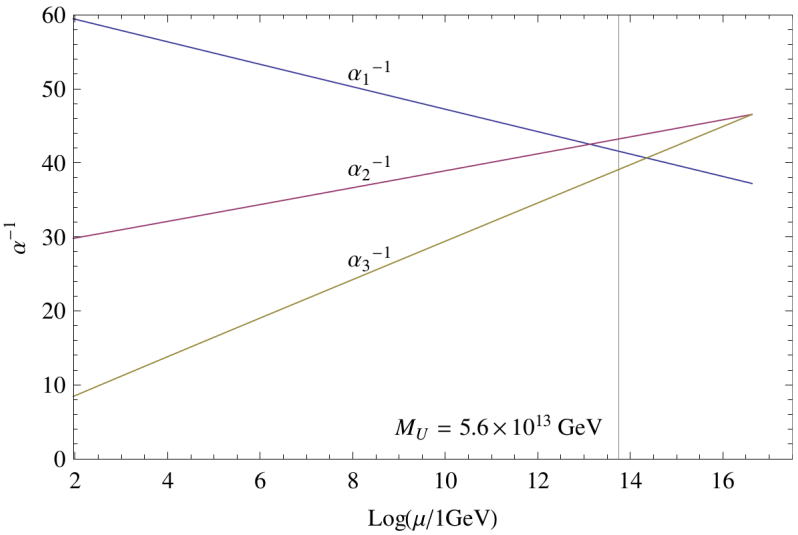

Figure 1.2 – Evolution of the SM gauge couplings with the scale μ. The couplings seems to converge but not exactly. This figure is taken from [45]

.

1.5.3 Gauge coupling unification

From the renormalization procedure and the renormalization group equations (RGE), one can calculate the evolution of the gauge couplings with the energy scale. In the standard model, one obtains the results of Fig. 1.2. That might hint toward a unification of the gauge couplings at a certain scale, however, in the standard model the convergence is definitely not perfect. Assuming that the gauge couplings have the same value at a specific high scale, one can think that the three gauge groups may be embedded in a single larger gauge group. This gauge group will be broken at the unification scale, which depends on the theory we consider (the RGE strongly depends on the content of particle and their interactions). The first model that has been developed in this context is based on $SU(5)$ which is then broken to G_{SM} [46]. Many models have followed involving various gauge groups where $SU(5)$, $SO(10)$, $E(6)$ and $E(8)$ rank among the most popular ones (ordered by size). Embedding the SM into a larger group is not a simple task and one has to face several issues. First, because of precise gauge coupling measurements, the simplest GUTs (Grand Unification Theories) are ruled out. Another important challenge is that in the most simple models, it is not possible to obtain the correct Yukawa values and one needs to consider additional extensions. But one of the biggest issue is the baryon number violating terms. In the standard model, the residual $U(1)_B$ ensures the proton stability, which is perfectly compatible with experiment: Bounds on the proton lifetime are rather high, around 10^{34} years from the Super-Kamiokande collaboration [47]. However, the unification group implies new gauge bosons that will generate baryon number violating operators at low scale. To satisfy the proton decay constraints, one needs to push the GUT scale rather high.

One way out is once again Supersymmetry. It turns out that Supersymmetric models favour gauge coupling unification and naturally drive the GUT scale higher than in the standard model (usually around 10^{16} GeV). Therefore, Supersymmetry is a suitable framework for GUT models.

Chapter 2 Supersymmetry

This chapter is dedicated to the discussion of Supersymmetry (SUSY) and its formalism. I will start by a short motivation. Then I will introduce the SUSY algebra and representations before going to the procedure on how to build SUSY invariant Lagrangians. This chapter will close on a quick discussion about the breaking of SUSY. Most of this chapter follows the notations and discussions of [48–50]. I leave for the next chapter the question of the MSSM as we will discuss it in more detail in the context of the non minimal flavour violation framework.

Helpful formulas and definitions for this chapter can be found in Appendix A.

2.1 Motivation for supersymmetry

2.1.1 The electroweak hierarchy problem revisited

As discussed in Sec. 1.5.2, one of the major issues associated to the SM is the electroweak hierarchy problem. It turns out that supersymmetry provides a solution. Indeed, as we will see later, SUSY predicts fermionic partners for bosonic degrees of freedom of the SM and bosonic partners for the fermionic degrees of freedom of the SM. Therefore, let us incorporate two additional scalars $\Phi_{L,R}$ to our toy model of Eq. (1.45), one for each component of the Dirac fermion and with the same mass.

The additional terms in the Lagrangian are

$$\mathcal{L}_S \subset \partial^\mu \Phi_A^\dagger \partial_\mu \Phi_A - \frac{M^2}{2}\Phi_A^\dagger \Phi_A - \lambda_1 \Phi_A^\dagger \Phi_B \phi - \lambda_2 |\Phi_A|^2 |\phi|^2 \tag{2.1}$$

where we are summing on $A, B = L, R$. We have now additional contributions to the scalar mass ϕ at one loop shown in Fig. 2.1.

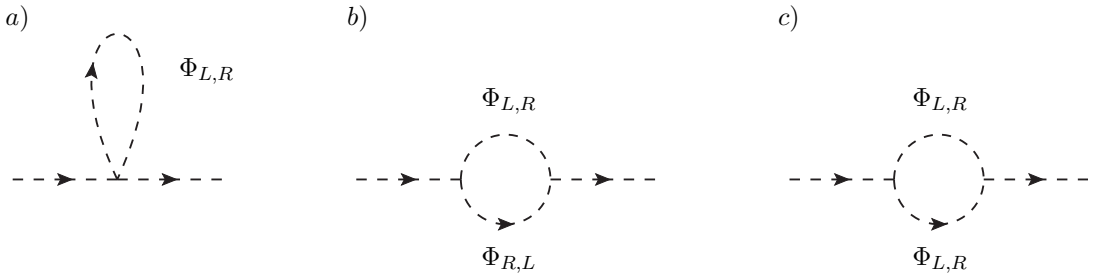

Figure 2.1 – Left and right new scalars contribution to the scalar mass.

However, the two last diagrams will not contribute to the mass correction because they will be given by B_0 scalar integrals, which vanish when considering the matching at $\mu = M$ as discussed in Sec. 1.5.2. Therefore, we only consider the contribution from the first diagram given by (neglecting the incoming momenta)

$$\mathcal{M}_s = -2\lambda_2 \int \frac{d^4q}{(2\pi)^4}\left(\frac{1}{q^2 - M^2} + \frac{1}{q^2 - M^2}\right). \tag{2.2}$$

The factor 2 in Eq. (2.2) comes from the symmetry of the diagram (see "Wick contraction" in [21]). Using the Passarino-Veltman decomposition we end up with the following contribution:

$$\delta^{\Phi}_{m^2} = -\frac{4\lambda_2}{(4\pi)^2} M^2. \tag{2.3}$$

Provided that $\lambda_2 = -y^2$, and that the heavy fermion and the heavy scalar are degenerated in mass, the contributions of Eqs. (1.49) and (2.3) exactly cancel. Therefore, introducing the scalars solves the hierarchy problem as no more large scale dependence enters in the Higgs boson mass. This feature is precisely what is obtained in SUSY theories.

As we will see, we will need to break SUSY and therefore the masses will not be degenerate. This will introduce a certain amount of fine tuning on the Higgs boson mass which increases as the same time as the SUSY breaking mass scale increases. Because of this reason, before starting experiments at the LHC, people thought that the SUSY scale would have been below the TeV scale. However, since no evidence of SUSY has been found so far, the SUSY scale has to be pushed higher, making the Higgs mass less natural (but still much more than in the SM).

2.1.2 A no-go theorem

In addition to the various phenomenological motivations we have discussed so far (dark matter, hierarchy problem, etc.), there is also a very appealing theoretical aspect in supersymmetry. In 1967, Sidney Coleman and Jeffrey Mandula proved a no-go theorem on the combination of dynamics with kinematics symmetries [51]. The theorem states that the only way to extend the Poincaré group with a Lie group, while respecting the properties of the S-matrix, is trivially: Taking T^a as the new symmetry generators we have

$$[T^a, P_\mu] = [T^a, M_{\mu\nu}] = 0, \tag{2.4}$$

where P_μ is the space time translation generator and $M_{\mu\nu}$ the Lorentz boost generators. This no-go theorem states that the only extensions we can implement need to be decoupled from the kinematics, which is by far reducing the possible ways of implementing new physics. However, the theorem presents a loophole in the case where the generators are not bosonic but fermionic. In that case, one falls into the Haag-Łopuzánski-Sohnius theorem [52]. In this context, the most general continuous symmetry of the S-matrix is that pertaining to a Z_2-graded Lie Algebra where the odd generators belong to the $(\frac{1}{2}, 0)$ and $(0, \frac{1}{2})$ of the Lorentz group while the even generators are a direct sum of the Poincaré generators with the other symmetry generators.

Introducing fermionic (odd) generators is exactly what we will call supersymmetry, meaning that supersymmetry is the only way to extend the Poincaré Algebra in a non-trivial way.

2.2 Supersymmetry Algebra

While it is possible to extend the Poincaré algebra by adding a set of N odd generators Q^I_α, where $I = 1...N$, we will consider only the simplest case where $N = 1$. It is quite useful for theoretical discussions to work in the chiral representation (see Appendix A). We will write un-dotted (resp. dotted) indices for the left-handed (resp. right-handed) fermions.

One can show that the commutation (and anti-commutation) relations are

$$\{Q_\alpha, \bar{Q}_{\dot{\beta}}\} = 2\sigma^\mu_{\alpha\dot{\beta}} P_\mu, \tag{2.5a}$$

$$\{Q_\alpha, Q_\beta\} = \{\bar{Q}_{\dot{\alpha}}, \bar{Q}_{\dot{\beta}}\} = 0, \tag{2.5b}$$

$$[Q_\alpha, P_\mu] = [\bar{Q}_{\dot{\alpha}}, P_\mu] = 0, \tag{2.5c}$$

$$\{Q_\alpha, M_{\mu\nu}\} = (\sigma_{\mu\nu})^\beta_\alpha Q_\beta, \tag{2.5d}$$

where α, β denote the spinorial index of the generators, since they are fermionic operators (carrying a Lorentz representation).

One important feature of the SUSY algebra is that, in a finite representation, we have the same number of bosonic and fermionic degrees of freedom. We start by introducing the fermion number operator N_f which acts on bosonic and fermionic states $|B\rangle$ and $|F\rangle$ as the following

$$(-1)^{N_f}|B\rangle = |B\rangle\,, \quad (-1)^{N_f}|F\rangle = -|F\rangle\,. \tag{2.6}$$

The SUSY generators turn a fermionic state into a bosonic one and vice versa

$$Q_\alpha|B\rangle = |F\rangle\,, \quad Q_\alpha|F\rangle = |B\rangle\,. \tag{2.7}$$

One can show that $\{(-1)^{N_f}, Q_\alpha\} = 0$. In the case of finite dimensions, one can compute the trace of $(-1)^{N_f}Q_\alpha$ and obtain

$$\mathrm{tr}\left((-1)^{N_f}\{Q_\alpha, \bar{Q}_{\dot\beta}\}\right) = \mathrm{tr}\left((-1)^{N_f}\sigma^\mu_{\alpha\dot\beta}P_\mu\right) = 0. \tag{2.8}$$

For $P_\mu \neq 0$, $\mathrm{tr}\left((-1)^{N_f}\right) = 0$, meaning that the number of states with eigenvalues $+1$ and -1 is the same.

2.2.1 Construction of the general supermultiplet representation

Spinors, vectors and scalars are representations of the Poincaré algebra. Since the Poincaré group is a subgroup of the SUSY group we expect that SUSY representations can be built in terms of these sub-blocks. In order to construct the general SUSY representation we can start from a scalar representation $\phi(x)$ and act with the SUSY fermionic generators. As SUSY is a graded Lie algebra, we will need to use the generalized Jacobi identities which include anticommutators

$$[\{A,B\},C] + \{[C,B],A\} + \{[C,A],B\} = 0, \tag{2.9a}$$
$$[\{A,B\},C] + [\{B,C\},A] + [\{C,A\},B] = 0. \tag{2.9b}$$

The procedure is the following: First, start from the scalar representation and act on it with the SUSY generators. Each new degree of freedom will be labeled as a new field inside the supermultiplet. Apply the SUSY operators on each new field and repeat the procedure until the algebra is closed and no new degree of freedom appears.

In the following, we will drop the x dependence of the fields. We thus start by

$$[Q_\alpha, \phi] = \psi_\alpha, \tag{2.10a}$$
$$[\bar{Q}^{\dot\alpha}, \phi] = \bar\chi^{\dot\alpha}, \tag{2.10b}$$

Where ψ (resp. $\bar\chi$) are left-handed (resp. right-handed) Weyl spinors. Acting with Q_α on ψ_β and using the Jacobi's identities and the SUSY algebra leads to

$$\{Q_\alpha, \psi_\beta\} = \{Q_\alpha, [Q_\beta, \phi]\} = -\{\psi_\alpha, Q_\beta\}, \tag{2.11}$$

meaning that

$$\{Q_\alpha, \psi_\beta\} = \epsilon_{\alpha\beta}F. \tag{2.12}$$

Similarly, we have

$$\{\bar{Q}^{\dot\alpha}, \bar\chi^{\dot\beta}\} = \epsilon^{\dot\alpha\dot\beta}E. \tag{2.13}$$

Here, F and E are scalar degrees of freedom. We can continue with

$$\{\bar{Q}^{\dot\alpha}, \psi_\beta\} = [2\sigma^{\mu\dot\alpha}_\beta P_\mu, \phi] - \{\bar\chi^{\dot\alpha}, Q_\beta\}. \tag{2.14a}$$

Defining $\{\bar{Q}^{\dot\alpha}, \psi_\beta\} = -2i\sigma^{\mu\dot\alpha}_\beta A_\mu$, we end with

$$\{\bar\chi^{\dot\alpha}, Q_\beta\} = -2i\sigma^{\mu\dot\alpha}_\beta(\partial_\mu\phi - A_\mu). \tag{2.15}$$

Therefore, only one new field emerges from the two different (anti)commutators. We can continue by acting the SUSY operators on E and F

$$[Q_\alpha, F] = \epsilon^{\gamma\beta}[Q_\alpha, \{Q_\beta, \psi_\gamma\}] = [F, Q_\alpha], \tag{2.16}$$

which leads to

$$[Q_\alpha, F] = 0. \tag{2.17}$$

Similarly we get

$$[\bar{Q}^{\dot{\alpha}}, E] = 0. \tag{2.18}$$

One can continue the procedure which presents no specific difficulties apart from some (time consuming) algebra. Finally, we have in addition to the previous fields

$$[\bar{Q}^{\dot{\alpha}}, F] = \bar{\mu}^{\dot{\alpha}}, \tag{2.19a}$$
$$[Q_\alpha, E] = \lambda_\alpha, \tag{2.19b}$$
$$[Q_\alpha, \lambda_\beta] = \epsilon_{\alpha\beta} D, \tag{2.19c}$$

while the other Jacobi identities either lead to trivial relations or can be expressed as functions of the other fields (see [53] for details).

The complete set of fields for the general supermultiplet are then: four complex scalar fields ($\phi,\ F,\ E,\ D$), one vector field (A_μ) and four complex Weyl spinors ($\bar{\chi},\ \psi,\ \bar{\mu},\ \lambda$). We thus have 16 bosonic degrees of freedom and 16 fermionic ones.

2.3 Superspace and superfields

2.3.1 Grassmann variables

Here we aim at briefly introducing Grassmann variables for the purpose of the SUSY formalism we will develop in the next sections.

A Grassmann variable η is an anticommuting variable such that

$$\eta\bar{\eta} + \bar{\eta}\eta = 0, \quad \eta^2 = \bar{\eta}^2 = 0, \quad \bar{\bar{\eta}} = \eta. \tag{2.20}$$

The previous conditions generate a Grassmann algebra. A general function f of such variables takes the form

$$f(\eta, \bar{\eta}) = f_0 + \eta f_1 + \bar{f}_2\bar{\eta} + f_3\eta\bar{\eta}, \tag{2.21}$$

where f_i are complex coefficients. One can define partial derivative such as

$$\frac{\partial(\bar{\eta}f)}{\partial\eta} = -f_1 \quad \text{and} \quad \frac{\partial(\eta f)}{\partial\bar{\eta}} = -\bar{f}_2. \tag{2.22}$$

Note in above that partial derivatives need to commute with η. We can define the integration procedure by following the Berezin integrations rules

$$\int d\eta\ \eta = \int d\bar{\eta}\ \bar{\eta} = 1, \tag{2.23a}$$
$$\int d\eta = \int d\bar{\eta} = \int d\eta \frac{\partial}{\partial\eta} f = \int d\bar{\eta} \frac{\partial}{\partial\bar{\eta}} f = 0. \tag{2.23b}$$

The Grassmann integration shows also two properties, linearity and translation invariance

$$\int d\eta \Big(\alpha f(\eta) + \beta g(\eta)\Big) = \alpha \int d\eta f(\eta) + \beta \int d\eta g(\eta), \tag{2.24a}$$
$$\int d\eta_i f(\eta_i + \eta_j) = \int d\eta_i f(\eta_i). \tag{2.24b}$$

For our purpose, in the following sections, we will use doublets of Grassmann variables. We can introduce θ_α and $\bar{\theta}^{\dot{\alpha}}$, where $\alpha, \dot{\alpha} = 1, 2$, which behave like left and right handed Weyl spinors.

These variables contract in the following way:

$$\theta\theta = \theta^\alpha \theta_\alpha, \quad \bar{\theta}\bar{\theta} = \bar{\theta}_{\dot{\alpha}} \bar{\theta}^{\dot{\alpha}}. \tag{2.25}$$

In addition we have the following identities that will be useful for the rest of the chapter:

$$\theta^\alpha \theta^\beta = -\frac{1}{2} \epsilon^{\alpha\beta} \theta\theta, \tag{2.26a}$$

$$\theta_\alpha \bar{\theta}_{\dot{\beta}} = \frac{1}{2} \sigma^\mu_{\alpha\dot{\beta}} (\bar{\theta}\bar{\sigma}_\mu \theta), \tag{2.26b}$$

$$\int d\theta_\alpha \ \theta^\beta = \delta^\beta_\alpha, \tag{2.26c}$$

$$\int d^2\theta \ \theta\theta = \int d^2\bar{\theta} \ \bar{\theta}\bar{\theta} = 1, \tag{2.26d}$$

where the measures are defined as

$$d^2\theta = \frac{1}{4} \epsilon_{\alpha\beta} d\theta^\alpha d\theta^\beta, \quad d^2\bar{\theta} = \frac{1}{4} \epsilon^{\dot{\alpha}\dot{\beta}} d\bar{\theta}^{\dot{\alpha}} d\bar{\theta}^{\dot{\beta}}. \tag{2.27}$$

2.3.2 Superfields and SUSY transformations in superspace

The superspace formalism [54] provides an elegant way to construct SUSY invariant Lagrangians. Indeed, by using an extended system of coordinates, more appropriate for the representation of SUSY transformations, SUSY invariant Lagrangians are easier to implement than using the usual Minkowski space.

The main idea is to add two new coordinates, θ and $\bar{\theta}$ which are two-components Grassmann variables. The superspace will be then composed by the following system of coordinates

$$x^\mu, \ \theta_\alpha, \ \bar{\theta}^{\dot{\alpha}}, \tag{2.28}$$

where x^μ is the usual space-time coordinates of the Minkowski space. Actually, one can build the superspace as a coset of the SuperPoincaré group by the Lorentz group. This procedure is very similar to the construction of Minkowski space by the coset of the Poincaré group by the Lorentz group. More details regarding this construction can be found in references [49, 50].

This particular choice of coordinates allows us to write down superfields, functions of the superspace. A generic superfield $\mathcal{F}(x, \theta, \bar{\theta})$ takes the following form

$$\mathcal{F}(x, \theta, \bar{\theta}) = \phi(x) + \theta\psi(x) + \bar{\theta}\bar{\chi}(x) + \theta\theta F(x) + \bar{\theta}\bar{\theta}E(x) + \theta\theta\bar{\theta}\bar{\mu}(x) + \theta\bar{\theta}\bar{\theta}\lambda(x) + \theta\theta\bar{\theta}\bar{\theta}D(x). \tag{2.29}$$

Basically, because θ_α and $\bar{\theta}^{\dot{\alpha}}$ are anti-commuting variables, this is the most general expression which is obtained by expanding the superfield in terms of the fermionic coordinates. As we can see, we recover the exact same degrees of freedom as in the case of the general supermultiplet construction from section 2.2.1.

We can now derive how the SUSY generators act on superfields. A SUSY transformation g will be parametrized by two fermionic variables ξ and $\bar{\xi}$. g will act on the superfield such as

$$\mathcal{F}(x, \theta, \bar{\theta}) \to \mathcal{F}'(x, \theta, \bar{\theta}) = g(\xi, \bar{\xi}) \mathcal{F}(x, \theta, \bar{\theta}) g^{-1}(\xi, \bar{\xi}), \tag{2.30}$$

with $g(\xi, \bar{\xi}) = e^{i(\xi^\alpha Q_\alpha + \bar{\xi}_{\dot{\alpha}} \bar{Q}^{\dot{\alpha}})}$. Because of the SUSY algebra, and like in the usual Poincaré group in Minkowski space, it is possible to write down

$$\mathcal{F}(x, \theta, \bar{\theta}) = h(x, \theta, \bar{\theta}) \mathcal{F}(0, 0, 0) h^{-1}(x, \theta, \bar{\theta}). \tag{2.31}$$

This leads to the following expression for the SUSY transformation of a superfield

$$\mathcal{F}(x,\theta,\bar{\theta}) \to \mathcal{F}'(x,\theta,\bar{\theta}) = g(\xi,\bar{\xi})h(x,\theta,\bar{\theta})\mathcal{F}(0,0,0)h^{-1}(x,\theta,\bar{\theta})g^{-1}(\xi,\bar{\xi}). \tag{2.32}$$

By the use of the Baker–Campbell–Hausdorff formula [55, 56], we end up with

$$\begin{aligned} g(\xi,\bar{\xi})h(x,\theta,\bar{\theta}) = \exp\Big\{ i\left(x^\mu P_\mu + (\xi^\alpha+\theta^\alpha)Q_\alpha + (\bar{\xi}_{\dot{\alpha}}+\bar{\theta}_{\dot{\alpha}})\bar{Q}^{\dot{\alpha}}\right) \\ -\frac{1}{2}\left[\xi^\alpha Q_\alpha + \bar{\xi}_{\dot{\alpha}}\bar{Q}^{\dot{\alpha}}, x^\mu P_\mu + \theta^\alpha Q_\alpha + \bar{\theta}_{\dot{\alpha}}\bar{Q}^{\dot{\alpha}}\right] + ...\Big\}. \end{aligned} \tag{2.33}$$

Evaluating the commutator (all other commutators vanishe), we end with the following expression

$$\mathcal{F}' = \mathcal{F}(x^\mu P_\mu + i\xi^\alpha\sigma^\mu_{\alpha\dot{\alpha}}\bar{\theta}^{\dot{\alpha}} + i\bar{\xi}_{\dot{\alpha}}\bar{\sigma}^{\mu\dot{\alpha}\alpha}\theta_\alpha,\ \xi^\alpha+\theta^\alpha,\ \bar{\xi}_{\dot{\alpha}}+\bar{\theta}_{\dot{\alpha}}), \tag{2.34}$$

where we have made used of relations described in Appendix A. For an infinitesimal transformation and expanding at the first order, one obtains:

$$\delta_{\xi,\bar{\xi}}\mathcal{F} = -i\left[\mathcal{F},\ \xi^\alpha Q_\alpha + \bar{\xi}_{\dot{\alpha}}\bar{Q}^{\dot{\alpha}}\right] = -i(\xi^\alpha\mathcal{Q}_\alpha + \bar{\xi}_{\dot{\alpha}}\bar{\mathcal{Q}}^{\dot{\alpha}})\mathcal{F} = \left(\delta x^\mu\partial_\mu + \delta\theta^\alpha\partial_\alpha + \delta\bar{\theta}_{\dot{\alpha}}\partial^{\dot{\alpha}}\right)\mathcal{F}, \tag{2.35}$$

where $\mathcal{Q}$ and $\bar{\mathcal{Q}}$ are the representations of Q and $\bar{Q}$ in terms of differential operators and

$$\partial_\alpha = \frac{\partial}{\partial\theta^\alpha}, \quad \partial_{\dot{\alpha}} = \frac{\partial}{\partial\bar{\theta}^{\dot{\alpha}}}. \tag{2.36}$$

In the rest of the manuscript, to avoid many notations we will write $\mathcal{Q}$ (resp. $\bar{\mathcal{Q}}$) as Q (resp. $\bar{Q}$), without distinguishing the generators from their differential representations. Finally, matching the expressions leads to the expressions of Q and $\bar{Q}$ in terms of differential operators:

$$Q_\alpha = i(\partial_\alpha + i\sigma^\mu_{\alpha\dot{\alpha}}\bar{\theta}^{\dot{\alpha}}\partial_\mu), \quad \bar{Q}^{\dot{\alpha}} = i(\partial^{\dot{\alpha}} + i\bar{\sigma}^{\mu\dot{\alpha}\alpha}\theta_\alpha\partial_\mu). \tag{2.37}$$

So far we have been dealing with general superfields. However, the generic superfield does not provide an irreducible SUSY representation. Starting from the general superfield $\mathcal{F}$, it is possible to build an irreducible representation by applying constraints $\mathcal{C}$ of the form

$$\mathcal{C}(\mathcal{F}) = 0. \tag{2.38}$$

In order to be consistent, the constraints need to commute with the SUSY operators

$$\delta_{\xi,\bar{\xi}}\mathcal{C}(\mathcal{F}) = \mathcal{C}(\delta_{\xi,\bar{\xi}}\mathcal{F}), \tag{2.39}$$

where δ denotes a SUSY transformation. One can build covariant derivatives

$$\mathcal{D}_\alpha = \partial_\alpha - i\sigma^\mu_{\alpha\dot{\alpha}}\bar{\theta}^{\dot{\alpha}}\partial_\mu, \quad \bar{\mathcal{D}}^{\dot{\alpha}} = \partial^{\dot{\alpha}} - i\bar{\sigma}^{\mu\dot{\alpha}\alpha}\theta_\alpha\partial_\mu, \tag{2.40a}$$

$$\mathcal{D}^\alpha = -\partial^\alpha + i\bar{\theta}_{\dot{\alpha}}\sigma^{\mu\dot{\alpha}\alpha}\partial_\mu, \quad \bar{\mathcal{D}}_{\dot{\alpha}} = -\partial_{\dot{\alpha}} + i\theta^\alpha\bar{\sigma}^\mu_{\alpha\dot{\alpha}}\partial_\mu, \tag{2.40b}$$

which satisfies the conditions of Eq. (2.39).

2.3.3 Chiral and antichiral superfields

A superfield Φ is called a chiral superfield if it satisfies the condition

$$\bar{\mathcal{D}}_{\dot{\alpha}}\Phi = 0, \tag{2.41}$$

and similarly, Ψ is antichiral if

$$\mathcal{D}_\alpha\Psi = 0. \tag{2.42}$$

We can note the property that if Φ is chiral, its conjugate $\Phi^\dagger$ will be antichiral.

Language	Q_α	$\bar{Q}_{\dot{\alpha}}$	$\mathcal{D}_\alpha$	$\bar{\mathcal{D}}_{\dot{\alpha}}$
Neutral	$-i(\partial_\alpha + i\sigma^\mu_{\alpha\dot{\alpha}}\bar{\theta}^{\dot{\alpha}}\partial_\mu)$	$i(\partial_{\dot{\alpha}} + i\theta^\alpha\sigma^\mu_{\alpha\dot{\alpha}}\partial_\mu)$	$\partial_\alpha - i\sigma^\mu_{\alpha\dot{\alpha}}\bar{\theta}^{\dot{\alpha}}\partial_\mu$	$-\partial_{\dot{\alpha}} + i\theta^\alpha\sigma^\mu_{\alpha\dot{\alpha}}\partial_\mu$
Chiral	$-i\partial_\alpha$	$i(\partial_{\dot{\alpha}} + 2i\theta^\alpha\sigma^\mu_{\alpha\dot{\alpha}}\partial_\mu)$	$\partial_\alpha - 2i\sigma^\mu_{\alpha\dot{\alpha}}\bar{\theta}^{\dot{\alpha}}\partial_\mu$	$-\partial_{\dot{\alpha}}$
Antichiral	$-i(\partial_\alpha + 2i\sigma^\mu_{\alpha\dot{\alpha}}\bar{\theta}^{\dot{\alpha}}\partial_\mu)$	$i\partial_{\dot{\alpha}}$	∂_α	$-\partial_{\dot{\alpha}} + 2i\theta^\alpha\sigma^\mu_{\alpha\dot{\alpha}}\partial_\mu$

Table 2.1 – Operators in different SUSY languages. The table presents the different operators in terms of chiral (y^μ) and antichiral ($\bar{y}^\mu$) coordinates. In case of chiral (resp. antichiral) language, the space time derivative takes the form $\partial_\mu = \partial/\partial y^\mu$ (resp. $\partial/\partial\bar{y}^\mu$).

In order to work out the field components of a chiral superfield, one can introduce a change in coordinates

$$y^\mu = x^\mu - i\theta\sigma^\mu\bar{\theta}, \quad \bar{y}^\mu = x^\mu + i\theta\sigma^\mu\bar{\theta}. \tag{2.43}$$

These are the so called (anti)chiral languages while using x^μ is the neutral language. In this case the expressions for the SUSY operators and the covariant derivatives are given in Table 2.1.

It is quite convenient, in order to find the expression of a chiral field, to use the chiral language. In such a case, it is sufficient that Φ does not depend on $\bar{\theta}$ to respect the constraint of Eq. (2.41). It is straightforward to write down the expression of Φ in chiral language

$$\Phi(y,\theta) = \phi(y) + \sqrt{2}\theta\psi(y) + \theta\theta F(y), \tag{2.44}$$

where the factor $\sqrt{2}$ is conventional. One can work out the expression in terms of neutral language and will find

$$\Phi(x,\theta,\bar{\theta}) = \phi(x) + \sqrt{2}\theta\psi(x) + \theta\theta F(x) - i\theta\sigma^\mu\bar{\theta}\partial_\mu\phi(x) - \frac{i}{\sqrt{2}}\theta\theta\bar{\theta}\bar{\sigma}^\mu\partial_\mu\psi(x) - \frac{1}{4}\theta\theta\bar{\theta}\bar{\theta}\partial^2\phi(x). \tag{2.45}$$

Similarly, the expression for the antichiral field is given by

$$\Phi^\dagger(x,\theta,\bar{\theta}) = \phi^\dagger(x) + \sqrt{2}\bar{\theta}\bar{\psi}(x) + \bar{\theta}\bar{\theta}F^\dagger(x) + i\theta\sigma^\mu\bar{\theta}\partial_\mu\phi^\dagger(x) - \frac{i}{\sqrt{2}}\bar{\theta}\bar{\theta}\theta\sigma^\mu\partial_\mu\bar{\psi}(x) - \frac{1}{4}\theta\theta\bar{\theta}\bar{\theta}\partial^2\phi^\dagger(x). \tag{2.46}$$

2.3.4 Vector superfields

We now introduce the concept of vector (real) superfield, which will be denoted by V. It can be built from a generic superfield imposing the reality constraint

$$V = V^\dagger. \tag{2.47}$$

It can be shown that the general expression for V, in neutral language, is

$$\begin{aligned} V(x,\theta,\bar{\theta}) = {} & C(x) + i\theta\chi(x) - i\bar{\theta}\bar{\chi}(x) + \frac{i}{2}\theta\theta M(x) - \frac{i}{2}\bar{\theta}\bar{\theta}M^\dagger(x) + \theta\sigma^\mu\bar{\theta}A_\mu \\ & + \theta\theta\bar{\theta}(i\bar{\lambda}(x) + \frac{1}{2}\bar{\sigma}^\mu\partial_\mu\chi(x)) - \bar{\theta}\bar{\theta}\theta(i\lambda(x) + \frac{1}{2}\bar{\sigma}^\mu\partial_\mu\bar{\chi}(x)) \\ & + \frac{1}{2}\theta\theta\bar{\theta}\bar{\theta}(D(x) + \frac{1}{2}\partial^\mu\partial_\mu C(x)), \end{aligned} \tag{2.48}$$

where C and D are real scalar fields, M is a complex scalar field, A_μ is a real four-vector field and χ and λ are complex Weyl spinors.

We can note, for a chiral superfield Φ, that $(\Phi + \Phi^\dagger)$ and $i(\Phi - \Phi^\dagger)$ are vector superfields since they do respect Eq. (2.47). We can thus define a "supergauge transformation" by transforming

$V \to V' = V + i(\Phi - \Phi^\dagger)$. By a proper gauge fixing, the Wess-Zumino (WZ) gauge, it is possible to get rid of several degrees of freedom. The vector superfield is then given by

$$V_{WZ} = \theta\sigma^\mu\bar{\theta}A_\mu + i\theta\theta\bar{\theta}\bar{\lambda} - i\bar{\theta}\bar{\theta}\theta\lambda + \frac{1}{2}\theta\theta\bar{\theta}\bar{\theta}D \tag{2.49}$$

Interestingly, working in the Wess-Zumino gauge will be simpler, as the WZ vector superfields satisfy

$$V_{WZ}^2 = \frac{1}{2}\theta\theta\bar{\theta}\bar{\theta}A^\mu A_\mu, \tag{2.50a}$$

$$V_{WZ}^n = 0 \quad \text{for} \quad n \geqslant 3. \tag{2.50b}$$

2.4 Building SUSY invariant Lagrangians

The purpose of this section is to give a general method for building SUSY invariant Lagrangians. In this context, the introduction of the superspace formalism will be very useful. The first thing to note is that any term like

$$\int d^2\theta d^2\bar{\theta}\ \mathcal{F}, \tag{2.51}$$

is SUSY invariant for $\mathcal{F}$ being any superfield. Indeed, because of translational invariance of the Grassmanian coordinates, we end with

$$\begin{aligned}\delta_{\xi,\bar{\xi}} \int d^2\theta d^2\bar{\theta}\ \mathcal{F} &= \int d^2\theta d^2\bar{\theta}\ \delta_{\xi,\bar{\xi}}\mathcal{F} \\ &= \int d^2\theta d^2\bar{\theta} \left\{ (i\xi\partial_\alpha + i\bar{\xi}\partial^{\dot{\alpha}})\mathcal{F} + \partial_\mu \left[(-\xi\sigma^\mu_{\alpha\dot{\alpha}}\bar{\theta}^{\dot{\alpha}} - \bar{\xi}\bar{\sigma}^{\mu\dot{\alpha}\alpha}\theta)\mathcal{F} \right] \right\},\end{aligned} \tag{2.52}$$

where we made use of Eq. (2.37) in the last step. The integration over the fermionic coordinates kills the first two terms as it would require powers of three in θ or $\bar{\theta}$ in $\mathcal{F}$ for them to be non vanishing. Up to total derivatives, we thus have a SUSY invariant Lagrangian. However, since generic superfields are not irreducible representations of SUSY, we will not use them as the main building blocks but rather terms involving chiral and vector superfields.

In the following we will encounter two types of terms which are SUSY invariant and made of vector and chiral superfields:

- D-terms, which arise from vector superfields

$$\int d^2\theta d^2\bar{\theta}\ V = V|_{\theta\theta\bar{\theta}\bar{\theta}}. \tag{2.53}$$

- F-terms, which arise from (anti)chiral superfields

$$\int d^2\theta\ \Phi = \Phi|_{\theta\theta} \quad \text{and} \quad \int d^2\bar{\theta}\ \Phi^\dagger = \Phi^\dagger|_{\bar{\theta}\bar{\theta}}. \tag{2.54}$$

2.4.1 Chiral superfield Lagrangians

We consider in this section Lagrangians for a chiral superfield Φ and its complex conjugate $\Phi^\dagger$. A first term which is SUSY invariant is the Kähler potential

$$\mathcal{L}_K = \int d^2\theta d^2\bar{\theta} K(\Phi, \Phi^\dagger), \tag{2.55}$$

where, for renormalizable theories, $K(\Phi, \Phi^\dagger) = \Phi^\dagger\Phi$ is the most general expression. Note that, since $\Phi^\dagger\Phi$ is a vector superfield, we have to pick the D-term.

From Eqs. (2.45) and (2.46), one can compute the expression for $\mathcal{L}_K$

$$\mathcal{L}_K = \Phi^\dagger\Phi|_{\theta\theta\bar{\theta}\bar{\theta}} = \partial^\mu\phi^\dagger\partial_\mu\phi + \frac{i}{2}(\psi\sigma^\mu\partial_\mu\bar{\psi} + \bar{\psi}\bar{\sigma}^\mu\partial_\mu\psi) + F^\dagger F + \text{total derivative}, \tag{2.56}$$

which is exactly the kinetic terms associated to one complex scalar field and one Majorana spinor. Using different chiral superfields, one can build Dirac spinors.

We can now ask the question: how can we write a F-term like in Eq. (2.54)? First, let us consider the superfield $W(\Phi)$ such as

$$W(\Phi) = \sum_n a_n \Phi^n, \tag{2.57}$$

where Φ is a chiral superfield. One can show (by applying the anti-chiral derivative) that $W(\Phi)$ is a chiral superfield too. $W(\Phi)$ is called the superpotential, as it will give rise to mass and interaction terms. We can thus write F-terms of the form $W(\Phi_i)|_{\theta\theta}$, where Φ_i denotes the various chiral superfields included in the theory. In case of renormalizable theories, $W(\Phi_i)$ must be at most cubic, because the mass dimension of the measure $d^4x\,d^2\theta$ is -3. Thus, the most general expression for $W(\Phi_i)$ is given by

$$W(\Phi_i) = f_i\Phi_i + \frac{1}{2}m_{ij}\Phi_i\Phi_j + \frac{1}{3!}g_{ijk}\Phi_i\Phi_j\Phi_k. \tag{2.58}$$

where m_{ij}, g_{ijk} are symmetric in the indices. Finally, the full Lagrangian for (anti)chiral superfields will be given by

$$\mathcal{L} = \Phi_i^\dagger\Phi_i|_{\theta\theta\bar{\theta}\bar{\theta}} + W(\Phi_i)|_{\theta\theta} + W(\Phi_i^\dagger)|_{\bar{\theta}\bar{\theta}}. \tag{2.59}$$

We can then expand the Lagrangian in terms of its field content and get

$$\begin{aligned}\mathcal{L} = {} & \partial^\mu\phi^\dagger\partial_\mu\phi + \frac{i}{2}(\psi\sigma^\mu\partial_\mu\bar{\psi} + \bar{\psi}\bar{\sigma}^\mu\partial_\mu\psi) + F^\dagger F \\ & + \left[\left(f_k + m_{ik}\phi_i + \frac{1}{2}g_{ijk}\phi_i\phi_j\right)F_k - \psi_i\psi_j\left(m_{ij} + g_{ijk}\phi_k\right) + \text{h.c.}\right].\end{aligned} \tag{2.60}$$

2.4.2 Gauge sector

We will now turn to the gauge sector of SUSY Lagrangians. As we have already seen, vector bosons appear in vector superfields V described in section 2.3.4. However, working out the SUSY transformation rules for the vector superfield components, we observe that there is an invariant sub-multiplet of V, composed of λ, $F_{\mu\nu}$ and D ($F_{\mu\nu}$ being the usual field strength tensor). Actually, in case of an abelian $U(1)$ symmetry one can build from V such supermultiplets in the following way:

$$W_\alpha = -\frac{1}{4}\bar{D}_{\dot{\alpha}}\bar{D}^{\dot{\alpha}}D_\alpha V, \tag{2.61a}$$

$$\overline{W}^{\dot{\alpha}} = -\frac{1}{4}D^\alpha D_\alpha\bar{D}^{\dot{\alpha}}V. \tag{2.61b}$$

Because $D^3 = \bar{D}^3 = 0$, W and $\overline{W}$ are respectively chiral and antichiral superfields. In addition, one can check that W and $\overline{W}$ are also SUSY gauge invariant, meaning invariant by a shift $i(\Lambda - \Lambda^\dagger)$. Computing the expression in Wess-Zumino gauge and in chiral (resp. antichiral) language, one finds

$$W_\alpha(y,\theta) = -i\lambda_\alpha + \theta_\alpha D + (\sigma^{\mu\nu})_\alpha^\beta\theta_\beta F_{\mu\nu} - \theta\theta\sigma^\mu_{\alpha\dot{\alpha}}\partial_\mu\bar{\lambda}^{\dot{\alpha}}, \tag{2.62a}$$

$$\overline{W}^\alpha(\bar{y},\theta) = i\bar{\lambda}^{\dot{\alpha}} - \bar{\theta}^{\dot{\alpha}}D + (\bar{\sigma}^{\mu\nu})_{\dot{\beta}}^{\dot{\alpha}}\theta_\beta F_{\mu\nu} + \bar{\theta}\bar{\theta}\bar{\sigma}^{\mu\dot{\alpha}\alpha}\partial_\mu\lambda_\alpha. \tag{2.62b}$$

We can thus write down the Lagrangian

$$\mathcal{L}_V = \frac{1}{4}WW|_{\theta\theta} + \frac{1}{4}\overline{WW}|_{\bar{\theta}\bar{\theta}} = -\frac{1}{4}F^{\mu\nu}F_{\mu\nu} + \frac{i}{2}(\lambda\sigma^\mu\partial_\mu\bar{\lambda} + \bar{\lambda}\bar{\sigma}^\mu\lambda) + \frac{1}{2}D^2. \tag{2.63}$$

This expression describes the free propagation of the gauge boson A_μ through its usual kinetic term and, in addition, we have a Majorana fermion. This Majorana fermion is called "gaugino" and is the supersymmetric partner of a SM gauge boson.

We are now interested in coupling gauge bosons to matter fields. Let us start by considering an abelian gauge transformation $U(1)$ acting on a chiral superfield of charge q_i,

$$\Phi_i \to e^{-iq_i\Lambda}\Phi_i. \tag{2.64}$$

The Kähler potential is manifestly invariant under a such transformation. However the superpotential $W(\Phi_i)$ is not:

$$W(\Phi_i) \to W'(\Phi_i) = e^{iq_i\lambda} f_i\Phi_i + e^{i\Lambda(q_i+q_j)}\frac{1}{2}m_{ij}\Phi_i\Phi_j + e^{i\Lambda(q_i+q_j+q_k)}\frac{1}{3}g_{ijk}\Phi_i\Phi_j\Phi_k, \tag{2.65}$$

and thus we have the following constraints for the superpotential

$$f_i = 0, \quad m_{ij} = 0 \text{ or } q_i + q_j = 0 \quad \text{and} \quad g_{ijk} = 0 \text{ or } q_i + q_j + q_k = 0. \tag{2.66}$$

If now we consider a local gauge transformation, in order to preserve supersymmetry, we need to promote Λ to a superfield $\Lambda(x, \theta, \bar{\theta})$ which depend on superspace coordinates. In addition, Λ is a chiral superfield, in order to preserve the chirality of the transformation. The Kähler potential will now transform as

$$K(\Phi, \Phi^\dagger) \to K'(\Phi, \Phi^\dagger) = \Phi^\dagger e^{iq_i(\Lambda-\Lambda^\dagger)}\Phi_i. \tag{2.67}$$

As it can be seen, the transformation is very similar to supersymmetric gauge transformation. One way to enforce gauge invariance, would be to modify the Kähler potential by inserting a vector superfield

$$K(\Phi_i, \Phi_i^\dagger) = \Phi_i^\dagger e^{-q_i V}\Phi_i, \tag{2.68}$$

enforcing that $V \to V' = V + i(\Lambda - \Lambda^\dagger)$, Φ transforms as in Eq. (2.64). We can work out the Lagrangian in the Wess-Zumino gauge

$$\mathcal{L}_K = (D^\mu\phi_i)^\dagger(D_\mu\phi_i) + \frac{i}{2}(\psi\sigma^\mu D_\mu\bar{\psi} - D_\mu\psi\sigma^\mu\bar{\psi}) + F_iF_i^\dagger - i\sqrt{2}q_i(\phi^\dagger\lambda\psi - \bar{\psi}\bar{\lambda}\phi_i) - \frac{1}{2}q_i\phi_i^\dagger D\phi_i, \tag{2.69}$$

where D_μ is the usual covariant derivative.

We will now consider the non-abelian case, where T^a are the generators of the group and $[T^a, T^b] = f^{abc}T^c$ with f^{abc} are the structure constant. Φ_i. The expression of the vector superfield is now given by

$$V_i^j = (V^aT^a)_i^j. \tag{2.70}$$

One can generalize the expressions for W and $\overline{W}$:

$$W_\alpha = -\frac{1}{4}\bar{D}_{\dot{\alpha}}\bar{D}^{\dot{\alpha}}e^{-V}D_\alpha e^V, \tag{2.71a}$$

$$\overline{W}^{\dot{\alpha}} = -\frac{1}{4}D^\alpha D_\alpha e^V\bar{D}^{\dot{\alpha}}e^{-V}. \tag{2.71b}$$

However these superfields are no longer SUSY gauge invariant by their own, but we can still build terms for the Lagrangian that preserve SUSY

$$\mathcal{L}_\mathcal{V} = \frac{1}{4}\int d^2\theta\ \mathrm{Tr}[WW] + \frac{1}{4}\int d^2\bar{\theta}\ \mathrm{Tr}[\overline{WW}]. \tag{2.72}$$

Concerning the interaction with matter superfields, the computation is very similar to the abelian case (while time-consuming) and can be found for e.g. in [48–50]. The main result is that, after

a redefinition of $V \to 2gV$ in order to explicit the coupling constant, one finds that the final Lagrangian for a non-abelian SUSY gauge theory is given by

$$\begin{aligned}\mathcal{L} = \frac{1}{16g^2}\left(\int d^2\theta\ \mathrm{Tr}[WW] + \int d^2\bar{\theta}\ \mathrm{Tr}[\overline{WW}]\right) + \int d^2\theta d^2\bar{\theta}\ \Phi^\dagger e^{2gV}\Phi \\ + \int d^2\theta\ W(\Phi) + \int d^2\bar{\theta}\ W(\Phi^\dagger).\end{aligned} \tag{2.73}$$

Therefore, we can express the Lagrangian in terms of field content and we end up with

$$\begin{aligned}\mathcal{L} = &-\frac{1}{4}F^a_{\mu\nu}F^{a\mu\nu} + i\lambda^a\sigma^\mu D_\mu\bar{\lambda}^a + \frac{1}{2}D^aD^a + (D^\mu\phi_i)^\dagger D_\mu\phi_i + \frac{i}{2}(\psi_i\sigma^\mu D_\mu\bar{\psi}_i - D_\mu\psi_i\bar{\sigma}^\mu\bar{\psi}_i) \\ &+ F_i^\dagger F_i + ig\sqrt{2}(\phi_i^\dagger(T^a)^{ij}\psi_j\lambda^a - \bar{\lambda}^a\bar{\psi}_i(T^a)^{ij}\phi_j) + gD^a\phi^\dagger(T^a)^{ij}\phi_j \\ &+ F_i\frac{\partial W}{\partial\phi_i} + F_i^\dagger\frac{\partial W^\dagger}{\partial\phi_i^\dagger} - \frac{1}{2}\psi_i\psi_j\frac{\partial^2 W}{\partial\phi_i\partial\phi_j} - \frac{1}{2}\bar{\psi}_i\bar{\psi}_j\frac{\partial^2 W^\dagger}{\partial\phi_i^\dagger\partial\psi_j^\dagger}\ ,\end{aligned} \tag{2.74}$$

where $W(\Phi^\dagger) = W^\dagger$.

2.4.3 Auxiliary fields and scalar potential

In the previous sections, we have not really specified the role of the F and D fields. However, this has to be understood as these fields will lead to additional mass terms in generic SUSY theories. As a starting point, we will consider a simple model made of a free propagating spinor ψ and a free propagating scalar ϕ. The Lagrangian simply reads

$$\mathcal{L} = \partial^\mu\phi^\dagger\partial_\mu\phi + i\psi\sigma^\mu\partial_\mu\bar{\psi}, \tag{2.75}$$

with the equation of motion given by:

$$\partial^2\phi = 0 \quad \text{and} \quad \bar{\sigma}^\mu\partial_\mu\psi = 0. \tag{2.76}$$

However, we face here a fundamental problem: The number of degrees of freedom (d.o.f.) is different for bosons and fermions, unless we consider that the equations of motion are satisfied. In order to solve this issue, one can add non propagating degrees of freedom to the theory which will give no further on-shell d.o.f. but will contribute off-shell. This is precisely the role of the F and D fields in the theory.

One can then recast Eq. (2.74) imposing the equations of motion for the F and D fields

$$F_i = -\frac{\partial W}{\partial\phi_i} \quad \text{and} \quad F_i^\dagger = -\frac{\partial W^\dagger}{\partial\phi_i^\dagger}, \quad D^a = -g\phi_i^\dagger(T^a)^{ij}\phi_j, \tag{2.77}$$

and obtain

$$\begin{aligned}\mathcal{L} = &-\frac{1}{4}F^a_{\mu\nu}F^{a\mu\nu} + i\lambda^a\sigma^\mu D_\mu\bar{\lambda}^a + (D^\mu\phi_i)^\dagger D_\mu\phi_i + \frac{i}{2}(\psi_i\sigma^\mu D_\mu\bar{\psi}_i - D_\mu\psi_i\bar{\sigma}^\mu\bar{\psi}_i) \\ &+ ig\sqrt{2}(\phi_i^\dagger(T^a)^{ij}\psi_j\lambda^a - \bar{\lambda}^a\bar{\psi}_i(T^a)^{ij}\phi_j) - \frac{1}{2}\psi_i\psi_j\frac{\partial^2 W}{\partial\phi_i\partial\phi_j} - \frac{1}{2}\bar{\psi}_i\bar{\psi}_j\frac{\partial^2 W^\dagger}{\partial\phi_i^\dagger\partial\psi_j^\dagger} - V(\phi_i,\phi_i^\dagger),\end{aligned} \tag{2.78}$$

where

$$V(\phi_i,\phi_i^\dagger) = F_i^\dagger F + \frac{1}{2}D^aD^a = \sum_i\left|\frac{\partial W}{\Phi_i}\right|^2_{\Phi_i=\phi_i} + \frac{1}{2}g^2\sum_a\left(\phi_j^\dagger(T^a)^{ij}\phi_i\right)^2. \tag{2.79}$$

As it can be seen, the scalar potential will lead to additional mass terms for scalar particles. We will discuss this feature in more detail when we will turn to the Minimal Supersymetric Standard Model (MSSM).

2.5 A word on R-symmetry and R-parity

It can be shown that the SUSY algebra exhibits a global $U(1)_R$ symmetry. This R symmetry leads to the following transformation for chiral superfields

$$\Phi \to e^{i\alpha R_\Phi}\Phi, \quad \Phi^\dagger \to e^{-i\alpha R_\Phi}\Phi^\dagger, \tag{2.80}$$

where Φ (resp. $\Phi^\dagger$) has R charge R_Φ (resp. $-R_\Phi$). Working out the charge for the superfields components while taking into account the R charge of the superspace coordinates θ and $\bar{\theta}$, one finds that

$$R(\phi) = R_\Phi, \quad R(\psi) = R_\Phi - 1, \quad R(F) = R_\Phi - 2. \tag{2.81}$$

Similarly for a vector superfield, for which $R(V) = 0$ because of the reality condition, one ends with:

$$R(A_\mu) = 0, \quad R(\lambda) = 1, \quad R(D) = 0. \tag{2.82}$$

Furthermore, if we consider a general gauge theory, we have in addition the assignment

$$R(\psi) = -1. \tag{2.83}$$

This additional assignment comes from the supergauge transformation of the vector superfield.

This new symmetry, if enforced, constrains the shape of the superpotential. However, this symmetry cannot be a true symmetry of nature. The main reason is that it forbids gaugino mass terms, and because of LHC negative-results for gaugino searches, we know that gauginos have non-vanishing masses. However, one can retain its discrete Z_2 subgroup called R-parity. An element g of the R-parity group is simply obtained considering $\alpha = \pi$ for $U(1)_R$ transformations, which leads to

$$g = e^{i\pi R} = (-1)^R. \tag{2.84}$$

The consequence of this is very interesting: Because of the previous charge assignments, we see that the R_p charge for vector bosons is always positive while the one of its fermionic partner is always negative. Regarding the chiral superfields, the R-parity charge assignment can be made in such a way that the SM model partner has always a negative R_p. In that case, all supersymetric partner of a SM particle have R-parity charge -1. This has very interesting phenomenological consequences, in particular that the lightest supersymetric partner (LSP) is stable and therefore, should it be neutral, provides a good candidate for Dark Matter (DM). One can write down the expression for the R_p charge in the case of lepton and baryon number conservation

$$R_p = (-1)^{3(B-L)+2S}, \tag{2.85}$$

where B and L stand for Baryon and Lepton number, and S for the spin of the considered field.

2.6 Explicit breaking of Supersymmetry

Because P^2 is a Casimir operator of the super-Poincaré group, all particles within a supermultiplet have the same mass. However, superpartners searches at collider are negative and thus it is clear that, if Supersymmetry is realized in Nature, it has to be broken.

The tricky part is that we do not have any knowledge about the mechanism that breaks Supersymmetry. This is why, we will consider the breaking of supersymetry in its most general form, by including explicit soft-breaking terms. Soft-terms are explicit Supersymetry breaking sources but we require that their addition to the Lagrangian does not spoil the nice SUSY feature of protecting the Higgs boson mass from quadratic scale contributions. Accordingly to this point, in this section we will explicit a method to access the most general expression of the soft-terms within a specific SUSY theory from a spurion approach.

Spurions have been used in particular for flavour physics to recover the shape of the explicit flavour symmetry breaking sources. It turns out that this approach can lead to similar results for SUSY breaking terms. The main idea is to promote free parameters to fields which respect the considered symmetry (in our case they will be superfields) and then to develop them around a background value (this is very similar to the Higgs field being developed around its vev). Before going into more details, let precise that the only fields that can be developed around a non-zero background value are scalars fields (this is enforced to respect Poincaré symmetry). Therefore, we will not include the spinor fields in the spurion superfields, as their background values must vanish. Finally, in the spurion approach, one can estimate the shape of the divergences introduced by the soft terms on the Higgs mass, making this approach very suitable for the soft term computation. We shall not discuss this aspect in details, but complementary information can be found in [57].

Let us start by considering the Lagrangian of a free chiral superfield Φ, this reduces to the usual Kähler potential

$$\mathcal{L} = \int d^2\theta d^2\bar{\theta}\ Z\Phi^\dagger\Phi, \tag{2.86}$$

where we promoted the coupling constant Z to a superfield. We can see that Z has to be real, i.e. $Z = Z^\dagger$. Performing the expansion in terms of background values, we end with

$$Z = 1 + (\theta\theta S + \text{h.c.}) + \theta\theta\bar{\theta}\bar{\theta}C, \tag{2.87}$$

where C is a real parameter while S can be complex. Performing the integration over the Grassmanian coordinates leads to the usual kinetics terms for ϕ and ψ plus an additional contribution

$$\mathcal{L} = \text{kinetics}(\phi,\psi) + F^\dagger F + S^\dagger F\phi^\dagger + SF^\dagger\phi + C\phi^\dagger\phi. \tag{2.88}$$

As usual, we can replace F and $F^\dagger$ by their equations of motion

$$F^\dagger = -S^*\phi^\dagger \quad \text{and} \quad F = -S\phi, \tag{2.89}$$

which leads to

$$\mathcal{L} = \text{kinetics}(\phi,\psi) + (C - |S|^2)\phi^\dagger\phi = \text{kinetics}(\phi,\psi) + C'\phi^\dagger\phi. \tag{2.90}$$

As can be seen, the spurion approach has generated an explicit SUSY breaking source for the scalar component of the chiral supermultiplet. This can be understood in the following way: Allowing non dynamical components for the $(\theta,\ \bar{\theta})$ coordinates break the translational invariance in the superfield coordinates. We now generalize the above procedure by simply including different generations of chiral superfields:

$$\mathcal{L} = \int d^2\theta d^2\bar{\theta}\ Z^{ij}\Phi_i^\dagger\Phi_j, \tag{2.91}$$

where i, j are generation indices. Because we should obtain canonical kinetics terms, Z^{ij} is given by

$$Z^{ij} = \delta^{ij} + (\theta\theta S^{ij} + \text{h.c.}) + \theta\theta\bar{\theta}\bar{\theta}C^{ij}. \tag{2.92}$$

which, after eliminating the auxiliary fields, leads to

$$\mathcal{L} = \text{kinetics}(\phi_i,\psi_i) + C'^{ij}\phi_i^\dagger\phi_j. \tag{2.93}$$

In case the coefficients do not vanish for $\neq j$, which is the general case, generation mixing occurs. The shape of these soft terms may be dictated by additional symmetries. For example, in the MSSM, the three gauge groups allow scalar partners with the same quantum numbers to mix. For instance, the sleptons can mix among each other as well as the squarks. Such mixing may lead to unobserved large contributions to flavour and CP observables (such as Kaon mixing), and therefore the general setup is challenged by current experiments. This is known as the SUSY flavour problem, and more on this topic will be discussed in the next chapter when we will investigate the MSSM for a general flavour mixing framework. In addition, these soft term may be driven by additional

flavour symmetries. We shall see an example in the context of flavoured GUT models, which will be the subject of Chapters 5 and 6.

For now, we will write down the most general soft terms using the spurion approach. Following [48, 57], we end up with

$$\begin{aligned} -\mathcal{L}_{SOFT} = &\left[\eta\left(-\frac{1}{3!}A^{ijk}\Phi_i\Phi_j\Phi_k + \frac{1}{2}B^{ij}\Phi_i\Phi_k - C^i\Phi_i + \frac{1}{2}M_a W^a W^a\right)\right]_{\theta\theta} + \text{h.c.} \\ &+ \left[\bar{\eta}\eta\Phi_i^\dagger (m^2)^{ij}(e^V)^{jk}\Phi_k\right]_{\theta\theta\bar{\theta}\bar{\theta}}, \end{aligned} \tag{2.94}$$

where $\eta = \theta\theta$ and $\bar{\eta} = \bar{\theta}\bar{\theta}$. The additional terms, such as S_{ij} in Eq. (2.92), can be absorbed into these contributions. In the case of the MSSM, the linear term C^i must vanish because of gauge invariance. The above terms contains the soft scalar masses m^{ij} (originating from the Kähler potential), the gaugino mass M_a (arrising from the gauge sector kinetic term) and the trilinear coupling A^{ijk} (from the Yukawa-type interaction in the superpotential) which couple three scalars. In addition, we have the bilinear term B^{ij}, which in the case of the MSSM couples the Higgs fields only (because of gauge invariance) and stands for the higgsino soft masses.

Chapter 3

The MSSM

This chapter is dedicated to the discussion of the Minimal Supersymetric Standard Model (MSSM), in particular in the context of the presence of non-minimally flavour violating terms. The discussion will be very useful for the rest of the manuscript, as the conventions are established here. Other chapters will be dedicated to SUSY GUT models, but as we will see, these models give back the MSSM once we integrate out the heavy degrees of freedom. Therefore, the MSSM will be our main theory when dealing with TeV scale physics. In this chapter, we will follow the discussion and notations of [48].

3.1 Lagrangian of the MSSM

The ambition is to provide a realistic extension of the SM. Therefore, Supersymmetry has to be broken in the MSSM.

We can decompose the MSSM Lagrangian in two parts

$$\mathcal{L}_{MSSM} = \mathcal{L}_{SUSY} + \mathcal{L}_{SOFT}. \tag{3.1}$$

While $\mathcal{L}_{SUSY}$ stands for the SUSY respecting part, $\mathcal{L}_{SOFT}$ includes the explicit SUSY breaking terms.

The SUSY preserving part includes the usual SM Lagrangian (up to a second Higgs doublet) as well as the dynamics and interactions of the superpartners. This part can be written in superfields formalism. On the other side, the soft breaking part provides additional contributions to the mass of the superpartners, as described in Sec. 2.6. We will use field content notation as only the superpartners are concerned here.

3.1.1 Superfield content of the MSSM

The MSSM is obtained from the usual SM by simply promoting the field content of the SM to superfields with the same charge assignments. However, the holomorphy property of the superpotential avoids any anti-chiral superfield in the interaction terms. Therefore, to recover the Yukawa interactions for the down quarks and charged leptons, one need to add an extra Higgs doublet. We will briefly list the set of superfields involved in the MSSM.

Let us start with the leptonic sector. As in the SM, there will be three generations of $SU(2)_L$ doublets L_i and three generations of $SU(2)$ singlets $\bar{E}_i$, for $i = 1, 2, 3$

$$L_1 = \begin{pmatrix} L_{\nu_e} \\ L_e \end{pmatrix}, \quad L_2 = \begin{pmatrix} L_{\nu_\mu} \\ L_\mu \end{pmatrix}, \quad L_1 = \begin{pmatrix} L_{\nu_\tau} \\ L_\tau \end{pmatrix}, \quad \bar{E}_1 = e^c_R, \quad \bar{E}_2 = \mu^c_R, \quad \bar{E}_3 = \tau^c_R, \tag{3.2}$$

where the c superscript stands for charge conjugation. The field content of the superfields L_i will be chiral Weyl fermions $\nu_i,\ e_{L,i},\ e^c_{R,i}$ with in addition their scalar partners $\tilde{\nu}_i,\ \tilde{e}_{L,i},\ \tilde{e}^*_{R,i}$. The quark

(squark) sector will be defined in the same manner as

$$\begin{aligned} Q_1 &= \begin{pmatrix} Q_u \\ Q_d \end{pmatrix}, \quad Q_2 = \begin{pmatrix} Q_c \\ Q_s \end{pmatrix}, \quad Q_1 = \begin{pmatrix} Q_t \\ Q_b \end{pmatrix}, \\ \bar{U}_1 &= u_R^c, \quad \bar{U}_2 = c_R^c, \quad \bar{U}_3 = t_R^c, \\ \bar{D}_1 &= d_R^c, \quad \bar{D}_2 = s_R^c, \quad \bar{D}_3 = b_R^c. \end{aligned} \tag{3.3}$$

As per the SM, the quark superfields have multiplicity of three in colour because they belong to the fundamental representation of $SU(3)_C$.

As discussed previously, the matter sector includes in addition two Higgs doublets (for the up and down sectors)

$$H_u = \begin{pmatrix} h_u^+ \\ h_u^0 \end{pmatrix}, \quad H_d = \begin{pmatrix} h_d^0 \\ h_d^- \end{pmatrix} \tag{3.4}$$

where the hypercharge of H_u is 1 (and -1 for H_d). Therefore, the superscripts $(+, -, 0)$ in (3.4) stand for the electric charge.

One needs also to define the gauge sector. Since the MSSM has the usual $G_{SM} = SU(3)_c \times SU(2)_L \times U(1)_Y$ gauge symmetry, we have to introduce a set of vector superfields

$$V^Y, \quad V^W, \quad V_g^a, \tag{3.5}$$

which includes the different gauge bosons.

3.1.2 SUSY part of the MSSM

Following the discussions of Sec. 2.4, we can write down the MSSM Lagrangian which includes the matter, gauge and Higgs sectors

$$\mathcal{L}_{SUSY} = \mathcal{L}_g + \mathcal{L}_M + \mathcal{L}_H. \tag{3.6}$$

The gauge part of the MSSM is given by

$$\mathcal{L}_g = \frac{1}{4} \int d^2\theta \left(W_g^a W_g^a + \vec{W}_W . \vec{W}_W + W_Y W_Y \right) + \text{h.c.} \,, \tag{3.7}$$

where the summation over a is implicit. The matter sector is given by

$$\begin{aligned} \mathcal{L}_M = \int d^2\theta d^2\bar{\theta} \Big[& L_i^\dagger e^{(g_2 \vec{V}_W . \vec{\sigma} + g_Y V^Y Y)} L_i + \bar{E}_i^\dagger e^{g_Y V^Y Y} \bar{E}_i + Q_i^\dagger e^{(g_s V_g^a \lambda^a + g_2 \vec{V}_W . \vec{\sigma} + g_Y V^Y Y)} Q_i \\ & + \bar{U}_i^\dagger e^{(g_s V_g^a \bar{\lambda}^a + g_Y V^Y Y)} \bar{U}_i + \bar{D}_i^\dagger e^{(g_s V_g^a \bar{\lambda}^a + g_Y V^Y Y)} \bar{D}_i \Big] , \end{aligned} \tag{3.8}$$

where $\vec{\sigma} = (\sigma_1, \sigma_2, \sigma_3)$ are the Pauli matrices and λ^a ($\bar{\lambda}^a$) are the Gell-Mann matrices (and hermitian conjugate). Finally, the Higgs sector will be described by

$$\mathcal{L}_H = \int d^\theta d^2\bar{\theta} \; H_m^\dagger e^{(g_2 \vec{V}_W . \vec{\sigma} + g_Y V^Y Y)} H_m + \left(\int d^2\theta \; W_{MSSM} + \text{h.c} \right), \tag{3.9}$$

where $m = u, d$ and W_{MSSM} is the MSSM superpotential. The expression of the superpotential is given by

$$W_{MSSM} = \mu H_d H_u - f_{ij}^e H_d L_i \bar{E}_j - f_{ij}^d H_d Q_i \bar{D}_j - f_{ij} H_u Q_i \bar{U}_j. \tag{3.10}$$

The shape of the MSSM superpotential is constrained by the requirement of R-parity conservation, defined in sec. 2.5.

As we did in the previous chapter, we can express the auxiliary fields F and D in terms of their equations of motion. Since we are dealing with $SU(2)_L$ doublets, we will define the components of

the doublets as $H^D_{u,d} = \epsilon_{DE} H^E_{u,d}$ (and similarly for sfermions). Therefore, the associated F^{*D}_f term will be given by

$$F^{*D}_f = -\frac{\partial W}{\partial f^D} \tag{3.11}$$

Working out the expressions, one finds (dropping the color indices)

$$F^{*D}_{H_d} = -\mu h^D_u + f^e_{ij}\tilde{e}^*_{jR}\tilde{l}^D_{iL} + f^d_{ij}\tilde{d}^*_{jR}\tilde{q}^D_{iL}, \tag{3.12a}$$
$$F^{*D}_{H_u} = \mu h^D_d - f^u_{ij}\tilde{u}^*_{jR}\tilde{q}^D_{iL}, \tag{3.12b}$$
$$F^{*D}_{L_i} = -f^e_{ij} h^D_d \tilde{e}^*_{jR}, \tag{3.12c}$$
$$F^{*D}_{Q_i} = -f^d_{ij} h^D_d \tilde{d}^*_{jR} + f^u_{ij} h^D_u \tilde{u}^*_{jR}, \tag{3.12d}$$
$$F^*_{\bar{E}_i} = f^e_{ji} h_d \tilde{l}_{jL}, \tag{3.12e}$$
$$F^*_{\bar{D}_i} = f^d_{ji} h_d \tilde{q}_{jL}, \tag{3.12f}$$
$$F^*_{\bar{U}_i} = f^u_{ji} \tilde{q}_{jL} h_u. \tag{3.12g}$$

The D terms can be replaced by the expressions

$$D^Y = -\frac{1}{2} g_Y \left(h^\dagger_u h_u - h^\dagger_d h_d - \frac{4}{3}\tilde{u}_{iR}\tilde{u}^\dagger_{iR} + \frac{2}{3}\bar{d}_{iR} d^\dagger_{iR} - \tilde{l}^\dagger_{iL}\tilde{l}_{iL} + 2\tilde{e}_{iR}\tilde{e}^*_{iR} \right), \tag{3.13}$$
$$\vec{D} = -g_2 \frac{1}{2} \left(h^\dagger_d \vec{\sigma} h_d + h^\dagger_u \vec{\sigma} h_u + \tilde{q}^\dagger_{iL}\vec{\sigma}\tilde{q}_{iL} + \tilde{l}^\dagger_{iL}\vec{\sigma}\tilde{l}_{iL} \right), \tag{3.14}$$
$$D^a = -\frac{1}{2} g_s \left(\tilde{q}^\dagger_{iL}\lambda^a \tilde{q}_{iL} + \tilde{u}^\dagger_{iL}\lambda^a \tilde{u}_{iL} + \tilde{d}^\dagger_{iL}\lambda^a \tilde{d}_{iL} \right). \tag{3.15}$$

Finally, the scalar potential for the MSSM is given by

$$V_{SUSY} = F^*_k F_k + \frac{1}{2}\left[{D^Y}^2 + \vec{D}^2 + D^a D^a \right]. \tag{3.16}$$

3.1.3 The soft breaking part of the MSSM

As discussed in Sec. 2.6, we include the most general soft terms for the MSSM. Using (2.94), we can write down the soft sector as

$$\begin{aligned} -\mathcal{L}_{SOFT} = {} & \tilde{q}^*_{iL}(M^2_{\tilde{Q}LL})_{ij}\tilde{q}_{jL} + \tilde{u}^*_{iR}(M^2_{\tilde{U}RR})_{ij}\tilde{u}_{jR} + \tilde{d}^*_{iR}(M^2_{\tilde{D}RR})_{ij}\tilde{d}_{jR} \\ & + \tilde{\ell}^*_{iL}(M^2_{\tilde{L}LL})_{ij}\tilde{\ell}_{jL} + \tilde{e}^*_{iR}(M^2_{\tilde{E}RR})_{ij}\tilde{e}_{jR} \\ & + \left[h_d \tilde{\ell}^*_{iL}(A^{e\dagger})_{ij}\tilde{e}_{jR} + h_d \tilde{q}^*_{iL}(A^{d\dagger})_{ij}\tilde{d}_{jR} + h_u \tilde{q}^*_{iL}(A^{u\dagger})_{ij}\tilde{u}_{jR} + \text{h.c.} \right] \\ & + m^2_d |h_d|^2 + m^2_u |h_u|^2 + (B\mu h_d h_u + \text{h.c.}) \\ & + \frac{1}{2}(M_1 \bar{\tilde{\lambda}}_Y P_L \tilde{\lambda}_Y + M^*_1 \bar{\tilde{\lambda}}_Y P_R \tilde{\lambda}_Y) + \frac{1}{2}(M_2 \bar{\vec{\tilde{\lambda}}} P_L \vec{\tilde{\lambda}} + M^*_2 \bar{\vec{\tilde{\lambda}}} P_R \vec{\tilde{\lambda}}) \\ & + \frac{1}{2}(M_3 \bar{\tilde{g}}^a P_L \tilde{g}^a + M^*_3 \bar{\tilde{g}}^a P_R \tilde{g}^a). \end{aligned} \tag{3.17}$$

Here, the LL, RR subscript stands for the chirality blocks of the full mass matrices where the soft matrices enters. For instance, $M_{\tilde{Q}LL}$ enters in the Left handed - Left handed block of the full squark mass matrices, which will be detailed later. The first and second lines correspond to the inclusion of soft mass matrices for the sfermions $M^2_{\tilde{f}}$, the third one involves the trilinear terms which couples left sfermions to right ones via a higgs field. The fourth line correspond to additional masses in the Higgs sector and finally the two last lines stand for the Majorana gaugino mass matrices.

As it can be seen, the soft Lagrangian can be decomposed into two blocks: The gaugino mass terms and a soft scalar potential. As discussed, these terms imply an explicit splitting in the superfield contents as only superpartner have this additional mass contribution.

3.2 The MSSM spectrum

When electroweak symmetry breaking (EWSB) occurs, the two Higgs doublets acquire vevs along the following directions

$$\langle h_d \rangle = \frac{1}{\sqrt{2}} \begin{pmatrix} v_d \\ 0 \end{pmatrix}, \quad \langle h_u \rangle = \frac{1}{\sqrt{2}} \begin{pmatrix} 0 \\ v_u \end{pmatrix}. \tag{3.18}$$

As in the SM, these vevs, combined to the Yukawa couplings will generate masses for the different particles. In the MSSM, it is usual to define the ratios of the vev as

$$\tan\beta = \frac{v_u}{v_d}, \quad v_u^2 + v_d^2 = v_{SM}^2 \sim (246 \text{ GeV})^2, \tag{3.19}$$

where v_{SM} is the SM Higgs vev. We will now investigate the spectrum of the MSSM.

3.2.1 Gauginos spectrum

After EWSB, the weak gauginos and the higgsinos mix. This can be traced back to different sources: First, there is a contribution which origin from the coupling between the Higgs and the weak gauginos and another which come from the Higgs bilinear term BH_dH_u from the soft Lagrangian. Finally, we have to include the gaugino Majorana masses, arising from the soft Lagrangian. The charged higgsino/gaugino mass Lagrangian will then read as

$$\mathcal{L}_m^c = -\frac{g}{\sqrt{2}}(v_d \lambda^+ \tilde{h}_d^- + v_u \lambda^- \tilde{h}_u^+ + \text{h.c.}) - (M_2 \lambda^+ \lambda^- + \mu \tilde{h}_d^- \tilde{h}_u^+ + \text{h.c.}). \tag{3.20}$$

One can rewrite this term as

$$-\mathcal{L}_m^c = (\psi^-)^T M_C \psi^+ + \text{h.c.} \tag{3.21}$$

with the definitions

$$\psi^+ = (\lambda^+, \tilde{h}_u^+)^T, \quad \psi^- = (\lambda^-, \tilde{h}_d^-)^T, \tag{3.22}$$

and

$$M_C = \begin{pmatrix} M_2 & \sqrt{2} M_W \sin\beta \\ \sqrt{2} M_W \cos\beta & \mu \end{pmatrix}. \tag{3.23}$$

A general matrix can be brought into a diagonal form by the use of two unitary matrices. This is called the Singular Value Decomposition (SVD). Therefore, we can bring the mass matrix to its diagonal form by rotating on the left and the right side $M_C^{diag} = U M_C V^\dagger$, where M_C^{diag} is diagonal. We therefore end with

$$\mathcal{L}_m^c = (\tilde{\chi}_1^- \ \tilde{\chi}_2^-) \begin{pmatrix} m_{C_1} & 0 \\ 0 & m_{C_2} \end{pmatrix} \begin{pmatrix} \tilde{\chi}_1^+ \\ \tilde{\chi}_2^+ \end{pmatrix}, \tag{3.24}$$

where the mass eigenstates associated to the charged higgsinos and gauginos $\tilde{\chi}^\pm$ are called charginos. The relation between the higgsinos/gauginos and the charginos is given by the two mixing matrices U and V as

$$\tilde{\chi}_k^+ = V_{km} \psi_m^+, \quad \tilde{\chi}_k^- = U_{km} \psi_m^-. \tag{3.25}$$

We can now perform a similar analysis for the neutral higgsinos and charginos. The mass Lagrangian reads

$$\mathcal{L}_m^n = -\frac{g_2}{2}\lambda_3 \left(v_d \tilde{h}_d^0 - v_u \tilde{h}_u^0\right) + \frac{g_Y}{2}\lambda_0 \left(v_d \tilde{h}_d^0 - v_u \tilde{h}_u^0\right) + \mu h_d^0 h_u^0 - \frac{1}{2} M_2 \lambda_3 \lambda_3 - \frac{1}{2} M_1 \lambda_0 \lambda_0 + \text{h.c.} \tag{3.26}$$

where λ_3 correspond to the neutral weak gaugino and λ_0 to the Bino (SUSY partner of the $U(1)_Y$ B boson). We can as before recast the previous equation into

$$\mathcal{L}_m^n = -\frac{1}{2}(\psi^0)^T M_N \psi^0, \tag{3.27}$$

where

$$\psi^0 = (\lambda_0,\ \lambda_3,\ h_d^0,\ h_u^0)^T. \tag{3.28}$$

The mass matrix is given by

$$M_N = \begin{pmatrix} M_1 & 0 & -M_Z\cos\beta\sin\theta_W & M_Z\sin\beta\sin\theta_W \\ 0 & M_2 & M_Z\cos\beta\cos\theta_W & -M_Z\sin\beta\cos\theta_W \\ -M_Z\cos\beta\sin\theta_W & M_Z\cos\beta\cos\theta_W & 0 & -\mu \\ M_Z\sin\beta\sin\theta_W & -M_Z\sin\beta\cos\theta_W & -\mu & 0 \end{pmatrix}, \tag{3.29}$$

where θ_W is the weak mixing angle. The mass matrix being symmetric, one needs only one unitary matrix N to diagonalize it. Therefore, we can express the mass term as

$$\mathcal{L}_m^n = \frac{1}{2}\sum_{i=1}^{4} M_i \tilde{\chi}_i^{0\ c}\tilde{\chi}_i^0, \tag{3.30}$$

where $\tilde{\chi}_i^0$ with $i = 1...4$ are the four neutralinos (mass eigenstates of the neutral higgsinos/gauginos). The relation between the interaction eigenstates and the mass eigenstates is obtained through the mixing matrix

$$\tilde{\chi}_i^0 = N_{im}\psi_m^0. \tag{3.31}$$

The lightest neutralino is a very good weakly interactive massive particle (WIMP) candidate for dark matter [58–60]. Indeed, within the MSSM with R-Parity, in case it is the lightest superpartner, χ_1^0 provides a stable and neutral $\mathcal{O}(100 \sim 1000)$ GeV particle which interacts only through weak interactions. However, there are other particles in the MSSM which can be suitable DM candidates [61, 62]. In the context of this manuscript we will always consider the neutralino as the DM candidate, which implies that it will be the lightest supersymetric particle.

3.2.2 Sfermion spectrum

We now turn to the sfermion sector of the MSSM. There are different contributions to the sfermion masses that can be decomposed as

$$V^{\tilde{f}} = V_{SOFT}^{\tilde{f}} + V_F^{\tilde{f}} + V_D^{\tilde{f}}, \tag{3.32}$$

where the subscript D and F stand for the contribution originating from the elimination of the F and D auxiliary fields. V_{SOFT} denotes the full contribution from $\mathcal{L}_{SOFT}$.

Collecting the full set of mass contributions, we will now write down the explicit matrices for the different sfermions in the MSSM, which enter the Lagrangian as

$$\mathcal{L}_{m_{\tilde{f}}} = \sum_{\tilde{f}} \tilde{f}^\dagger M_{\tilde{f}}^2 \tilde{f}, \tag{3.33}$$

where the $\tilde{f}$ vector is simply given by

$$\tilde{f} = \begin{pmatrix} \tilde{f}_L^i \\ \tilde{f}_R^j \end{pmatrix}. \tag{3.34}$$

where i, j are generation indices. For example, the up-squark vector will be given by

$$\tilde{u} = (\tilde{u}_L, \tilde{c}_L, \tilde{t}_L, \tilde{u}_R, \tilde{c}_R, \tilde{t}_R)^T. \tag{3.35}$$

Therefore, apart from the sneutrino mass matrix which has dimension 3×3, the sfermion mass matrices will have dimension 6×6. The general expression for the sfermion masses is

$$M_{\tilde{f}}^2 = \begin{pmatrix} M_{\tilde{F}LL}^2 + D_{LL}^{\tilde{f}}\ \mathbb{1} + m_f m_f^\dagger & -\frac{v_f}{\sqrt{2}}\left(A^{f\dagger} + \mu f(\beta) y_f\right) \\ -\frac{v_f}{\sqrt{2}}\left(A^f + \mu^* f(\beta) y_f^\dagger\right) & M_{\tilde{F}RR} + D_{RR}^{\tilde{f}}\ \mathbb{1} + m_f^\dagger m_f \end{pmatrix}, \tag{3.36}$$

where $M^2_{\tilde{F}\{LL,RR\}}$ and A^f are the 3×3 soft matrices from Eq. (3.17) where LL (resp. RR) denotes the matrix entering into the left-handed - left-handed term (resp. right - right). $Q_{\tilde{f}}$ and $T^{\tilde{f}}_{3L}$ are the charge and weak isospin of $\tilde{f}$. y_f stands for the f Yukawa coupling and v_f for the associated Higgs vev. In addition, m_f stands for the associated SM fermion mass and $f(\beta)$ is given by

$$f(\beta) = \begin{cases} \tan\beta & \text{if } \tilde{f} = \tilde{d}, \tilde{e} \\ \cot\beta & \text{if } \tilde{f} = \tilde{u} \end{cases} . \tag{3.37}$$

Finally, $D^{\tilde{f}}_{LL,RR}$, which are sourced by the D auxiliary fields, are given by

$$D^{\tilde{f}}_{LL} = M_Z^2(T^{\tilde{f}}_{3L} - Q_{\tilde{f}}\sin^2\theta_W)\cos(2\beta), \qquad D^{\tilde{f}}_{RR} = Q_{\tilde{f}}M_Z^2\cos(2\beta)\sin^2\theta_W. \tag{3.38}$$

For a simpler form, we will often write down the mass matrix in terms of four 3×3 matrices as

$$M^2_{\tilde{f}} = \begin{pmatrix} M^2_{\tilde{f}LL} & M^2_{\tilde{f}LR} \\ M^{2\dagger}_{\tilde{f}LR} & M^2_{\tilde{f}RR} \end{pmatrix}, \tag{3.39}$$

where the matrices $M^2_{\tilde{f}AA}$, for $A = L, R$, are hermitian (but not necessary for the $M_{\tilde{f}LR}$ ones). In case $\tilde{f} = \tilde{\nu}$, only the LL entry of the mass matrix is non-zero because of the absence of right handed neutrinos/sneutrinos in the standard MSSM.

3.2.3 Super-CKM basis (SCKM)

The mass matrices from the previous section are given in the flavour basis. However, for phenomenological purposes, it is more convenient to work in a different basis, called the Super-CKM basis (SCKM) [63]. To obtain this basis, one simply performs the same rotations on the SM quarks and on the squarks in order to get diagonal SM Yukawa couplings. This basis allows us to work in the mass basis for SM particles and therefore it is more appropriate for studying low scale observables and non minimal flavour violating effects. In Sec. 1.4.3, we defined the quark rotations that bring the Yukawa terms to diagonal form. Therefore the squarks in the SCKM basis are defined by

$$\tilde{u}'_L = V_{u_L}\tilde{u}_L, \quad \tilde{u}'_R = V_{u_R}\tilde{u}_R, \quad \tilde{d}'_L = V_{d_L}\tilde{d}_L, \quad \tilde{d}'_R = V_{d_R}\tilde{d}_R, \tag{3.40}$$

where the primed fields stand for the original basis while the unprimed ones are in the SCKM basis.

As a first step, we can work out the down squark rotations. We have the following transformations for the mass matrix elements of the down squark sector:

$$A^d = V^\dagger_{d_R}A'^d V_{d_L}, \tag{3.41a}$$
$$m_d = \mathrm{diag}(m_{d_1}, m_{d_2}, m_{d_3}), \tag{3.41b}$$
$$M^2_{\tilde{D}RR} = V^\dagger_{d_R}M'^2_{\tilde{D}RR}V_{d_R}, \tag{3.41c}$$
$$M^2_{\tilde{D}LL} = V^\dagger_{d_L}M'^2_{\tilde{D}LL}V_{d_L}, \tag{3.41d}$$

while all other terms in $M^2_{\tilde{d}}$ are left invariant. However, we shall emphasize that, because of the $SU(2)_L$ doublet representation for up and down-squarks, $M'^2_{\tilde{D}LL} = M'^2_{\tilde{U}LL} \equiv M'^2_{\tilde{Q}LL}$. In order to keep track of this dependence, we have $M'^2_{\tilde{Q}LL} = V_{d_L}M^2_{\tilde{Q}LL}V^\dagger_{d_L}$ and therefore $M^2_{\tilde{D}LL} = M^2_{\tilde{Q}LL}$. We can now turn to the up-squark rotations which lead to the following transformations:

$$A^u = V^\dagger_{u_R}A'^u V_{u_L}, \tag{3.42a}$$
$$m_u = \mathrm{diag}(m_{u_1}, m_{u_2}, m_{u_3}), \tag{3.42b}$$
$$M^2_{\tilde{U}RR} = V^\dagger_{u_R}M'^2_{\tilde{U}RR}V_{u_R}, \tag{3.42c}$$
$$M^2_{\tilde{U}LL} = V^\dagger_{u_L}V_{d_L}M^2_{\tilde{Q}LL}V^\dagger_{d_L}V_{u_L}, \tag{3.42d}$$

which completes the SCKM transformations. We can then write the mass matrix for down-squarks as

$$M_{\tilde{d}}^2 = \begin{pmatrix} M_{\tilde{Q}LL}^2 + D_{LL}^{\tilde{d}}\,\mathbb{1} + m_d^\dagger m_d & -\frac{v_d}{\sqrt{2}}\left(A^{d\dagger} + \mu f(\beta) y_d\right) \\ -\frac{v_d}{\sqrt{2}}\left(A^d + \mu^* f(\beta) y_d^\dagger\right) & M_{\tilde{D}RR} + D_{RR}^{\tilde{d}}\,\mathbb{1} + m_d^\dagger m_d \end{pmatrix}, \tag{3.43}$$

and for up-squarks as

$$M_{\tilde{u}}^2 = \begin{pmatrix} V_{CKM} M_{\tilde{Q}LL}^2 V_{CKM}^\dagger + D_{LL}^{\tilde{u}}\,\mathbb{1} + m_u^\dagger m_u & -\frac{v_u}{\sqrt{2}}\left(A^{u\dagger} + \mu f(\beta) y_u\right) \\ -\frac{v_u}{\sqrt{2}}\left(A^u + \mu^* f(\beta) y_u^\dagger\right) & M_{\tilde{U}RR} + D_{RR}^{\tilde{u}}\,\mathbb{1} + m_u^\dagger m_u \end{pmatrix}, \tag{3.44}$$

where y^f are diagonal matrices. For a large part of the rest of the manuscript we will work in the SCKM basis. Let us note that an analogous basis exists for leptons when working with massive neutrinos, the so called Super-PMNS (SPMNS) basis.

3.3 Flavour mixing

As it can be seen for the sfermion mass matrices, new sources of flavour violation can arise from the soft terms. One can check from Eq. (3.36), that all the terms apart from the soft ones are either proportional to the SM mass matrices or the identity, meaning that they are all diagonalizable in the same way as the SM Yukawa couplings, bringing no new sources of flavour violation with respect to the usual CKM matrix. This particular setup is called the minimal flavour violation (MFV) framework [64]: MFV is a BSM hypothesis that states that any new couplings involving SM generations are either proportional to the identity or the SM Yukawas. However, the presence of generic off diagonal soft terms implies a breaking of the MFV paradigm. Therefore, additional potential sources of flavour violation arise which might lead to (unobserved) flavour violating effects. To return to the usual MFV paradigm, one simply puts to 0 the off-diagonal elements of the soft terms in the SCKM basis [1], in which case the sfermion soft terms are diagonal in flavour space. However, keeping the off-diagonal elements non-vanishing, one falls into the so-called Non-Minimal Flavour Violation (NMFV) framework. In that case, generation changing interactions appear at tree level. This is the setup we should discuss and study for the next chapters of the manuscript.

Before going into additional details, let us simply discuss the squark mass eigenstates. Starting from the matrices in Eqs. (3.44) and (3.43), we can define rotation matrices that bring the squark mass matrices to their diagonal form

$$M_{\Delta\tilde{d}}^2 = R^{\tilde{d}^\dagger} \hat{M}_{\tilde{d}}^2 R^{\tilde{d}}, \qquad M_{\Delta\tilde{u}}^2 = R^{\tilde{u}^\dagger} \hat{M}_{\tilde{u}}^2 R^{\tilde{u}}, \tag{3.45}$$

where $M_{\Delta\tilde{q}}^2$ is diagonal. We have similar transformations for sleptons and sneutrinos. In case we follow the MFV paradigm, no intergenerational mixing is generated and the rotation matrices simply mix the different sfermion helicity states.

The associated eigenstates change is the following

$$(\tilde{u}_L, \tilde{c}_L, \tilde{t}_L, \tilde{u}_R, \tilde{c}_R, \tilde{t}_R) \to (\tilde{u}_1, \tilde{u}_2, \tilde{u}_3, \tilde{u}_4, \tilde{u}_5, \tilde{u}_6), \tag{3.46}$$

where the convention is chosen such that $m_{\tilde{u}_i} < m_{\tilde{u}_{i+1}}$. For the up-squark sector, the mass eigenstates can be expressed in terms of flavour eigenstates as

$$\tilde{u}_i = \sum_j R_{ij}^{\tilde{u}} \tilde{u}_j', \tag{3.47}$$

where the prime here stands for flavour eigenstates. The same holds for the different sfermion sectors. Therefore, in Eq. (3.47) in NMFV framework, the squark mass eigenstates are composed by different up-generation flavour eigenstates. This is extended to different sleptons sector if the NMFV framework holds there.

[1] Properly speaking, one needs also to set the diagonal elements either proportional to the identity or to the diagonal yukawa couplings. However, we will refer this setup as "strict MFV" when needed while we will keep using "MFV" framework for our less strict parametrization.

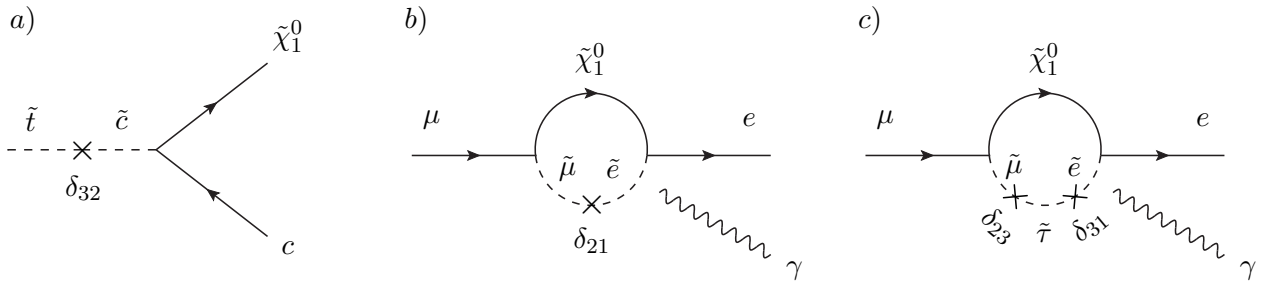

Figure 3.1 – The *a*) panel shows the decay of a stop to the lightest neutralino and charm quark through the insertion of one flavour violating δ parameter. The panels *b*) and *c*) show contributions to the decay $\mu \to e\gamma$ for resp. one and two δ insertions (diagram *c*) involves a $\tilde{\tau}$ in the loop).

3.3.1 Mass insertion approximation

There is a very useful way to parametrize the amount of flavour violation in SUSY models with NMFV framework. Working in the SCKM basis, one can rescale the off-diagonal elements with respect to the diagonal ones and obtain what we will call δ parameters. Different definitions for these parameters can be found in the literature, however the common approach is to rescale with respect to the diagonal soft matrices elements.

We will define the δ parameters as the following:

$$(\delta^{\tilde{f}}_{AA})_{ij} = \frac{(M^2_{\tilde{F}AA})_{ij}}{\sqrt{(M^2_{\tilde{F}AA})_{ii}(M^2_{\tilde{F}AA})_{jj}}}, \qquad (\delta^{\tilde{f}}_{RL})_{ij} = \frac{v_f}{\sqrt{2}}\frac{(A^f)_{ij}}{\sqrt{(M^2_{\tilde{F}AA})_{ii}(M^2_{\tilde{F}AA})_{jj}}}, \tag{3.48}$$

where $v_f = v_u,\ v_d$ depending on the sfermion under consideration and $A = L, R$. From the above definition, it is clear that $(\delta_{LR}) = (\delta_{RL})^\dagger$. We can note also that because of the $SU(2)$ relations, we have

$$(\delta^{\tilde{u}}_{LL}) = (\delta^{\tilde{d}}_{LL}) \equiv (\delta^{\tilde{Q}}_{LL}), \qquad (\delta^{\tilde{\nu}}_{LL}) = (\delta^{\tilde{l}}_{LL}) \equiv (\delta^{\tilde{L}}_{LL}), \tag{3.49}$$

keeping in mind that the CKM matrix (and PMNS matrix if present) rotates the δ matrices in the corresponding sector. Let us emphasize here that in general the off diagonal elements have to be smaller than the respective diagonal ones. If not, one would end with a negative squared mass for one of the sfermions. By the use of these definitions, one can get an approximation for the sfermion mass matrix (Super-CKM-PMNS basis) by rewriting

$$\hat{M}^2_{\tilde{f}} \sim \begin{pmatrix} \widetilde{M}^2_{\tilde{F}LL}(\delta^{\tilde{f}}_{LL}) + D^{\tilde{f}}_{LL}\ \mathbb{1} + \hat{m}^\dagger_f m_f & -\frac{v_f}{\sqrt{2}}\mu f(\beta)\hat{y}_f + \widetilde{M}_{\tilde{F}LL}\widetilde{M}_{\tilde{F}RR}(\delta^{\tilde{f}}_{RL})^\dagger \\ -\frac{v_f}{\sqrt{2}}\mu^* f(\beta)\hat{y}^\dagger_f + \widetilde{M}_{\tilde{F}LL}\widetilde{M}_{\tilde{F}RR}(\delta^{\tilde{f}}_{RL}) & \widetilde{M}^2_{\tilde{F}RR}(\delta^{\tilde{f}}_{RR}) + D^{\tilde{f}}_{RR}\ \mathbb{1} + \hat{m}^\dagger_f m_f \end{pmatrix}, \tag{3.50}$$

where $\widetilde{M}^2_{\tilde{F}AA}$ is the average of the LL and RR diagonal soft matrix elements. Using this approximation, we can see that the flavour violation effects are determined by the δ matrices.

As an example of the use of this notation, let us first consider the flavour violating decay $\tilde{t}_L \to \tilde{c}_L\chi^0_1$. In case of the MFV framework, the decay is suppressed by the $(V_{CKM})_{23}$ element and appears at the one loop level. However, in case we switch on the off-diagonal elements of the δ matrices, additional sources of flavour violation enter in the decay. We can therefore parametrize the contribution in terms of the δ parameters. Fig. 3.1 presents two flavour violating processes, $\tilde{t}_L \to \tilde{c}_L\chi^0_1$ and $\mu \to e\gamma$ where we included the δ insertions. Note that different type of δ (LL, RR, RL) can contribute to the diagrams.

3.3.2 NMFV: Motivations and experimental constraints

As we mentioned before, flavour violating terms are very constrained by current experiments. Therefore, the question of the motivation to consider the NMFV framework arises. First, since there is

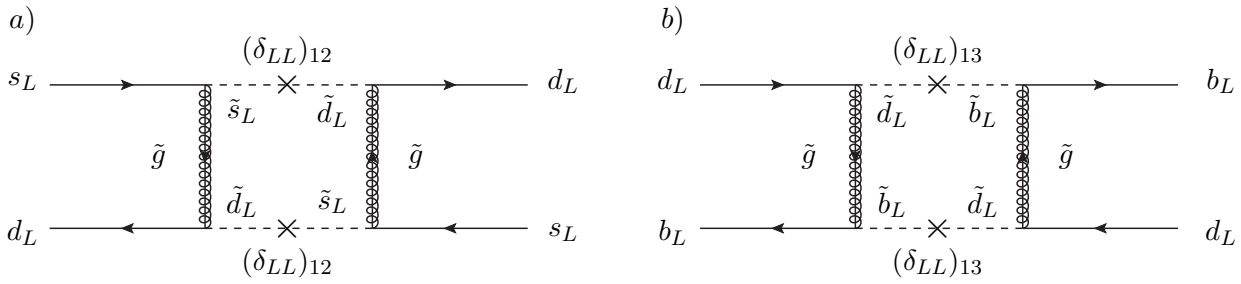

Figure 3.2 – The a) panel shows a QCD SUSY contribution to $K^0 - \bar{K}^0$ oscillation while the b) panel shows a similar contribution to the $B^0 - \bar{B}^0$ oscillation. Both diagrams are non-vanishing in case of the non minimal flavour violation framework, when the off-diagonal elements of the δ matrices are non-vanishing.

no systematic dynamical way to enforce MFV, and because MFV is only motivated to avoid facing experimental constraints (if not motivated by an extended framework), we shall consider NMFV as the most general framework. As a second point, a recent publication has shown that mixing in the squark sector is weakening the limits set at the LHC on the squark mass [65]. The main reason is that in case of single-flavoured eigenstate, the channel studied at LHC for searches of a squark is among others $pp \to \tilde{u}_1\tilde{u}_1 \to tt/cc + \not{E}_T$. If one allows a significant mixing in the stop-scharm sector, a new channel opens where a charm quark is produced at the same time as a top quark. This channel is currently not under investigation. On the other hand, even by taking into account flavour constraints from the hadronic sector, there is still sizable room left for the flavour violating parameters. This is shown in [66] where the authors have performed a Markov Chain Monte-Carlo (MCMC) parameter scan for the flavour violating δ parameters in the hadronic sector. Applying constraints and considering accessible energy scales at the LHC, the results are showing that the amount of flavour violation can be significant. Moreover, the NMFV framework is highly motivated by flavoured (with flavour symmetry) grand unification theories (GUT) where off-diagonal elements in the soft terms are predicted and controlled by the flavour symmetry. More on this topic will be discussed later on, in Chapters 5 and 6.

After this short motivation for the NMFV framework, we need to discuss what type of experimental constraints are relevant for this context. We aim here at discussing different experimental constraints that can have a crucial impact on the flavour structure of SUSY theories. However we emphasize that the list to be discussed is non-exhaustive.

We start by considering the hadronic sector. One of the most important constraint on hadronic δ come from the meson mixing experimental limits. To illustrate, we draw in Fig. 3.2 two QCD contribution to the B^0 and K^0 meson mixing. Both diagrams are proportional to the square of off-diagonal elements of the δ matrices, leading to four-quark operators. Therefore, meson mixing is a crucial observable when considering NMFV framework.

As an other illustration, remaining in the hadronic sector, one can consider the branching ratio of $B_s \to \mu\mu$ which can pick up SUSY contributions in the context of NMFV and in the context of MFV (Fig. 3.3). However, if the MFV framework is employed, the diagram will be CKM suppressed. In case of NMFV, the δ matrices are once again the source of the diagram. Moreover, the diagram is now directly proportional to the δ elements, unlike the case of the meson mixing contribution discussed before.

We can now turn to the leptonic side. We already mentioned the $\mu \to e\gamma$ decay in the previous section 3.3.1. In addition to the multiple $\ell_i \to l_j\gamma$ constraints, we can also have three body leptonic decays such as $\ell_i \to \ell_j\ell_k\bar{\ell}_k$. It turns out that leptonic constraints are very strong when considering NMFV. Indeed, a look at Table 3.1 shows that the leptonic branching ratios are very well constrained and that the bounds are very strong. This is because these channels are very neat from an experimental perspective.

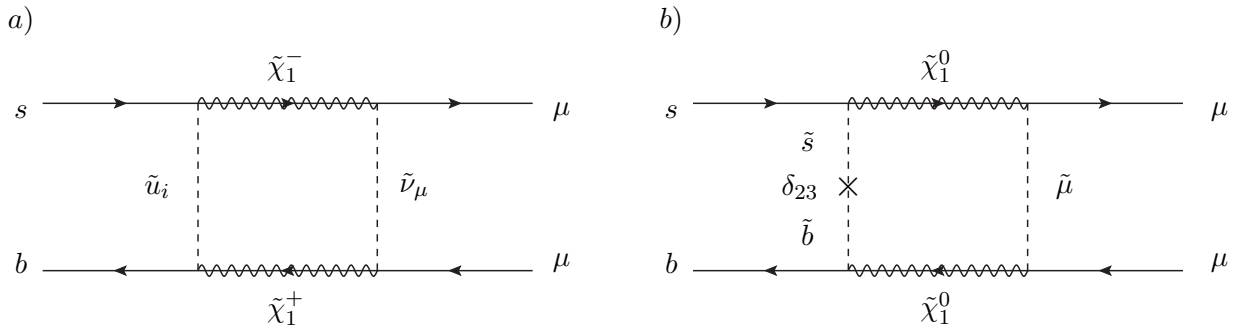

Figure 3.3 – The *a*) and *b*) panels show SUSY contributions to $B_s \to \mu\mu$. While the diagram shown in *a*) can appear in the MFV framework but will be CKM suppressed, the second diagram presented in *b*) only arises in case of the NMFV framework.

We close here the discussion of experimental constraints on NMFV, leaving the reader with Table 3.1 as a non exhaustive reminder of the various constraints that should be considered when dealing with non-trivial flavour structure.

Observable	Constraint	Remarks	Refs.
$\mathrm{BR}(\mu \to e\gamma)$	$< 4.2 \times 10^{-13}$	90% (exp.)	[67]
$\mathrm{BR}(\mu \to 3e)$	$< 1.0 \times 10^{-12}$	90% (exp.)	[67]
$\mathrm{BR}(\tau \to e\gamma)$	$< 3.3 \times 10^{-8}$	90% (exp.)	[67]
$\mathrm{BR}(\tau \to \mu\gamma)$	$< 4.4 \times 10^{-8}$	90% (exp.)	[67]
$\mathrm{BR}(\tau \to 3e)$	$< 2.7 \times 10^{-8}$	90% (exp.)	[67]
$\mathrm{BR}(\tau \to 3\mu)$	$< 2.1 \times 10^{-8}$	90% (exp.)	[67]
$\mathrm{BR}(\tau \to e^-\mu\mu)$	$< 2.7 \times 10^{-8}$	90% (exp.)	[67]
$\mathrm{BR}(\tau \to e^+\mu\mu)$	$< 1.7 \times 10^{-8}$	90% (exp.)	[67]
$\mathrm{BR}(\tau \to \mu^- ee)$	$< 1.8 \times 10^{-8}$	90% (exp.)	[67]
$\mathrm{BR}(\tau \to \mu^+ ee)$	$< 1.5 \times 10^{-8}$	90% (exp.)	[67]
$\mathrm{BR}(B \to X_s\gamma)$	$(3.32 \pm 0.18) \times 10^{-4}$	2σ (exp.)	[68]
$\mathrm{BR}(B_s \to \mu\mu)$	$(2.7 \pm 1.2) \times 10^{-9}$	2σ (exp.)	[67]
ΔM_{B_s}	$(17.757 \pm 0.042 \pm 2.7)$ ps^{-1}	2σ (exp.)	[67, 69]
ΔM_K	$(3.1 \pm 1.2) \times 10^{-15}$ GeV	2σ (th.)	[67, 70]
ϵ_K	2.228 ± 0.29	2σ (th.)	[67, 70]

Table 3.1 – Non exhaustive list of relevant flavour constraint for NMFV. The th. uncertainties are dominated by hadronic contributions (i.e. forms factors) for the meson parameters.

Chapter 4

Accessing the squark flavour structure

As we discussed in the previous chapter, the NMFV framework is to be considered as the most general one. Therefore, a question arises when considering the soft Lagrangian: Is it possible, from an experimental point of view, to access the underlying flavour structure of the theory?

This chapter is dedicated to this question and is based on the publication [71].

4.1 Objectives and setup

The main goal of the following study is to investigate different methods for reconstructing the flavour content of an observed squark state. Indeed, this information would be of a fundamental importance to identify the underlying features of the soft breaking sectors as well as imposing constraints on further SUSY model attempts. While we perform the analysis in the context of the MSSM, we would like to emphasize that possible applications of the methods presented here might be extended, to some degree, to other BSM models exhibiting a non trivial flavour structure. We would like to write down a disclaimer: while this study may trigger further analysis, it is not an "out of the box" method we propose. We rather aim at illustrating the feasibility of the analysis and explicitly show that accessing information on the squark flavour structure is possible. Finally, let us precise that the underlying assumption of the following analysis is a squark is to be observed at the LHC.

The assumption of NMFV in the squark sector has received considerable attention throughout the last decade [72–88]. In particular, as mentioned in Sec. 3.3.2, it has recently been shown that non-minimal flavour mixing between the second and third generation squarks can easily be accommodated with respect to current experimental constraints from flavour and precision data [66, 89, 90]. Even more recently, it has become apparent that the current limits published by the ATLAS and CMS collaborations cannot directly be applied in such a configuration, but will be considerably weakened [65, 91]. In maximal mixing cases, squarks would even be likely to completely escape detection. Consequently, a dedicated search for characteristical signatures of non-minimal flavour violation in the squark sector is necessary. Such a strategy is proposed in Ref. [65] based on the search for mixed final states containing a top quark together with a charm-flavoured jet and missing transverse energy. In the following, we assume that this final state can be accessed with sufficient luminosity at the LHC as discussed in Ref. [65], allowing to include the currently uncovered parameter region.

Assuming the discovery of a squark-like state at the LHC, e.g., through the channel mentioned above, it will be crucial to understand its exact nature and in particular reveal its flavour content. It is the main goal of the present analysis to investigate different methods for reconstructing the flavour content of an observed squark state. To simplify this first attempt, we concentrate on squarks containing top and charm flavour. This situation is less constrained by flavour and precision data [66] as compared to mixing with first generation flavours [73]. Moreover, squarks containing top flavour are easier to access from the experimental point of view. However, the methods presented in the present analysis are general and can be extended to the first generation or to the sectors of down-type squarks and sleptons.

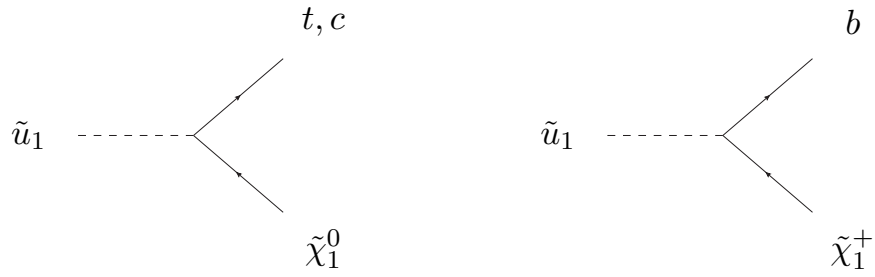

Figure 4.1 – Flavour mixed squark decay into a quark and a neutralino or a chargino.

Our study will rely on the pair production of a flavour-mixed squark [74] and its subsequent decays into either top or charm quarks plus missing transverse energy [85], or into bottom quarks and charginos as described in Fig. 4.1. A direct reconstruction of the squark rotation matrix would in principle be possible, provided that we have access to the corresponding branching ratios, potentially with the help of top-polarization measurements [92–95], plus complete information on the neutralino and chargino sector. In practice, having precise access to these information is not an option.

We therefore discuss methods aiming at inferring the top and charm content of the observed squark and obtain information about the flavour structure requiring a minimal amount of prior knowledge. More precisely, we will apply two methods: the first based on a likelihood inference, the second relying on multi-variate analysis techniques. Again, we emphasize that the present discussion does not aim at constructing a complete analysis, but rather show that these two methods may provide interesting approaches to the above question, provided complementary investigation for a more concrete analysis.

The framework under consideration is therefore the mixing between the first and second generation for the squark sector where the lightest squark can be represented as an admixture of top flavoured and charm flavoured squark, i.e.

$$\tilde{u}_1 = (R^{\tilde{u}})_{12}\tilde{c}_L + (R^{\tilde{u}})_{13}\tilde{t}_L + (R^{\tilde{u}})_{15}\tilde{c}_R + (R^{\tilde{u}})_{16}\tilde{t}_R, \tag{4.1}$$

where $R^{\tilde{u}}$ is the up-squark rotation matrix and $\tilde{u}_1$ is the lightest up-type squark mass eigenstate. Let us mention here that we leave aside the question of CP violation and therefore we are dealing with real parameters.

Simplifying a bit more, we will consider the following (less precise but meaningful) quantity $x_{\tilde{t}}$ called the "top-content"

$$x_{\tilde{t}} = (R^{\tilde{u}})^2_{13} + (R^{\tilde{u}})^2_{16}. \tag{4.2}$$

In order to sample the parameter space, we introduce here two "helicity" mixing angles $\theta_{\tilde{c}}$ and $\theta_{\tilde{t}}$, that account for the mixing between left and right scalar partners in the charm and top sectors

$$\begin{aligned} (R^{\tilde{u}})_{13} &= \sqrt{x_{\tilde{t}}}\cos\theta_{\tilde{t}}, \qquad (R^{\tilde{u}})_{16} = \sqrt{x_{\tilde{t}}}\sin\theta_{\tilde{t}}, \\ (R^{\tilde{u}})_{12} &= \sqrt{1-x_{\tilde{t}}}\cos\theta_{\tilde{c}}, \qquad (R^{\tilde{u}})_{15} = \sqrt{1-x_{\tilde{t}}}\sin\theta_{\tilde{c}}. \end{aligned} \tag{4.3}$$

Therefore, the cases $x_{\tilde{t}} = 0$ and $x_{\tilde{t}} = 1$ correspond to the two limit MFV cases where the squark is either a pure scharm or a pure stop. Additionally, the limit where $\theta_{\tilde{q}} = 0, \pi/2$ stands for a pure left or a pure right squark.

Our goal in the following analysis will be to access the top-content $x_{\tilde{t}}$ of a given test point which will be generated using simulation according to setup described in the next sections.

4.2 Observables related to flavour violation at LHC

If a squark should be observed at the Large Hadron Collider or any future hadron collider, it will most likely be produced from (flavour-conserving) gluon-initiated processes and manifest through its decay into quarks and gauginos. In our setup, this corresponds to the decay modes

$$\tilde{u}_1 \to t\tilde{\chi}_1^0\,, \qquad \tilde{u}_1 \to c\tilde{\chi}_1^0\,, \qquad \tilde{u}_1 \to b\tilde{\chi}_1^+\,, \tag{4.4}$$

which are simultaneously open if the squark is a mixture of the two flavours, i.e. if $0 < x_{\tilde{t}} < 1$. Here, the neutralinos manifest as missing transverse energy, while the charginos will decay further into W-bosons and neutralinos.

Our study is based on the assumption that these decays are observed, and that we have access to the observables

$$m_{\tilde{u}_1}, \quad m_{\tilde{\chi}_1^0}, \quad m_{\tilde{\chi}_1^+}, \quad R_{c/t} = \frac{\mathrm{BR}(\tilde{u}_1 \to c\chi_1^0)}{\mathrm{BR}(\tilde{u}_1 \to t\chi_1^0)}, \quad R_{b/t} = \frac{\mathrm{BR}(\tilde{u}_1 \to b\chi_1^+)}{\mathrm{BR}(\tilde{u}_1 \to t\chi_1^0)}\,. \tag{4.5}$$

Note that the production cross-section of the squarks, as well as their branching ratios alone, are difficult to access. We therefore choose to work with the ratios defined above rather than with the pure associated event rates. The mixed "top-charm" production channel at the LHC may be used to obtain the observable $R_{c/t}$, together with the standard "top-top" channel. Analytical expressions for the relevant decay rates in the NMFV framework can be found in Ref. [74]. Note that in the definition of the ratios $R_{c/t}$ and $R_{b/t}$, we assume without loss of generality that the decay into top quarks is always open.

For further study, it is interesting to examine the expressions for the different decay modes in order to find the $x_{\tilde{t}}$-dependence of the observables in certain limits concerning the nature of the involved neutralinos and charginos. For example, assuming a pure higgsino-like neutralino and neglecting the neutralino mass with respect to the squark mass, we obtain

$$R_{c/t}\Big|_{\tilde{\chi}_1^0=\tilde{H}^0,\ m_{\tilde{u}_1}\gg m_{\tilde{\chi}_1^0}} = \frac{m_c^2}{m_t^2}\,\frac{1-x_{\tilde{t}}}{x_{\tilde{t}}}\,. \tag{4.6}$$

As a second example, we assume a pure bino-like neutralino and obtain

$$R_{c/t}\Big|_{\tilde{\chi}_1^0=\tilde{B}^0,\ m_{\tilde{u}_1}\gg m_{\tilde{\chi}_1^0}} = \frac{1-x_{\tilde{t}}+\kappa_c\big(R^{\tilde{u}}\big)^2_{15}}{x_{\tilde{t}}+\kappa_t\big(R^{\tilde{u}}\big)^2_{16}} \quad\longrightarrow\quad \frac{1-x_{\tilde{t}}}{x_{\tilde{t}}}\,, \tag{4.7}$$

where $\kappa_q = e_q^2/\big(e_q - T_q^3\big)^2 - 1 = 15$ for $q = c, t$, and the last expression holds for a pure "left-handed" or a pure "right-haded" squark. Finally, for a pure wino-like neutralino, the ratio becomes

$$R_{c/t}\Big|_{\tilde{\chi}_1^0=\tilde{W}^0} = \frac{B_c\,\lambda_c^{1/2}}{B_t\,\lambda_t^{1/2}}\,\frac{\big(R^{\tilde{u}}\big)^2_{12}}{\big(R^{\tilde{u}}\big)^2_{13}} \quad\longrightarrow\quad \frac{B_c\,\lambda_c^{1/2}}{B_t\,\lambda_t^{1/2}}\,\frac{1-x_{\tilde{t}}}{x_{\tilde{t}}}\,, \tag{4.8}$$

where $\lambda_q = m_{\tilde{u}_1}^4 + m_{\tilde{\chi}_1^0}^4 + m_q^4 - 2(m_{\tilde{u}_1}^2 m_{\tilde{\chi}_1^0}^2 + m_{\tilde{u}_1}^2 m_q^2 + m_{\tilde{\chi}_1^0}^2 m_q^2)$ denotes the usual Källén function associated to the squark decay and $B_q = m_{\tilde{u}_1}^2 - m_{\tilde{\chi}_1^0}^2 - m_q^2$ for $q = c, t$. Here, the last expression holds for a pure "left-handed" squark.

In order to gain a better understanding of these ratios, we start by randomly scanning over the parameters governing the lightest squark, neutralino, and chargino. More precisely, we vary the physical squark mass $m_{\tilde{u}_1}$, and the parameters $x_{\tilde{t}}$, $\theta_{\tilde{t}}$, and $\theta_{\tilde{c}}$ defining its flavour decomposition.

In the gaugino sector, we vary the bino, wino, and Higgsino mass parameters M_1, M_2, and μ. The physical gaugino masses are obtained by diagonalizing the mass matrices at the tree-level.

As the expressions in Eqs. (4.6) – (4.8) do not exhibit a dependence on $\tan\beta$, we conclude that this parameter only has a mild impact on the observables of our interest. We therefore fix $\tan\beta = 10$

Variable	Range
$m_{\tilde{u}_1}$	$[700, 2000]$
$x_{\tilde{t}}$	$[0, 1]$
$\cos\theta_{\tilde{t}}$	$[0, 1]$
$\cos\theta_{\tilde{c}}$	$[0, 1]$

Variable	Range
M_1	$[600, 2000]$
M_2	$[600, 2000]$
μ	$[600, 2000]$

Table 4.1 – Scanned ranges of the parameters associated to the squark (left) and gaugino sector (right). All masses are given in GeV.

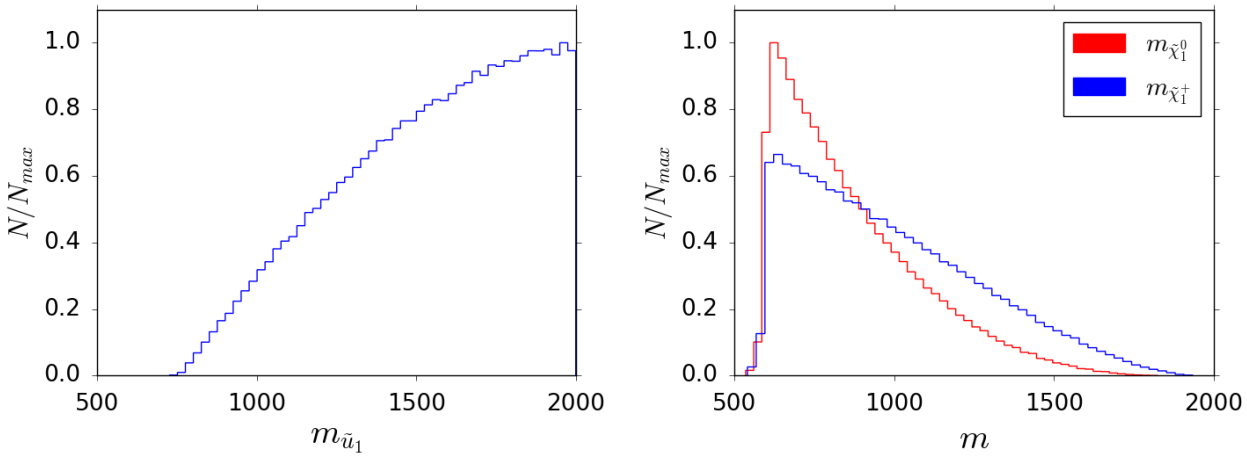

Figure 4.2 – Distributions of the squark (left) and gaugino (right) masses obtained from the scan summarized in Table 4.1. The masses are given in GeV. The distributions show the number N of points per bin normalized to the maximum value $N_{\max}$.

throughout the presented analyses. All parameters are scanned over in a uniform manner (flat distribution) according to the ranges given in Table 4.1. The corresponding parameter distributions are illustrated in Fig. 4.2 for the relevant physical masses and Fig. 4.3 for the corresponding mixing parameters, respectively. The shape of the mass distributions are explained by the fact that we require the decay modes mentioned above to be kinematically allowed, which favours larger squark and smaller gaugino masses. Since we impose a flat distribution of the stop content $x_{\tilde{t}}$, the elements $(\mathcal{R}^{\tilde{u}})_{1i}$ $(i = 2, 3, 5, 6)$ of the up-squark rotation matrix follow a parabolic distribution. As the distributions of $(\mathcal{R}^{\tilde{u}})_{1i}$ for $i = 3, 5, 6$ are similar to the one of $(\mathcal{R}^{\tilde{u}})_{12}$, they are not shown separately in Fig. 4.3.

For each parameter point, the gaugino masses and the ratios $R_{c/t}$ and $R_{b/t}$ of our interest are computed using the full analytical expressions of Ref. [74]. The results are depicted in Fig. 4.4, where we indicate as colour code the dominant component of the involved neutralino as well as the nature of the decaying squark. As expected from Eqs. (4.6) – (4.8), distinct regions are observed in the distributions of $R_{c/t}$. The same kind of feature appears for the ratio $R_{b/t}$. More precisely, the two ratios depend strongly on the neutralino decomposition and the "chirality" (expressed in terms of $\theta_{\tilde{t}}$ and $\theta_{\tilde{c}}$ defined in Eqs. (4.3)) of the decaying squark.

The width of each band in Fig. 4.4 is due to the fact that the majority of the parameter points feature mixed gauginos and squarks rather than corresponding to the limit cases discussed above. Nevertheless, the presence of the observed rather distinct regions is an important feature which will turn out to be crucial in the identification of the squark flavour decomposition from the observables given in Eq. (4.5).

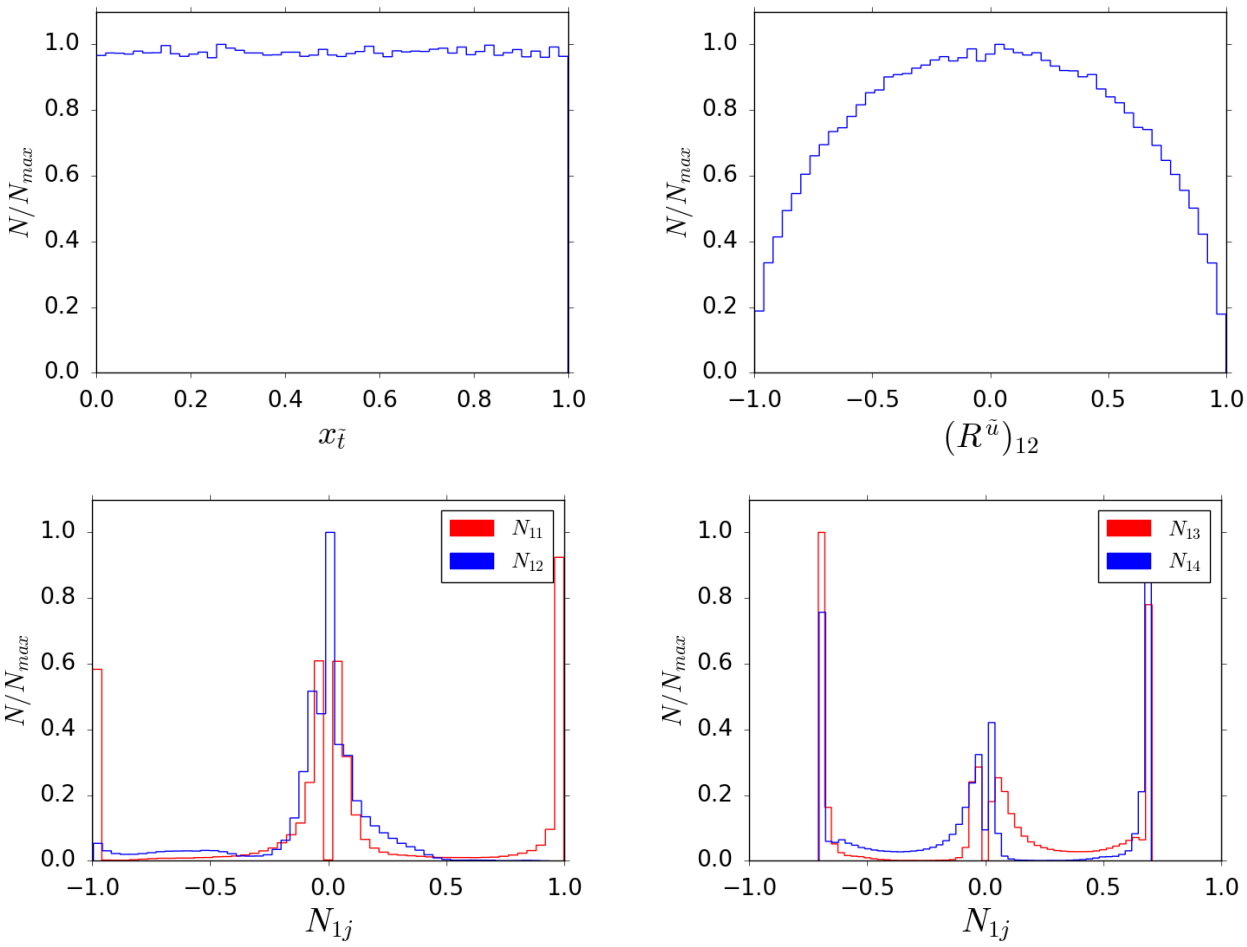

Figure 4.3 – Distributions of the squark (upper row) and neutralino (lower row) mixing parameters associated to the masses shown in Fig. 4.2. The distributions are shown on a linear scale.

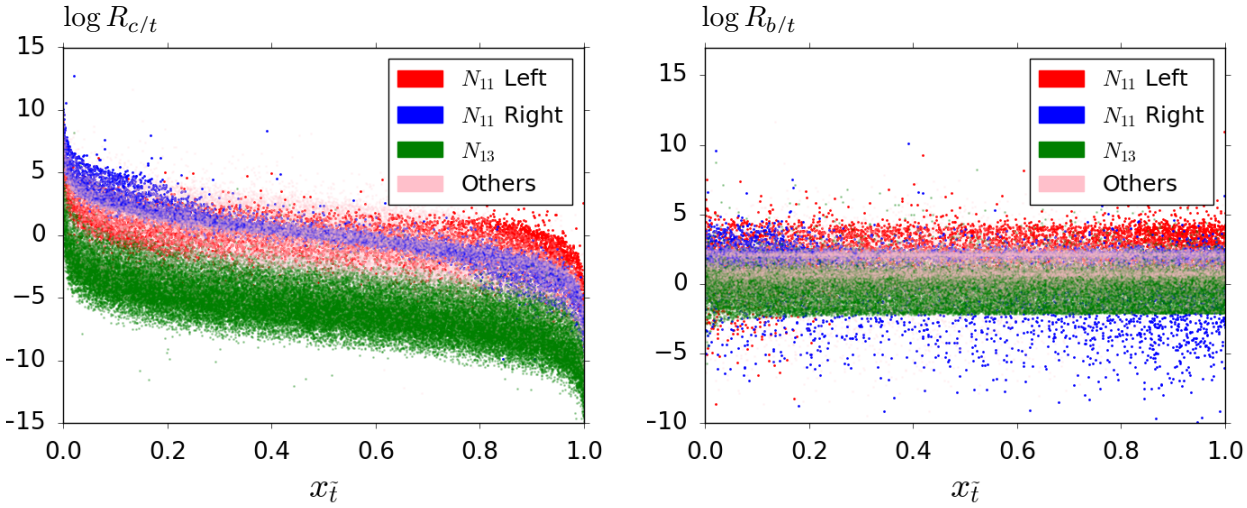

Figure 4.4 – Distributions of the ratios $R_{c/t}$ (left) and $R_{b/t}$ (right) of the decay modes defined in Eq. (4.5) in dependence of the stop composition $x_{\tilde{t}}$ of the decaying squark. The colour code refers to different combinations of neutralino compositions and squark "chiralities".

Data set	$m_{\tilde{u}_1}$	$m_{\tilde{\chi}_1^\pm}$	$m_{\tilde{\chi}_1^0}$	$x_{\tilde{t}}$	σ_i/D_i	inferred $x_{\tilde{t}} \pm \sigma(x_{\tilde{t}})$
P_1	1015.73	699.60	604.39	0.66	0.25	0.57 ± 0.16
P_2	1798.29	303.02	267.66	0.04	0.25	0.04 ± 0.03
P_3	1488.78	321.53	244.21	0.08	0.25	0.15 ± 0.08
P_4	1422.50	1001.11	637.85	0.83	0.25	0.76 ± 0.12
P_5	1369.07	281.13	276.32	0.04	0.35	0.03 ± 0.03
P_6	1770.52	717.95	511.39	0.65	0.35	0.00 ± 0.90

Table 4.2 – Parameters of the test data sets together with the assumed relative error σ_i/D_i and the stop component obtained from the likelihood fits illustrated in Figs. 4.5 – 4.6. All masses are given in GeV.

4.3 Likelihood inference in a simplified model

In order to infer the stop component $x_{\tilde{t}}$ of the observed squark, we start by constructing a maximum likelihood estimator. For the given set of data

$$D \;=\; \{m_{\tilde{u}_1}, m_{\tilde{\chi}_1^0}, m_{\tilde{\chi}_1^\pm}, R_{c/t}, R_{b/t}\} \tag{4.9}$$

supposed to be obtained at the LHC, we associate a likelihood value to each point of an ensemble of random parameter points. Assuming uncorrelated parameters and thus a Gaussian distribution, this likelihood takes the form

$$\ln \mathcal{L}(\theta) \;=\; -\frac{1}{2}\sum_i \left(\frac{\theta_i - D_i}{\sigma_i}\right)^2 \tag{4.10}$$

with θ being the set of parameters associated to the parameter point under consideration and σ_i being the error associated to the observable D_i. Even if in practice the parameters of interest are correlated, a Gaussian distribution constitues a reasonable approximation, as will be seen in the following.

We now divide the interval $x_{\tilde{t}} \in [0,1]$ into N bins of equal size. For each bin $j = 1, \ldots, N$, we then compute the average likelihood $\hat{\mathcal{L}}_j(x_{\tilde{t}})$ of all random parameter points having their value of $x_{\tilde{t}}$ inside the given bin. From the obtained values of $\hat{\mathcal{L}}_j(x_{\tilde{t}})$ over the interval $x_{\tilde{t}} \in [0,1]$, we can fit a Gaussian distribution in order to find the maximum of likelihood corresponding to the inferred value of the stop component $x_{\tilde{t}}$. The associated uncertainty $\sigma(x_{\tilde{t}})$ is then based on the standard deviation value of the Gaussian fit.

As a first step, for the sake of simplicity, and in order to illustrate the proposed inference method, we fix the parameters associated to the neutralino and chargino decomposition as

$$N_{1l} = 0.5\,, \qquad U_{11} = V_{12} = 1\,, \qquad U_{12} = V_{11} = 0\,, \tag{4.11}$$

where N, U, and V denote the mixing matrices associated to the neutralinos and charginos. In other words, we consider a maximally mixed neutralino. For the present example, we have performed a random scan over the five parameters of Eq. (4.9) leading to an ensemble of $5 \cdot 10^8$ parameter points. Moreover, we assign a common value of $\sigma_i = 0.25 D_i$ to the uncertainties entering the likelihood calculation.

Assuming four different test parameter points P_i $(i = 1, \ldots, 4)$ representing different configurations, we perform the analysis described above and infer the stop component $x_{\tilde{t}}$ using a Gaussian likelihood fit. The results are illustrated in Fig. 4.5 and summarized in the upper part of Table 4.2.

More precisely, for each test parameter point, we show in Fig. 4.5 the average likelihood $\hat{\mathcal{L}}_j(x_{\tilde{t}})$ obtained for each bin together with the Gaussian fit. As can be seen, our method manages to recover the actual stop component within the resulting uncertainty from the Gaussian fit.

As second and final step, we relax the assumption on the gaugino decompositions given in Eq. (4.11), and include the gaugino mixing parameters in the random scan. Again, we generate an

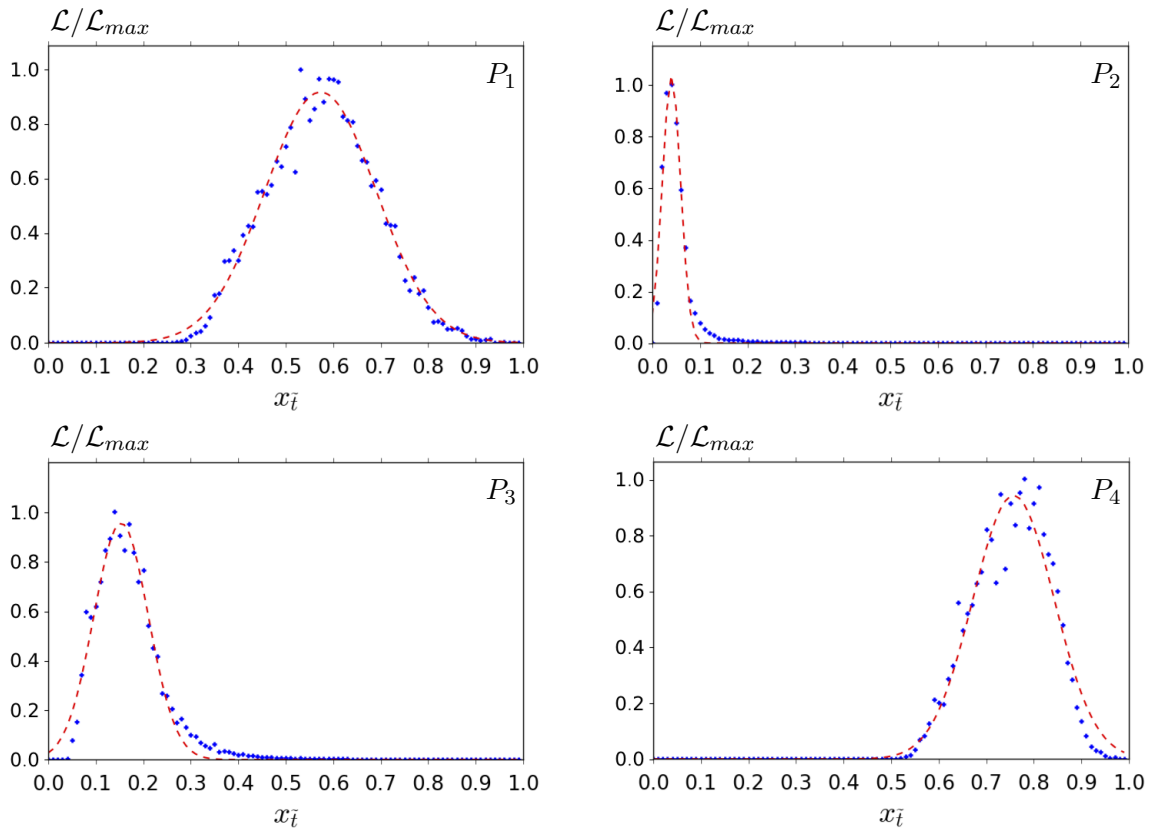

Figure 4.5 – Likelihood fit for four test data sets featuring a fixed gauginos composition as in Eq. (4.11). The resulting inferred values of the stop component are listed in Table 4.2. The distributions show the averaged likelihood $\hat{\mathcal{L}}$ normalized to the maximum value $\hat{\mathcal{L}}_{\text{max}}$.

ensemble of $5 \cdot 10^8$ parameter points with $\sigma_i = 0.35 D_i$, and apply our reconstruction method to two data sets P_5 and P_6.

The results are shown in Fig. 4.6 and summarized in the lower part of Table 4.2. Even if the true stop components lie within the infered intervals, the uncertainties are much larger in this case, such that the results may become meaningless in certain cases. In addition, from Fig. 4.6 we can see that the likelihood is no longer Gaussian. This is due to the fact that here different regions of the parameters present a concentration of points able to explain the data.

Let us briefly discuss the impact of the uncertainties, which we have investigated by varying the value of σ_i $(i = 1, \ldots, 5)$ for a given reference point. As it can be expected, increasing the uncertainties σ_i leads to an increase in the uncertainty $\sigma(x_{\tilde{t}})$ obtained from the Gaussian fit. However, special care has to be taken when reducing the value of σ_i. First, the quality of the Monte Carlo sampling plays a crucial role. Indeed, if the parameter space is not populated well enough, the Gaussian fit "breaks down", i.e. cannot yield a meaningful result. Second, if one considers the more general setup, e.g., without fixing the gaugino parameters, degeneracies between the observables and the top-content $x_{\tilde{t}}$ appear, as can be seen in Fig. 4.4. This may lead to additional complications concerning the treatment of uncertainties.

In this first attempt of reconstructing the top-content $x_{\tilde{t}}$, we do not perform a dedicated analysis of the impact of the uncertainties σ_i. However, this question will need to be addressed properly in the case of an actual observation of a squark-like state. In this situation, the analysis proposed here will become crucial, and information about the underlying uncertainties will be known.

The uncertainties associated to the ratios $R_{c/t}$ and $R_{t/b}$ will be the most limiting factors of the analysis. In particular, $R_{c/t}$ is the most constraining observable, since it shows a strong correlation

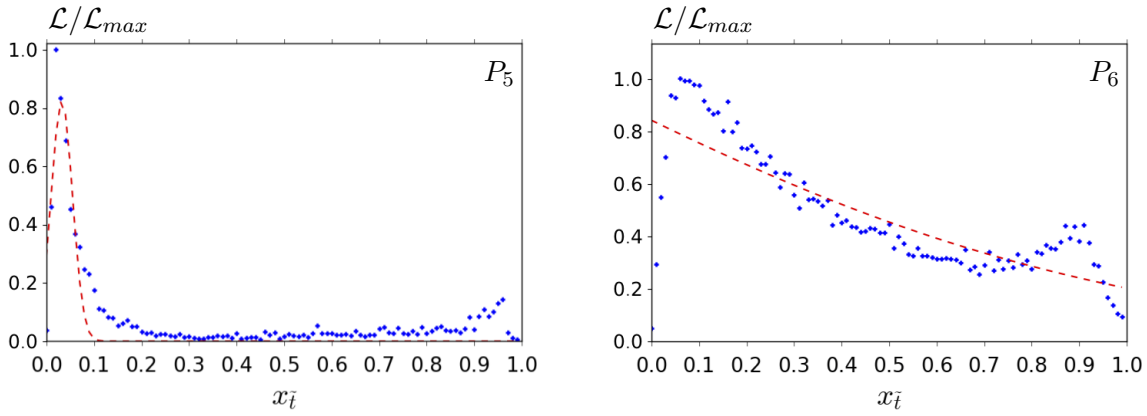

Figure 4.6 – Same as Fig. 4.5 for two test parameter points obtained by scanning in addition over the parameters related to the gaugino sector.

with the parameter $x_{\tilde{t}}$, as can be seen in Fig. 4.4. As a last comment, let us emphasize that the observables D_i should have different relative uncertainties σ_i.

We conclude that the present method is not suitable if no additional independent knowledge on the gaugino sector, nor other relevant observables, are available. Here, we do not aim at studying the limit of the present method associated to the quality of the parameter space sampling, which will be necessary for a concrete analysis rather than for the simplified setup under consideration here.

4.4 Multivariate analysis in a simplified model

In order to go beyond the likelihood inference presented in the previous Section, especially in a more realistic setup such as, e.g., the more complete Minimal Supersymmetric Standard Model (MSSM) discussed in Ref. [66], we now employ a multivariate analysis (MVA) classifier. We start by presenting results obtained from a multi-layer perceptron (MLP) provided by `ROOT` through the `TMVA` package [96] for the simplified setup already used in Secs. 4.2 and 4.3. The discussion of the complete MSSM with squark generation mixing of Ref. [66] will follow in Sec. 4.5.

In this context, the goal of our analysis is slightly different with respect to the previous Section. While the likelihood inference aims at estimating the actual stop component of the observed squark, a multivariate classifier is designed to efficiently classify different configurations. In order to provide a simple illustration, we define two categories based on the stop composition $x_{\tilde{t}}$, which remains the key quantity of our interest. We will divide the parameter space into "top-flavoured" squarks and "charm-flavoured" squarks according to

$$x_{\tilde{t}} < 0.5 \quad \Longleftrightarrow \quad \text{“charm} - \text{flavoured”}\,, \tag{4.12}$$

$$x_{\tilde{t}} > 0.5 \quad \Longleftrightarrow \quad \text{“top} - \text{flavoured”}\,. \tag{4.13}$$

Let us note that these categories are for the moment rather arbitrary and aim at the illustration of the method rather than representing specific physical regions. In particular, additional categories can be defined in order to refine the analysis. Such a case will be discussed in Sec. 4.5. Based on the two categories, the MLP can be trained on the parameter points obtained from a random scan, and subsequently tested on a subset of points, the test sample, in order to compute the efficiency and the misidentification rate of the classifier. The analysis presented here is based on a training sample of 10^6 points, which have been obtained by uniformly scanning as indicated in Table 4.1.

The classifier basically combines the set of obervables given in Eq. (4.5), i.e. $m_{\tilde{u}_1}$, $m_{\tilde{\chi}_1^0}$ $m_{\tilde{\chi}_1^+}$, $R_{c/t}$, and $R_{b/t}$ into a single variable, the so-called MLP response comprised between 0 and 1. The algorithm will associate an MLP value to each parameter point of the scan, depending on the set of

observables that maximizes the separation between the two categories. The obtained MLP response will be presented as an histogram containing the distributions associated to the two categories to be separated. If the MLP is rather efficient, the two distributions peak at the extremities 0 and 1, respectively.

A key point of such an analysis is the danger of so-called "overtraining", meaning that training the algorithm on a too small dataset may enforce the identification of unphysical regions, i.e. statistical fluctuations, as physical ones. We have performed an overtraining check by comparing the classification performance on the training sample and on the test sample. The behavior of the algorithm being the same on the two samples, we conclude that there are no statistical fluctuations having an impact on the classification.

The rather simple situation of having only two categories will also serve to study the influence of the underlying prior distribution, in particular of the stop component $x_{\tilde{t}}$. We start from the same setup as in Sec. 4.2, where the random parameter scan has been performed such that the stop component $x_{\tilde{t}}$ exhibits a flat distribution. For this case, we show the obtained MLP response for the two categories in Fig. 4.7, together with the prior distribution of the stop component (see also Fig. 4.3). If a set of observables leads, e.g., to an MLP response close to 1, the parameter point is likely to belong to the category of "charm-like" stages ($x_{\tilde{t}} < 0.5$, shown in red), while for MLP responses close to 0, the associated points are likely to belong to the "top-like" category ($x_{\tilde{t}} > 0.5$, shown in blue). The ratio "top-like" over "charm-like" is quite large for small MLP values, while the opposite ratio is large for high MLP responses. Note that the histograms are presented on a logarithmic scale.

In the present case, the classifier manages to seperate the two categories with a rather good efficiency. For a given misidentification rate, the associated efficiency, i.e. the number of points of a chosen class surviving the misidentification cut, of the classifier can be computed based on a cut on the MLP response. To give an example, the efficiency for the "charm-like" (red) category is obtained as the ratio of the "charm-like" area above the cut and the total "charm-like" area. The cut is chosen such that the ratio of the "top-like" (blue) area over the "charm-like" (red) area above the cut corresponds to the misidentification rate imposed for the "charm-like" (red) category. It is to be noted that decreasing the misidentification rate (by increasing the cut value) will lead to a decrease of the efficiency. The efficiency for the "top-like" category is analogously obtained considering the corrresponding areas below a cut on the MLP response.

Here, for a misidentification rate of 10%, we obtain an efficiency of 54% for the "top-like" squark region and of 64% for the "charm-like" case. In other words, we can tag respectively approximately 54% and 64% of the points at 90% confidence level.

As a second example, we employ the classifier to the case of a non-uniform prior distribution of the stop-content $x_{\tilde{t}}$. Inspired by the results of Ref. [66], we choose a prior distribution peaking at its "MFV-like" extremities $x_{\tilde{t}} \approx 0$ and $x_{\tilde{t}} \approx 1$. Apart from the prior distribution (and thus the squark rotation matrix elements), the sample has the same characteristics as the previous one. The prior distribution and the resulting MLP response are shown in Fig. 4.8. While it is approximately symmetric in the case of a flat prior, the MLP response associated to the two categories is clearly non-symmetric in the present case. This can be traced to the fact that the observables used to classify are non-symmetric with respect to "top-flavoured" and "charm-flavoured" squarks.

In this example, for the misidentification rate of 10%, we obtain an efficiency of 64% for the "top-flavoured" category and an efficiency of 60% for the "charm-flavoured" category. It appears that the efficiency depends on the prior distribution. More precisely, considering the more peaked prior, the classifier becomes more efficient in identifying the "top-flavoured" category, but slighly less performant concerning the "charm-flavoured" category.

The increasing classification power coming from the prior distribution can intuitively be understood as the two categories are now more different. The border between the two cases, i.e. $x_{\tilde{t}} \sim 0.5$, where it is phenomenologically difficult to assign a given point to a single category, are less populated in the second case with non-uniform prior. It is therefore easier to maximize the

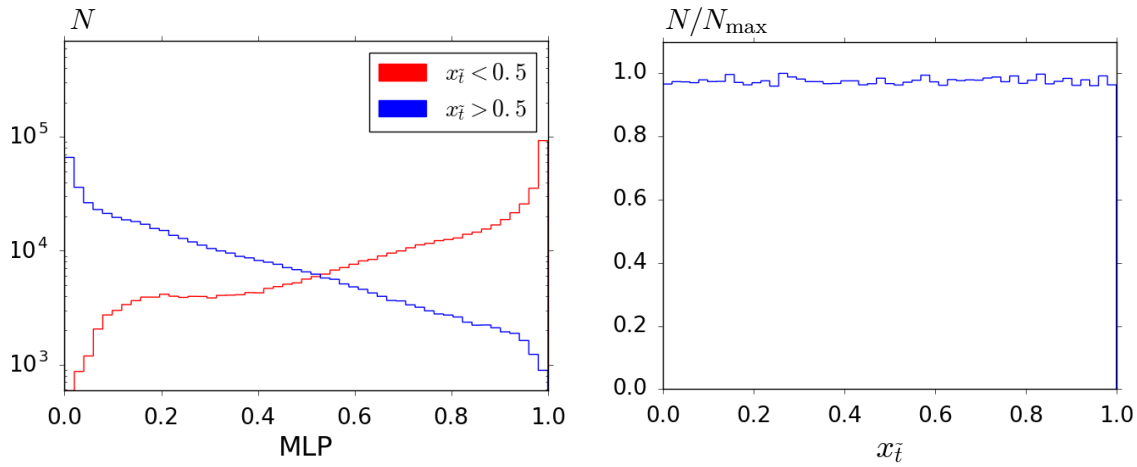

Figure 4.7 – MLP response (number of points N, left panel) on the simplified scan based on a uniform prior (number of points N normalized to the maximum value $N_{\max}$, right panel) of the stop component $x_{\tilde{t}}$. The colour code corresponds to the seperation of "top-like" (blue) and "charm-like" (red) squarks.

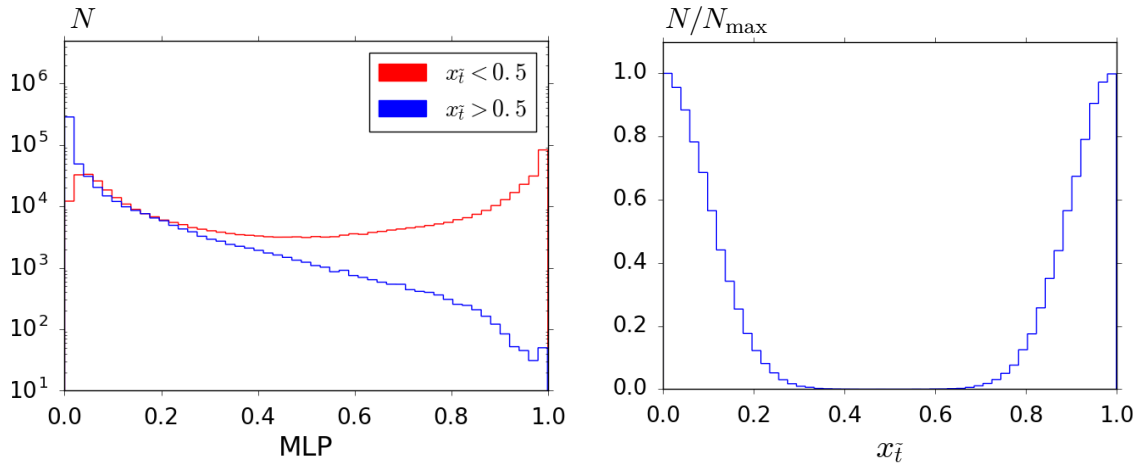

Figure 4.8 – Same as Fig. 4.7 for an example of a non-uniform prior of the stop component $x_{\tilde{t}}$.

separation. As a final comment, we would like to emphasize that the prior dependence is not a limitation of the present method, but a feature that the user should be aware of. After this first analysis within the simplified setup, we now aim at applying the MLP method to a more complete model.

4.5 Application to the MSSM with mixed top-charm squarks

As announced in the previous Section, we finally apply the multivariate analysis (MVA) classifier to the Minimal Supersymmetric Standard Model (MSSM) with non-minimal flavour mixing between charm- and top-flavoured squarks. In order to work with a rather "realistic" setup, as basis of our study we choose to use the parameter points obtained in Ref. [66] by means of a Markov Chain Monte Carlo (MCMC) algorithm. These parameter points defined at the TeV scale have been shown to fulfill all relevant constraints coming from flavour and precision measurements, in particular the Higgs-boson mass, the decays $B \to X_s\gamma$ and $B \to X_s\mu\mu$, and the meson oscillation parameter ΔM_{B_s}, to name the most relevant ones. For all details on the applied constraints and the related MCMC study of the MSSM with non-minimal flavour violation in the squark sector, the reader is

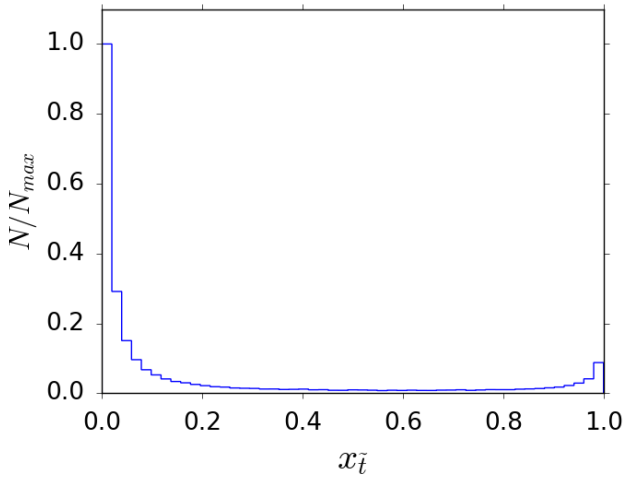

Figure 4.9 – Prior distribution (Number of points N per bin normalized to the maximum value $N_{\max}$) of the stop composition $x_{\tilde{t}}$ from the MCMC analysis of Ref. [66].

referred to Ref. [66].

Following the preliminary study of the simplified setup in Sec. 4.4, it is interesting to examine the prior distribution of the quantity that we want to address, i.e. the stop component $x_{\tilde{t}}$ of the lightest up-type squark. As can be seen from its representation in Fig. 4.9, the distribution strongly peaks at the "MFV-like" ends. Moreover, flavour and precision data tend to favour a high charm content with respect to top content in the lightest squark. Note that this situation is similar to the non-uniform prior tested in Sec. 4.4, which turned out to yield a higher efficiency than the simpler uniform prior. However, in the present case, the prior distribution is non-symmetric between the MFV-like ends, the "charm-like" case being favoured.

Let us note that even in the case of such a peaked prior, the possibility of important flavour mixing is not ruled out. As a consequence, the question of identifying the flavour content of an observed squark is still of high interest. As discussed in Sec. 4.4, the prior distribution has an impact on the efficiency of the method, but not on its applicability. Finally, let us note that, although still relying on certain simplifications, the study of Ref. [66] is at our knowledge the most general phenomenogically analysis of the squark-flavour violating MSSM, and therefore the resulting parameter points represent a suitable sample to study in the given context.

We now perform the same MLP classification using a training sample containing about $6 \cdot 10^5$ points obtained from the MCMC analysis of Ref. [66] [1]. Starting from the prior distribution shown in Fig. 4.9, we divide the ensemble of points into four categories defined as follows:

$$\begin{aligned} 0.00 \leq x_{\tilde{t}} < 0.05 &\iff \text{"charm MFV"} \\ 0.05 < x_{\tilde{t}} < 0.50 &\iff \text{"charm NMFV"} \\ 0.50 < x_{\tilde{t}} > 0.95 &\iff \text{"top NMFV"} \\ 0.95 < x_{\tilde{t}} \leq 1.00 &\iff \text{"top MFV"} \end{aligned} \tag{4.14}$$

Note that, although the given definition of the above categories is again somewhat arbitrary, the exact value of the cuts between MFV and NMFV does not have a major impact on the methods presented in the following. It might, however, affect the efficiency of the proposed analysis, and the exact definition of the categories may in practice depend on the problem under consideration.

Here, we use the MVA classifier to seperate each of the four above categories from its complement, i.e. the ensemble comprising the three other classes. In Fig. 4.10, we show the MLP responses

[1] For the present study, we have extended the sample resulting from the analysis presented in Ref. [66] using exactly the same computational setup.

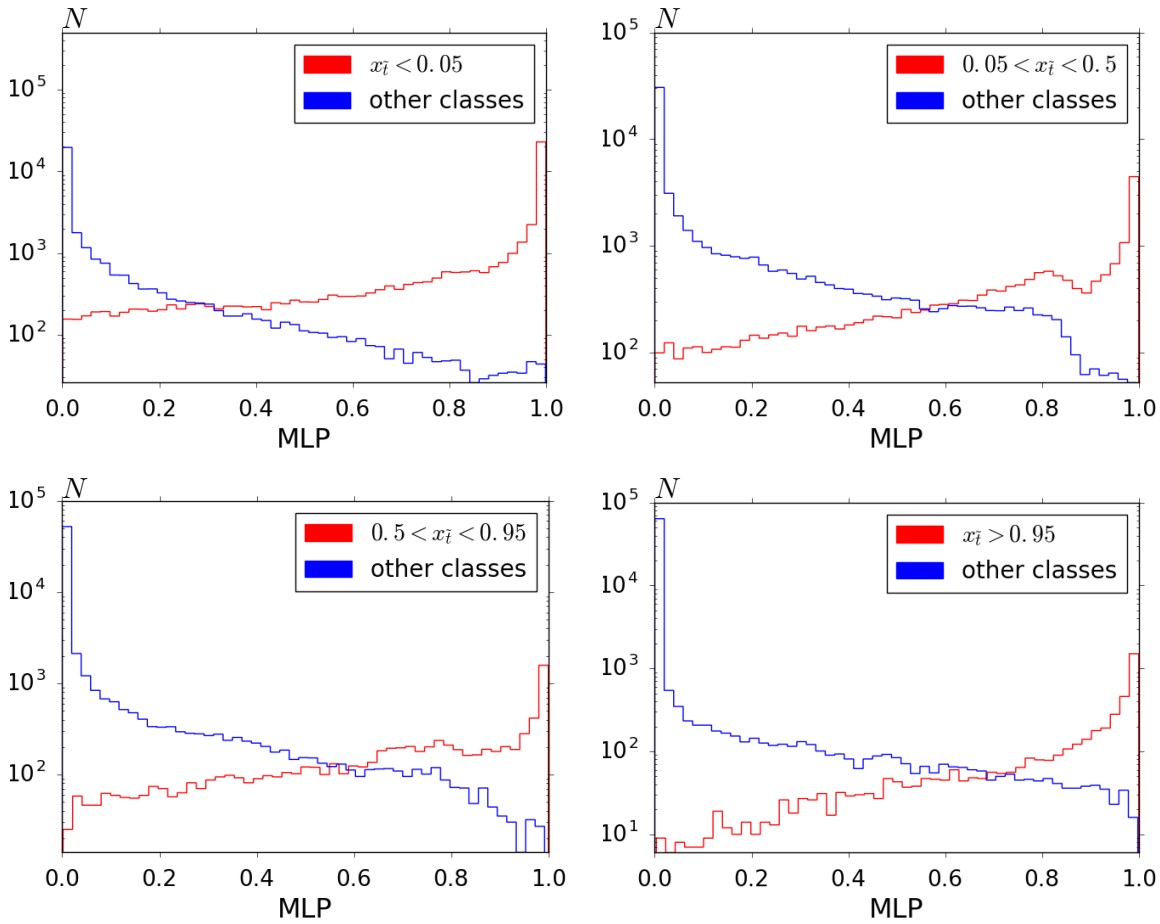

Figure 4.10 – MLP response (number of points N) on the NMFV-MSSM of Ref. [66] for the seperation the "charm MFV" (upper left), "charm NMFV" (upper right), "top NMFV" (lower left), and "top MFV" (lower right) categories (red) from the remaining parameter points (blue).

obtained for the four cases. As expected from the overpopulated prior region, the "charm MFV" category is rather well identified. However, the identification is less efficient for the two NMFV categories, which are underpopulated in the prior distribution. For the sake of a numerical comparison between the categories, and also to the cases presented in Sec. 4.4, we summarize the obtained efficiencies of the classifier in Table 4.3. In terms of physical interpretation, the efficiency of 95% for the "charm MFV" category is to be understood as follows: The probability to count an actual "charm MFV" parameter point correctly into this category is 95%, assuming that only 10% of the other parameter points (not belonging to this category) are wrongly classified as "charm MFV" (misidentification).

Overall, the performance of the classifier is better than for the simplified situations presented in Sec. 4.4. This can be traced to the underlying prior distribution of the stop content $x_{\tilde{t}}$ (see Fig.

Categories		Efficiency
"charm" MFV	$0.00 \leq x_{\tilde{t}} < 0.05$	95%
"charm" NMFV	$0.05 < x_{\tilde{t}} < 0.50$	51%
"top" NMFV	$0.50 < x_{\tilde{t}} < 0.95$	41%
"top" MFV	$0.95 < x_{\tilde{t}} \leq 1.00$	69%

Table 4.3 – Efficiencies of the classification method for the four categories of our interest assuming a misidentification rate of 10%.

4.9). The categories which are most difficult to identify, i.e. the two NMFV categories, are less populated in this particular model. The algorithm is therefore less performant in distinguishing these categories. The small bump observed around MLP $\sim 0.7 \ldots 0.8$ in both NMFV categories is an artefact of the employed multi-class MLP due to the presence of phenomenologically different regions.

Let us finally mention that we have also tested the likelihood inference method discussed in Sec. 4.3 on the present case of the NMFV-MSSM of Ref. [66]. However, for this method it turns out that inferring in a region of rather low density is quite difficult (contrary to the case of a uniform prior applied in Sec. 4.3). In addition, the strongly peaked prior distribution of the stop component $x_{\tilde{t}}$ leads to a certain bias, such that the obtained results are not reliable any more. We therefore do not discuss this method further for the given model.

4.6 Perspectives of the method

As a starting point, we have considered a rather simple but typical set of collider observables related to inter-generational mixing between top- and charm-flavoured squarks. The quantity of our interest is the top-flavour content of the observed squark state, since it may give valuable information on the flavour structure of the theory.

We first have employed a likelihood inference method, which basically allows to infer the top-flavour content of the observed squark. With the help of a simplified model incorporating non-minimal flavour violation between the top- and charm-flavoured squarks, we have obtained viable information on the squark flavour structure assuming that additional information, in particular concerning the gaugino sector, is provided. In the absence of such information on the neutralino and chargino nature, the likelihood inference is less viable. However, the more additional information is available, e.g. on the gaugino sector (even if not fully determined), the more efficient this method will be. We also tried to use the likelihood inference method to the more general situation of the Minimal Supersymmetric Standard Model (MSSM) with additional top-charm mixing in the squark sector. However, it turns out to be inapplicable due to the somewhat extreme prior distribution of the top-flavour content and the available number of parameter points in the considered test sample based on previous work.

The second method consists of a multi-variate analysis classifier, which can efficiently separate two categories among a sample making use of a given set of observables. Performing this analysis on both the simplified setup and on the more general MSSM framework has led to promising results concerning the seperation between the Minimal and Non-Minimal Flavour Violation hypotheses. It turns out that this method can better deal with the strongly peaked prior distribution as it is the case in the considered MSSM with top-charm flavour mixing.

We want to emphasize the fact that the two methods are not addressing the same question. While the multi-variate analysis does not return an actual value for the top-flavour content of the squark, the likelihood inference can provide a reasonable estimation. However, the likelihood inference needs additional information, especially on the gaugino sector, and cannot handle very extreme prior distributions. These inconvenients can in turn be avoided by the use of the multivariate analysis, which already allows to gain valuable information on the flavour structure.

As this is a first attempt of the reconstruction of the squark flavour structure, the presented analysis relies on rather simple observables. Designing improved analyses inspired from this work should lead to a considerable improvement of the performances. As an example, one might consider additional observables related to the same parameters, such as, e.g., the top polarization from the squark decay or event rates stemming from gluino production and decay. From the machine-learning point of view, many algorithms exist for parameter-fitting problems and with a specific analysis it may be possible to access the actual value of the top-flavour content in a generic gaugino sector. Furthermore, considering new types of algorithms and additional observables may give access to the actual entries of the squark rotation matrix.

Since we did not assume any specific values for the masses nor any other observables in our scan of the parameter space, we show the feasibility of the proposed study in a generic way. For a concrete case, i.e. in case of an actual observation of a squark-like state at the LHC, this study has to be adapted to the actual signal. A more complete analysis of the proposed methods will therefore be in order. However, such an analysis, including in particular experimental details and uncertainties, is beyond the scope of the present discussion and will be necessary in order to render the proposed study well adapted to the actual observation. The experimental uncertainties fixed in our likelihood-based analysis of Sec. 4.3 can be adapted to the actual uncertainties associated to an observation. Concerning the multivariate analysis, the study proposed in Sec. 4.4 does not exploit the associated uncertainties. This will be rather technical to address and will rely again on experimental knowledge associated to the actual observation.

Chapter 5

Flavoured SUSY SU(5) GUT models

After investigating experimental aspects to access the squark flavour structure, we aim here at discussing how the NMFV framework naturally arises in the context of well motivated flavoured SUSY GUT models. This chapter is devoted to introduce the basics of SUSY grand unification theories featuring a discrete flavour symmetry. First, we will discuss the motivation and framework of flavour symmetries in a general way. This part will be also helpful for the last chapter of the manuscript when we will consider flavoured leptoquarks extensions of the SM. Then, we will present basic ingredients of $SU(5)$ GUT models in the context of SUSY theories. Finally, we will briefly comment on specific features when combining flavour symmetries and $SU(5)$.

5.1 Flavour symmetries

5.1.1 Motivation for flavour symmetries

Among the shortcomings of the SM discussed in Sec. 1.5, the question of the origin and structure of flavour is also an open question. A look at Fig. 5.1 raises the question of the hierarchy in the fermion masses and the mixing matrices elements. Indeed, the lepton sector exhibits smaller masses than the quark sector, and this is even more impressive when the (light) neutrino masses are considered. On the other hand, the mixing matrix associated to the leptonic sector, the PMNS matrix, has very large off-diagonal entrance suggesting a strong mixing of the flavour eigenstates while the CKM matrix is nearly diagonal.

In addition to this hierarchy problem, the fundamental question of why there are three generations for quarks and leptons is not answered in the Standard Model.

A first approach to this feature could be simply to argue that nature may be anarchic and that the parameters of the SM are simply random. However, this anthropic argument could be considered to be non sufficient for physicists. Indeed, we would rather prefer a dynamical way to generate such hierarchies in the flavour sector. Furthermore, most of the degrees of freedom of the Standard Model originate from the Yukawa couplings and therefore, the question of dynamically generating the Yukawa reinforces the motivation to go beyond the anthropic argument.

As a particle physicist, a usual way out is to consider extended symmetries. Removing the Yukawa parameters of the standard model, one restores a full $U(3)^5$ flavour symmetry ($U(3)^6$ if considering right-handed neutrinos). Many efforts, Refs. [99–105] among a long list of publications, have been done in order to identify an underlying flavour symmetry above the electroweak scale. For our purpose, we will focus on discrete flavour symmetries as they can explain the specific patterns associated to the PMNS and CKM matrices. We will also mention $U(1)$ Froggatt-Nielsen symmetries, that can account for the mass hierarchies.

Discrete flavour symmetries have various advantages with respect to continuous ones. Indeed, the number of irreducible representations is finite and the parameters describing the transformations are discrete, meaning less additional parameters added to the usual SM Lagrangian. Additionally, they can be traced back from higher dimension compactifications [106]. The leptonic sector has received considerable attention, because the sizable entrances of the PMNS matrices may be explained

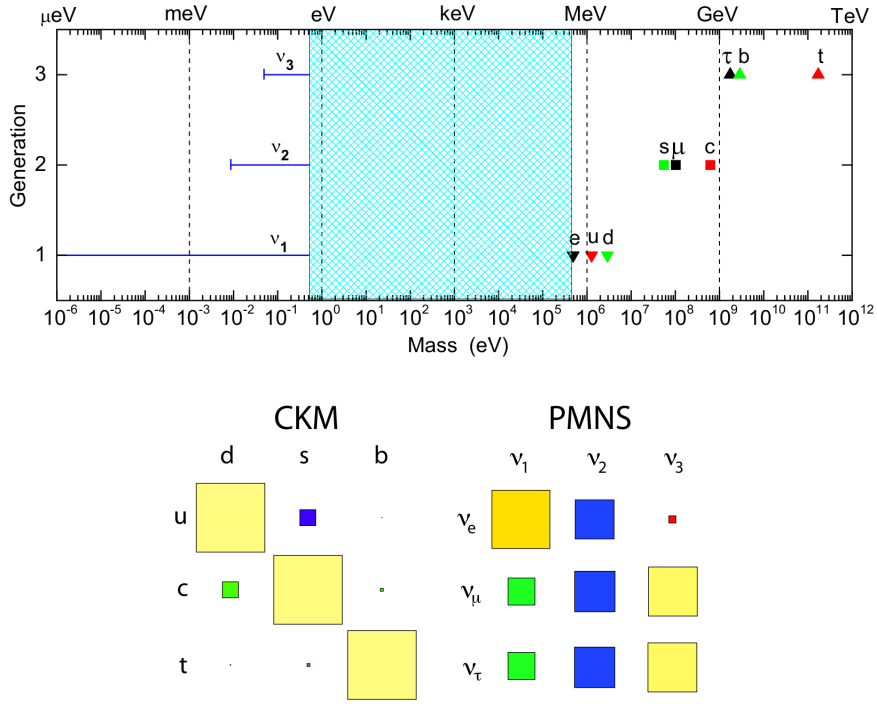

Figure 5.1 – The top figure [97] represents the the SM mass hierarchy puzzle while the bottom one [98] presents the magnitude of the CKM and PMNS matrix elements.

using rather small groups. On the other hand, accommodating precisely the CKM matrix would require very large groups as the off-diagonal elements are very small. However, suitable groups are able to explain the Cabibbo mixing pattern [107] which is a very good approximation of the full CKM matrix (describes the first two generation mixing).

5.1.2 Froggatt-Nielsen U(1)$_{\mathbf{FN}}$ flavour symmetry

We first illustrate the principle of flavour symmetries in the context of the Froggatt-Nielsen symmetry mechanism [108] to explain the fermion mass hierarchy. This attempt, being one of the simplest examples, remains still appealing. Indeed, a plethora of models, Refs. [109, 110] among them, are combining a Froggatt-Nielsen symmetry with discrete symmetries in order to predict the quark and lepton Yukawa couplings with the correct mixing patterns and mass hierarchies. In our example, let us consider the quark sector and write down the mass hierarchies

$$\frac{m_u}{m_t} \sim \epsilon^8, \quad \frac{m_c}{m_t} \sim \epsilon^4, \quad \frac{m_d}{m_b} \sim \epsilon^5, \quad \frac{m_s}{m_b} \sim \epsilon^2, \tag{5.1}$$

where $\epsilon \sim 0.2$.

In addition, the CKM matrix exhibits similarly an underlying hierarchical structure

$$V_{us} \sim \epsilon, \quad V_{uc} \sim \epsilon^3, \quad V_{ub} \sim \epsilon^3. \tag{5.2}$$

The above structure can be deduced from the Wolfenstein parametrization of the CKM matrix introduced in Eq. (1.44).

The idea behind the Froggatt-Nielsen mechanism is to generate the correct Yukawa couplings that can lead to these different ratios. The idea is very simple: One introduces a new $U(1)_{FN}$ global symmetry in the SM Lagrangian. To spontaneously break this symmetry, one introduces a scalar field ϕ, singlet under the SM gauge group but with FN charge $Q_{FN}(\phi) = -1$. Below some scale M, the scalar acquires a vev that breaks $U(1)_{FN}$. Therefore, one can build effective Yukawa couplings

of the form

$$\mathcal{L} \subset y_{ij}\bar{Q}_i H u_j \left(\frac{\langle\phi\rangle}{M}\right)^{n_{ij}}, \tag{5.3}$$

where $n_{ij} = Q_{FN}(u_j) - Q_{FN}(Q_i)$. Note that in this context, all the y_{ij} are order one coefficients.

Choosing the ratio $\langle\phi\rangle/M \sim \epsilon$ together with correct charge assignments leads to the specific hierarchical patterns described in Eqs. (5.1) and (5.2). In particular, choosing the same charge for Q_3 and u_3 allows for renormalizable y_t. Therefore, the top quark mass will be of order $m_t \sim v/\sqrt{2} \sim 170$ GeV. Interestingly, the CKM elements are roughly given by powers of ϵ, depending of the charge of the different quark doublets

$$V_{ij} \sim \left(\frac{\langle\phi\rangle}{M}\right)^{c_{ij}}, \quad \text{with} \quad c_{ij} = Q_{FN}(Q_j) - Q_{FN}(Q_i). \tag{5.4}$$

Following this indication, we end with the prediction

$$V_{ub} \sim V_{us}V_{cb}, \tag{5.5}$$

which indeed agrees with the determination of the CKM matrix elements.

Although we have presented an EFT approach, it is possible to build UV complete models, usually by introducing new heavy (vector) fermions (see for instance [111, 112] among many).

5.1.3 Discrete flavour symmetry: An A_4 example for the lepton sector

This section aim at providing an illustration, through a concrete example, of how non-abelian discrete symmetries may be used to predict structure of fermionic mixing. We will closely follow the Altarelli-Feruglio discussion [100, 113], where they built an explicit model for the lepton sector based on the group A_4. Complementary and pedagogical discussions can also be found in [114].

They aimed at incorporating neutrino masses together with the leptonic mixing matrix, the PMNS matrix, defined as the mismatch between charged lepton and (effective) neutrino Yukawa couplings [1]

$$U_{PMNS} = V_\ell^\dagger V_\nu, \tag{5.6}$$

where $V_{l,\nu}$ diagonalize the charged lepton and neutrino Yukawa couplings.

The neutrino mass

$$\mathcal{L}_{m_\nu} = \frac{1}{2}\bar{\nu}^c m_\nu \nu, \tag{5.7}$$

is assumed here to arise from the dimension five Weinberg operator.

A good approximation for the leading order PMNS matrix is the so-called tri-bimaximal (TMB) form [115]

$$U_{TBM} = \begin{pmatrix} \sqrt{\frac{2}{3}} & \frac{1}{\sqrt{3}} & 0 \\ -\frac{1}{\sqrt{6}} & \frac{1}{\sqrt{3}} & -\frac{1}{\sqrt{2}} \\ -\frac{1}{\sqrt{6}} & \frac{1}{\sqrt{3}} & \frac{1}{\sqrt{2}} \end{pmatrix}. \tag{5.8}$$

The TBM form for the leptonic mixing matrix is however ruled out by the observation of a non-zero θ_{13} value in neutrino oscillations [116]. However, it is still possible to reach the correct experimental values starting from this leading order assumption, see [117, 118] among others, by extending the charged lepton sector such that small perturbations from the TBM form arise.

We will now discuss how the TBM mixing matrix is naturally predicted by the A_4 group. The alternating group A_4 is the group of even permutations of four elements. It can also be seen as the group which leaves invariant a rigid regular tetrahedron. As presented in Fig. 5.2, A_4 is generated

[1] After integrating out heavy right handed neutrinos, in seesaw models, an effective Yukawa coupling is generated out of the right handed Majorana mass matrix and Dirac yukawa coupling.

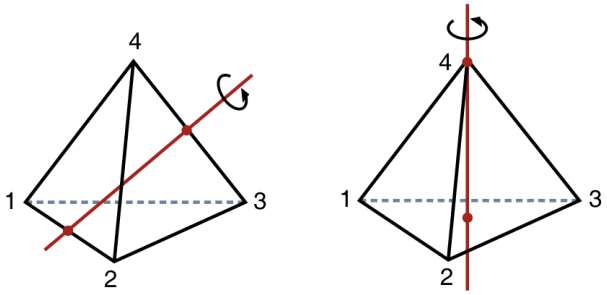

Figure 5.2 – Tetrahedron symmetry generators. Figure taken from [114].

by two generators T and S which stand for rotations and reflexions. The generators satisfy the relations

$$S^2 = 1, \quad T^3 = 1, \quad (ST)^3 = 1. \tag{5.9}$$

The group is made of twelve elements that belong to four equivalence classes which can be characterized by the different powers of T. The A_4 group has four irreducible representations, three are dimension one and will be named $\mathbf{1}$, $\mathbf{1'}$ and $\mathbf{1''}$; last one is a dimension three representation.

One can work out the different generator representations for the one dimensional representations as

$$\begin{aligned} &\mathbf{1}: \ S = 1, \ T = 1, \\ &\mathbf{1'}: \ S = 1, \ T = \omega, \\ &\mathbf{1''}: \ S = 1, \ T = \omega^2, \end{aligned} \tag{5.10}$$

where $\omega = e^{i2\pi/3}$ is the cubic root of unity. As for the triplet representation, we will work in the T-diagonal basis where we have

$$\mathbf{3}: \ S = \frac{1}{3}\begin{pmatrix} -1 & 2 & 2 \\ 2 & -1 & 2 \\ 2 & 2 & -1 \end{pmatrix}, \ T = \begin{pmatrix} 1 & 0 & 0 \\ 0 & \omega & 0 \\ 0 & 0 & \omega^2 \end{pmatrix}. \tag{5.11}$$

Additionally, we can write down the different laws for the representation products

$$\begin{aligned} &\mathbf{1} \times \mathbf{n} = \mathbf{n} \quad \text{where } \mathbf{n} \text{ stands for any representation,} \\ &\mathbf{1'} \times \mathbf{1'} = \mathbf{1''}, \quad \mathbf{1'} \times \mathbf{1''} = \mathbf{1}, \\ &\mathbf{1''} \times \mathbf{1''} = \mathbf{1'}, \\ &\mathbf{3} \times \mathbf{3} = \mathbf{1} + \mathbf{1'} + \mathbf{1''} + \mathbf{3_A} + \mathbf{3_S} \quad \text{where } A, S \text{ stand for anti-symmetric and symmetric.} \end{aligned} \tag{5.12}$$

We recall that different Clebsch-Gordan coefficients appear in the different products. A list of those coefficients can be found in [114].

We can now make the key observation that leads A_4 to be a good candidate for TBM mixing. The point is that, in the basis where the charged lepton mass matrix is diagonal (so $U_{PMNS} = U_\nu$), a mass matrix that respects

$$S^T m_\nu S = m_\nu, \tag{5.13}$$

gives precisely rise to U_{TBM} [2]. Achieving a diagonal charged lepton mass matrix will be done by imposing that the lepton mass term remains invariant under the action of T while in the neutrino sector we will enforce the invariance under S.

[2] Actually, one also requires that the neutrino mass matrix is also invariant under a $\mu - \tau$ symmetry.

	L	e^c	μ^c	τ^c	$H_{u,d}$	ϕ_T	ϕ_S	ξ
A_4	3	1	$1''$	$1'$	1	3	3	1
Z_3	ω	ω^2	ω^2	ω^2	1	1	ω	ω

Table 5.1 – Field and charges content of the Altarelli-Feruglio model.

Therefore the basic mechanism is to break A_4 in two subgroups generated by S and T for the neutrino and the charged lepton sector. For this purpose, we will introduce additional flavons ϕ_S and ϕ_T, charged under A_4 which will acquire vevs along the S and T directions. Manifestly, the following vevs are invariant under T and S respectively:

$$\langle \phi_T \rangle = (v_T, 0, 0)^T, \quad \langle \phi_S \rangle = (v_S, v_S, v_S)^T. \tag{5.14}$$

We now illustrate the typical Altarelli-Feruglio model. First, we are working in the context of Supersymmetry. As discussed in their model, SUSY is not needed but it turns out to be a useful ingredient that helps to achieve the correct flavon alignment that leads to the vevs of Eq. (5.14). We introduce an additional Z_3 symmetry. This new symmetry, called auxiliary (or driving) symmetry, is needed to distinguish the flavons ϕ_T and ϕ_S so they couple to the correct sectors, as the flavons are singlets under G_{SM}. We also introduce a flavon ξ, singlet under A_4, that couples to neutrinos. The field content is given in table 5.1.

One can write down the superpotential lepton mass term

$$\begin{aligned} W = &\frac{y_e}{\Lambda} e^c H_d (L\phi_T)_1 + \frac{y_\mu}{\Lambda} \mu^c H_d (L\phi_T)_{1'} + \frac{y_\mu}{\Lambda} \tau^c H_d (L\phi_T)_{1''} \\ &+ \frac{x_a}{\Lambda^2} \xi H_u H_u (LL)_1 + \frac{x_b}{\Lambda^2} H_u H_u (LL\phi_S)_1 + \text{higher orders}. \end{aligned} \tag{5.15}$$

The flavour symmetry is then broken by the vevs of Eq. (5.14) and $\langle \xi \rangle = v_\xi$. The mass matrices resulting from this particular setup are then

$$m_e = \frac{v_d v_T}{\sqrt{2}\Lambda} \begin{pmatrix} y_e & 0 & 0 \\ 0 & y_\mu & 0 \\ 0 & 0 & y_\tau \end{pmatrix}, \qquad m_\nu = \frac{v_u^2}{\Lambda} \begin{pmatrix} a + 2b/3 & -b/3 & -b/3 \\ -b/3 & 2b/3 & a - b/3 \\ -b/3 & a - b/3 & 2b/3 \end{pmatrix}, \tag{5.16}$$

where

$$a = \frac{2 x_a v_\xi}{\Lambda}, \qquad b = \frac{2 x_b v_S}{\Lambda}. \tag{5.17}$$

Diagonalizing this matrix, one finds that the resulting PMNS matrix is precisely of the TBM form, as expected from the residual invariance under S.

The above results are valid up to higher order terms. We can explicitly see that the hierarchy of the masses is not explained in this framework. Usually, one introduces also a seesaw mechanism that leads to natural neutrino masses. In addition, it is possible to combine the above model with a Froggatt-Nielsen symmetry such that the lepton masses are also natural.

The simplified setup presented here is not complete. Indeed, the flavon alignments are arbitrary, while in a complete model we should aim at reaching the correct vev from a dynamical process. Investigating this aspect is beyond the scope of the simplified presentation given here, the reader is left with the original paper from Altarelli and Feruglio [113] where both higher order contributions and flavon alignment are discussed.

5.2 SU(5): the simplest GUT model

As discussed in Sec. 1.5.3, the gauge couplings almost meet in the SM at a very high scale. It turns out that in the context of the MSSM, the unification is much better [119] as can be seen if Fig. 5.3.

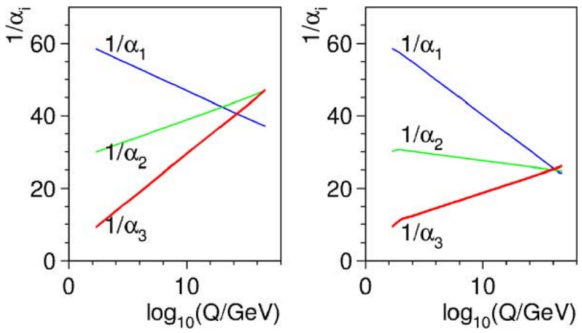

Figure 5.3 – Gauge coupling unification in the SM and the MSSM. Figure taken from [120].

This is a very appealing aspect in favour of using one single gauge group (and therefore one unique gauge coupling) to describe the three interactions of the standard model.

The first attempt in this direction has been proposed by Georgi and Glashow [46] and relies on $SU(5)$. This version was a non-SUSY model has been ruled out after precise gauge coupling measurements. However, going beyond the vanilla model without SUSY can still predict correct gauge couplings at low scale [121]. Nevertheless, we will remain in the context of SUSY in this Chapter.

What are the requirements for a gauge group to be a good GUT candidate? First of all, we would like that $G_{GUT} \subset G_{SM}$, as the SM, despite the flaws already discussed, remains very successful. To achieve this, it is required that G_{GUT} be at least a rank four Lie group (four commuting generators) because G_{SM} itself is of rank four. The smallest group which contains G_{SM} is $SU(5)$. Because of this characteristic, $SU(5)$ has been widely studied and constitutes a very attractive playground for studying GUT models.

5.2.1 Basic structure of SU(5) models

First, we would like to explicit the fact that all the SM fermions for a given generation fit into two representations of $SU(5)$, the **10** and the $\bar{\mathbf{5}}$. Recall that the different MSSM fields in left-handed notation have the $G_{SM} = SU(3)_C \times SU(2)_L \times U(1)_{Y/2}$ transformation properties

$$\begin{gathered} Q = (\mathbf{3}, \mathbf{2}, 1/6), \quad d^c = (\bar{\mathbf{3}}, \mathbf{1}, 1/3), \quad u^c = (\bar{\mathbf{3}}, \mathbf{1}, -2/3), \\ L = (\mathbf{1}, \mathbf{2}, -1/2), \quad e^c = (\mathbf{1}, \mathbf{1}, 1). \end{gathered} \tag{5.18}$$

Assuming the breaking pattern $SU(5) \to G_{SM}$ let us write an $SU(3) \times SU(2)$ transformation as a block-diagonal 5×5 matrix that stands for an $SU(5)$ transformation. The $SU(2)$ matrix will be labeled as U_2, the $SU(3)$ one as U_2 and the $SU(5)$ one as U_5. The form of the $SU(5)$ transformation is then

$$U_5 = \begin{pmatrix} U_3 & 0 \\ 0 & U_2 \end{pmatrix}. \tag{5.19}$$

Additionally, because $SU(5)$ is of rank 4 (4 commuting generators), there is an other generator that commutes with the above $SU(3) \times SU(2)$ transformation:

$$Y/2 = C \begin{pmatrix} -1/3 & 0 & 0 & 0 & 0 \\ 0 & -1/3 & 0 & 0 & 0 \\ 0 & 0 & -1/3 & 0 & 0 \\ 0 & 0 & 0 & 1/2 & 0 \\ 0 & 0 & 0 & 0 & 1/2 \end{pmatrix}, \tag{5.20}$$

where C is a normalization constant. This normalization will be later on absorbed in the definition of the hypercharge coupling, therefore we will drop it for now. This generator correspond to the hypercharge generator $Y/2$ of the SM.

From there, we can explicitly check that the $\mathbf{5}$ decomposes under G_{SM} as

$$\mathbf{5} \to (\mathbf{3}, \mathbf{1}, -1/3) + (\mathbf{1}, \mathbf{2}, 1/2), \tag{5.21}$$

and therefore

$$\bar{\mathbf{5}} \to (\bar{\mathbf{3}}, \mathbf{1}, 1/3) + (\mathbf{1}, \mathbf{2}, -1/2). \tag{5.22}$$

We would like now to investigate the decomposition of the $\mathbf{10}$ under G_{SM}. First, let us notice that the $\mathbf{10}$ can be obtained by the product of two $\mathbf{5}$: $\mathbf{5} \otimes \mathbf{5} = \mathbf{10} + \mathbf{15}$. The $\mathbf{10}$ is antisymmetric while the $\mathbf{15}$ is symmetric. Performing the representation products we get

$$\begin{aligned} \mathbf{5} \otimes \mathbf{5} &\to [(\mathbf{3}, \mathbf{1}, -1/3) + (\mathbf{1}, \mathbf{2}, 1/2)] \otimes [(\mathbf{3}, \mathbf{1}, -1/3) + (\mathbf{1}, \mathbf{2}, 1/2)] \\ &= (\mathbf{6} + \bar{\mathbf{3}}, \mathbf{1}, -2/3) + (\mathbf{3}, \mathbf{2}, 1/6) + (\mathbf{3}, \mathbf{2}, 1/6) + (\mathbf{1}, \mathbf{1} + \mathbf{3}, 1), \end{aligned} \tag{5.23}$$

where we used the fact that in $SU(3)$ we have $\mathbf{3} \otimes \mathbf{3} = \bar{\mathbf{3}} + \mathbf{6}$ ($\bar{\mathbf{3}}$ is antisymmetric and $\mathbf{6}$ is symmetric) and in $SU(2)$ $\mathbf{2} \otimes \mathbf{2} = \mathbf{1} + \mathbf{3}$ ($\mathbf{1}$ is antisymmetric and $\mathbf{3}$ is symmetric).

Therefore, one immediately sees that $\mathbf{10} \supset (\bar{\mathbf{3}}, \mathbf{1}, -2/3) + (\mathbf{1}, \mathbf{1}, 1)$ while $\mathbf{15} \supset (\mathbf{6}, \mathbf{1}, -2/3) + (\mathbf{1}, \mathbf{3}, 1)$. However, we see that we need to add to both the $\mathbf{10}$ and the $\mathbf{15}$ decompositions one $(\mathbf{3}, \mathbf{2}, 1/6)$ to get the correct number of states. We can explicitly compute the antisymmetric product to show that the $\mathbf{10}$ representation includes a specific combination of the two $(\mathbf{3}, \mathbf{2}, 1/6)$. In order to do this, let us consider two vectors u_5 and u'_5 belonging to $\mathbf{5}$ of $SU(5)$. These vectors can be decomposed as two subvectors $u_3 + u_2$ (resp. $u'_3 + u'_2$) that transform under $SU(3)$ and $SU(2)$, i.e.

$$u_5 = u_3 + u_2 = \begin{pmatrix} \alpha_i \\ 0 \\ 0 \end{pmatrix} + \begin{pmatrix} 0 \\ 0 \\ 0 \\ \beta_j \end{pmatrix}, \quad u'_5 = u'_3 + u'_2 = \begin{pmatrix} \alpha'_i \\ 0 \\ 0 \end{pmatrix} + \begin{pmatrix} 0 \\ 0 \\ 0 \\ \beta'_j \end{pmatrix}, \tag{5.24}$$

where $i = 1, 2, 3$ and $\beta = 1, 2$.

The antisymmetric part of $u_5 \otimes u'_5$ is defined as

$$u_5 \otimes_A u'_5 = u_5 \otimes u'_5 - u'_5 \otimes u_5. \tag{5.25}$$

Using the decomposition (5.24), we end with

$$\begin{aligned} u_5 \otimes_A u'_5 = {} & u_3 \otimes u'_3 - u'_3 \otimes u_3 + u_2 \otimes u'_2 - u'_2 \otimes u_2 \quad (\mathrm{L}_1) \\ & + u_3 \otimes u'_2 + u_2 \otimes u'_3 - u'_2 \otimes u_3 - u'_3 \otimes u_2 \quad (\mathrm{L}_2). \end{aligned} \tag{5.26}$$

The first line (L_1) in Eq. (5.26) corresponds to $(\bar{\mathbf{3}}, \mathbf{1}, -2/3) + (\mathbf{1}, \mathbf{1}, 1)$. Performing the tensor product of the second line (L_2) we get

$$\mathrm{L}_2 = \begin{pmatrix} 0 & 0 & 0 & -\alpha'_1\beta 1 + \alpha_1\beta'_1 & -\alpha'_1\beta 2 + \alpha_1\beta'_2 \\ 0 & 0 & 0 & -\alpha'_2\beta 1 + \alpha_2\beta'_1 & -\alpha'_2\beta 2 + \alpha_2\beta'_2 \\ 0 & 0 & 0 & -\alpha'_3\beta 1 + \alpha_3\beta'_1 & -\alpha'_3\beta 2 + \alpha_3\beta'_2 \\ \alpha'_1\beta 1 - \alpha_1\beta'_1 & \alpha'_2\beta 1 - \alpha_2\beta'_1 & \alpha'_3\beta 1 - \alpha_3\beta'_1 & 0 & 0 \\ \alpha'_1\beta 2 - \alpha_1\beta'_2 & \alpha'_2\beta 2 - \alpha_2\beta'_2 & \alpha'_3\beta 2 - \alpha_3\beta'_2 & 0 & 0 \end{pmatrix}. \tag{5.27}$$

This corresponds exactly to an antisymmetric $(\mathbf{3}, \mathbf{2}, 1/6)$. Finally, we reach the conclusion that

$$\mathbf{10} \to (\bar{\mathbf{3}}, \mathbf{1}, -2/3) + (\mathbf{3}, \mathbf{2}, 1/6) + (\mathbf{1}, \mathbf{1}, 1). \tag{5.28}$$

It is now clear that the complete set of representations of the MSSM in Eq. (5.18) can be embedded into $\mathbf{10} + \bar{\mathbf{5}}$ in $SU(5)$. We can now give a matrix expression for the $SU(5)$ representations in terms of the MSSM matter field content as

$$\bar{\mathbf{5}} = \begin{pmatrix} d_r^c \\ d_g^c \\ d_b^c \\ \ell^- \\ -\nu \end{pmatrix}, \quad \mathbf{10} = \begin{pmatrix} 0 & -u_g^c & u_b^c & -u_r & -d_r \\ u_g^c & 0 & -u_r^c & -u_g & -d_g \\ -u_b^c & u_r^c & 0 & -u_b & -d_b \\ u_r & u_g & u_b & 0 & -e^c \\ d_r & d_g & d_b & e^c & 0 \end{pmatrix}. \tag{5.29}$$

For the rest of the manuscript, we will denote by F and by T the $\bar{\mathbf{5}}$ and $\mathbf{10}$ representations for the fermionic content. Let us emphasize that it is not possible to gather u^c and L in the same representation because of the hypercharge generator. However, variations introducing an additional $U(1)$ symmetry exist where it is possible to switch d^c and u^c. These models go under the name of flipped $SU(5)$ [122].

We can now investigate the gauge sector. $SU(5)$ has $5^2 - 1 = 24$ generators which live in the adjoint representation $\mathbf{24}$. We can investigate the decomposition of the adjoint representation under G_{SM} and we will get

$$\mathbf{24} \to (\mathbf{8}, \mathbf{1}, 0) + (\mathbf{1}, \mathbf{3}, 0) + (\mathbf{1}, \mathbf{1}, 0) + (\mathbf{3}, \mathbf{2}, -5/6) + (\bar{\mathbf{3}}, \mathbf{2}, 5/6). \tag{5.30}$$

Therefore, the gauge sector of $SU(5)$ contains the usual eight gluons, three weak bosons and the hypercharge boson of G_{SM}. In addition, we have twelve bosons charged under $SU(3)_C \times SU(2)_L \times U(1)_{Y/2}$. These new gauge bosons violate lepton and baryon numbers and generate operators leading to proton decay. However, even if the parameter space tends to be very constrained [123, 124], there is still plausibly some room left for viable SUSY $SU(5)$ [125].

Let us now discuss the Yukawa sector of $SU(5)$. First of all, the MSSM Higgs doublets H_5^u and H_5^d belong to respectively a $\mathbf{5}$ and a $\bar{\mathbf{5}}$

$$H_5^u = \begin{pmatrix} \Delta \\ H_u \end{pmatrix}, \quad H_5^d = \begin{pmatrix} \bar{\Delta} \\ H_d \end{pmatrix}, \tag{5.31}$$

where Δ (resp. $\bar{\Delta}$) is a colour triplet (resp. anti-triplet) and $H_{u,d}$ are the MSSM Higgs doublets. We can construct the Yukawa superpotential terms in the following way

$$W_Y = T Y_{10} T H_5^u + F Y_5 T H_5^d. \tag{5.32}$$

Here, Y_{10} corresponds to the up-type (s)quarks Yukawa of the MSSM while Y_5 is associated to both L and d superfields.

Finally, before moving on to several aspects of $SU(5)$ models, we mention that the breaking $SU(5) \to G_{SM}$ can be accomplished by introducing an adjoint representation H_{24}. Allowing for this field to acquire a specific vev leads to the wanted breaking pattern.

5.2.2 Consequences of SU(5) models

$SU(5)$ models present interesting features. One of the first we note is, due to the gathering of u and u^c into the T representation while d^c and L belong to the F representation, specific relationships hold for the Yukawa couplings. The relations translate into the MSSM Yukawa couplings and we have

$$Y_u = Y_u^t, \quad Y_e = Y_d^t. \tag{5.33}$$

This very predictive shape for the Yukawa is under constraints because of the masses of the SM particles. However it is possible to go beyond this scope by introducing an H_{45} field which

transforms as an $\overline{\mathbf{45}}$ of $SU(5)$. This is known as the Georgi-Jarlskog mechanism [126]. Therefore, the down quark and lepton Yukawa couplings originate from a combination of a Y_5 and a Y_{45}. From there, specific Clebsch-Gordan coefficients modify the different values of the SM Yukawa matrices and enforce different relations that satisfy better the experimental constraints.

Furthermore, under the assumption that the SUSY breaking mediator transforms as a singlet of $SU(5)$, the relations (5.33) transfer to the trilinear soft terms of the MSSM and we obtain

$$A_u = A_u^t, \quad A_e = A_d^t. \tag{5.34}$$

Such configurations are more than welcome for phenomenological purposes. Indeed, imposing such relations restricts greatly the number of free parameters.

In addition to this particular flavour structure, $SU(5)$ models address the problem of charge quantization. As we already have seen before in Eq. (5.20), the commuting generator $Y/2$ takes discrete values up to a normalization C. The normalization constant can be fixed by imposing that

$$\mathrm{Tr}[T_a T_b] = \frac{1}{2}\delta^{ab}. \tag{5.35}$$

Therefore we obtain that

$$C = \sqrt{\frac{3}{5}}. \tag{5.36}$$

As already mentioned, this normalization factor can be reabsorbed in the definition of the coupling constant $g_{Y/2}$ leading to

$$g_{Y/2} = \sqrt{\frac{3}{5}} g_5. \tag{5.37}$$

Turning now to the gaugino sector, it is quite intuitive that, if one assumes that gaugino soft breaking masses are generated above the GUT scale, all fermionic partners of the gauge bosons have the same mass above M_{GUT} for a simple model. This particular feature leads to approximate mass relations at the SUSY scale [127]

$$M_1 : M_2 : M_3 \sim 1 : 2 : 6. \tag{5.38}$$

However, it is possible to relax this prediction by considering non-universal gaugino masses, as it has been shown in different models [128–130]. We do not aim at discussing this point which is beyond the scope of this manuscript but we will take for granted that considering non-universal gaugino masses in the next chapter is well motivated.

Before concluding this section and discussing the flavoured $SU(5)$ models we mention the doublet-triplet splitting problem in $SU(5)$ models. As described in Eq. (5.31), the MSSM Higgs fields belong to the same representation of the colour triplets. While the MSSM Higgs fields are required to be massless, the colour triplet needs to be massive enough to avoid large contributions to proton decay. Various possibilities can be considered, [131] for instance, but we are not aiming at discussing it further.

5.3 SUSY SU(5) meeting flavour symmetry

In this short section we aim at discussing several aspects of SUSY $SU(5)$ models coupled to a horizontal symmetry. The motivations behind such models are multiple. One of the most attractive parts is that because of the $SU(5)$ unification, both leptons and quarks are controlled by the same flavour symmetry. Therefore, the same shaping flavour symmetry dictates the Yukawa couplings of the full fermionic sector. Within a gravity mediated SUSY breaking framework, the flavour symmetry imposed patterns translate immediately to the soft terms and reduce drastically the

number of free parameters and/or their ranges. However, when building such models, several cares have to be taken.

A typical SUSY GUT flavoured model is usually based on a global non-abelian discrete symmetry (NADS) alongside of an global $U(1)_{FN}$ symmetry. The Froggat-Nielsen symmetry is present to ensure correct hierarchy for the masses of the SM particles while the NADS controls the fermionic mixing. Usually, one builds such models as EFT with non-renormalizable operators. In case of supersymmetry, one needs also to include higher operators in the Kähler potential in the following way

$$K(\Phi_1, ..., \Phi_N) = \sum \frac{a_n}{M^n} \Phi_i^\dagger \Phi_j \phi_k \ ... \tag{5.39}$$

where Φ_i are matter superfields, a_n are order one coefficients, M is the cutoff scale and ϕ_k are flavon insertions in order to build invariant Lagrangians under the flavour symmetry. We omitted here the gauge interactions for the sake of simplicity. Eq. (5.39) has to be understood as the sum over all the (super)fields that are invariant under the global flavour symmetries and gauge symmetries up to a given order.

However, we have seen in Sec. 2.4 that the Kähler potential controls the kinetic terms of the SM particles as well as the SUSY partners. Therefore, in general, non diagonal kinetic terms appear. This lead to a non-diagonal Kähler metric $\mathcal{K}$ which can be written in the following way:

$$\mathcal{L}_{kin} = \mathcal{K}_{ij}(\partial^\mu \tilde{f}_i^* \partial_\mu \tilde{f}_j + i f_i^* \bar{\sigma}^\mu \partial_\mu f_j), \tag{5.40}$$

with $\mathcal{K} \neq 1$.

Therefore, one needs to perform a change of basis, called the canonical normalization, in order to extract meaningful results. The basic strategy [132, 133] is to rotate the fields in such a way that

$$\mathcal{K}' = (P_A^\dagger)^{-1} \mathcal{K} P_A = 1, \tag{5.41}$$

where P_A is a non unitary transformation that acts on the superfield A as

$$A = (P_A)^{-1} A'. \tag{5.42}$$

In typical $SU(5)$ we have $A = T, F, N$ where T, F stand for the $\mathbf{10}$ and $\bar{\mathbf{5}}$ fermionic representations and N is for the right handed neutrinos, if present in the model. This transformation plays an important role as it will modify the Yukawa couplings (and soft terms) of a significant amount (see for instance [109]).

In the next chapter, we shall discuss with a concrete example, the phenomenology of $SU(5) \times A_4$ inspired models, including constraints. However, no specific breaking pattern for A_4 will be considered and therefore, we will not need to perform the canonical normalization as we will consider a general setup. However, this feature has to be kept in mind when dealing with complete flavoured models.

Finally, before moving to the next chapter, we wish to make a comment about possible UV completions of such models. An example can be found in [134], where the authors built an explicit UV completion by considering additional messengers for the flavour sector. Building a full UV complete flavour model produces a very predictive framework where the flavour violating terms are controlled by a small number of parameters. However, the UV completion of flavoured GUT models is well beyond the scope of this manuscript and we will remain in the context of an EFT description.

Chapter 6

Phenomenology of A_4 inspired GUT models

After introducing the framework of flavoured SUSY $SU(5)$ GUT models in the previous chapter, we dedicate here a chapter to the discussion and study of their phenomenology. We will investigate a somehow simplified model based on the A_4 group, as an illustration of parameter study in the context of flavoured GUT models. This is a simplified setup in the sense that the model will not assume any particular flavour symmetry breaking pattern. Therefore, we aim here at varying the flavour violating terms around benchmarks points to study the consequences on low scale flavour violating observables. The discussion will be based on the publication [135].

6.1 Context of the study

The link between NMFV terms at the TeV scale and the GUT scale is interesting from both the phenomenological and model-building point of view. Although they may be numerically rather different, flavour violating interactions in the squark and slepton sectors are linked if NMFV is implemented in a unification framework at the high-scale, as it has been discussed in Sec. 5.3. The same source of flavour violation may therefore be challenged by experimental data from both sectors.

In a recent paper [136], such a scenario was discussed in the framework of an $SU(5)$ GUT combined with an A_4 family symmetry[1]. The idea was that the three $\overline{\mathbf{5}}$ representations form a single triplet of the family symmetry with a unified soft mass m_F, while the three $\mathbf{10}$ representations are singlets with independent soft masses m_{T_1}, m_{T_2}, m_{T_3}. Assuming MFV, it was shown that in order to account for the muon anomalous magnetic moment $(g-2)_\mu$, dark matter and LHC data, non-universal gaugino masses M_i $(i = 1, 2, 3)$ at the high scale are required in the framework of the MSSM.

The authors of [136] focussed on a region of parameter space that has not been studied in detail before characterised by low higgsino mass $\mu \approx -300$ GeV, as required by $(g-2)_\mu$. The latter also required a right-handed smuon $\tilde{\mu}_R$ with a mass around 100 GeV, and a neutralino $\tilde{\chi}_1^0$ several GeV lighter which allows successful relic density for dark matter. The LHC will be able to fully test this scenario with the upgraded luminosity via muon-dominated tri- and di-lepton signatures resulting from higgsino dominated $\tilde{\chi}_1^\pm \tilde{\chi}_2^0$ and $\tilde{\chi}_1^+ \tilde{\chi}_1^-$ production, as well as direct smuon production searches in the above region of parameter space.

The above study [136] was clearly concerned with the implications of the flavoured GUT model for the superpartner spectrum consistent with $(g-2)_\mu$ and the Dark Matter relic density. However, for simplicity, it was assumed that there was no flavour violation at the GUT scale, whereas it is well known that such flavour violation is expected in flavoured GUT models [109, 137, 138]. The goal of the present study is to extend this work to the NMFV framework by introducing off-diagonal squark and slepton mass-squared terms in the Lagrangian at the GUT scale, motivated by the analyses in Refs. [109, 137, 138] which show that such flavour violation is generically expected. Here, we take a phenomenological (or model independent) approach, and simply introduce flavour violating

[1] Note that the A_4 may be replaced by S_4 or $SO(3)$ or indeed any family symmetry which contains both triplet and singlet representations.

terms at high energy to explore their effect on low energy observables. To this end we consider two MFV reference parameter points, one of which is inspired by the findings of Ref. [136] and involves a very light smuon capable of accounting for $(g-2)_\mu$, and the other one with a heavier smuon, harder to discover at the LHC, but not able to account for $(g-2)_\mu$. In both cases, we then perturb around these points, switching on off-diagonal mass terms, consistently with $SU(5)$, arising from A_4 breaking effects. We find interesting correlations between the flavour violating parameters at the GUT scale consistent with the stringent lepton flavour violating processes $\mu \to e\gamma$.

As a first step, we summarize within the present context the discussions of chapters 5 and 3. The notation will slightly change with respects to the previous chapters (in particular the soft terms) but this is to match the conventions used in [135] and provide a self-consistent chapter. We then present the numerical approach employed before discussing the results of the analysis.

6.2 Model review

Although the exact breaking mechanism is not completely understood, it is well known that Supersymmetry (SUSY) must be broken to some degree. The associated SUSY-breaking Lagrangian contains all terms which do not necessarily respect SUSY but hold to the tenets of gauge invariance and renormalisability. Considering the Minimal Supersymmetric Standard Model (MSSM), the SUSY-breaking Lagrangian reads

$$\begin{aligned}\mathcal{L}_{\text{soft}}^{\text{MSSM}} = &-\frac{1}{2}(M_1\widetilde{B}\widetilde{B} + M_2\widetilde{W}\widetilde{W} + M_3\widetilde{g}\widetilde{g} + \text{h.c.}) \\ &- M_{\widetilde{Q}}^2\widetilde{Q}^\dagger\widetilde{Q} - M_{\widetilde{L}}^2\widetilde{L}^\dagger\widetilde{L} - M_{\widetilde{U}}^2\widetilde{U}^*\widetilde{U} - M_{\widetilde{D}}^2\widetilde{D}^*\widetilde{D} - M_{\widetilde{E}}^2\widetilde{E}^*\widetilde{E} \\ &- (A_U\widetilde{U}^*H_u\widetilde{Q} + A_D\widetilde{D}^*H_d\widetilde{Q} + A_E\widetilde{E}^*H_d\widetilde{L} + \text{h.c.}) \\ &- m_{H_u}^2H_u^*H_u - m_{H_d}^2H_d^*H_d - (bH_u^*H_d + \text{h.c.})\,.\end{aligned} \tag{6.1}$$

While the soft mass and trilinear parameters appearing in Eq. (6.1) are assumed to be diagonal matrices in flavour space within the MFV framework, they may comprise non-diagonal entries when relaxing this hypothesis and considering a NMFV scenario. It should be noted that generic SUSY models do not possess any symmetry preventing large off-diagonal elements in soft-SUSY parameters. The soft mass matrices are defined in the Super-CKM (SCKM) basis as:

$$\begin{aligned}M_Q^2 &= \begin{pmatrix}(M_Q)_{11}^2 & (\Delta_{12}^Q)^2 & (\Delta_{13}^Q)^2 \\ \cdot & (M_Q)_{22}^2 & (\Delta_{23}^Q)^2 \\ \cdot & \cdot & (M_Q)_{33}^2\end{pmatrix}, \\ M_U^2 &= \begin{pmatrix}(M_U)_{11}^2 & (\Delta_{12}^U)^2 & (\Delta_{13}^U)^2 \\ \cdot & (M_U)_{22}^2 & (\Delta_{23}^U)^2 \\ \cdot & \cdot & (M_U)_{33}^2\end{pmatrix}, \qquad M_D^2 = \begin{pmatrix}(M_D)_{11}^2 & (\Delta_{12}^D)^2 & (\Delta_{13}^D)^2 \\ \cdot & (M_D)_{22}^2 & (\Delta_{23}^D)^2 \\ \cdot & \cdot & (M_D)_{33}^2\end{pmatrix}, \\ M_L^2 &= \begin{pmatrix}(M_L)_{11}^2 & (\Delta_{12}^L)^2 & (\Delta_{13}^L)^2 \\ \cdot & (M_L)_{22}^2 & (\Delta_{23}^L)^2 \\ \cdot & \cdot & (M_L)_{33}^2\end{pmatrix}, \qquad M_E^2 = \begin{pmatrix}(M_E)_{11}^2 & (\Delta_{12}^E)^2 & (\Delta_{13}^E)^2 \\ \cdot & (M_E)_{22}^2 & (\Delta_{23}^E)^2 \\ \cdot & \cdot & (M_E)_{33}^2\end{pmatrix}\end{aligned} \tag{6.2}$$

which are associated to the left-handed squarks, right-handed up- and down-type squarks, left-handed sleptons and sneutrinos, and right-handed sleptons, respectively. In addition, there are the

trilinear coupling matrices:

$$A_U = \begin{pmatrix} (A_U)_{11} & \Delta_{12}^{AU} & \Delta_{13}^{AU} \\ \Delta_{21}^{AU} & (A_U)_{22} & \Delta_{23}^{AU} \\ \Delta_{31}^{AU} & \Delta_{32}^{AU} & (A_U)_{33} \end{pmatrix}, \quad A_D = \begin{pmatrix} (A_D)_{11} & \Delta_{12}^{AD} & \Delta_{13}^{AD} \\ \Delta_{21}^{AD} & (A_D)_{22} & \Delta_{23}^{AD} \\ \Delta_{31}^{AD} & \Delta_{32}^{AD} & (A_D)_{33} \end{pmatrix}, \\ A_E = \begin{pmatrix} (A_E)_{11} & \Delta_{12}^{AE} & \Delta_{13}^{AE} \\ \Delta_{21}^{AE} & (A_E)_{22} & \Delta_{23}^{AE} \\ \Delta_{31}^{AE} & \Delta_{32}^{AE} & (A_E)_{33} \end{pmatrix} \tag{6.3}$$

for the up- and down-type squarks and the sleptons. Detailed expressions for the diagonal elements of the matrices given in Eqs. (6.2) and (6.3) can be found in Ref. [139]. Note that the soft mass matrices in Eq. (6.2) are symmetric due to the requirement for hermiticity.

It is convenient to parametrize the off-diagonal, i.e. flavour violating, elements of the above matrices in a dimensionless manner by normalizing them to the respective diagonal entries of the sfermion mass matrices. In the SCKM basis, this leads to the following parameters [73];

$$(\delta_{LL}^{Q})_{ij} = \frac{(\Delta_{ij}^{Q})^2}{(M_Q)_{ii}(M_Q)_{jj}}, \quad (\delta_{RR}^{U})_{ij} = \frac{(\Delta_{ij}^{U})^2}{(M_U)_{ii}(M_U)_{jj}}, \quad (\delta_{RR}^{D})_{ij} = \frac{(\Delta_{ij}^{D})^2}{(M_D)_{ii}(M_D)_{jj}}, \\ (\delta_{RL}^{U})_{ij} = \frac{v_u}{\sqrt{2}} \frac{\Delta_{ij}^{AU}}{(M_Q)_{ii}(M_U)_{jj}}, \quad (\delta_{RL}^{D})_{ij} = \frac{v_d}{\sqrt{2}} \frac{\Delta_{ij}^{AD}}{(M_Q)_{ii}(M_D)_{jj}}, \\ (\delta_{LL}^{L})_{ij} = \frac{(\Delta_{ij}^{L})^2}{(M_L)_{ii}(M_L)_{jj}}, \quad (\delta_{RR}^{E})_{ij} = \frac{(\Delta_{ij}^{E})^2}{(M_E)_{ii}(M_E)_{jj}}, \quad (\delta_{RL}^{E})_{ij} = \frac{v_d}{\sqrt{2}} \frac{\Delta_{ij}^{AE}}{(M_L)_{ii}(M_E)_{jj}}, \tag{6.4}$$

with v_u and v_d being the vacuum expectation values of the up- and down-type Higgs doublets, respectively. Note that these definitions hold at any scale. In the following, the scales of interest will be the GUT and TeV scales. Moreover, the situation where all off-diagonal NMFV parameters defined in Eq. (6.4) vanish corresponds to a scenario with quite minimal flavour violation.

We now consider the gauge group $SU(5)$, which is the smallest group containing the SM gauge group, and can accomodate its matter fields in the $F = \overline{\mathbf{5}}$ and $T = \mathbf{10}$ representations according to

$$F = \overline{\mathbf{5}} = \begin{pmatrix} d_r^c \\ d_b^c \\ d_g^c \\ e^- \\ -\nu_e \end{pmatrix}_L, \qquad T = \mathbf{10} = \begin{pmatrix} 0 & u_g^c & -u_b^c & u_r & d_r \\ . & 0 & u_r^c & u_b & d_b \\ . & . & 0 & u_g & d_g \\ . & . & . & 0 & e^c \\ . & . & . & . & 0 \end{pmatrix}_L, \tag{6.5}$$

where r, b, g denote the quark colours, and c denotes CP-conjugated fermions. The Higgs doublets H_u and H_d, which break the electroweak symmetry, may arise from $SU(5)$ multiplets $H_{\mathbf{5}}$ and $H_{\overline{\mathbf{5}}}$, provided the colour triplet components are heavy. The $SU(5)$ gauge group may be broken by an additional Higgs multiplet in the **24** representation developing a vacuum expectation value

$$SU(5) \;\rightarrow\; SU(3)_C \times SU(2)_L \times U(1)_Y\,, \tag{6.6}$$

where complete SM quark and lepton families (Q, u^c, d^c, L, e^c) fit into the representations as

$$\begin{aligned} F(\overline{\mathbf{5}}) &= d^c(\overline{\mathbf{3}}, \mathbf{1}, 1/3) \oplus L(\mathbf{1}, \overline{\mathbf{2}}, -1/2)\,, \\ T(\mathbf{10}) &= u^c(\overline{\mathbf{3}}, \mathbf{1}, -2/3) \oplus Q(\mathbf{3}, \mathbf{2}, 1/6) \oplus e^c(\mathbf{1}, \mathbf{1}, 1)\,. \end{aligned} \tag{6.7}$$

Including the above arguments into a supersymmetric framework, $SU(5)$ symmetry provides relationships between the soft terms belonging to the supermultiplets within a given representation.

For the MSSM under consideration here, we can write down the soft-breaking Lagrangian in terms of $SU(5)$ fields:

$$\begin{aligned}\mathcal{L}_{\text{soft}}^{\text{SU(5)MSSM}} = &-\frac{1}{2}(M_1\widetilde{B}\widetilde{B} + M_2\widetilde{W}\widetilde{W} + M_3\widetilde{g}\widetilde{g} + \text{h.c.}) \\ &- M_F^2\widetilde{F}^\dagger\widetilde{F} - M_T^2\widetilde{T}^\dagger\widetilde{T} \\ &- (A_{TT}\widetilde{T}^* H_u\widetilde{T} + A_{FT}\widetilde{F}^* H_d\widetilde{T} + \text{h.c.}) \\ &- m_{H_u}^2 H_u^* H_u - m_{H_d}^2 H_d^* H_d - (bH_u^* H_d + \text{h.c.}),\end{aligned} \tag{6.8}$$

where $\widetilde{F}$ and $\widetilde{T}$ are the superpartner fields of F and T given in Eq. (6.5). Comparing this with Eq. (6.1) leads to the relations

$$\begin{aligned} M_Q^2 = M_U^2 = M_E^2 &\equiv M_T^2\,, \\ M_D^2 = M_L^2 &\equiv M_F^2\,, \\ A_D = (A_E)^T &\equiv A_{FT}\,, \\ A_U &\equiv A_{TT}\,, \end{aligned} \tag{6.9}$$

that hold at the GUT scale. Note that renormalization group evolution towards lower scales will spoil these relations.

In addition to the $SU(5)$ grand unification, we impose an A_4 flavour symmetry on the model under consideration. To this end, we unify the three families of $F = \bar{\mathbf{5}} = (d^c, L)$ into the triplet of A_4 leading to a unified soft mass parameter m_F for the three generations[2]. The three families of $T_i = \mathbf{10}_i = (Q, u^c, e^c)_i$ are singlets of A_4, which means that the three generations may have independent soft mass parameters m_{T_1}, m_{T_2}, m_{T_3} [110, 137, 140–142].

Through breaking the discrete symmetry just below the GUT scale, we can induce flavour violation in our soft parameters. We express this primordial flavour violation as the matrices M_T^2, M_F^2, A_{FT}, and A_{TT} analogously to Eq. (6.2) in the flavour basis of A_4, that is, before rotation to the SCKM:

$$M_T^2 = \begin{pmatrix} m_{T_1}^2 & (\Delta_{12}^T)^2 & (\Delta_{13}^T)^2 \\ \cdot & m_{T_2}^2 & (\Delta_{23}^T)^2 \\ \cdot & \cdot & m_{T_3}^2 \end{pmatrix}, \qquad M_F^2 = \begin{pmatrix} m_F^2 & (\Delta_{12}^F)^2 & (\Delta_{13}^F)^2 \\ \cdot & m_F^2 & (\Delta_{23}^F)^2 \\ \cdot & \cdot & m_F^2 \end{pmatrix},$$

$$A_{FT} = \begin{pmatrix} (A_{FT})_{11} & \Delta_{12}^{FT} & \Delta_{13}^{FT} \\ \Delta_{21}^{FT} & (A_{FT})_{22} & \Delta_{23}^{FT} \\ \Delta_{31}^{FT} & \Delta_{32}^{FT} & (A_{FT})_{33} \end{pmatrix}, \qquad A_{TT} = \begin{pmatrix} (A_{TT})_{11} & \Delta_{12}^{TT} & \Delta_{13}^{TT} \\ \Delta_{21}^{TT} & (A_{TT})_{22} & \Delta_{23}^{TT} \\ \Delta_{31}^{TT} & \Delta_{32}^{TT} & (A_{TT})_{33} \end{pmatrix}, \tag{6.10}$$

Note that the breaking of A_4 enforces off-diagonal elements of the M_T^2 and A_{FT} matrices in Eq. (6.10) to be smaller than the diagonal entries, and we also assume that off-diagonal elements in the other matrices are small[3]. This provides a theoretical motivation for small, but-non-zero flavour violation in such a class of models. $SU(5)$ gives the following relationships between the dimensionless NMFV parameters in the basis before rotation to the SCKM (as denoted by the

[2] In principle, any group that admits triplet representations can give degenerate soft masses here.

[3] This assumption becomes inevitable when one considers an additional U(1) symmetry as per Ref. [136], which is required for the Froggatt-Nielsen mechanism and to supply correct flavon vev alignment.

subscript '0'):

$$\begin{aligned} \delta^{Q_0}_{LL} &= \delta^{U_0}_{RR} = \delta^{E_0}_{RR} \equiv \delta^{T}, \\ \delta^{D_0}_{RR} &= \delta^{L_0}_{LL} \equiv \delta^{F}, \\ \delta^{D_0}_{RL} &= (\delta^{E_0}_{RL})^{T} \equiv \delta^{FT}, \\ \delta^{U_0}_{RL} &\equiv \delta^{TT} \end{aligned} \tag{6.11}$$

These four matrices parameterise the flavour violation in the $A_4 \times SU(5)$ setup studied here. Note that δ^T, δ^F and δ^{TT} are necessarily symmetric whereas δ^{FT} is not (see Eqs. (6.8) and (6.10)) leading to a total of 15 NMFV parameters at the GUT scale.

It is apparent that we have flavour violation at phenomenological scales from two distinct sources: The presence of off-diagonal elements in various coupling matrices at the GUT scale due to A_4 breaking, and further effects on the off-diagonal elements induced by RGE running. We do not consider a specific breaking mechanism or pattern for the discrete symmetry.

6.3 Method and numerical setup

6.3.1 MFV benchmark points

In order to focus on the impact of NMFV terms in the Lagrangian of our model, we start by choosing suitable reference scenarios respecting the MFV paradigm. From previous work [136] it is apparent that successfully imposing the dark matter relic density as well as the anomalous magnetic moment of the muon on the $A_4 \times SU(5)$ framework requires rather specific parameter configurations. More precisely, the corresponding parameter points feature a physical spectrum where the "right-handed" smuon is light and almost mass-degenerate with the lightest neutralino, which is bino-like. This allows to simultaneously satisfy the $(g-2)_\mu$ and relic density constraints [67, 143]. For our study, we choose two MFV reference scenarios, which are summarized in Table 6.1.

The first reference point of our choice corresponds to the scenario labelled 'BP4' in Ref. [136]. For practical reasons, mainly due to including NMFV terms at the GUT scale, we do not make use of the same version of the spectrum generator `SPheno`. In consequence, effects from renormalization group running differ slightly, and we have adapted the input parameters of the original BP4 reference scenario to the ones given in Table 6.1. However, note that, although there is a small deviation for the TeV scale parameters as compared to scenario BP4 of [136], the phenomenological aspects of our reference scenario at the TeV scale are unaffected. Let us recall that the rather low smuon mass parameter, $m_{T_2} = 200$ GeV, which leads to the physical mass $m_{\tilde{\mu}_R} = 102.1$ GeV, is required in order to satisfy simultaneously the $(g-2)_\mu$ and relic density constraints as discussed in [136]. This particular choice for m_{T_2} is an assumption in this work.

While current limits on "right-handed" smuons still allow masses as low as about 100 GeV [144], this first scenario is going to be severely challenged by ongoing LHC searches. For this reason, we choose to include a second reference point which is inspired by the first one but features larger smuon and neutralino masses. This still fulfilling the relic density constraint due to efficient co-annihilation and avoids LHC limits to be published in the near future. Note that, however, the higher smuon mass $m_{\tilde{\mu}_R} \sim 250$ GeV does not resolve the tension between the Standard Model and the experimental value of $(g-2)_\mu$. Let us emphasize that both reference scenarios capture the essential results of [136], namely almost mass-degenerate "right-handed" smuon and bino-like neutralino, while all other MSSM states are essentially decoupled.

In both reference scenarios, the required neutralino relic density is met thanks to efficient co-annihilation with the smuon and even smuon pair annihilation. All (co)annihilation contributions are summarized in Table 6.2. Neutralino pair annihilation mainly proceeds through t- and u-channel smuon exchange, while smuon pair annihilation proceeds through neutralino t- or u-channel exchange. Moreover, the relative importance of the co-annihilation and smuon pair annihilation

	Parameter/Observable	Scenario 1	Scenario 2
MFV Parameters at GUT scale	m_F	5000	5000
	m_{T_1}	5000	5000
	m_{T_2}	200	233.2
	m_{T_3}	2995	2995
	$(A_{TT})_{33}$	-940	-940
	$(A_{FT})_{33}$	-1966	-1966
	M_1	250.0	600.0
	M_2	415.2	415.2
	M_3	2551.6	2551.6
	m_{H_u}	4242.6	4242.6
	m_{H_d}	4242.6	4242.6
	$\tan\beta$	30	30
	μ	-2163.1	-2246.8
Physical masses	m_h	126.7	127.3
	$m_{\tilde{g}}$	5570.5	5625.7
	$m_{\tilde{\mu}_L}$	4996.7	4997.5
	$m_{\tilde{\mu}_R}$	102.1	254.4
	$m_{\tilde{\chi}_1^0}$	94.6	250.4
	$m_{\tilde{\chi}_2^0}$	323.6	322.0
	$m_{\tilde{\chi}_3^0}$	2248.8	2331.1
	$m_{\tilde{\chi}_4^0}$	2248.8	2331.2
	$m_{\tilde{\chi}_1^\pm}$	323.8	322.2
	$m_{\tilde{\chi}_2^\pm}$	2249.8	2332.2
	$\Omega_{\tilde{\chi}_1^0}h^2$	0.116	0.120
	$\sigma_{\rm SI}^{\rm proton}/10^{-14}\,{\rm pb}$	2.987	1.055
	$\sigma_{\rm SI}^{\rm neutron}/10^{-14}\,{\rm pb}$	3.249	0.986

Table 6.1 – GUT scale inputs together with selected physical masses and relevant TeV scale parameters for the two MFV reference scenarios. First and second generation trilinear couplings are set to zero. Further squark and slepton masses which are beyond the reach of current experiments are not shown. Unless otherwise illustrated, dimensionful quantities are given in GeV. DM direct detection cross-sections are given for both protons and neutrons.

Annihilation channel	Relative contribution to $\Omega_{\tilde{\chi}_1^0} h^2$	
	Scenario 1	Scenario 2
$\tilde{\chi}_1^0 \tilde{\chi}_1^0 \to \mu \bar{\mu}$	27%	2%
$\tilde{\chi}_1^0 \tilde{\mu}_R \to \mu \gamma$	45%	31%
$\tilde{\chi}_1^0 \tilde{\mu}_R \to \mu Z^0$	8%	8%
$\tilde{\mu}_R \tilde{\mu}_R \to \mu \mu$	10%	37%
$\tilde{\mu}_R \tilde{\mu}_R^* \to \gamma \gamma$	3%	11%

Table 6.2 – Dominant annihilation channels contributing to the annihilation cross-section and the neutralino relic density in the two MFV reference scenarios of Table 6.1.

with respect to the neutralino pair annihilation is governed by the Boltzmann factor involving the mass difference of the two particles [145]. The smuon mass therefore plays a central role in this context. Considering NMFV, the off-diagonal elements of the matrices in Eqs. (6.2) and (6.3) not only violate flavour but can in addition have a significant impact on the smuon mass and thus on the relic density.

6.3.2 Introducing NMFV

Starting from the two MFV reference points, we study the impact of flavour violating soft terms by perturbing around this scenario. Keeping the MFV parameters fixed at the values given in Table 6.1, we perform a random scan on the flavour violating parameters introduced in Eq. (6.11) at the GUT scale using flat prior distributions. In practice, we vary the NMFV parameters both independently and as part of a multi-dimensional scan over all parameters simultaneously. We subsequently study the impact of the constraints detailed in Table 6.3.

More precisely, we require the Higgs-boson mass to be reasonably close to the observed value of about 125 GeV, where we account for a theory uncertainty of 2.5 GeV from the `SPheno` calculation. For the B_s-meson oscillation, we consider the experimental value $\Delta M_{B_s} = (17.757 \pm 0.021)$ ps^{-1} [67] and add a theory uncertainty of 1.35 ps^{-1} [69] which dominates over the experimental error. For the neutralino relic density, we require that the lightest neutralino accounts for the totality of observed cold dark matter. The error given by the Planck collaboration is augmented in order to take into account the 1% accuracy of the theoretical calculation of the relic density by `micrOMEGAs`. For further details on experimental constraints we refer the reader to Table 6.3 and the references therein.

Finally, note that although the reference scenarios defined in Table 6.1 have in part been obtained considering the anomalous magnetic moment of the muon as a key observable [136], we do not take into account this constraint here. Since $(g-2)_\mu$ is a flavour-conserving process, we do not expect sizeable effects from NMFV terms on this observable within the ranges that are allowed from the other constraints.

For numerical evaluation, we make use of the spectrum generator `SPheno 4.0.3` [146, 147], where we have included the MSSM with general flavour mixing using the `Mathematica` package `SARAH 4.12.3` [152–155]. From the resulting code `SPhenoMSSM` we obtain through two-loop renormalization group equations for the soft-breaking parameters and the physical mass spectrum at the TeV scale, as well as numerical predictions for flavour observables listed in Table 6.3. The neutralino relic density $\Omega_{\tilde{\chi}_1^0} h^2$ is computed using the public package `micrOMEGAs 4.3.5` [149–151]. Again, we have used `SARAH` to obtain the `CalcHEP` model files necessary to accomodate NFMV effects in the calculation. Our computational setup is summarized in Fig. 6.1. The mass spectrum obtained from `SPhenoMSSM` is handed to `micrOMEGAs` by making use of the *SUSY Les Houches Accord 2* [63]. Note that, since the spin-independent scattering cross-sections related to direct dark matter detection given in Table 6.1 are relatively low as compared to the corresponding experimental limits, we do

Observable	Constraint	Remarks	Refs.
m_h	(125.2 ± 2.5) GeV	(SPheno th.)	[67, 146, 147]
$\mathrm{BR}(\mu \to e\gamma)$	$< 4.2 \times 10^{-13}$	90% (exp.)	[67]
$\mathrm{BR}(\mu \to 3e)$	$< 1.0 \times 10^{-12}$	90% (exp.)	[67]
$\mathrm{BR}(\tau \to e\gamma)$	$< 3.3 \times 10^{-8}$	90% (exp.)	[67]
$\mathrm{BR}(\tau \to \mu\gamma)$	$< 4.4 \times 10^{-8}$	90% (exp.)	[67]
$\mathrm{BR}(\tau \to 3e)$	$< 2.7 \times 10^{-8}$	90% (exp.)	[67]
$\mathrm{BR}(\tau \to 3\mu)$	$< 2.1 \times 10^{-8}$	90% (exp.)	[67]
$\mathrm{BR}(\tau \to e^-\mu\mu)$	$< 2.7 \times 10^{-8}$	90% (exp.)	[67]
$\mathrm{BR}(\tau \to e^+\mu\mu)$	$< 1.7 \times 10^{-8}$	90% (exp.)	[67]
$\mathrm{BR}(\tau \to \mu^- ee)$	$< 1.8 \times 10^{-8}$	90% (exp.)	[67]
$\mathrm{BR}(\tau \to \mu^+ ee)$	$< 1.5 \times 10^{-8}$	90% (exp.)	[67]
$\mathrm{BR}(B \to X_s\gamma)$	$(3.32 \pm 0.18) \times 10^{-4}$	2σ (exp.)	[148]
$\mathrm{BR}(B_s \to \mu\mu)$	$(2.7 \pm 1.2) \times 10^{-9}$	2σ (exp.)	[67]
ΔM_{B_s}	$(17.757 \pm 0.042 \pm 2.7)$ ps^{-1}	2σ (exp.), (th.)	[67, 69]
ΔM_K	$(3.1 \pm 1.2) \times 10^{-15}$ GeV	2σ (th.)	[67, 70]
ϵ_K	2.228 ± 0.29	2σ (th.)	[67, 70]
$\Omega_{\mathrm{CDM}}h^2$	0.1198 ± 0.0042	2σ (exp.), 1% (th.)	[143, 149–151]

Table 6.3 – Experimental constraints imposed on the $A_4 \times SU(5)$ MSSM parameter space in our study. Upper limits are given at the 90% confidence level, while two-sided limits are understood at the 2σ confidence level.

not explicitly evaluate these cross-section in our NMFV scan.

Before running `SPheno`, we first need to perform a CKM transformation to certain GUT scale matrices to comply with the basis that `SPheno` requires for the input parameters (see Appendix B. Let us note that, for typical values of Yukawa parameters inserted into our MFV reference points, CKM matrix running between the GUT and TeV scales has been found to be negligible (order 10% for the smallest element). We therefore assume that the CKM matrix is identical across all scales.

In the full multi-dimensional scan, the studied range for each parameter is set empirically to give reasonable computational efficiency as informed by one-dimensional scans over individual parameters. The obtained ranges have been increased slightly to be able to study whether correlations between the different NMFV parameters may result in larger allowed ranges as compared to the one-dimensional scan. The applied limiting values for each MFV scenario under consideration and for each NMFV parameter are given in Table 6.4.

Already from the individual scans, it becomes apparent that for certain NMFV parameters, especially in the case of Scenario 1, small deviations from the MFV case can induce either a charged dark matter candidate (the smuon in this case) or tachyonic mass spectra. We therefore set

$$(\delta^T)_{23} \;=\; (\delta^{FT})_{21} \;=\; (\delta^{FT})_{32} \;=\; 0 \tag{6.12}$$

throughout the analysis of Scenario 1, and scan over the remaining 12 NMFV parameters according to Table 6.4. This situation does not occur for Scenario 2, where we vary all 15 NMFV parameters.

Starting from parameters at the GUT scale, we test each point against the observables listed in Table 6.3. Points which do not satisfy all the imposed constraints within the associated uncertainties are collected in the prior distribution only, while those which comply with all constraints are in addition recorded as part of the posterior distribution. In examining the latter, we obtained the allowed ranges for each of the NMFV parameters. In addition, by comparing the prior and posterior

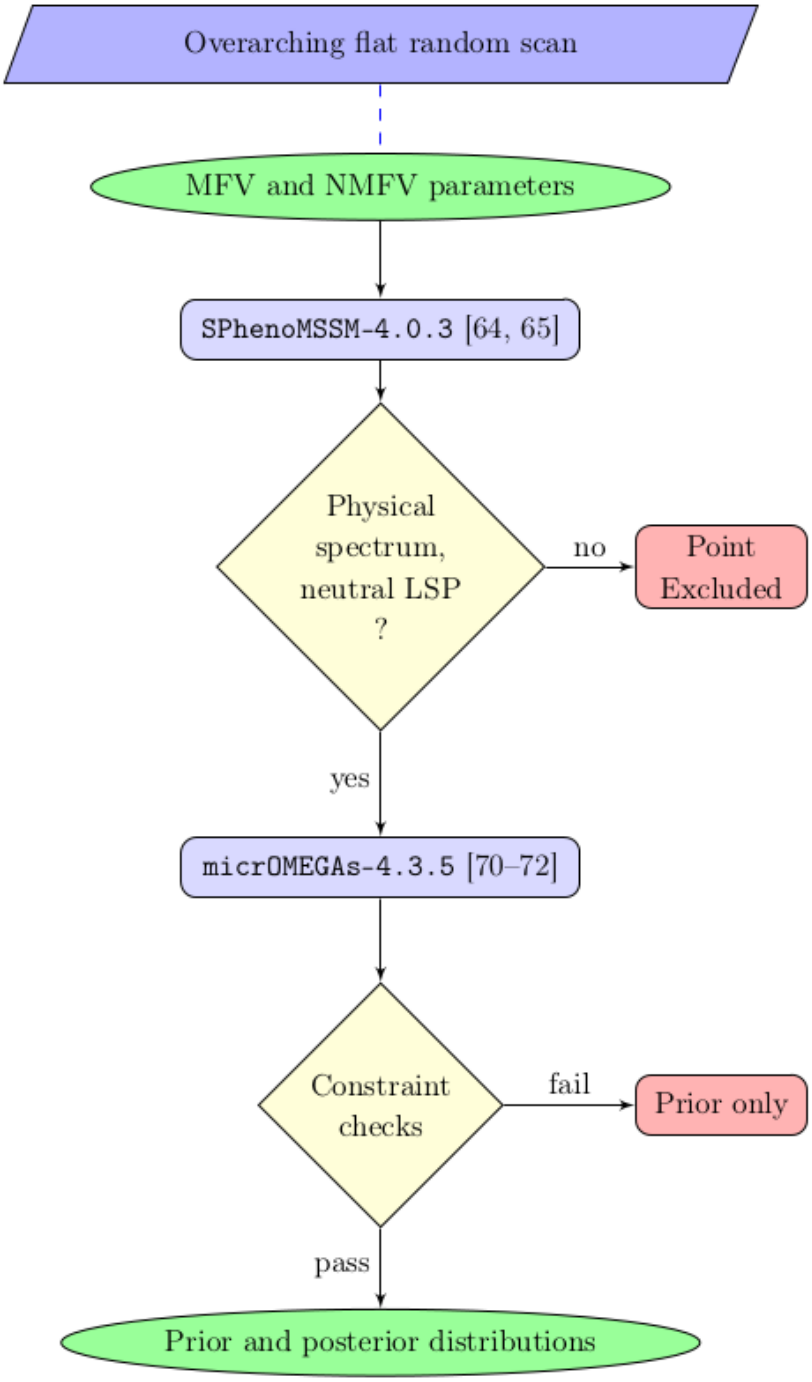

Figure 6.1 – Illustration of the computational procedure applied to each individual point of our parameter scan.

Parameters	Scenario 1	Scenario 2
$(\delta^T)_{12}$	$[-2.00, 2.00] \times 10^{-2}$	$[-5.57, 5.15] \times 10^{-2}$
$(\delta^T)_{13}$	$[-8.01, 8.01] \times 10^{-2}$	$[-0.267, 0.301]$
$(\delta^T)_{23}$	0.0	$[-5.73, 5.73] \times 10^{-2}$
$(\delta^F)_{12}$	$[-8.00, 8.00] \times 10^{-3}$	$[-8.00, 8.00] \times 10^{-3}$
$(\delta^F)_{13}$	$[-1.00, 1.00] \times 10^{-2}$	$[-8.00, 8.00] \times 10^{-2}$
$(\delta^F)_{23}$	$[-1.60, 1.60] \times 10^{-2}$	$[-8.00, 8.00] \times 10^{-2}$
$(\delta^{TT})_{12}$	$[-8.69, 10.43] \times 10^{-4}$	$[-7.46, 8.95] \times 10^{-4}$
$(\delta^{TT})_{13}$	$[-1.74, 1.74] \times 10^{-3}$	$[-3.48, 1.74] \times 10^{-3}$
$(\delta^{TT})_{23}$	$[-0.0174, 0.145]$	$[-0.0871, 0.124]$
$(\delta^{FT})_{12}$	$[-4.64, 4.64] \times 10^{-5}$	$[-5.47, 5.47] \times 10^{-5}$
$(\delta^{FT})_{13}$	$[-7.74, 7.74] \times 10^{-5}$	$[-3.87, 3.87] \times 10^{-4}$
$(\delta^{FT})_{21}$	0.0	$[-1.04, 1.04] \times 10^{-4}$
$(\delta^{FT})_{23}$	$[-1.16, 1.16] \times 10^{-4}$	$[-2.32, 2.32] \times 10^{-4}$
$(\delta^{FT})_{31}$	$[-1.39, 1.39] \times 10^{-5}$	$[-8.81, 8.81] \times 10^{-5}$
$(\delta^{FT})_{32}$	0.0	$[-1.49, 1.49] \times 10^{-4}$

Table 6.4 – Ranges of the NMFV parameters defined at the GUT scale (see Eq. (6.11)) for our multi-dimensional scans around the reference scenarios. Those parameters given as 0.0 have been switched off, since even small variations lead to tachyonic mass spectra and/or a charged LSP.

distributions, and taking into account posterior distributions based on a single constraint, we identify the most important constraints among those listed in Table 6.3 for each NMFV parameter. The results are presented in the next Section.

6.4 Results and Discussion

In this Section we present the results of our analysis. Before coming to a more detailed discussion, we start by presenting the general aspects and the obtained limits on the NMFV parameters, presented in Table 6.5. Ultimately, we perform two different kinds of scan on the parameter space: "individual" scans, where only a single δ is varied and all others are set to zero, and "simultaneous" scans where all of the NMFV parameters are varied at the same time according to the ranges given in Table 6.4.

From the multi-dimensional scan, we conclude that for the majority of the considered NMFV parameters, the most sensitive observables are the branching ratios of $\mu \to e\gamma$ and $\mu \to 3e$, as well as the neutralino relic density $\Omega_{\tilde{\chi}_1^0} h^2$. As discussed in Section 6.3, the impact of the relic density can be attributed to the small mass difference between the neutralino and the smuon, which depends strongly on the off-diagonal elements in the slepton mass matrix. Since both our reference scenario exhibit a relatively small value of $(m_T)_{22}$, already rather tiny flavour violating elements can be excluded by current data.

Although the experimental limit is more stringent (by about a factor of two) for the decay $\mu \to e\gamma$, the $\mu \to 3e$ decay has about the same constraining power and is in certain cases even the dominant constraint. This is explained as follows: The amplitude of $\mu \to e\gamma$ is helicity-suppressed, and therefore contains a suppression factor m_e/m_μ. While this is also the case for $\mu \to 3e$ diagrams related to those of $\mu \to e\gamma$, there are additional four-point diagrams, where the helicity suppression

Parameters	Scenario 1	Most constraining obs. 1	Scenario 2	Most constraining obs. 2
$(\delta^T)_{12}$	[-0.015, 0.015]	$\mu \to 3e$, $\mu \to e\gamma$, $\Omega_{\tilde{\chi}_1^0}h^2$	[-0.12, 0.12]†	$\Omega_{\tilde{\chi}_1^0}h^2$, $\mu \to e\gamma$
$(\delta^T)_{13}$	]-0.06, 0.06[	$\Omega_{\tilde{\chi}_1^0}h^2$	[-0.3, 0.3]†	$\Omega_{\tilde{\chi}_1^0}h^2$
$(\delta^T)_{23}$	[0,0]*	$\Omega_{\tilde{\chi}_1^0}h^2$, $\mu \to 3e$, $\mu \to e\gamma$	[-0.1, 0.1]†	$\Omega_{\tilde{\chi}_1^0}h^2$, $\mu \to 3e$, $\mu \to e\gamma$,
$(\delta^F)_{12}$	[-0.008, 0.008]	$\mu \to 3e$, $\mu \to e\gamma$	[-0.015, 0.015]†	$\mu \to 3e$, $\mu \to e\gamma$
$(\delta^F)_{13}$	]-0.01, 0.01[	$\mu \to e\gamma$	[-0.15, 0.15]†	$\mu \to 3e$, $\mu \to e\gamma$
$(\delta^F)_{23}$	]-0.015, 0.015[	$\mu \to e\gamma$, $\Omega_{\tilde{\chi}_1^0}h^2$	[-0.15, 0.15]†	$\Omega_{\tilde{\chi}_1^0}h^2$, $\mu \to e\gamma$, $\mu \to 3e$
$(\delta^{TT})_{12}$	[-3, 3.5] $\times 10^{-5}$	prior	[-1, 1.5]† $\times 10^{-3}$	prior, $\Omega_{\tilde{\chi}_1^0}h^2$
$(\delta^{TT})_{13}$	]-6, 7[$\times 10^{-5}$	prior, $\Omega_{\tilde{\chi}_1^0}h^2$	[-4, 2.5]† $\times 10^{-3}$	prior, $\Omega_{\tilde{\chi}_1^0}h^2$
$(\delta^{TT})_{23}$	]-0.5, 4[$\times 10^{-5}$	prior, $\Omega_{\tilde{\chi}_1^0}h^2$	[-0.25, 0.2]†	prior, $\Omega_{\tilde{\chi}_1^0}h^2$
$(\delta^{FT})_{12}$	[-0.0015, 0.0015]	$\Omega_{\tilde{\chi}_1^0}h^2$	[-1.2, 1.2]† $\times 10^{-4}$	$\mu \to 3e$, $\Omega_{\tilde{\chi}_1^0}h^2$, $\mu \to e\gamma$
$(\delta^{FT})_{13}$	]-0.002, 0.002[	$\Omega_{\tilde{\chi}_1^0}h^2$	[-5, 5] $\times 10^{-4}$	$\Omega_{\tilde{\chi}_1^0}h^2$, $\mu \to 3e$, $\mu \to e\gamma$
$(\delta^{FT})_{21}$	[0,0]*	prior	[-1.2, 1.2]† $\times 10^{-4}$	$\Omega_{\tilde{\chi}_1^0}h^2$, prior
$(\delta^{FT})_{23}$	]-0.0022, 0.0022[	$\Omega_{\tilde{\chi}_1^0}h^2$	[-6, 6]† $\times 10^{-4}$	$\mu \to 3e$, $\Omega_{\tilde{\chi}_1^0}h^2$, $\mu \to e\gamma$
$(\delta^{FT})_{31}$	]-0.0004, 0.0004[	$\Omega_{\tilde{\chi}_1^0}h^2$	[-2, 2]† $\times 10^{-4}$	$\Omega_{\tilde{\chi}_1^0}h^2$
$(\delta^{FT})_{32}$	[0,0]*	prior	[-1.5, 1.5] $\times 10^{-4}$	$\Omega_{\tilde{\chi}_1^0}h^2$

Table 6.5 – Estimated allowed GUT scale flavour violation for both reference scenarios and impactful constraints ordered from the most to the least constraining. Where square brackets are shown open, we scan up to these values but even if we noticed some impact from constraints, it seems that the allowed region can be larger and extrapolation to concrete limits is not straightforward. * denotes parameters fixed to 0 in order to satisfy LSP and physical mass spectrum requirements. † stands for extrapolated ranges, meaning that the posterior does not actually drop to 0 but extrapolation to a limit is reasonable. A parameter that is constrained by 'prior' is limited by LSP and physical mass requirement.

is lifted since no photon is involved. Despite the additional gauge coupling and the greater degree of loop suppression, these diagrams are numerically competitive to those of $\mu \to e\gamma$.

One can see that NMFV parameters mixing the first or second generation with the third generation are also mainly constrained by the decays $\mu \to e\gamma$ and $\mu \to 3e$ rather than by the corresponding τ decays such as $\tau \to \mu\gamma$ or $\tau \to e\gamma$. This can be traced to the better experimental precision of the muonic decay measurements with respect to the analogous tau decays. Even though NMFV parameters mediating $e - \tau$ or $\mu - \tau$ transitions lead to the dominant contributions of the tau decays, these parameters also can enter into the muon decay amplitudes. For example, if the $\mu \to e\gamma$ process includes a stau in the loop, the corresponding amplitude is proportional to terms including products of the type $(\delta)_{23}(\delta)_{13}$. See Fig. 6.2 for a diagrammatic representation. Since the muon decay limits are stronger than the tau decay limits by four to five orders of magnitude, the $e - \tau$ and $\mu - \tau$ mixing parameters are constrained by the $e - \mu$ processes first. We have explicitly checked this by artificially lowering the bounds on tau decays. In this case, the tau decay becomes the dominant constraint for the $(\delta)_{13}$ and $(\delta)_{23}$ parameters.

Finally, we observe that the constraints coming from the hadronic sector, such as the decays $B \to X_s\gamma$ or $B_s \to \mu^+\mu^-$, which are dominant in the case of NMFV in the squark sector alone [66], are not competitive as compared to the leptonic constraints mentioned above. This can be traced to the greater experimental precision of dedicated leptonic measurements compared to meson decays.

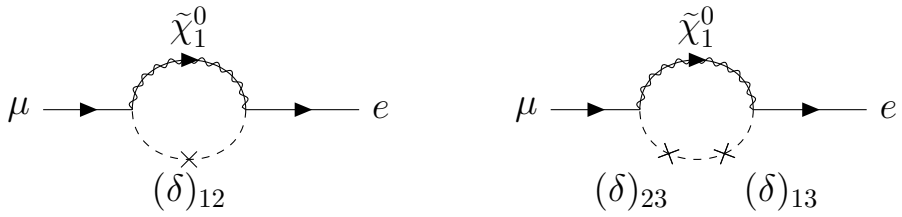

Figure 6.2 – Feynman diagrams that contribute to $\mu \to e\gamma$, dashed line represents a slepton and δ denotes mass insertion parameters. Photon should be taken to be emitted from any particle charged under QED.

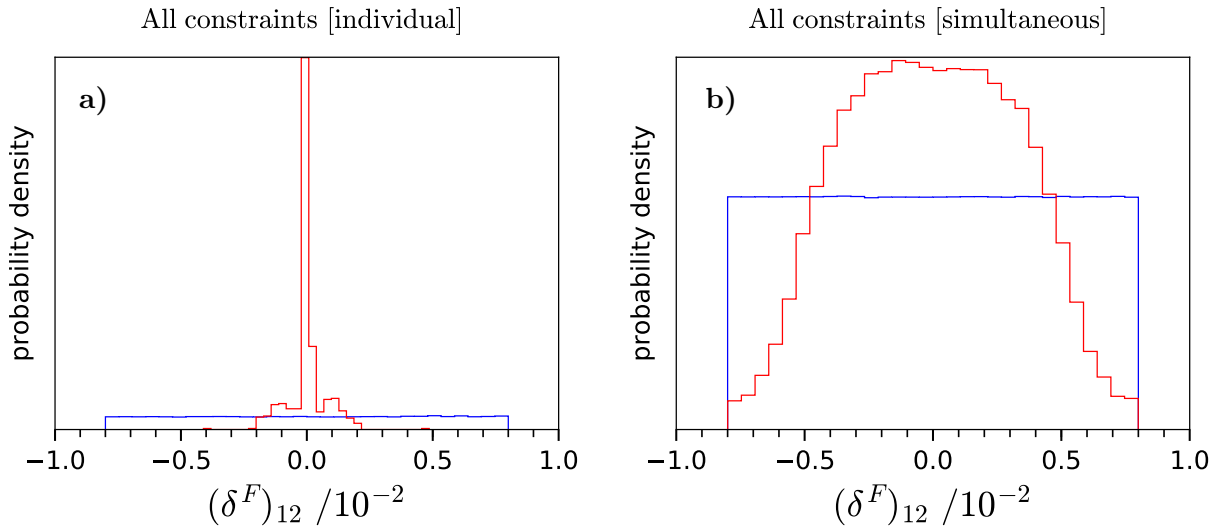

Figure 6.3 – Comparison of individual (panel a)) vs. simultaneous (panel b)) scan of the NMFV parameter $(\delta^F)_{12}$ around Scenario 1. Each panel shows the prior (blue) together with the posterior (red) distributions.

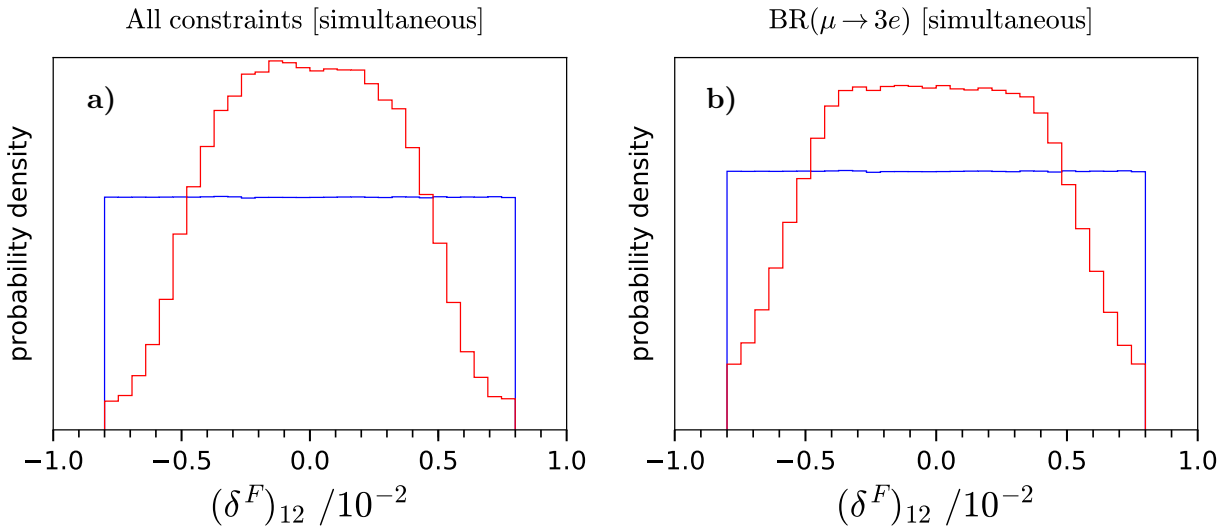

Figure 6.4 – Dominant constraints on the parameter $(\delta^F)_{12}$ from simultaneous scan around Scenario 1. Prior distributions are given in blue and posterior distribution are given in red.

6.4.1 Scan around Scenario 1

We discuss here in detail the results obtained for the full NMFV scan around the reference scenario 1. The MFV parameters are fixed at the values given in Table 6.1, while we scan over the NMFV parameters according to the ranges given in Table 6.4, either individually (i.e. keeping all but one parameter to zero), or simultaneously. For each performed scan, we record the prior distribution containing all points featuring a physical mass spectrum and neutralino dark matter candidate (see also Fig. 6.1) as well as the posterior distribution obtained when imposing either one or all constraints summarized in Table 6.3.

Fig. 6.3 shows the obtained prior and posterior distributions for the NMFV parameter $(\delta^F)_{12}$. The viable region for this parameter with respect to the imposed constraints is much larger for the case of the simultaneous scan as compared to the individual scan result. Indeed, it is possible that more than one of the NMFV parameters enters the calculation of one or more observables. In such a case, interferences and/or cancellations between the contributions induced by different NMFV parameters can occur. As a consequence, they give rise to viable regions of parameter space that would not be fully explored when varying each parameter in isolation. This is seen quantitatively as a broadening of posterior distributions when comparing a simultaneous scan result against a histogram from an individual scan. Let us emphasize that this feature is present for several of the flavour violating parameters under consideration in our study.

Fig. 6.4, panel b) shows the action of a single observable, BR($\mu \to 3e$), on the same parameter $(\delta^F)_{12}$ for simulultaneous scan, and can thus be directly compared to Fig. 6.3 [4]. Since the shape of the single-constraint posterior almost matches the posterior obtained imposing all constraints, we conclude that this parameter is mainly limited by the $\mu \to 3e$ lepton decay bound. The $\mu \to e\gamma$ observable is less important in this case (see Table 6.5, corresponding posterior not shown).

Coming to the parameter $(\delta^T)_{12}$ shown in Fig. 6.5 including all constraints, note that the obtained viable interval is again broadened when comparing the simultaneous scan, leading to $|(\delta^T)_{12}| \lesssim 0.2 \times 10^{-2}$, with the individual one yielding the range $|(\delta^T)_{12}| \lesssim 1.6 \times 10^{-2}$. For the same NMFV parameter $(\delta^T)_{12}$, we detail in Fig. 6.6 the effect of the three most important experimental constraints in the simultaneous scan. The $\mu \to e\gamma$ constraint can be seen to admit the entirety of the scanned region of parameter space in the simultaneous scan, whereas it is far the most stringent constraint in the individual scan (see Fig. 6.5). Indeed, $\mu \to 3e$ is the most constraining observable for this parameter when varied along with other flavour violating entries of mass matrices. In addition, Fig. 6.6 illustrates how the obtained shape of the posterior distribution is due to the influence of three experimental constraints imposed on the parameter space.

We now discuss the parameter $(\delta^T)_{13}$ shown in Fig. 6.7. We can notice that it is constrained only by the neutralino relic density and that the flavour constraints have no effect. This gives insight on the unexpected shape of the posterior distribution: As we have seen for two examples above, other NMFV parameters are allowed under flavour constraints to shift significantly away from zero. This has a marked effect in reducing superpartner masses which are determined by diagonalising the mass-squared matrices from Eq. (6.2). This applies in particular to the "right-handed" smuon mass, as the initial smallness of m_{T_2} means that small NMFV parameters can slightly lower the smuon mass. As a further consequence, the relic density is then reduced due to the smaller mass difference between smuon and neutralino, which increases the importance of co-annihilation and smuon pair annihilation. However, the smuon mass also is influenced by $(\delta^T)_{13}$, which by virtue of being unconstrained by flavour observables, may be non-zero. Moreover, this particular parameter increases the lightest smuon mass due to the specific hierarchies in the mass matrix. The smuon mass being decreased by other non-zero NMFV parameters, $(\delta^T)_{13}$ being non-zero then re-establishes the initial mass difference between the smuon and neutralino allowing the relic density to stay within the Planck limits. If one relaxes the assumption that the neutralino $\tilde{\chi}_1^0$ is the only dark matter candidate, i.e. relax the lower limit on the relic density, then the caracteristic shape observed for

[4] Note that panel b) of Fig. 6.3 is identical to panel a) in Fig. 6.4.

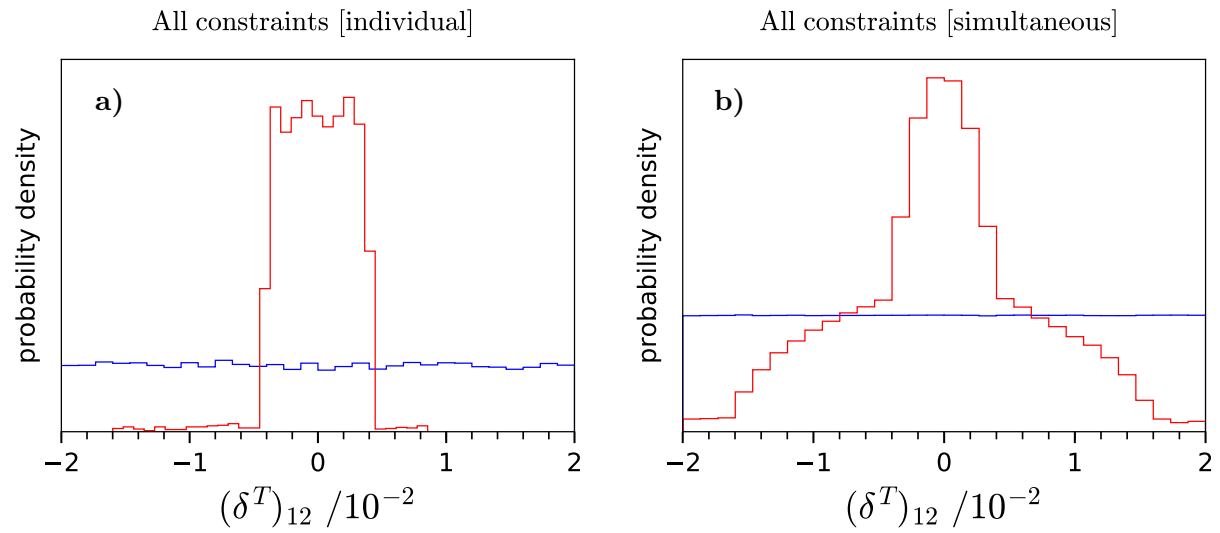

Figure 6.5 – Comparison of individual (left) vs. simultaneous (right) scan of the NMFV parameter $(\delta^T)_{12}$ around Scenario 1. Each panel shows the prior (blue) together with the posterior (red) distributions.

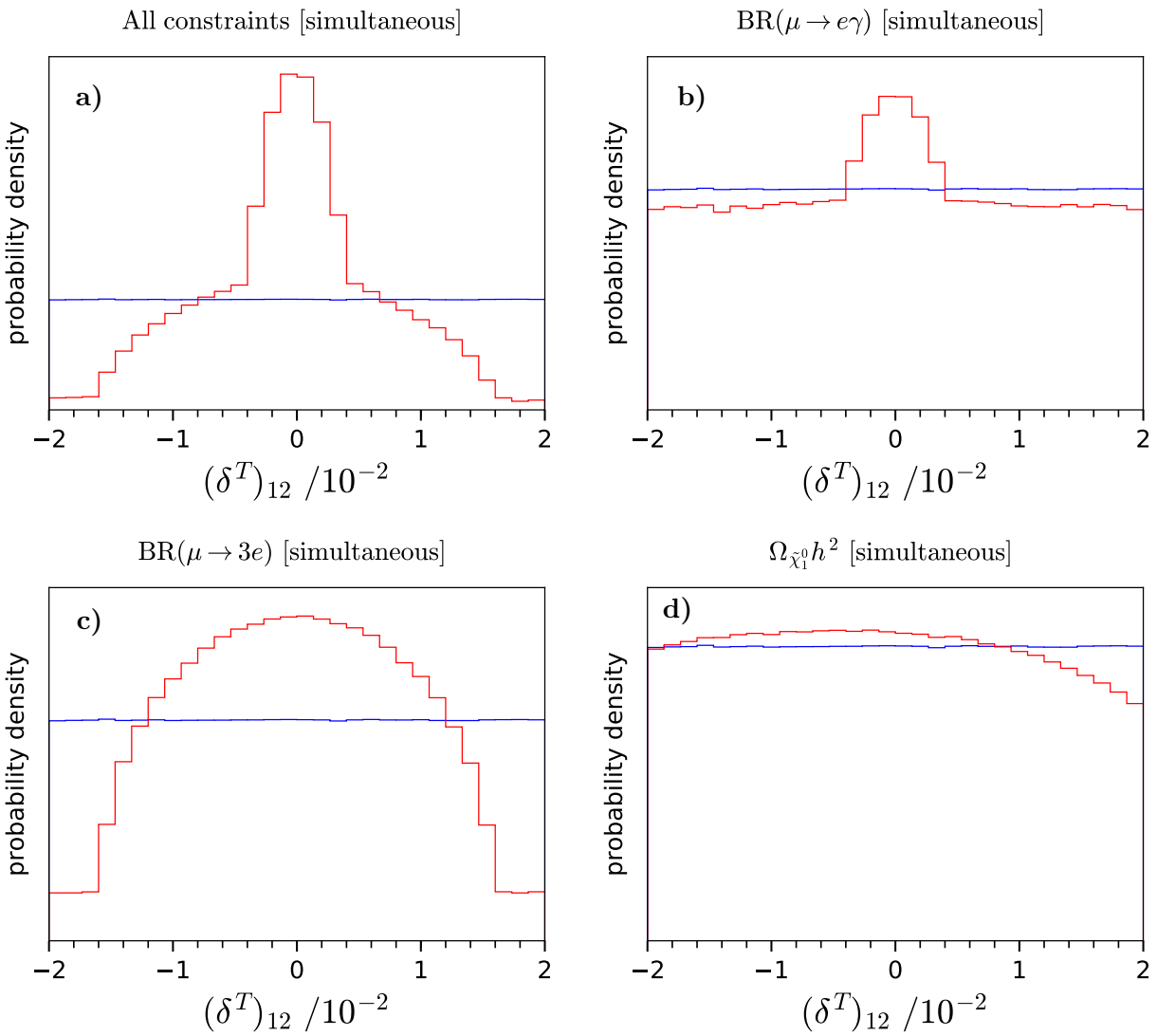

Figure 6.6 – Dominant constraints on the parameter $(\delta^T)_{12}$ from simultaneous scan around Scenario 1. Prior distributions are given in blue and posterior distribution are given in red.

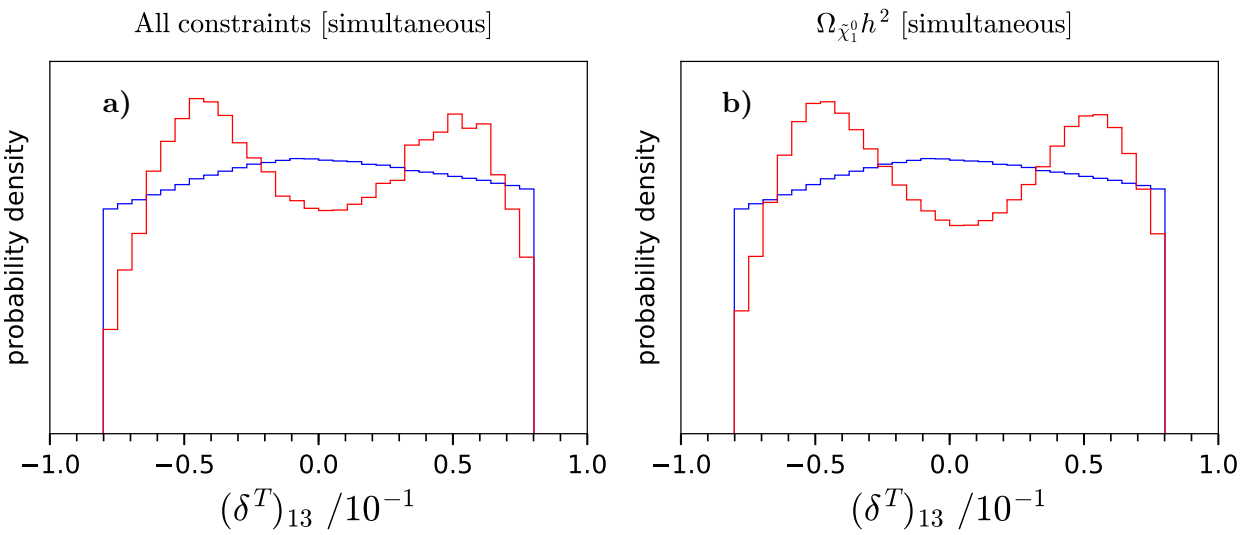

Figure 6.7 – Dominant constraints on the parameter $(\delta^T)_{13}$ from simultaneous scan around Scenario 1. Prior distributions are given in blue and posterior distribution are given in red.

$(\delta^T)_{13}$ in Fig. 6.7 disappears.

Any NMFV parameters among those listed in Table 6.4 whose distributions are not detailed here do not have any interesting phenomena associated with the imposed constraints, therefore the reader can deduce the full effect and resulting ranges from Table 6.5. Recall that for this scenario, the parameters $(\delta^T)_{23}$, $(\delta^{FT})_{21}$, and $(\delta^{FT})_{32}$ have been set to zero due to requirements for a physical spectrum and neutral LSP. For all δ^{TT} parameters, the main requirements are for a physically relevant spectrum and uncharged LSP, hence we conclude that the *prior* distribution dominantes over flavour observables that we test against here. Finally, we do not discuss the δ^{FT} parameters as the corresponding results are much the same as for the scan around Scenario 2 presented in the following.

From the discussed results related to reference Scenario 1, it is clear that varying the NMFV parameters individually is not sufficient to properly explore the entirety of parameter space. For this reason, we do not discuss individual variations any further.

6.4.2 Scan around Scenario 2

Here, we discuss selected results of the simultaneous scan of all 15 NMFV parameters around Scenario 2. NMFV parameters are varied according to the ranges given in Table 6.4, while the MFV parameters are fixed to the values given in Table 6.1. Note that the change of the MFV parameters as compared to Scenario 1 allows the variation of all 15 NMFV parameters, while three of them were set to zero for Scenario 1. This yields limits on the full range of flavour violation allowed in Scenario 2.

Starting the discussion with the parameter $(\delta^T)_{13}$ for which we present the resulting prior and posterior distributions in Fig. 6.8, we observe the same feature as for Scenario 1 (see Fig. 6.7), but more pronounced. Again, slightly positive or negative values for $(\delta^T)_{23}$ counteract the effects of other NMFV parameters on the neutralino relic density as explained previously.

Coming to the parameter $(\delta^F)_{13}$, Fig. 6.9 shows that, rather than a single observable having a clear effect, cumulatively $\mu \to e\gamma$, $\mu \to 3e$, and $\Omega_{\tilde{\chi}_1^0}h^2$ constrain the parameter together with each having a similar effect. Here, we see particularly the effect of flavour violating muon decays on $(\delta)_{13}$ parameters as elaborated upon in the beginning of Section 6.4.

In the same way as for Scenario 1, all δ^{TT} parameters are constrained by the "prior" requirement of a physical mass spectrum and a neutralino dark matter candidate. Flavour observables

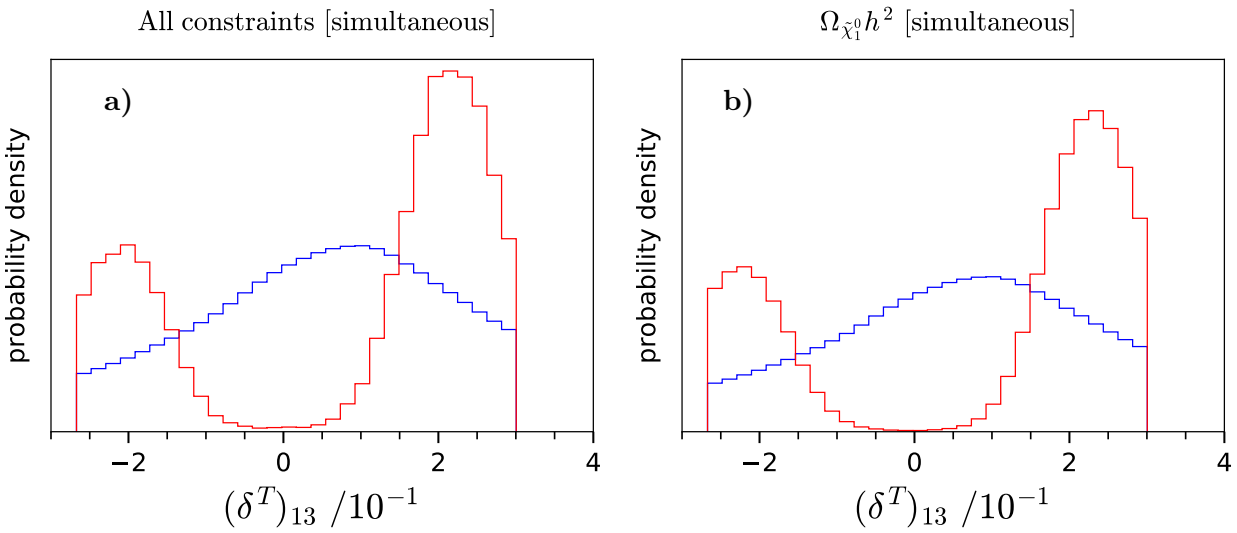

Figure 6.8 – Dominant constraints on the parameter $(\delta^T)_{13}$ from simultaneous scan around Scenario 2. Prior distributions are given in blue and posterior distribution are given in red.

have a negligible effect (see Table 6.5).

An example of the posterior distribution for δ^{FT} parameters is shown in Fig. 6.10, namely for $(\delta^{FT})_{13}$. This parameter is constrained almost entirely by the relic density bound, as can be seen in the similarity of the two panels. Let us recall that complete information on limits and dominant constraints of all NMFV parameters associated with Scenario 2 is summarized in Table 6.5.

6.4.3 SUSY Scale NMFV parameters for Scenario 2

While from the model-building point of view it is useful to explore the allowed level of flavour violation at the GUT scale, it is equally important to explore the resulting physics at the SUSY scale. Renormalization group running from the GUT scale to the SUSY scale will break the unification conditions given in Eq. (6.9) and consequently in Eq. (6.11). The fact that these relations are not valid any more below the GUT scale is an essential and intrinsic part of Grand Unification. The present Section is devoted to highlighting selected results related to the NMFV parameters obtained at the SUSY scale. More precisely, we study the behaviour of different SUSY scale NMFV parameters which stem from a single NMFV parameter at the GUT scale.

In Fig. 6.11 we show the example of $(\delta^F)_{12}$, defined at the GUT scale, and the two resulting SUSY scale parameters $(\delta^L_{LL})_{12}$ and $(\delta^D_{RR})_{12}$, which belong to the slepton and down-type squark sectors, respectively. First, we see that the prior distribution is altered by the renormalization group effects between the GUT scale in panel a) and the SUSY scale distributions in panels b) and c). The imposed flat priors at the GUT scale are transformed into almost Gaussian-like distributions at the SUSY scale. Looking at the corresponding posteriors, the SUSY scale distributions look even more peaked than the corresponding GUT scale histrograms.

Second, it is interesting to note that, at the SUSY scale, the allowed range for the hadronic parameter $(\delta^D_{RR})_{12}$ is wider than that for the related leptonic parameter $(\delta^L_{LL})_{12}$ in the simultaneous scan. This behaviour is somewhat unexpected, since the gluino running, which is blind to flavour, drives the diagonal squark mass parameters higher, while it leaves the leptonic ones unaffected. In turn, this is expected to reduce the squark NMFV parameters once normalized as per Eq. (6.4) [73]. We find that this behaviour is confirmed for all NMFV parameters stemming from *individual* scans (see examples in Fig. 6.11 panels d) and e)), agreeing with the results presented in Ref. [73]. However, for the δ^F parameters, the reverse is true when considering the *simultaneous* scan. We suspect that strong renormalization group effects are the cause of this feature, due to the fact that

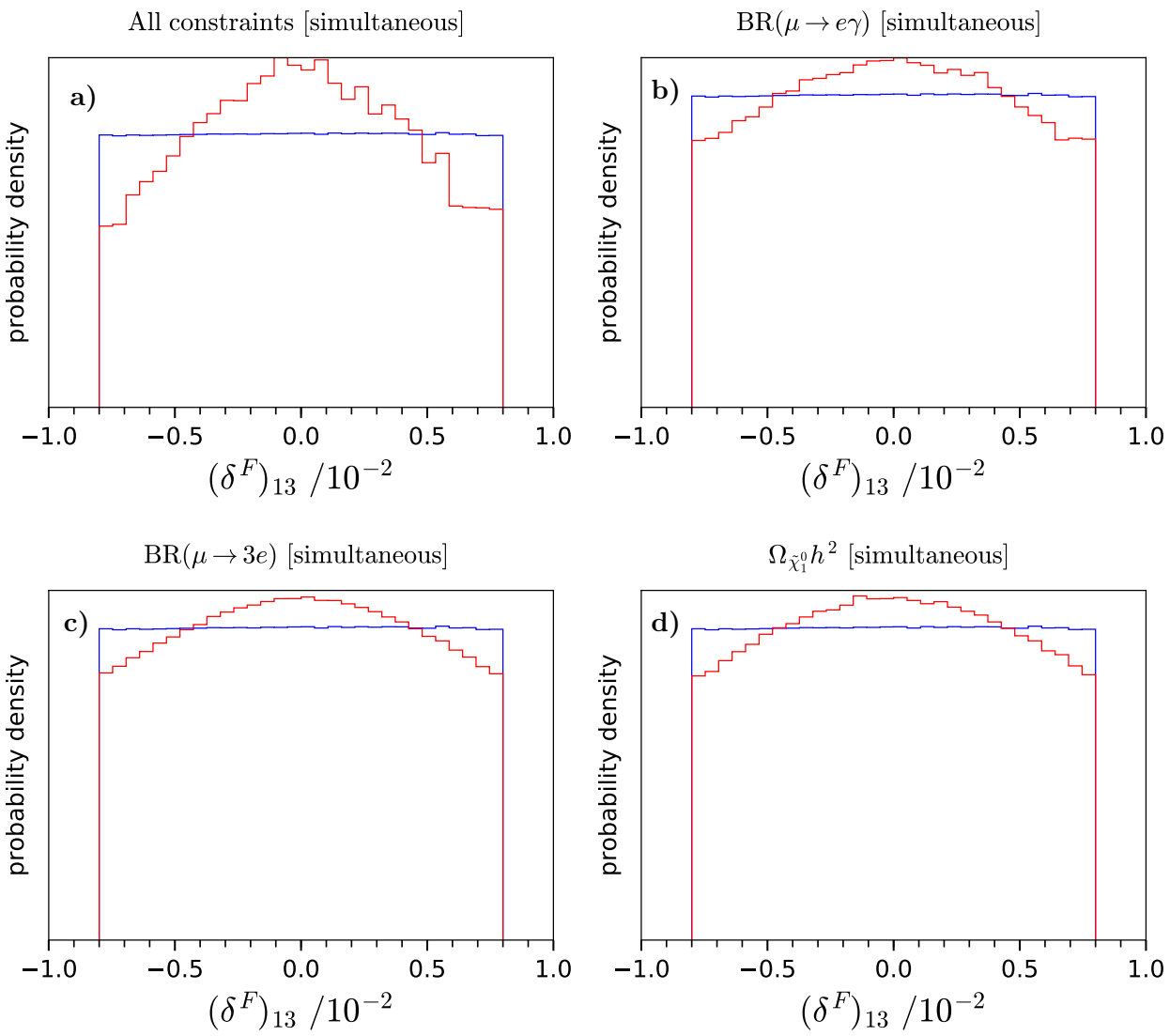

Figure 6.9 – Dominant constraints on the parameter $(\delta^F)_{13}$ from simultaneous scan around Scenario 2. Prior distributions are given in blue and posterior distribution are given in red.

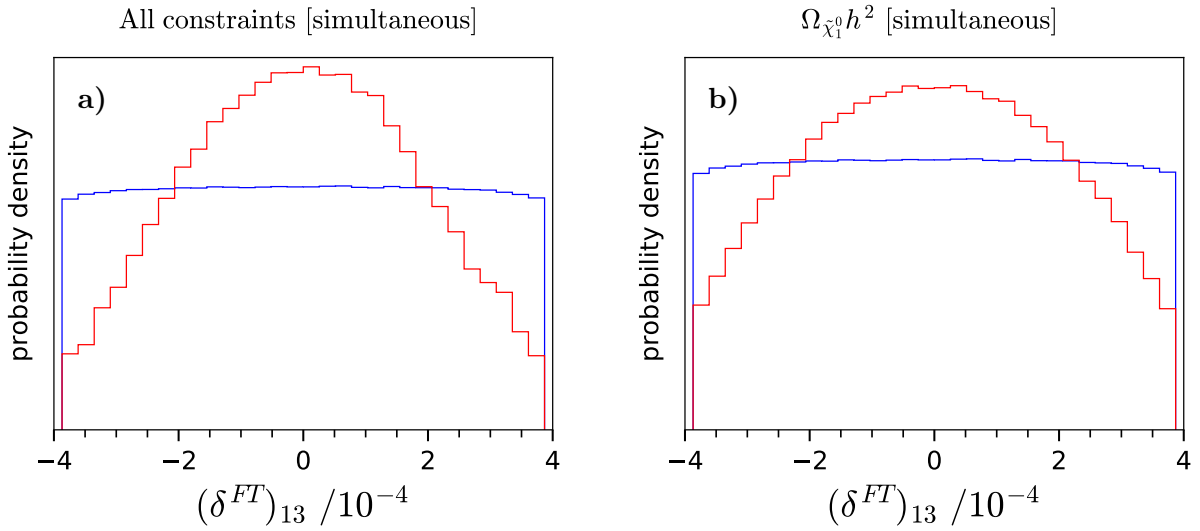

Figure 6.10 – Dominant constraints on the parameter $(\delta^{FT})_{13}$ from simultaneous scan around Scenario 2. Prior distributions are given in blue and posterior distribution are given in red.

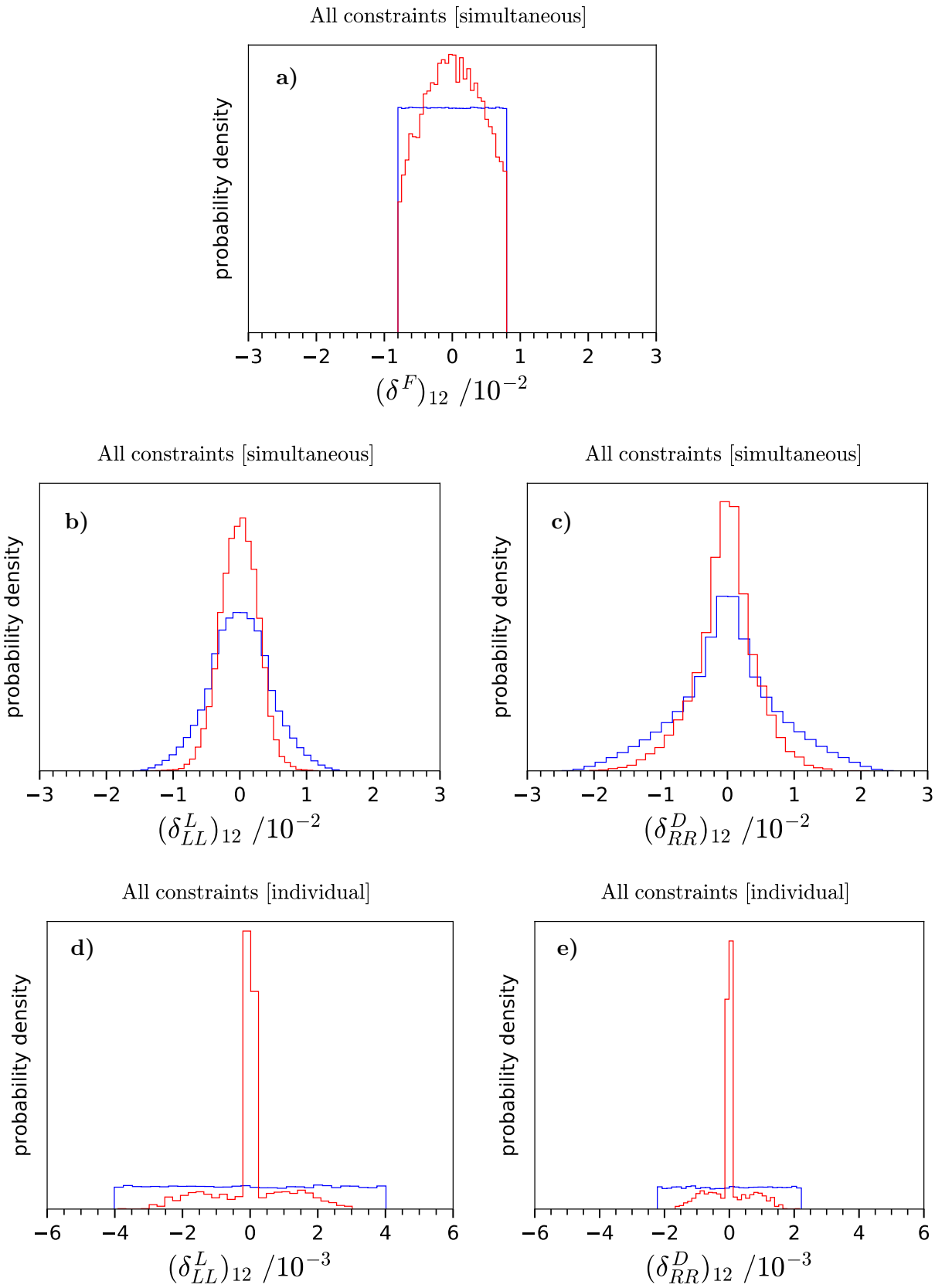

Figure 6.11 – Distributions obtained for the GUT-scale parameter $(\delta^F)_{12}$ and the associated SUSY-scale parameters $(\delta^L_{LL})_{12}$ and $(\delta^D_{RR})_{12}$ (see Eq. (6.4)) from simultaneous (b) and c)) and individual (d) and e)) scan around Scenario 2. Analogously to other results, prior distributions are shown in blue and posterior distributions are shown in red.

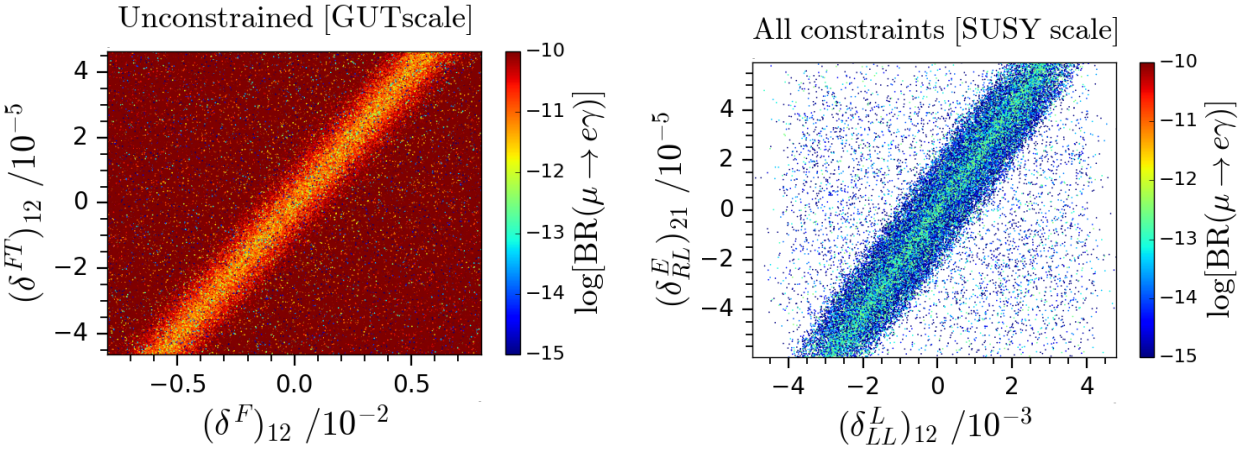

Figure 6.12 – Correlation of the GUT-scale parameters $(\delta^F)_{12}$ and $(\delta^{FT})_{12}$ (left panel) and associated correlation of the SUSY-scale parameters $(\delta^L_{LL})_{12}$ and $(\delta^E_{RL})_{12}$ (right panel) for Scenario 1. While the first plot shows the results for the full scan, the second one shows only the surviving points once the constraints of Table 6.3 are applied.

multiple NMFV parameters interact with each other during the evolution from the GUT scale to the SUSY scale.

6.4.4 Parameter Correlations

In this section, we examine more closely the correlation between certain NMFV parameters, mentioned already several times in the above discussion, and being the reason that scanning over all parameters simultaneously is ultimately required. The key is that cancellations may exist between the contributions from certain parameters in the calculation of a given observable. However, dealing with analytical results for the different experimental constraints is difficult and beyond the scope of this work. Instead, we choose to take advantage of the numerical results, showing posterior distributions of more than one NMFV parameter together.

The first panel in Fig. 6.12 shows viable parameter points that seem to follow a "golden line", with an increased density of points concentrated around a linear relationship between the GUT scale parameters $(\delta^F)_{12}$ and $(\delta^{FT})_{12}$. Indeed, the impact of BR($\mu \to e\gamma$) is suppressed in this line due to cancellation between the two parameters in the analytic expression for this observable. One can also see this in the right panel that only those points lying close to or along said correlation line are consistent with the experimental limits. Said correlation could provide an interesting hint for future SUSY GUT model building.

The analytic expression for the decay rate of $\mu \to e\gamma$ can be written as [73]

$$\frac{\mathrm{BR}(\ell_i \to \ell_j \gamma)}{\mathrm{BR}(\ell_i \to \ell_j \nu_i \nu_j)} = \frac{48\pi^3 \alpha}{G_F^2}(|F_L^{ij}|^2 + |F_R^{ij}|^2) \tag{6.13}$$

where the branching ratio of the decay $\ell_i \to \ell_j \nu_i \nu_j$ is a constant with respect to the NMFV parameters under consideration in the present work. For real NMFV parameters, the form factors $F_{L,R}$ are related to the flavour violating parameters at the SUSY scale according to

$$\begin{aligned} F_L^{ij} &= c_1(\delta^L_{LL})_{ij} + c_2(\delta^E_{RL})_{ij}\,, \\ F_R^{ij} &= c_3(\delta^L_{RR})_{ij} + c_4(\delta^E_{RL})_{ji}\,. \end{aligned} \tag{6.14}$$

The coefficients c_i $(i = 1, \ldots, 4)$ are combinations of loop factors, masses, and other numerical inputs which can be assumed to be constant in our analysis. Minimizing the form factors $F_{L,R}$ in

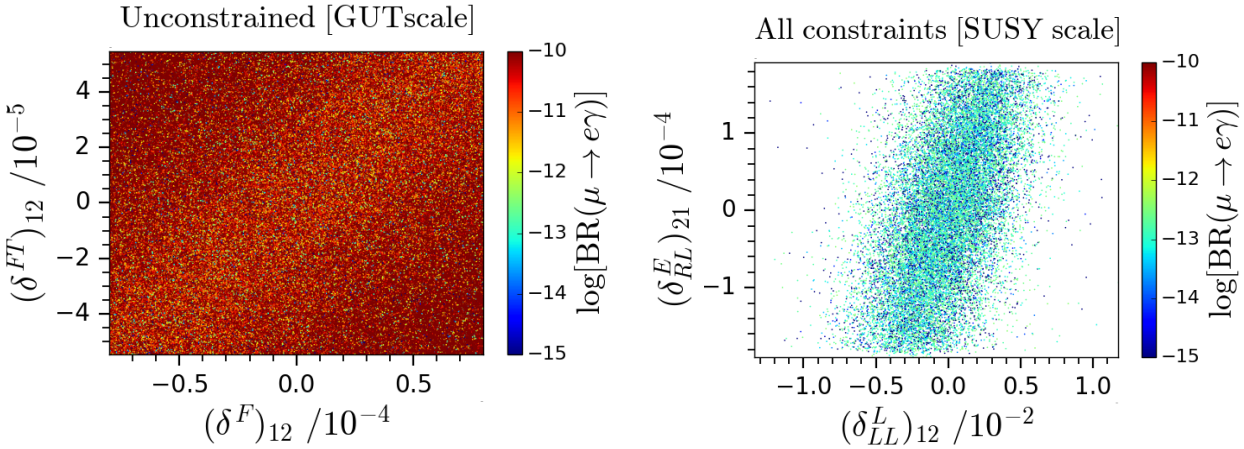

Figure 6.13 – Correlation of the GUT-scale parameters $(\delta^F)_{12}$ and $(\delta^{FT})_{12}$ (left panel) and associated correlation of the SUSY-scale parameters $(\delta^L_{LL})_{12}$ and $(\delta^E_{RL})_{12}$ (right panel) for Scenario 2. While the first plot shows the results for the full scan, the second one shows only the surviving points once the constraints of Table 6.3 are applied.

Eq. (6.14) to yield small $\mu \to e\gamma$ branching ratios and hence satisfy the experimental constraint leads to relations of the form

$$(\delta^L_{LL})_{ij} \;=\; -\frac{2c_2}{c_1}\,(\delta^E_{RL})_{ij}\,, \tag{6.15}$$

corresponding to the observed lines in Figs. 6.12 and 6.13. As such, the "golden line" that we recover purely from our numerical analysis is consistent with the analytic formulae for this lepton flavour-violating decay.

6.5 Conclusion and further projects

In this analysis we have considered CP-conserving non-minimal flavour violation in $A_4 \times SU(5)$ inspired Supersymmetric Grand Unified Theories (GUTs), focussing on the regions of parameter space where Dark Matter is successfully accommodated due to a light right-handed smuon a few GeV heavier than the lightest neutralino dark matter candidate. Such regions of parameter space are obtained by choosing the second generation T_2 to have a light soft mass, while the heavy gluino mass ensured that all squarks in this multiplet are heavy after RG running to low energy. We have considered two scenarios along those lines, one with a very light right-handed smuon, which is capable of being discovered or excluded by the LHC very soon, but which can account for the $(g-2)_\mu$ results, and another scenario with a somewhat heavier smuon. In such regions of parameter space we have found that some of the flavour violating parameters, in particular $(\delta^T)_{13}$ and $(\delta^{FT})_{32}$, are constrained by the requirement of dark matter relic density, due to the delicate interplay between the smuon and neutralino masses.

By scanning over many of the GUT scale flavour violating parameters, constrained by low energy quark and lepton flavour violating observables, we have discovered a striking difference between the results in which individual parameters are varied to those where multiple parameters are varied simultaneously, where the latter relaxes the constraints on flavour violating parameters due to cancellations and/or correlations. Since charged lepton flavour violation provides the strongest constraints within a GUT framework, due to relations between quark and lepton flavour violation, we have examined in detail a prominent correlation between the flavour violating parameters $(\delta^F)_{12}$ and $(\delta^{FT})_{12}$ at the GUT scale consistent with the stringent lepton flavour violating process $\mu \to e\gamma$.

By switching on both flavour violating parameters together, we have seen that much larger flavour violation is allowed than if only one of them were permitted separately. We have examined this correlation also in terms of the resulting low energy flavour violating parameters in the quark and lepton sectors, and have provided some analytic estimates to understand the origin of the observed correlation.

Precision flavour physics measurements could present challenges to this work and warrant further attention. Particularly, situations such as this often predict small-but-non-zero branching ratios for the LFV decays $\mu \to e\gamma$ and $\mu \to 3e$, hence stricter bounds on such processes will further limit the amount of NMFV allowed in such scenarios. Figs. 6.12 and 6.13 are purely data-driven and shows the regions that experimental data prefers; a model which predicts such a correlation could allow reasonable flavour violation and still be preferred over other such models.

In general, we have examined the relation between GUT scale and low scale flavour violating parameters, for both quarks and leptons, and shown how the usual expectations may be violated due to the correlations when multiple parameters are varied simultaneously. We have presented results in the framework of non-minimal flavour violation in $A_4 \times SU(5)$ inspired Supersymmetric Grand Unified Theories, with smuon assisted dark matter. Such a framework is interesting since it allows both successful dark matter and contributions to $(g-2)_\mu$, as well as providing the smoking gun prediction of a light right-handed smuon accessible at LHC energies.

To go beyond this scope, we are actually investing a more complete flavoured GUT model, described in [109]. The model includes a specific breaking pattern and therefore is giving rise to Yukawa coupling predictions for the SM particles. In addition, the see-saw mechanism is implemented to ensure correct mass hierarchy for the neutrinos. This model is highly predictive, and therefore, our current strategy is to run an MCMC code to fit the parameters, taking into account SM measurements such as the SM particle masses and fermionic mixing patterns as well as the contributions from the SUSY partners in terms of flavour violating observables and DM relic density.

Chapter 7

Leptoquarks and flavour symmetries

In this chapter, we leave the SUSY framework and focus on a BSM extension which add leptoquarks to the SM content. These new fields will couple to the leptons and the quarks and can lead to a very rich phenomenology. Leptoquarks have regained interest in the past few years, in particular since the observation of the ratios $R_{K^{(*)}}$ by the LHCb and Belle collaborations [17, 18]. The observations suggest discrepancies between the SM predictions and the experimental measures, which hint towards new physics to be explained. However, new updates presented in Moriond 2019 [156] place the experimental measurements closer to the SM predictions. Nevertheless, leptoquarks are motivated by different frameworks and remain an interesting BSM extension.

In this chapter, we will adopt a flavour symmetry framework, which can be used to enforce the leptoquark couplings, a priori general, to have a very specific and predictive structure. We will then develop a strategy to identify various flavour groups that can lead to viable fermionic mixing matrices alongside with highly predictive leptoquark coupling patterns. This chapter is based on the publication [157].

7.1 Introduction

Flavoured phenomena are amongst the best measured, and least theoretically understood, of the Standard Model (SM) of particle physics. Accounting for Dirac (Majorana) neutrinos, the extended SM permits at least 20 (22) free parameters associated to fermionic mass and mixing, and all but one (three) have reliable constraints provided by experiment — early hints at the leptonic Dirac CP-violating phase exist, albeit with large uncertainties (see e.g. [116]). Furthermore, while all of these unexplained free parameters are associated to Yukawa terms, the strong and electroweak interactions of the SM are otherwise flavour blind; gluons, $W^{\pm}$, and Z gauge bosons couple equally to each fermion species. The SM's flavour expectations are therefore strikingly different between its scalar and vector interactions, with the former furnishing the so-called *flavour problem* described above, and the latter providing opportunities for precision tests of fermion universality through the decays of heavy mesons (among other tests).

Intriguingly, recent hints from LHCb [17, 18] indicate deviations from SM predictions through lepton non-universal (LNU) decays of B-mesons, in particular in the ratio observables

$$R_{K^*,[a,b]} = \frac{\int_a^b dq^2 \ [d\Gamma(B \to K^* \mu^+ \mu^-)/dq^2]}{\int_a^b dq^2 \ [d\Gamma(B \to K^* e^+ e^-)/dq^2]} \,. \tag{7.1}$$

Here, q^2 is the invariant mass of the dilepton final state, and $[a, b]$ represent bin boundaries in GeV^2. Experimentally, Eq. (7.1) is measured as a double ratio with respect to the resonant high-statistics J/Ψ channel for dilepton production, in order to cancel uncertainties in the measurement efficiencies of the signal modes, and is further shown to only probe Lepton Non-Universality (LNU) in flavour changing neutral current (FCNC) decays by testing explicit universality in the J/Ψ production channels, which are observed to be consistent with the SM [158]. Coupling this robust experimental strategy with rather precise predictions in the SM, where scale and other theory uncertainties for the

Ratio	Bin (GeV^2)	Data	Experimental Reference
R_K	[1, 6]	$0.745^{+0.090}_{-0.074} \pm 0.036$	LHCb [18]
R_{K^*}	[1.1, 6.0]	$0.685^{+0.113}_{-0.069} \pm 0.047$	LHCb [17]
	[0.045, 1.1]	$0.66^{+0.11}_{-0.07} \pm 0.03$	LHCb [17]

Table 7.1 – $R_{K^{(*)}}$ as measured by the LHCb collaboration. Also see [162] and footnote 1.

individual decay channels cancel in the ratio [159], it is broadly agreed that one can safely regard Eq. (7.1) as clean tests of LNU. Since LHCb results for both R_K and R_{K^*} deviate individually between 2-3 σ from the SM expectation [159, 160] — cf. Table 7.1[1] — it is then worth considering the sorts of new physics that can generate these early hints of LNU.

Several theory papers have addressed the anomalous data in Table 7.1, including model-independent fits to the operators of low-energy effective field theory (EFT) [163–170] as well as concrete beyond-the-Standard Model (BSM) constructions employing composite- or multi-Higgs, leptoquark, or Z' fields (to name a few) [171–198]. In what follows we explore scenarios where the SM flavour problem is addressed alongside of $R_{K^{(*)}}$,[2] and we will do so by incorporating one of the following leptoquark representations into the SM Lagrangian:

$$\Delta_3 \sim (\bar{3}, 3, 1/3)\,, \quad \Delta_1^\mu \sim (3, 1, 2/3)\,, \quad \Delta_3^\mu \sim (3, 3, 2/3)\,, \tag{7.2}$$

where the charges given are those of the SM gauge group defined by $\mathcal{G}_{SM} \equiv SU(3)_C \times SU(2)_L \times U(1)_Y$. We will respectively refer to the states in Eq. (7.2) as the scalar triplet, vector singlet, and vector triplet, and all can account for $R_{K^{(*)}} < 1$ [167]. When added to the field content of the SM they source the following new $\mathcal{G}_{SM}$-invariant terms in the Lagrangian:

$$\begin{aligned}
\Delta_3: &\quad \mathcal{L} \supset y^{LL}_{3,ij} \bar{Q}^{C\,i,a}_L \epsilon^{ab} (\tau^k \Delta^k_3)^{bc} L^{j,c}_L + z^{LL}_{3,ij} \bar{Q}^{C\,i,a}_L \epsilon^{ab} ((\tau^k \Delta^k_3)^\dagger)^{bc} Q^{j,c}_L + \text{h.c.} \\
\Delta_1^\mu: &\quad \mathcal{L} \supset x^{LL}_{1,ij} \bar{Q}^{i,a}_L \gamma^\mu \Delta_{1,\mu} L^{j,a}_L + x^{RR}_{1,ij} \bar{d}^i_R \gamma^\mu \Delta_{1,\mu} e^j_R + x^{\overline{RR}}_{1,ij} \bar{u}^i_R \gamma^\mu \Delta_{1,\mu} \nu^j_R + \text{h.c.} \\
\Delta_3^\mu: &\quad \mathcal{L} \supset x^{LL}_{3,ij} \bar{Q}^{i,a}_L \gamma^\mu \left(\tau^k \Delta^k_{3,\mu}\right)^{ab} L^{j,b}_L + \text{h.c.}
\end{aligned} \tag{7.3}$$

where $\{a, b\}$ are SU(2) indices, $\{i, j\}$ are flavour indices, and $k = 1, 2, 3$ for the Pauli matrices. As can be seen, the scalar triplet generates a diquark operator that can source proton decay, and the vector singlet introduces new physical interactions between right-handed (RH) fields — see [199] for a thorough review of the physics of leptoquarks.

Generically, the coefficients in Eq. (7.3) are 3×3 complex matrices in flavour space, just like the Yukawa couplings of the SM. Particular textures in (e.g.) $x^{LL}_{1,3}$ or y^{LL}_3 will then generate different phenomenology [200–203], and so only special patterns for these couplings are capable of explaining $R_{K^{(*)}} < 1$ (or any other observable sensitive to their inclusion). Predictions in such models therefore require that one either 1) *assumes* a particular form for $x^{LL}_{1,3}$, y^{LL}_3 or 2) *structures* them within an extended theoretical framework, perhaps including a flavour symmetry $\mathcal{G}_\mathcal{F}$. Only the latter allows to simultaneously address the observed scalar and vector LNU, and to that end multiple collaborations have attempted specific 'flavourings' of the SM and its $R_{K^{(*)}}$-inspired leptoquark extensions (see e.g. [171, 173, 177, 178, 186–188, 190, 192–195]). Our goal is to instead determine what sorts of $\mathcal{G}_\mathcal{F}$ can generate successful patterns of CKM, PMNS, and leptoquark mixing matrices (associated to $x^{LL}_{1,3}$, y^{LL}_3) in a model-*independent* fashion.

[1] Results for an updated value of R_K incorporating Run 2 data from the LHCb collaboration have recently been presented in [156, 161]. While the tension with the SM remains at $\sim 2.5\sigma$ if both Run 1 and Run 2 data sets are included, the Run 2 data appears consistent with unity when analyzed alone.

[2] Note however that the formalism we develop is generic, and can be applied to other Lagrangians addressing different combinations of experimental signals.

Although we want to determine viable $\mathcal{G}_\mathcal{F}$ without committing to specific model-building assumptions, e.g. the dynamics of flavour symmetry breaking, we will focus on a particular class of $\mathcal{G}_\mathcal{F}$: non-Abelian discrete symmetries (NADS), which are well-motivated by both infrared (IR) and ultra-violet (UV) physics. Furthermore, we will study NADS in the context of the residual flavour symmetry (RFS) mechanism, where one assumes that $\mathcal{G}_\mathcal{F}$ breaks to global Abelian flavour symmetries $\mathcal{G}_a$ ($a \in \{u, d, l, \nu\}$) in some or all of the SM mass terms and (now) also the leptoquark-sourced terms in Eq. (7.3). The residual $\mathcal{G}_a$ then control the shapes of the relevant Yukawa-like couplings in the IR, and the specific forms of the generators that action them can be used to 'reconstruct' the parent $\mathcal{G}_\mathcal{F}$. The RFS framework generalizes the symmetry-breaking patterns of entire classes of popular flavour models, and as a result has become a useful tool for studying flavour both analytically and numerically within the SM [101, 107, 204–225] — reviews can be found in [100, 226, 227]. In fact, RFS have been used to define a novel set of 'Simplified Models of Flavourful Leptoquarks' [171], where (highly-restrictive) consequences were derived when the *same* RFS representations are assumed to act in SM and leptoquark terms. However, in [171], the authors did not use the generators of $\mathcal{G}_a$ to reconstruct viable $\mathcal{G}_\mathcal{F}$. Here we perform this closure using a bottom-up and automated technique developed in [107, 216], both for the symmetry breaking described in [171] and for a highly natural relaxation of it. The method employs scripts written with the computational finite algebra package `GAP` [228, 229], and we will use them to scan over NADS capable of sourcing interesting phenomenology. Importantly, our approach is applicable to any flavoured leptoquark scenario, and therefore will remain relevant regardless of the experimental status of $R_{K^{(*)}}$.

The Chapter develops as follows: In Sec. 7.2 we review the RFS mechanism, first in the context of the SM alone and then when leptoquarks are included. We also distinguish two specific symmetry-breaking environments (labeled SE1 and SE2) to scan over, and further derive the 'leptoflavour basis' where all relevant physical mixings in the theory can be communicated to our `GAP` scripts. In Section 7.3 we review our bottom-up approach for scanning NADS and give details regarding the current BSM leptoquark application. Finally, we perform the `GAP` scans for SE1 and SE2 respectively in Sections 7.4-7.5, where additional details relevant to each are presented and a plethora of $\mathcal{G}_\mathcal{F}$ are discovered. Closing remarks are provided in Section 7.6.

7.2 Residual Flavour Symmetries with Leptoquarks

Before continuing to study the SM when enhanced by a new leptoquark field, we first review the Residual Flavour symmetry (RFS) mechanism in the context of the SM alone [101, 107, 204–223]. As stated above, the core assumption in the RFS framework is that, regardless of the symmetry-breaking mechanism or any dynamics associated to it, a UV flavour symmetry $\mathcal{G}_\mathcal{F}$ breaks to global Abelian flavour symmetries $\mathcal{G}_a$ in some or all of the SM mass terms:

$$\mathcal{G}_\mathcal{F} \to \begin{cases} \mathcal{G}_\mathcal{L} \to \begin{cases} \mathcal{G}_\nu \\ \mathcal{G}_\mathrm{l} \end{cases} \\ \mathcal{G}_\mathcal{Q} \to \begin{cases} \mathcal{G}_\mathrm{u} \\ \mathcal{G}_\mathrm{d} \end{cases} \end{cases} \tag{7.4}$$

where for illustration we have sketched a symmetry-breaking chain to all four fermion families through two intermediate non-Abelian symmetries $\mathcal{G}_{\mathcal{L},\mathcal{Q}}$ that control only leptons or quarks. Other breaking patterns are of course also conceivable. Regardless, the scenario outlined in Eq. (7.4) appears quite natural as, after all, the mass terms of SM charged fermions and (if present) Dirac neutrinos already exhibit accidental $U(1)^3$ global symmetries associated to independent rephasings of each generation. If neutrinos are instead Majorana fields they respect an accidental $\mathbb{Z}_2 \times \mathbb{Z}_2$ Klein symmetry. To see this explicitly we write down the SM Yukawa sector after EWSB, in the fermion

mass basis:

$$\mathcal{L}^{SM}_{mass} \supset \frac{1}{2}\bar{\nu}^c_L\, m_\nu\, \nu_L + \bar{E}_R\, m_l\, l_L + \bar{d}_R\, m_d\, d_L + \bar{u}_R\, m_u\, u_L + \text{h.c.} \tag{7.5}$$

where for now we have included a Majorana neutrino mass term, as may be generated in a any seesaw mechanism [230], to illustrate our point. Here m_a are all diagonal matrices of mass eigenvalues. We now observe that Eq. (7.5) is invariant under the following operations on its fields:

$$\begin{aligned} &\nu_L \to T_{\nu_i}\nu_L, \quad \text{with} \quad T_{\nu 1} = diag\,(1,-1,-1) \quad \text{and} \quad T_{\nu 2} = diag\,(-1,1,-1)\,, \\ &f \to T_f f, \quad \text{with} \quad T_f = diag\left(e^{i\alpha_f}, e^{i\beta_f}, e^{i\gamma_f}\right) \quad \text{for} \quad f \in \{e_R, l_L, d_R, d_L, u_R, u_L\}. \end{aligned} \tag{7.6}$$

In Eq. (7.6) we have simply arranged the action of the aforementioned accidental Abelian symmetries into (reducible) triplet representations whose diagonal elements distinguish different generations. Clearly $T_{\nu_{1,2}}$ generate the Klein four-group and T_f generates the respective $U(1)^3$ of Dirac fermions.[3] If one instead wishes to identify a discrete subgroup of $U(1)^3$, as we will below in order to identify NADS, the free phases get quantized as

$$\{\alpha,\beta,\gamma\}_f \overset{!}{=} \frac{2\pi}{m}\{a,b,c\}_f \tag{7.7}$$

with m the order of the cycle symmetry $\mathbb{Z}_m$ being generated. Cyclic product subgroups with more than one generator are also possible and potentially interesting.

In the RFS framework, the symmetries described by Eq. (7.6) are no longer accidental — they represent the infrared (IR) signatures of a complete flavour theory controlled by $\mathcal{G}_\mathcal{F}$, which commutes with the entire SM (or any BSM completion, e.g. an $SU(5)$ grand unified theory). For example, $\mathcal{G}_a$ may appear when, in some or all SM Yukawa operators, scalar flavon fields break $\mathcal{G}_\mathcal{F}$ via vacuum expectation values (VEVs) aligned along special directions of flavour space. Thinking from the top down, these special alignments (and therefore the particular $\mathcal{G}_a$ realized) are a consequence of the form of a $(\mathcal{G}_\mathcal{F} \times \mathcal{G}_{(\mathcal{B})\mathcal{SM}})$-invariant scalar potential. On the other hand, from a bottom-up perspective, different phase configurations for the RFS generators T_a, once 'chosen,' correspond to different (phenomenologically relevant) configurations of fermion mixing matrices.

This latter point is best seen in the SM flavour basis, where the charged-current interactions of the SM are diagonal, but its mass matrices are not:

$$\mathcal{L}^{SM}_{flav} \supset \frac{1}{2}\bar{\nu}^c_L V^\star_\nu m_\nu V^\dagger_\nu \nu_L + \bar{e}_R V_{e_R} m_l V^\dagger_l l_L + \bar{d}_R V_{d_R} m_d V^\dagger_{d_L} d_L + \bar{u}_R V_{u_R} m_u V^\dagger_{u_L} u_L + \text{h.c.} \tag{7.8}$$

The V transformations are 3×3 unitary matrices, and the physical CKM and PMNS mixing matrices of the SM are defined in terms of those acting on the LH fields participating in the charged interactions:

$$V_{CKM} \equiv V^\dagger_{u_L} V_{d_L}, \qquad U_{PMNS} \equiv V^\dagger_l V_\nu. \tag{7.9}$$

One now observes the following invariance of Eq. (7.8):

$$a \to T_{aU}\, a \quad \text{with} \quad T_{aU} = U_a T_a U^\dagger_a\,, \tag{7.10}$$

with a representing all fermions, including neutrinos. This invariance is interpreted as a symmetry of the mass matrix,

$$m_{aU} = T^\dagger_{aU} m_{aU} T_{aU}, \tag{7.11}$$

where the Hermitian conjugate '†' gets replaced with a transpose 'T' for Majorana neutrinos.

One now also sees how the mixing of particle species can be connected directly to the parent group structure. In Eq. (7.10), the generators are written explicitly as functions of the physical

[3] Note that, in a generic flavour symmetry framework, the right-handed (RH) fermions need not transform under the same representation as the left-handed (LH) ones. It is after the flavour symmetry is broken (either to residual subgroups or not) that the mass term requires LH and RH fermions to transform in a related way.

mixing matrices. Assuming that our flavour symmetry $\mathcal{G}_\mathcal{F}$ breaks down to the RFS present in Eq. (7.4), then one can 'reconstruct' the $\mathcal{G}_\mathcal{F}$ as the group generated by $\{T_{\nu iU}, T_{lU}, T_{dU}, T_{uU}\}$ or any allowed combination therein (in the event $\mathcal{G}_\mathcal{F}$ does not break to all four families). This bottom-up approach to studying flavour is not merely a mathematical trick. It describes the symmetry-breaking patterns of entire classes of flavour models,[4] including the famous Altarelli-Feruglio model of leptonic mass and mixing [113]. There, $\mathcal{G}_L \cong A_4$ is broken by flavon fields whose VEVs align themselves in different directions in the charged lepton and neutrino mass terms, leaving residual $\mathbb{Z}_{3,2}$ symmetries (to be identified as $\mathcal{G}_{l,\nu}$) in these respective sectors. The associated mass-basis generators $T_{l,\nu}$, when rotated through Eq. (7.10) with $U_a = U_{TBM}$,[5] the tri-bimaximal mixing matrix [115] that the model predicts, immediately close the original A_4 group.

7.2.1 Isospin Decomposition of Leptoquark Couplings

We now wish to extend the above analysis to include the leptoquark representations of Eq. (7.3), although for brevity we will typically only show details for the scalar triplet Δ_3; the vector singlet and triplet analyses follow in precisely the same way, and any special caveats will be mentioned when relevant.

As in [199], we define new combinations of the isospin components of Δ_3 as

$$\Delta_3^{4/3} = \left(\Delta_3^1 - i\Delta_3^2\right)/\sqrt{2}, \qquad \Delta_3^{-2/3} = \left(\Delta_3^1 + i\Delta_3^2\right)/\sqrt{2}, \qquad \Delta_3^{1/3} = \Delta_3^3, \tag{7.12}$$

with exponents denoting electric charges and $SU(2)$ indices on the left- and right-hand sides, respectively. Contracting $SU(2)$ indices, we can write the scalar triplet Lagrangian in Eq. (7.3) explicitly in the mass basis of the SM fermions, obtaining

$$\begin{aligned}\mathcal{L}^{LQ}_{mass} \supset\ & \underbrace{-(V_{d_L}^T y_3^{LL} V_\nu)_{ij}}_{\lambda_{d\nu}}\, \bar{d}_L^{C\,i} \Delta_3^{1/3} \nu_L^j \underbrace{-\sqrt{2}(V_{d_L}^T y_3^{LL} V_l)_{ij}}_{\lambda_{dl}}\, \bar{d}_L^{C\,i} \Delta_3^{4/3} l_L^j \\ & + \underbrace{\sqrt{2}(V_{u_L}^T y_3^{LL} V_\nu)_{ij}}_{\lambda_{u\nu}}\, \bar{u}_L^{C\,i} \Delta_3^{-2/3} \nu_L^j \underbrace{-(V_{u_L}^T y_3^{LL} V_l)_{ij}}_{\lambda_{ul}}\, \bar{u}_L^{C\,i} \Delta_3^{1/3} l_L^j \\ & + \text{h.c.}\end{aligned} \tag{7.13}$$

where we leave aside the diquark operators, although the residual symmetries can also apply there.[6] Here it is clear that the λ_{QL} combinations we have defined can all be written in terms of a single coupling,

$$\lambda_{d\nu} = \frac{1}{\sqrt{2}} \lambda_{dl}\, U_{PMNS}, \quad \lambda_{ul} = \frac{1}{\sqrt{2}} V_{CKM}^\star\, \lambda_{dl}, \quad \lambda_{u\nu} = -V_{CKM}^\star\, \lambda_{dl}\, U_{PMNS}. \tag{7.14}$$

We have chosen to normalize to λ_{dl}, the matrix we can constrain via measurements of $R_{K^{(\star)}}$, and where we have used the definitions of the CKM and PMNS matrices in Eq. (7.9). The analogous relationships for Δ_3^μ are given by

$$\lambda_{d\nu}^{V_3} = -\sqrt{2}\, \lambda_{dl}^{V_3}\, U_{PMNS}, \qquad \lambda_{ul}^{V_3} = -\sqrt{2}\, V_{CKM}\, \lambda_{dl}^{V_3}, \qquad \lambda_{u\nu}^{V_3} = -V_{CKM}\, \lambda_{dl}^{V_3}\, U_{PMNS}, \tag{7.15}$$

where we have distinguished these from the scalar triplet through the additional 'V_3' label (the conjugation structure of the fields in Eq. (7.3) yields a slightly different normalization for the $d-l$

[4] These are referred to as 'direct' and 'semi-direct' models in the taxonomy of [226]. Other 'indirect' models, where the accidental symmetries of Eq. (7.6) and Eq. (7.10) are not controlled by subgroups of $\mathcal{G}_\mathcal{F}$, are of course also popular in the flavoured model-building literature — see [231] for a successful and recent example.

[5] Note that in [113] the charged lepton mass matrix is already diagonal, so $U_e = \mathbb{1}$ and therefore $U_\nu = U_{PMNS}$.

[6] As discussed in more detail in [171], the residual symmetries can also readily control the flavour structure of the diquark couplings and alleviate issues of proton decay.

coupling: $\lambda_{dl}^{V_3} \equiv -(U_d^\dagger x_3^{LL} U_l)$.). On the other hand, we only have one such correspondence for the vector singlet, since we do not have RH analogues to the CKM and PMNS matrices:

$$\lambda_{u\nu}^{V_1} = V_{CKM}\, \lambda_{dl}^{V_1}\, U_{PMNS}, \tag{7.16}$$

with the redefined $d-l$ coupling now given by $\lambda_{dl}^{V_1} \equiv (U_d^\dagger x_1^{LL} U_l)$. As it turns out, the $SU(2)$ relations in Eqs. (7.14)-(7.16) are extremely important not only in determining the overall shape of the relevant RFS generators in a chosen basis, but also in restricting the experimentally allowed phases controlling the order of any given generator.

7.2.2 The Fermion Mass Basis

Including all relevant terms, the full Yukawa sector of our Δ_3-enhanced Lagrangian, in the mass basis of the SM fermions, now reads

$$\begin{aligned}\mathcal{L}_{mass} \supset\ & \frac{1}{2}\bar{\nu}_L^c\, m_\nu\, \nu_L + \bar{E}_R\, m_l\, l_L + \bar{d}_R\, m_d\, d_L + \bar{u}_R\, m_u\, u_L \\ & + \bar{d}_L^C\, \lambda_{dl}\, l_L\, \Delta_3^{4/3} + \bar{d}_L^C\, \lambda_{d\nu}\, \nu_L\, \Delta_3^{1/3} + \bar{u}_L^C\, \lambda_{ul}\, l_L\, \Delta_3^{1/3} + \bar{u}_L^C\, \lambda_{u\nu}\, \nu_L\, \Delta_3^{-2/3} \\ & + \text{h.c.}\end{aligned} \tag{7.17}$$

with m_a diagonal matrices of mass eigenvalues, and the λ_{QL} defined as in Eqs. (7.13) and (7.14). Since we are in the fermion mass basis, the leptoquark Yukawa couplings are generically non-diagonal, with rows and columns identifiable in a generation specific way. For example, λ_{dl} can be written as [173]

$$-\sqrt{2}\,\left(V_{d_L}^T\, y_3^{LL}\, V_l\right) \equiv \lambda_{dl} = \begin{pmatrix} \lambda_{de} & \lambda_{d\mu} & \lambda_{d\tau} \\ \lambda_{se} & \lambda_{s\mu} & \lambda_{s\tau} \\ \lambda_{be} & \lambda_{b\mu} & \lambda_{b\tau} \end{pmatrix}. \tag{7.18}$$

Given Eq. (7.18), the starting assumption of our analysis is that

$$\exists\ \{Q, L\},\quad T_Q^{(T,\dagger)}\, \lambda_{QL}\, T_L \stackrel{!}{=} \lambda_{QL}, \tag{7.19}$$

where T_Q is transposed 'T' (daggered '†') when considering scalar (vector) leptoquark(s). That is, we assume that residual symmetries also constrain the matrix elements of at least one leptoquark coupling, and of course in what follows we will always include λ_{dl}, so that we have theoretical control over R_{K^*}. Eq. (7.19) further implies that the *same* generator representations T_a acting on fermion fields in their respective SM mass terms also action the RFS in (at least one of) the new leptoquark couplings. This assumption is of course not required from the model-building perspective, however it is highly plausible. So, while building explicit models that realize Eq. (7.19) is beyond the scope (and in fact antithetical to the purpose) of this analysis, we will briefly mention possible explanations for its origins below, where we consider two interesting cases of Eq. (7.19) that have also already been explored in the literature, either directly or indirectly. Namely, we study Eq. (7.19) in the following 'symmetry environments:'

1. **Symmetry Environment 1 (SE1) — Fully-Reduced Matrices:** The same RFS hold in all four SM mass terms *and* all four $SU(2)$ related leptoquark couplings. This scenario corresponds to the 'Simplified Models of Flavourful Leptoquarks' presented in detail in [171], where it was shown that the arbitrary 3×3 complex matrices of λ_{QL} are simplified to matrices with only a single real parametric degree of freedom, as shown in Table 7.2. These 'fully-reduced' matrices can be realized, e.g., in effective models where the operators in Eq. (7.3) are enhanced to include 1) flavon(s) to structure the λ_{QL} via their VEVs, and 2) other scalars that can distinguish the members of $SU(2)$ doublets after EWSB (in a way that preserves Eq. (7.14)).

2. **Symmetry Environment 2 (SE2) — Partially-Reduced Matrices:** RFS hold in some or all of the SM mass terms, but only SM down quark and/or charged lepton symmetries are active in the leptoquark sector, controlling the shape of λ_{dl}.[7] Symmetries are respected by $\lambda_{d\nu,ul,u\nu}$ because they are inherited from λ_{dl} via $SU(2)$ relations. These represent relaxed versions of the simplified models of [171], and generalize the complete models written down in [173], which are realized by single-flavon enhancements of the operators in Eq. (7.3). Hence they do not require additional non-trivial SU(2) scalars, and in this sense may be more minimal than models constructed in SE1. However, as their name suggests, the resulting λ_{QL} have more parametric degrees of freedom — they are only 'partially reduced.'

In both SE1 and SE2, the T generators are again represented by diagonal matrices with three phases, such that an equality of the following form appears (e.g.) for λ_{dl} [171]:

$$\begin{pmatrix} e^{i(\alpha_d+\alpha_l)}\lambda_{de} & e^{i(\alpha_d+\beta_l)}\lambda_{d\mu} & e^{i(\alpha_d+\gamma_l)}\lambda_{d\tau} \\ e^{i(\beta_d+\alpha_l)}\lambda_{se} & e^{i(\beta_d+\beta_l)}\lambda_{s\mu} & e^{i(\beta_d+\gamma_l)}\lambda_{s\tau} \\ e^{i(\gamma_d+\alpha_l)}\lambda_{be} & e^{i(\gamma_d+\beta_l)}\lambda_{b\mu} & e^{i(\gamma_d+\gamma_l)}\lambda_{b\tau} \end{pmatrix} \overset{!}{=} \begin{pmatrix} \lambda_{de} & \lambda_{d\mu} & \lambda_{d\tau} \\ \lambda_{se} & \lambda_{s\mu} & \lambda_{s\tau} \\ \lambda_{be} & \lambda_{b\mu} & \lambda_{b\tau} \end{pmatrix}. \tag{7.20}$$

In the event that only quark or lepton symmetries are active in SE2, then only the phases associated to T_d or T_l are non-zero in Eq. (7.20), respectively. Importantly, the solutions to Eq. (7.20) that are LNU (following the implications of $R_{K^{(*)}}$) and which distinguish multiple generations in each family, as would be expected for a family symmetry, are few in number.

The matrix elements of Eq. (7.20) are of course also constrained by a variety of different experimental observables, in particular lepton flavour violating (LFV) processes (e.g. $\mu \to e\gamma$), B-meson mixing, and indeed the LNU ratios $R_{K^{(*)}}$ — see [163, 167, 171, 173, 200, 232] for their specific implications on λ_{dl}. Furthermore, when one considers the combined application of Eqs. (7.14) and (7.20) as is required in SE1, the measured values of the PMNS and CKM matrices become relevant, as the RFS may want to enforce a zero in λ_{QL} that cannot be realized experimentally. All of these considerations have been made in [171], where the allowed patterns for λ_{QL} were derived in SE1, assuming that they distinguish at least two of three fermion species and that leptoquark couplings mimic SM ones (couplings to heavier fermions are taken to be larger than those to lighter ones). The explicit matrices obtained in [171] for λ_{dl}, as well as all of the associated phase relationships amongst the generators $T_{u,d,l,\nu}$ for the three leptoquarks considered here, are catalogued in Table 7.2. We scan over various NADS that can predict these patterns alongside of special PMNS and CKM matrices in Section 7.4. On the other hand, SE2 represents a relaxation of the assumptions made in [171]. We will discuss the consequences of this relaxation below and in more detail in Section 7.5, where we also perform another scan to find predictive NADS. However, both sets of scans described in Section 7.4-7.5 require us to find a basis where our RFS generators know about the physical mixing patterns we want to connect to $\mathcal{G}_\mathcal{F}$, precisely as we did above when we rotated to the SM flavour basis in Eq. (7.8), so that $T_{\nu U}$ was an explicit function of U_{PMNS}. We now write this basis down.

7.2.3 The Leptoflavour Basis

We will in general have new rotations that appear in our leptoquark extension of the SM, namely those that further diagonalize Eq. (7.18). And so, in order to use the reconstruction technique outlined in Section 7.3, we must find a basis where information about these new rotations (and hence about λ_{dl}) can simultaneously be extracted along with information about the CKM and PMNS matrices of the SM.

Let us begin in the mass basis of Eq. (7.17), where the special patterns of Table 7.2 were derived, and where each generation of quark and lepton can be uniquely identified. We recall that

[7] We consider then that any other symmetry present is understood as accidental, i.e. not controlled by an explicit subgroup of $\mathcal{G}_\mathcal{F}$. This scenario is again analogous to the Altarelli-Feruglio model [113], where the neutrino mass matrix predicted is invariant under a $\mu - \tau$ operator generating a $\mathbb{Z}_2$ symmetry that is *not* a subgroup of A_4.

λ_{QL}		Phase Equalities	λ_{dl}
λ_{QL}^{e3A}	Δ_3	$\{\ \beta_d,\ \gamma_d,\ -\alpha_\nu,\ -\beta_\nu,\ -\alpha_l,\ \beta_u,\ \gamma_u\ \}$	$\lambda_{be}\begin{pmatrix} 0 & 0 & 0 \\ -\frac{V_{ub}}{V_{us}} & 0 & 0 \\ 1 & 0 & 0 \end{pmatrix}$
	Δ_3^μ	$\{\ \beta_d,\ \gamma_d,\ \alpha_\nu,\ \beta_\nu,\ \alpha_l,\ \beta_u,\ \gamma_u\ \}$	
	Δ_1^μ	$\{\ \beta_d, \gamma_d, \alpha_l\ \}\ \{\ \alpha_\nu, \beta_\nu, \beta_u, \gamma_u\ \}$	
λ_{QL}^{e3B}	Δ_3	$\{\ \beta_d,\ \gamma_d,\ -\alpha_\nu,\ -\beta_\nu,\ -\alpha_l,\ \alpha_u,\ \gamma_u\ \}$	$\lambda_{be}\begin{pmatrix} 0 & 0 & 0 \\ -\frac{V_{cb}}{V_{cs}} & 0 & 0 \\ 1 & 0 & 0 \end{pmatrix}$
	Δ_3^μ	$\{\ \beta_d,\ \gamma_d,\ \alpha_\nu,\ \beta_\nu,\ \alpha_l,\ \alpha_u,\ \gamma_u\ \}$	
	Δ_1^μ	$\{\ \beta_d, \gamma_d, \alpha_l\ \}\ \{\ \alpha_\nu, \beta_\nu, \alpha_u, \gamma_u\ \}$	
λ_{QL}^{e3C}	Δ_3	$\{\ \beta_d,\ \gamma_d,\ -\alpha_\nu,\ -\beta_\nu,\ -\alpha_l,\ \alpha_u,\ \beta_u\ \}$	$\lambda_{be}\begin{pmatrix} 0 & 0 & 0 \\ -\frac{V_{tb}}{V_{ts}} & 0 & 0 \\ 1 & 0 & 0 \end{pmatrix}$
	Δ_3^μ	$\{\ \beta_d,\ \gamma_d,\ \alpha_\nu,\ \beta_\nu,\ \alpha_l,\ \alpha_u,\ \beta_u\ \}$	
	Δ_1^μ	$\{\ \beta_d, \gamma_d, \alpha_l\ \}\ \{\ \alpha_\nu, \beta_\nu, \alpha_u, \beta_u\ \}$	
$\lambda_{QL}^{e\mu 1A}$	Δ_3	$\{\ \beta_d,\ \gamma_d,\ -\beta_\nu,\ -\gamma_\nu,\ -\alpha_l,\ -\beta_l,\ \beta_u,\ \gamma_u\ \}$	$\lambda_{b\mu}\begin{pmatrix} 0 & 0 & 0 \\ \frac{V_{ub}}{V_{us}}\frac{U_{21}}{U_{11}} & -\frac{V_{ub}}{V_{us}} & 0 \\ -\frac{U_{21}}{U_{11}} & 1 & 0 \end{pmatrix}$
	Δ_3^μ	$\{\ \beta_d,\ \gamma_d,\ \beta_\nu,\ \gamma_\nu,\ \alpha_l,\ \beta_l,\ \beta_u,\ \gamma_u\ \}$	
	Δ_1^μ	$\{\ \beta_d, \gamma_d, \alpha_l, \beta_l\ \}\ \{\ \beta_\nu, \gamma_\nu, \beta_u, \gamma_u\ \}$	
$\lambda_{QL}^{e\mu 1B}$	Δ_3	$\{\ \beta_d,\ \gamma_d,\ -\beta_\nu,\ -\gamma_\nu,\ -\alpha_l,\ -\beta_l,\ \alpha_u,\ \gamma_u\ \}$	$\lambda_{b\mu}\begin{pmatrix} 0 & 0 & 0 \\ \frac{U_{21}}{U_{11}}\frac{V_{cb}}{V_{cs}} & -\frac{V_{cb}}{V_{cs}} & 0 \\ -\frac{U_{21}}{U_{11}} & 1 & 0 \end{pmatrix}$
	Δ_3^μ	$\{\ \beta_d,\ \gamma_d,\ \beta_\nu,\ \gamma_\nu,\ \alpha_l,\ \beta_l,\ \alpha_u,\ \gamma_u\ \}$	
	Δ_1^μ	$\{\ \beta_d, \gamma_d, \alpha_l, \beta_l\ \}\ \{\ \beta_\nu, \gamma_\nu, \alpha_u, \gamma_u\ \}$	
$\lambda_{QL}^{e\tau 1A}$	Δ_3	$\{\ \beta_d,\ \gamma_d,\ -\beta_\nu,\ -\gamma_\nu,\ -\alpha_l,\ -\gamma_l,\ \beta_u,\ \gamma_u\ \}$	$\lambda_{b\tau}\begin{pmatrix} 0 & 0 & 0 \\ \frac{U_{31}}{U_{11}}\frac{V_{ub}}{V_{us}} & 0 & -\frac{V_{ub}}{V_{us}} \\ -\frac{U_{31}}{U_{11}} & 0 & 1 \end{pmatrix}$
	Δ_3^μ	$\{\ \beta_d,\ \gamma_d,\ \beta_\nu,\ \gamma_\nu,\ \alpha_l,\ \gamma_l,\ \beta_u,\ \gamma_u\ \}$	
	Δ_1^μ	$\{\ \beta_d, \gamma_d, \alpha_l, \gamma_l\ \}\ \{\ \beta_\nu, \gamma_\nu, \beta_u, \gamma_u\ \}$	
$\lambda_{QL}^{e\tau 1B}$	Δ_3	$\{\ \beta_d,\ \gamma_d,\ -\beta_\nu,\ -\gamma_\nu,\ -\alpha_l,\ -\gamma_l,\ \alpha_u,\ \gamma_u\ \}$	$\lambda_{b\tau}\begin{pmatrix} 0 & 0 & 0 \\ \frac{U_{31}}{U_{11}}\frac{V_{cb}}{V_{cs}} & 0 & -\frac{V_{cb}}{V_{cs}} \\ -\frac{U_{31}}{U_{11}} & 0 & 1 \end{pmatrix}$
	Δ_3^μ	$\{\ \beta_d,\ \gamma_d,\ \beta_\nu,\ \gamma_\nu,\ \alpha_l,\ \gamma_l,\ \alpha_u,\ \gamma_u\ \}$	
	Δ_1^μ	$\{\ \beta_d, \gamma_d, \alpha_l, \gamma_l\ \}\ \{\ \beta_\nu, \gamma_\nu, \alpha_u, \gamma_u\ \}$	
$\lambda_{QL}^{\mu\tau 1A}$	Δ_3	$\{\ \beta_d,\ \gamma_d,\ -\beta_\nu,\ -\gamma_\nu,\ -\beta_l,\ -\gamma_l,\ \beta_u,\ \gamma_u\ \}$	$\lambda_{b\tau}\begin{pmatrix} 0 & 0 & 0 \\ 0 & \frac{U_{31}}{U_{21}}\frac{V_{ub}}{V_{us}} & -\frac{V_{ub}}{V_{us}} \\ 0 & -\frac{U_{31}}{U_{21}} & 1 \end{pmatrix}$
	Δ_3^μ	$\{\ \beta_d,\ \gamma_d,\ \beta_\nu,\ \gamma_\nu,\ \beta_l,\ \gamma_l,\ \beta_u,\ \gamma_u\ \}$	
	Δ_1^μ	$\{\ \beta_d, \gamma_d, \beta_l, \gamma_l\ \}\ \{\ \beta_\nu, \gamma_\nu, \beta_u, \gamma_u\ \}$	
$\lambda_{QL}^{\mu\tau 1B}$	Δ_3	$\{\ \beta_d,\ \gamma_d,\ -\beta_\nu,\ -\gamma_\nu,\ -\beta_l,\ -\gamma_l,\ \alpha_u,\ \gamma_u\ \}$	$\lambda_{b\tau}\begin{pmatrix} 0 & 0 & 0 \\ 0 & \frac{U_{31}}{U_{21}}\frac{V_{cb}}{V_{cs}} & -\frac{V_{cb}}{V_{cs}} \\ 0 & -\frac{U_{31}}{U_{21}} & 1 \end{pmatrix}$
	Δ_3^μ	$\{\ \beta_d,\ \gamma_d,\ \beta_\nu,\ \gamma_\nu,\ \beta_l,\ \gamma_l,\ \alpha_u,\ \gamma_u\ \}$	
	Δ_1^μ	$\{\ \beta_d, \gamma_d, \beta_l, \gamma_l\ \}\ \{\ \beta_\nu, \gamma_\nu, \alpha_u, \gamma_u\ \}$	

Table 7.2 – The 'fully-reduced' patterns derived in [171] after the application of SE1 symmetry and experimental constraints, including associated phase equalities required in the generators T_a for all leptoquarks considered in this paper. NOTE: $U^{ij}_{PMNS} \equiv U_{ij}$ and $(V^{ij}_{CKM})^\star \equiv V_{ij}$. For the vectors $\Delta^\mu_{(1,3)}$, replace $V_{ij} \to V^\star_{ij}$.

here the charged-current interactions of the SM are given by

$$\mathcal{L}^{CC}_{mass} = \frac{g}{\sqrt{2}}\bar{l}_L U_{PMNS}\gamma^\mu \nu_L W^+_\mu + \frac{g}{\sqrt{2}}\bar{d}_L V^\dagger_{CKM}\gamma^\mu u_L W^+_\mu + \text{h.c.} \tag{7.21}$$

with the CKM and PMNS matrices defined in Eq. (7.9) as the mismatch between up/down and charged lepton/neutrino mixing matrices, respectively. In moving to a basis where λ_{dl} is generically diagonal, one must be sure to label any further rotations in a manner that respects this (physical) definition. One way to do so is to rotate fields such that the SM charged currents are simultaneously diagonal with λ_{dl}, which we refer to as the *leptoflavour basis*.[8] This can be achieved by reabsorbing any misalignment introduced in the charged currents by rotations in the charged lepton and down quark sectors via transformations on the neutrino and the up quark fields. We therefore construct the leptoflavour basis via the following operations:

$$\begin{aligned} &l_L \to \Lambda^\dagger_l l'_L, && d_L \to \Lambda^\dagger_d d'_L, && \nu_L \to U^\dagger_{PMNS}\Lambda^\dagger_l \nu'_L, && u_L \to V_{CKM}\Lambda^\dagger_d u'_L, \\ &E_R \to \Lambda^\dagger_E E'_R, && d_R \to \Lambda^\dagger_D d'_R, && \nu_R \to \Lambda^\dagger_R \nu'_R, && u_R \to \Lambda^\dagger_U u'_R, \end{aligned} \tag{7.22}$$

where by definition we obtain a new diagonal matrix λ'_{dl} given by

$$\lambda'_{dl} \equiv \Lambda^*_d \lambda_{dl} \Lambda^\dagger_l. \tag{7.23}$$

Note that while the right-handed rotations in Eq. (7.22) are not physical in the SM, they can become so in its leptoquark extensions although, for the particular case of the scalar triplet written explicitly below, they are again redundant. However, this is not the case for the vector singlet, and we therefore include them in all associated equations below for completeness.

Upon applying Eq. (7.22), the corresponding Δ_3-enhanced Lagrangian is then found in the leptoflavour basis as

$$\begin{aligned} \mathcal{L} \supset\ & \frac{g}{\sqrt{2}}\bar{l}'_L\gamma^\mu\nu'_L W^+_\mu + \frac{g}{\sqrt{2}}\bar{d}'_L\gamma^\mu u'_L W^+_\mu \\ &+ \frac{1}{2}\bar{\nu}'^c_L \Lambda^*_l U^*_{PMNS} m_\nu U^\dagger_{PMNS}\Lambda^\dagger_l \nu'_L + \bar{E}'_R\Lambda_E m_l \Lambda^\dagger_l l'_L + \bar{d}'_R \Lambda_D m_d \Lambda^\dagger_d d'_L + \bar{u}'_R \Lambda_U m_u V_{CKM}\Lambda^\dagger_d u'_L \\ &+ \frac{1}{\sqrt{2}}\bar{d}'^c_L \Lambda^*_d \lambda_{dl}\Lambda^\dagger_l \nu'_L \Delta_3^{1/3} + \bar{d}'^c_L \Lambda^*_d \lambda_{dl}\Lambda^\dagger_l l'_L \Delta_3^{4/3} + \bar{u}'^c_L \Lambda^*_d \lambda_{dl}\Lambda^\dagger_l \nu'_L \Delta_3^{-2/3} + \frac{1}{\sqrt{2}}\bar{u}'^c_L \Lambda^*_d \lambda_{dl}\Lambda^\dagger_l l'_L \Delta_3^{1/3} \\ &+ \text{h.c.}, \end{aligned} \tag{7.24}$$

where we have already used the $SU(2)$ equalities of Eq. (7.14). We now recall the main assumption of the analysis, namely that the SM RFS control (at least one of) the Yukawa-like terms in Eq. (7.24) sourced by the leptoquark representation. In the mass basis this is enforced on the leptoquark terms via Eq. (7.19), and there is a corresponding relation in the leptoflavour basis:

$$T^{(T,\dagger)'}_Q \lambda'_{QL} T'_L \stackrel{!}{=} \lambda'_{QL}, \tag{7.25}$$

with λ'_{QL} generically denoting the leptoquark Yukawa couplings in the new basis (c.f. Eq. (7.23) for the $d-l$ coupling). The extent to which Eq. (7.25) is explicitly enforced depends on the breaking of $\mathcal{G}_\mathcal{F}$ to $\mathcal{G}_a$ in a complete model, and so we now explore it for the two environments discussed above.

RFS Invariance in SE1

In the scenario with fully-reduced matrices, Eq. (7.25) holds $\forall\ \{Q, L\}$, and from Eq. (7.24) we can then read off the explicit expressions for the leptoflavour basis RFS generators, obtaining

$$T'_l = \Lambda_l T_l \Lambda^\dagger_l, \quad T'_\nu = \Lambda_l U_{PMNS} T_\nu U^\dagger_{PMNS}\Lambda^\dagger_l, \quad T'_d = \Lambda_d T_d \Lambda^\dagger_d, \quad T'_u = \Lambda_d V^\dagger_{CKM} T_u V_{CKM}\Lambda^\dagger_d, \tag{7.26}$$

[8] This is essentially a basis where all the flavour violation is in the mixing matrices.

for the left-handed generators and

$$T_E^{'} = \Lambda_E T_l \Lambda_E^\dagger, \quad T_R^{'} = \Lambda_R T_\nu \Lambda_R^\dagger, \quad T_D^{'} = \Lambda_D T_d \Lambda_D^\dagger, \quad T_U^{'} = \Lambda_U T_u \Lambda_U^\dagger, \tag{7.27}$$

for the right-handed generators ($T_R^{\prime}$ holds only in the case of Dirac neutrinos). One can easily show that these leave the Lagrangian invariant, as seen explicitly (e.g.) for the $d-\nu$ term:

$$\begin{aligned}
\frac{1}{\sqrt{2}}\vec{d}_L^{\,c}\Lambda_d^*\lambda_{dl}\Lambda_l^\dagger\nu_L'\Delta_3^{1/3} \;\longrightarrow\; & \frac{1}{\sqrt{2}}\vec{d}_L^{\,c}\Lambda_d^* T_d^T\Lambda_d^T\Lambda_d^*\lambda_{dl}\Lambda_l^\dagger\Lambda_l U_{PMNS}T_\nu U_{PMNS}^\dagger\Lambda_l^\dagger\nu_L'\Delta_3^{1/3} \\
&= \frac{1}{\sqrt{2}}\vec{d}_L^{\,c}\Lambda_d^* T_d^T\left[\lambda_{dl}U_{PMNS}\right]T_\nu U_{PMNS}^\dagger\Lambda_l^\dagger\nu_L'\Delta_3^{1/3} \\
&= \frac{1}{\sqrt{2}}\vec{d}_L^{\,c}\Lambda_d^*\left[\lambda_{dl}U_{PMNS}\right]U_{PMNS}^\dagger\Lambda_l^\dagger\nu_L'\Delta_3^{1/3} \\
&= \frac{1}{\sqrt{2}}\vec{d}_L^{\,c}\Lambda_d^*\lambda_{dl}\Lambda_l^\dagger\nu_L'\Delta_3^{1/3} \qquad \text{Q.E.D.}
\end{aligned} \tag{7.28}$$

In moving from the second to third lines we used Eq. (7.14) (the bracketed term is simply $\sqrt{2}\lambda_{d\nu}$) and Eq. (7.25). Similar equalities hold for all other terms in Eq. (7.24). We therefore identify Eq. (7.26) as the generating set for $\mathcal{G}_\mathcal{F}$ when RFS are active in all four fermion families, with the phases of $T_{u,d,l,\nu}$ constrained as per Table 7.2, and we use them to scan over various possible $\mathcal{G}_\mathcal{F}$ in Section 7.4 below. Also note that in the limit where leptoquarks do not mix, $\Lambda_{d,l} \to \mathbb{1}$, Eq. (7.26) returns the generators required to reconstruct a $\mathcal{G}_\mathcal{F}$ that controls SM mixing only, as expected! Finally, it is easy to show that the transformations in Eq. (7.22) and the resulting generators in Eq. (7.26) also hold when considering vector singlet and triplet leptoquarks, since conjugation differences in the corresponding Lagrangians get compensated by the differing SU(2) relations between couplings, cf. Eqs. (7.14)-(7.16).

RFS Invariance in SE2

In the scenario with partially-reduced matrices one only demands that Eq. (7.25) hold for $Q = d$ and $L = l$. As mentioned above, this can happen when Eq. (7.3) is enhanced by a single flavon, whose VEV then leaves an overall RFS in y_3^{LL} after flavour symmetry breaking. In this case and upon decomposing isospin indices, moving to the fermion mass basis, and normalizing all couplings to λ_{dl}, one can easily derive that the RFS acting on the leptoquarks are actioned by:

$$T_d^{LQ} = T_d, \quad T_l^{LQ} = T_l, \quad T_u^{LQ} = V_{CKM}\,T_d^{LQ}\,V_{CKM}^\dagger, \quad T_\nu^{LQ} = U_{PMNS}^\dagger\,T_l^{LQ}\,U_{PMNS}, \tag{7.29}$$

where in general we have been careful to label these operations with 'LQ' to distinguish them from the RFS controlling the SM masses, but where in the first two equations we have also already identified the down quark and charged lepton actions with their SM counterparts $T_{d,l}$ (one of our assumptions). Now, Eq. (7.24) of course knows nothing about any RFS, and so the generic shape of the generators in Eq. (7.26) also holds in SE2. However, we must now be careful to distinguish the actions on the SM and leptoquark components of Eq. (7.24). Plugging Eq. (7.29) into Eq. (7.26) (with appropritae 'LQ' labels implied), one immediately sees that the neutrino and up quark generators become redundant:

$$T_\nu^{\prime\,LQ} = T_l^{\prime\,LQ} = T_l', \quad T_u^{\prime\,LQ} = T_d^{\prime\,LQ} = T_d'. \tag{7.30}$$

This is to be expected, since in this symmetry environment we have no way of distinguishing the components of the $SU(2)$ fermion doublets in Eq. (7.3). To see that the invariance of Eq. (7.24)

still holds under RFS, we repeat the sample calculation above for the $d-\nu$ term:

$$\begin{aligned}\frac{1}{\sqrt{2}}\vec{d}_L^{\,c}\Lambda_d^*\lambda_{dl}\Lambda_l^\dagger\nu_L'\Delta_3^{1/3} \;\longrightarrow\; &\frac{1}{\sqrt{2}}\vec{d}_L^{\,c}\Lambda_d^*T_d^T\Lambda_d^T\Lambda_d^*\lambda_{dl}\Lambda_l^\dagger\Lambda_l T_l\Lambda_l^\dagger\nu_L'\Delta_3^{1/3}\\ &= \frac{1}{\sqrt{2}}\vec{d}_L^{\,c}\Lambda_d^*T_d^T\left[\lambda_{dl}\right]T_l\Lambda_l^\dagger\nu_L'\Delta_3^{1/3}\\ &= \frac{1}{\sqrt{2}}\vec{d}_L^{\,c}\Lambda_d^*\lambda_{dl}\Lambda_l^\dagger\nu_L'\Delta_3^{1/3} \qquad \text{Q.E.D.}\end{aligned} \tag{7.31}$$

In the second line one notes the subtle difference with respect to Eq. (7.28): the symmetry at work in the $d-\nu$ term is coming from the equality $T_d^T\lambda_{dl}T_l \overset{!}{=} \lambda_{dl}$, not $T_d^T\lambda_{d\nu}T_\nu \overset{!}{=} \lambda_{d\nu}$, which corresponds precisely to the difference in the symmetry assumptions between SE1 and SE2. The same is true for the $u-\nu$ and $u-l$ terms not shown, and all invariances again proceed analogously for the vector $\Delta^\mu_{(1,3)}$ Lagrangians.[9]

Of course, the up quark and neutrino mass terms may still be controlled by a respective RFS, and those will still be given by the second and fourth terms in Eq. (7.26). Therefore, practically speaking, the complete set of generating matrices in the leptoflavour basis are still given by Eqs. (7.26)-(7.27). However, there are no longer any phase relationships in $T_{u,d,l,\nu}$ (cf. Table 7.2) between any two sectors other than (potentially) the down quarks and charged leptons. One is also not required to include all four $T'_{u,d,l,\nu}$ in the generating set of $\mathcal{G}_\mathcal{F}$, as it is conceivable that $\mathcal{G}_\mathcal{F}$ only breaks directly to RFS in certain fermion families. We will consider three such possibilities in Section 7.5.

7.2.4 On Dirac vs. Majorana Neutrinos

While we have chosen to include a Majorana neutrino mass term in the above equations, the analysis proceeds equivalently in the presence of a Dirac mass, whose form is given by

$$\begin{aligned}\mathcal{L} \;&\supset\; \bar{\nu}_R\, m_\nu\, \nu_L\,, && \text{(Fermion mass basis)}\\ \mathcal{L} \;&\supset\; \bar{\nu}'_R\,\Lambda_R\, m_\nu\, U^\dagger_{PMNS}\,\Lambda_l^\dagger\,\nu'_L\,, && \text{(Leptoflavour basis)}\end{aligned} \tag{7.32}$$

where we have written it in both the fermion mass and leptoflavour bases. Applying Eq. (7.26) to the latter, one recovers the original expression as desired:

$$\begin{aligned}\bar{\nu}'_R\,\Lambda_R\, m_\nu\, U^\dagger_{PMNS}\,\Lambda_l^\dagger\,\nu'_L \;\longrightarrow\; &\bar{\nu}'_R\,\Lambda_R\, T_\nu^\dagger\,\Lambda_R^\dagger\Lambda_R\, m_\nu\, U^\dagger_{PMNS}\,\Lambda_l^\dagger\Lambda_l\, U_{PMNS}\, T_\nu\, U^\dagger_{PMNS}\,\Lambda_l^\dagger\,\nu'_L\\ &= \bar{\nu}'_R\,\Lambda_R\,\left[T_\nu^\dagger\, m_\nu\, T_\nu\right]\, U^\dagger_{PMNS}\,\Lambda_l^\dagger\,\nu'_L\\ &= \bar{\nu}'_R\,\Lambda_R\, m_\nu\, U^\dagger_{PMNS}\,\Lambda_l^\dagger\,\nu'_L \qquad \text{Q.E.D.}\end{aligned} \tag{7.33}$$

Recall that the equality between the second and third lines is just the natural RFS of the SM masses, cf. Eq. (7.6). Hence the form of the RFS generators given in Eq. (7.26) is the same for both Dirac and Majorana neutrinos. However, we have already seen in Eq. (7.6) that the phases of the fermion mass-basis generators T_a potentially differ between the two scenarios, as the maximal RFS for a Majorana mass term is given by a Klein $\mathbb{Z}_2\times\mathbb{Z}_2$ [204]. Indeed, the tacit assumption throughout Sections 7.2.2-7.2.3 is that $\mathcal{G}_a$ is generated by a single matrix representation T_a, regardless of whether or not neutrinos are Dirac or Majorana. In the event it is instead described by a cyclic product group of the form

$$\mathcal{G}_a \sim \mathbb{Z}_a^1\times\mathbb{Z}_a^2\times ..., \tag{7.34}$$

then Eq. (7.25) must be met for each associated $T_a^{i\prime}$, whose shape is again given by Eq. (7.26), up to the differing phases of the individual T_a^i.

[9] Note that the distinction between SE1 and SE2 is not meaningful for the RH terms of the vector singlet, as these do not involve SU(2) doublets from the outset. They are in any event not included in the scans below.

7.2.5 On Unambiguous Mixing Predictions

We now wish to emphasize that the complete three-generation fermionic mixing matrices cannot be fully controlled by the RFS of $\mathcal{G}_\mathcal{F}$ unless all three fermion species are distinguished by the respective $\mathcal{G}_a$. For SM mixing patterns this is perhaps easier to see in the flavour basis Eq. (7.10), where the generators T_{aU} are functions of the mixing matrices U_a predicted. However, if T_a has equal phases in its (i,j) entries, then T_{aU} is equivalent to the same matrix rotated through the (i,j) sector:

$$T_{aU} = U_a\, T_a^{ii=jj}\, U_a^\dagger = U_a\, R_a^{ij}\, T_a^{ii=jj}\, R_a^{ji\star}\, U_a^\dagger, \quad \text{with} \quad R^{ij} \equiv \begin{pmatrix} \cos\theta_{ij} & \sin\theta_{ij}\, e^{-i\delta_{ij}} \\ -\sin\theta_{ij}\, e^{i\delta_{ij}} & \cos\theta_{ij} \end{pmatrix}. \tag{7.35}$$

This invariance translates to an ambiguity in the change of basis itself, leading to additional free contributions to the CKM and PMNS matrices. Explicitly, one can write down the transformations to pass from the mass basis to the flavour basis as

$$f_a \to R_a^{ij} U_a^\dagger f_a^0, \tag{7.36}$$

where f_a^0 is the usual flavour eigenstate. One immediately sees that in this case the RFS generator transforms as shown on the RHS of Eq. (7.35), meaning that $\mathcal{G}_\mathcal{F}$ cannot unambiguously control fermionic mixing, as the predicted CKM and PMNS matrices may still exhibit a dependence on R_a^{ij},

$$V_{CKM} \Leftrightarrow R_u^{ji\star}\, U_{CKM}\, R_d^{mn}, \qquad U_{PMNS} \Leftrightarrow R_l^{ji\star}\, U_{PMNS}\, R_\nu^{mn}, \tag{7.37}$$

that $\mathcal{G}_\mathcal{F}$ cannot distinguish. In Eq. (7.37) we are of course not implying that the degeneracies need to be in the same plane for either $T_{u,l}$ nor $T_{d,\nu}$, and clearly $R_a = \mathbb{1}$ if T_a has three eigenvalues. That is, the RFS controls portions of the mixing, but permits additional free parameter(s). In this case a product group like Eq. (7.34) would be required for the RFS to pin down an exact U_a, and in fact this is always true for Majorana neutrinos, since a $\mathbb{Z}_2$ symmetry only has two distinct eigenvalues. Finally, we note that the ambiguity in Eq. (7.37) also holds in the leptoflavour basis that we reconstruct $\mathcal{G}_\mathcal{F}$ in.

Of course it is entirely plausible that in a complete model the RFS does not control all of the observed mixing, but instead allows free parameters to be fit to data or includes some other mechanism (perhaps auxiliary symmetries) not captured in our simplified framework that solidifies the prediction. This happens in [113], for example, where $\mathcal{G}_\mathcal{F}$ only breaks to $\mathcal{G}_\nu \sim \mathbb{Z}_2$, but the model unambiguously predicts $U_{PMNS} = U_{TBM}$. We will therefore state clearly our assumptions in each relevant scan presented in Sections 7.4-7.5.

7.3 Closing Finite Groups: the Bottom-Up Approach

We now have all relevant information required to close NADS capable of explaining fermionic mixing in the SM and special patterns of leptoquark Yukawa couplings, and to do so we will follow a bottom-up approach that tracks the symmetry breaking backwards in Eq. (7.4), using the generators of $\mathcal{G}_a$ to close the larger $\mathcal{G}_\mathcal{F}$. We will effectively automate this procedure by taking particular forms for the relevant mixing matrices in question, discretizing the free parameters in those matrices and all phases of T_a, and scanning over experimentally allowed ranges using the `GAP` computational finite algebra package [228, 229]. This is a naíve but powerful way to quickly gain information about phenomenologically relevant $\mathcal{G}_\mathcal{F}$, and has been applied to matrices in both the lepton [216] and quark [107] sector. We detail the basic steps below for completeness and to highlight any special points relevant to this new application to leptoquarks.

7.3.1 Approximating the CKM and PMNS Matrices

A key input to Eq. (7.26) are the CKM and PMNS mixing matrices of the SM, for which one expects the RFS of $\mathcal{G}_\mathcal{F}$ to have some control over. The RFS mechanism was in fact pioneered to search for

$\mathcal{G}_\mathcal{F}$ that can predict their parameters in a model-independent way, and multiple collaborations have used `GAP` or other tools/techniques to find such predictive NADS [101, 107, 204–223]. The take-away conclusions from those papers are, within the strict (semi-)direct symmetry-breaking approach embodied in Eqs. (7.51)-(7.56), that only large groups of $\mathcal{O}(10^2)$ are capable of predicting all three measured mixing angles of the PMNS matrix θ_i^l, while even larger groups are required to explain complete CKM mixing angles θ_i^q (or even PMNS mixing simultaneously with the Cabibbo angle).[10] Hence it may be more natural to consider smaller groups that quantize these matrices to 'leading order' (LO), thereby controlling only the dominant observed mixing. Other smaller mixing angles are then left unconstrained by the RFS, and can either be fitted to free parameters the RFS allows or be realized via other mechanisms that the RFS cannot describe, e.g. Renormalization Group evolution from the flavour breaking scale or next-to-leading order (NLO) terms in the operator product expansion (OPE) in flavons defining the effective theory of flavour.

Regardless, following the discussion in Section 7.2.4 it is clear from Table 7.2 and Eq. (7.26) that none of the models in SE1 are capable of predicting all three angles in either the CKM or the PMNS matrices anyway; not only do the isolation patterns predict $\theta_{13}^l = 0$, but degenerate phases exist in both the quark and lepton sectors, although they are aligned such that the Cabibbo angle of the CKM can (potentially) be predicted in all models except λ_{QL}^{e3C}. All two-columned SE1 patterns also permit a free parameter in the (1,3) element of the PMNS matrix which is, when instead *predicted* by the RFS, partially responsible for generating the large (undesirable) groups mentioned above, due to the smallness of the 'reactor' angle θ_{13}^l. We will further see in Section 7.5 that SE2 environments also require degenerate phases in the quark sector to account for $R_{K^{(*)}}$.

It therefore makes sense for us to approximate the forms of the PMNS and CKM matrices in Eq. (7.26) in a way that 1) is more likely to recover small, natural $\mathcal{G}_\mathcal{F}$ and 2) that can actually capture the unambiguous predictions of most of our simplified models. To that end we assume the following LO forms:

$$U_{PMNS} \simeq U_{\mu\tau} \equiv \frac{1}{\sqrt{2}} \begin{pmatrix} \sqrt{2}\cos\theta_{\mu\tau} & \sqrt{2}\sin\theta_{\mu\tau} & 0 \\ -\sin\theta_{\mu\tau} & \cos\theta_{\mu\tau} & 1 \\ \sin\theta_{\mu\tau} & -\cos\theta_{\mu\tau} & 1 \end{pmatrix} + \mathcal{O}\left(\theta_{13}^l\right), \tag{7.38}$$

$$V_{CKM} \simeq V_C \equiv \begin{pmatrix} \cos\theta_C & \sin\theta_C & 0 \\ -\sin\theta_C & \cos\theta_C & 0 \\ 0 & 0 & 1 \end{pmatrix} + \mathcal{O}\left(\theta_C^2, \theta_C^3\right). \tag{7.39}$$

The $\mu-\tau$ invariant matrix in Eq. (7.38) can still provide an excellent description of leptonic mixing up to the small correction required from θ_{13}^l. It includes many popular patterns explored in prior leptonic flavour models, including the tri-bimaximal [115], golden ratio [233, 234], bi-maximal [235], and hexagonal matrices [236, 237]:

$$U_{\mu\tau}\left(\theta_{\mu\tau}\right) \to \begin{cases} U_{TBM} & \rightleftarrows \tan\theta_{\mu\tau} = \frac{1}{\sqrt{2}} \\ U_{BM} & \rightleftarrows \tan\theta_{\mu\tau} = 1 \text{ or } \theta_{\mu\tau} = \frac{\pi}{4} \\ U_{GR_1} & \rightleftarrows \tan\theta_{\mu\tau} = \frac{2}{(1+\sqrt{5})} \\ U_{GR_2} & \rightleftarrows \theta_{\mu\tau} = \frac{\pi}{5} \\ U_{HM} & \rightleftarrows \tan\theta_{\mu\tau} = \frac{1}{\sqrt{3}} \text{ or } \theta_{\mu\tau} = \frac{\pi}{6} \end{cases} \tag{7.40}$$

One observes that any model allowing a free rotation in the (2,3) or (1,3) sectors of this matrix can then successfully account for all experimental constraints on U_{PMNS}.

Similarly, the Cabibbo matrix in Eq. (7.39) describes the dominant CKM mixing between first and second generation quarks excellently, and exterior off-diagonal elements are anyway suppressed

[10] Again, flavour models that do not exhibit the symmetry-breaking patterns in Eq. (7.4) are not considered in these statements. Indirect models like that of [231] can control complete three-generation mixing with small finite groups, although NLO terms in the OPE still become relevant for the model's phenomenology.

by one or two orders of magnitude in comparison. While free parameter(s) introduced through RFS-allowed rotations of the form in Eq. (7.35) can further quantize additional element(s), especially in the (2,3) sector, the large hierarchies present in the CKM matrix could also indicate a sub-leading origin for some (or all) of the missing matrix elements in Eq. (7.39).

Following on these assumptions we then discretize the free parameters in Eqs. (7.38)-(7.39) using the schemes in Eqs. (7.45a)-(7.45b). Sets of matrices that fulfill the phenomenological constraints we impose, namely

$$0.5 \leq \sin\theta_{\mu\tau} \leq 0.72, \tag{7.41}$$

$$0.2 \leq \sin\theta_{C} \leq 0.225, \tag{7.42}$$

are then collected to form unique mixing matrices, which are then used to form T'_ν and T'_u in Eq. (7.26). We have chosen a relatively large window for $\sin\theta_{\mu\tau}$ that encompasses all of the leading order patterns in Eq. (7.40), and a much narrower window for the (extremely well measured, and typically RGE stable [238–240]) Cabibbo angle.

7.3.2 Symmetry Assignment and Discretization

We assign the simplest possible (discrete) RFS to each family sector, namely that mediated by a single cyclic group:

$$\mathcal{G}_a \cong \mathbb{Z}_a^{n_a} \tag{7.43}$$

with n_a the order of the symmetry. Accordingly, the matrices represented by Eq. (7.26) are the core group-theoretic and phenomenological engines of our study.

Continuing, we want to find NADS by closing structures generated by the multiple Abelian subgroups of Eq. (7.43). We therefore construct the explicit representations found in Eq. (7.26). We also intend to exploit the `SmallGroup` library of finite groups documented in the `GAP` package, so we must choose a scheme where the free parameters of these matrices (e.g. α_d, β_d, ..., $\theta_{\mu\tau}$, θ_C, ..., $\lambda_{se}/\lambda_{be}$, ...) are explicitly quantized, otherwise we would not close finite groups. Hence we must choose a 'discretization scheme' which can be scanned over. In previous studies [107, 216] the generator representations depended only on phases and trigonometric functions (fermionic mixing angles). For the matrices in Eq. (7.26), however, we must also include the types of parameters entering $\Lambda_{d,l}$, which are just the (generically speaking, unknown) values of ratios of the matrix elements of λ_{dl}. We therefore choose the following schemes for the different types of parameters in T'_a, where in all cases we take $\{n, m\} \in \mathbb{Z}^2$:

- **Leptoquark Matrix Elements:** For the ratios of λ_{dl} matrix elements we choose a simple 'root-rational' discretization scheme:

$$\lambda_i \stackrel{!}{=} \left(+\sqrt{\frac{n}{m}}\right)_i, \tag{7.44a}$$

  where the square root operation in `GAP` is given by 'ER' for a rational number, i.e. $\sqrt{n/m} \leftrightarrow ER(n/m)$. We are therefore implying that these couplings are real, which can be derived as a consequence of SE1 [171], but represents a further assumption in SE2. However, since we have little knowledge of the structure of λ_{dl} other than weak bounds on the overall magnitude of some of its elements, this simple scheme will prove sufficient for our current purposes.

- **Fermionic Mixing Angles:** All mixing angles appearing in U_{CKM} and U_{PMNS} are quantized as either

$$\theta_i \stackrel{!}{=} \pi\left(\frac{n}{m}\right)_i \quad \text{or} \tag{7.45a}$$

$$\tan(\theta_i) \stackrel{!}{=} \left(+\sqrt{\frac{n/m}{1-n/m}}\right)_i. \tag{7.45b}$$

In the first scheme we restrict ourselves to $\theta \in \{0, 2\pi\}$ to avoid degeneracy, and in the second we restrict ourselves to the unit circle. Of course, these appear in different trigonometric functions in most parameterizations of U_{CKM} and U_{PMNS}, so we also give the corresponding `GAP` objects for cosines and sines that we construct. For Eq. (7.45a) one finds

$$\begin{aligned} \cos(n\pi/m) &= \frac{E(2m)^n + E(2m)^{-n}}{2}, \\ \sin(n\pi/m) &= \frac{E(2m)^n - E(2m)^{-n}}{2E(4)}, \end{aligned} \tag{7.46}$$

with $E(N) = e^{\frac{2\pi i}{N}}$, whereas for Eq. (7.45b) one obtains

$$\begin{aligned} \cos(\theta) &= ER\left(1 - \frac{n}{m}\right), \\ \sin(\theta) &= ER\left(\frac{n}{m}\right). \end{aligned} \tag{7.47}$$

Since in Eq. (7.45b) we restricted ourselves to the unit circle, $n/m \in [0, 1]$ there and in Eq. (7.47).

- **Free Phases in RFS Generators:** We also quantize the free phases to multiples of 2π in all fermion mass-basis generators T_a:

$$\phi_i \stackrel{!}{=} 2\pi \left(\frac{n}{m}\right)_i . \tag{7.48}$$

Hence we simply create `GAP` objects of the form

$$T = \text{diag}\left(E(m)^{n_\alpha}, E(m)^{n_\beta}, E(m)^{n_\gamma}\right) \tag{7.49}$$

in our scripts.

These simple schemes are well-motivated by the representation theory of finite groups, and indeed in Sections 7.4-7.5 we will show that they are sufficient to reconstruct of a diversity of non-Abelian $\mathcal{G}_\mathcal{F}$.

Given these core parametric inputs, our automation scripts must then have a range of values for $\{n, m\}_i$ to scan over. These domains will not only determine the number of quantizations of $U_{PMNS,CKM}$ and $\Lambda_{d,l}$ entering T'_a, but also even the order n_a of the cyclic groups $\mathbb{Z}_a$ that get distributed to each family sector. In all scans in Sections 7.4-7.5 we choose the following:

$$\begin{aligned} \{n, m\}_\lambda &\in \{1, 1..5\}, \quad \{n, m\}_{\theta_C} \in \{1, 14..15\}, \\ \{n, m\}_{\phi_a} &\in \{0..n_a, 2..n_a\}, \quad \{n, m\}_{\theta_{\mu\tau}} \in \{1, 1..5\}, \end{aligned} \tag{7.50}$$

with λ in the first line sometimes called x or y below, and ϕ_a representing an arbitrary free phase in a fermion mass-basis generator T_a. While these windows may seem small, they generate a wealth of different group structures, and in any event can be trivially changed given updated experimental or theoretical input. We then scan across all relevant combinations of Eq. (7.50), and then cull results that do not give phenomenologically relevant quantizations. This procedure yields a finite number of generating sets $\{T'_a\}$, where the number of matrices in each set is determined by the symmetry-breaking patterns assumed.

7.3.3 Group Closure and Analysis

The output of Sections 7.3.1-7.3.2 are representations for the generators of our RFS that incorporate all relevant symmetry and experimental constraints applicable to the simplified models under

consideration. They are sets of 3×3 unitary matrices without any free variables — all have been quantized under one of the above discretization schemes. Our scripts then collect these unique sets of generators and insist that a parent symmetry $\mathcal{G}_\mathcal{F}$ is formed from their closure. To do so we call the `GroupWithGenerators` command of the `GAP` language. In SE1 we assume the symmetry-breaking patterns in Eq. (7.4), and so the generating set includes four matrices. On the other hand, in SE2 we are free to assume a variety of different symmetry breaking situations. For example, it is plausible that the mechanism or symmetry responsible for PMNS mixing could have origins independent of that controlling CKM mixing. For each special pattern of λ_{dl} considered, we therefore close the groups generated by the following matrices:

$$\begin{aligned}
(\textbf{SE1}\text{: Leptoquarks, PMNS, \& CKM}): &\quad \mathcal{G}_F \sim \{T'_d, T'_l, T'_u, T'_\nu\} && (7.51)\\
(\textbf{SE1}\text{: Leptoquarks, PMNS, \& CKM}): &\quad \mathcal{G}_F \sim \{T'_d, T'_u\} \times \{T'_l, T'_\nu\} && (7.52)\\
(\textbf{SE2}\text{: Leptoquarks, PMNS, \& CKM}): &\quad \mathcal{G}_F \sim \{T'_d, T'_l, T'_u, T'_\nu\} && (7.53)\\
(\textbf{SE2}\text{: Leptoquarks, PMNS, \& CKM}): &\quad \mathcal{G}_F \sim \{T'_d, T'_u\} \times \{T'_l, T'_\nu\} && (7.54)\\
(\textbf{SE2}\text{: Leptoquarks \& PMNS}): &\quad \mathcal{G}_F \sim \{T'_l, T'_\nu\} && (7.55)\\
(\textbf{SE2}\text{: Leptoquarks \& CKM}): &\quad \mathcal{G}_F \sim \{T'_u, T'_d\} && (7.56)
\end{aligned}$$

where we have indicated that these closures respectively treat the cases where a single flavour symmetry $\mathcal{G}_\mathcal{F}$ addresses fermionic mixing and $R_{K^{(*)}}$ Eqs. (7.51)-(7.54) or either PMNS or CKM mixing alongside of $R_{K^{(*)}}$ Eqs. (7.55)-(7.56). For Eqs. (7.51) and (7.53) we ask that a single NADS be closed by the generators of all four residual symmetries, whereas in Eqs. (7.52) and (7.54) we consider the case sketched in Eq. (7.4), where $\mathcal{G}_\mathcal{F} \cong \mathcal{G}_\mathcal{Q} \times \mathcal{G}_\mathcal{L}$. Note that this is not equivalent to simply taking the products of Eqs. (7.55) and (7.56), since additional phase equalities are required amongst T_a when all $\mathcal{G}_a$ are active — $\mathcal{G}_\mathcal{Q} \times \mathcal{G}_\mathcal{L}$ represents a subset of the product of Eqs. (7.55) and (7.56). In principle we could also define the group $\mathcal{G}_{LQ} \sim \{T'_d, T'_l\}$ in SE2, which would have control over λ_{dl} and therefore $R_{K^{(*)}}$, but no control over fermionic mixing in the SM. However we have found that $\mathcal{G}_{LQ}$ can only be Abelian given our assumptions above and below in Section 7.5 — $T'_{d,l}$ are always diagonal — and so we cannot reconstruct a NADS for $\mathcal{G}_{LQ}$ unless these are softened.

Upon closing the groups in Eqs. (7.51)-(7.56) we must still do some culling, as not all will be finite, non-Abelian, of small order, etc. `GAP` includes a number of internal commands that can be used to filter results based on user-defined preferences. We impose cuts such that we only reconstruct relatively small,

$$\mathcal{O}\left(\mathcal{G}_\mathcal{F}, \mathcal{G}_\mathcal{L}\right) \leq 100, \;\; \mathcal{O}\left(\mathcal{G}_\mathcal{Q}\right) \leq 50, \tag{7.57}$$

and non-Abelian finite groups, and then identify the remaining flavour symmetry candidates with the `GroupID` and `StructureDescription` commands.[11] The latter often returns non-Abelian product structures in terms of Abelian subgroups, and so we recall the corresponding isomorphisms for many common finite group series (see [241] for a comprehensive mathematical review of NADS):

$$\begin{aligned}
&\Sigma(3N^2) \cong (Z_N \times Z_N) \rtimes Z_2,\\
&\Delta(3N^2) \cong (Z_N \times Z_N) \rtimes Z_3,\\
&\Delta(6N^2) \cong ((Z_N \times Z_N) \rtimes Z_3) \rtimes Z_2,\\
&\Sigma(3N^3) \cong Z_N \times \Delta\left(3N^2\right) \;\text{ for }\; N/3 \neq \mathit{Integer},\\
&\Sigma(3 \cdot 3^3) \cong (Z_3 \times Z_3 \times Z_3) \rtimes Z_3.
\end{aligned} \tag{7.58}$$

Note that for brevity we will only report unique combinations of NADS and physical parameter quantizations. That is, we will not report two results where the same symmetry $\mathcal{G}_\mathcal{F}$ predicts the

[11] Observe that `StructureDescription` is *not* an isomorphism invariant command; two groups that are not isomorphic can return the same string while isomorphic groups in different representations can return different strings. The *GroupID* command is unique, however.

same physical parameter(s), but with different phase configurations in the RFS generators T_a. Of course these phases are relevant to the additional free parameters that the model allows, cf. Eq. (7.35), and so in certain cases we make specific demands about their alignments; this will be noted when relevant below. Finally, we also omit results of the form $Z_N \times D$, where D is a NADS already identified by the scans.

In addition to giving this information on $\mathcal{G}_\mathcal{F}$, our scripts also carefully archive the parameters associated to it. In this way we have all relevant information on the representations of the residual generators, which is necessary if one wishes to construct a consistent model from our results.

7.4 Scanning Fully-Reduced Matrices in SE1

In this section we investigate the different viable leptoquark patterns derived in [171]. By computing the explicit shape of the leptoquark mixing matrices $\Lambda_{d,l}$, and using the CKM and PMNS assumptions from Eqs. (7.38) and (7.39), we obtain representations for the RFS generators in the leptoflavour basis, which can then be closed to specific group structures as described in Section 7.3.3

We obtain $\Lambda_{d,l}$ by utilizing a Singular Value Decomposition (SVD) algorithm, which relies on the fact that a generic matrix $\mathcal{M}$ is diagonalizable by two unitary matrices $\mathcal{U}$ and $\mathcal{V}$,

$$\mathcal{M}^D = \mathcal{U}\mathcal{M}\mathcal{V}^\dagger, \tag{7.59}$$

where $\mathcal{M}^D$ is diagonal. In the event $\mathcal{M}$ is symmetric (or Hermitian, for a $\mathbb{C}$-matrix), only one matrix is required. In this way we diagonalize the various leptoquark patterns from Table 7.2 and extract the Λ_d and Λ_l mixing matrices corresponding to the transformation

$$\lambda'_{dl} = \Lambda_d^* \lambda_{dl} \Lambda_l^\dagger, \tag{7.60}$$

where λ'_{dl} is diagonal. We will present the explicit forms of Λ_d and Λ_l in all cases, before performing the GAP scans.

In what follows we will first study the isolation patterns of Table 7.2, and then move on to the two-columned matrices. We will form groups according to Eqs. (7.51)-(7.52). In all cases we restrict the RFS generators to

$$2 \leq \mathcal{O}(T_{l,\nu}) \leq 5, \quad 2 \leq \mathcal{O}(T_{u,d}) \leq 3\,, \tag{7.61}$$

which, when combined with the phenomenological parameter and group-order bounds of Sections 7.3.1-7.3.3, yields thousands of generator combinations. In particular, we scan over 23880(4620) and 42864(8664) RFS generator combinations for $\Delta_3^{(\mu)}$ and Δ_1^μ, respectively, in the isolation(two-columned) patterns . In all cases we present our results in tables that include, from left to right, the relevant quantization of the mixing parameters $\theta_{\mu\tau,C}$,[12] the phase alignments of all four RFS generators $T_{u,d,l,\nu}$, the corresponding GAP `SmallGroup` ID of the NADS closed, the common name (GAP `StructureDescription`) for the NADS, and an indication of how many of the (A, B, C) patterns from Table 7.2 are predicted.

7.4.1 Isolation Patterns

The electron isolation patterns $\lambda_{dl}^{[e3X]}$, with $X = A, B, C$, are given by

$$\lambda_{dl}^{[e3X]} = \lambda_{be} \begin{pmatrix} 0 & 0 & 0 \\ x_X & 0 & 0 \\ 1 & 0 & 0 \end{pmatrix}, \quad \text{with} \quad x_X = -\frac{V_{u_X b}}{V_{u_X s}}. \tag{7.62}$$

[12] In this section we only consider the Eq. (7.45b) discretization of $\theta_{\mu\tau}$, which is sufficiently general. In Section 7.5.2 we will study both Eqs. (7.45a) and (7.45b), observing that the former generates no further groups.

Electron Isolation and Fermionic Mixing in SE1							
$\{t_{\theta_{\mu\tau}}, \theta_C\}$	T_l^{ii}	T_d^{ii}	T_u^{ii}	T_ν^{ii}	GAP-ID	$\mathcal{G}_\mathcal{F}$	A/B
$\{\star, \frac{\pi}{14}\}$	[1,1,-1]	[-1,1,1]	[-1,1,1]	[1,1,-1]	[56, 5]	D_{56}	✓/ ✓
$\{t_{\theta_{\mu\tau}}, \theta_C\}$	T_l^{ii}	T_d^{ii}	T_u^{ii}	T_ν^{ii}	GAP-ID	$\mathcal{G}_\mathcal{Q} \times \mathcal{G}_\mathcal{L}$	A/B
$\{\star, \frac{\pi}{c}\}$	[1,ω_3,ω_3^2]	[-1,1,1]	[-1,1,1]	[1,1,-1]	([N,d],[6,1])	$D_N \times S_3$	✓/✓
$\{\star, \frac{\pi}{c}\}$	[1,1,-1]	[-1,1,1]	[-1,1,1]	[1,1,-1]	([N,d],[8,3])	$D_N \times D_8$	✓/✓
$\{\star, \frac{\pi}{c}\}$	[1,ω_5,ω_5^4]	[-1,1,1]	[-1,1,1]	[1,1,-1]	([N,d],[10,1])	$D_N \times D_{10}$	✓/✓
$\{\star, \frac{\pi}{c}\}$	[1,1,-1]	[-1,1,1]	[-1,1,1]	[1,1,ω_4]	([N,d],[32,11])	$D_N \times \Sigma(32)$	✓/✓
$\{\star, \frac{\pi}{c}\}$	[1,ω_4,-ω_4]	[-1,1,1]	[-1,1,1]	[1,1,ω_3]	([N,d],[36,6])	$D_N \times (Z_3 \times (Z_3 \rtimes Z_4))$	✓/✓
$\{\star, \frac{\pi}{c}\}$	[1,1,-1]	[-1,1,1]	[-1,1,1]	[1,1,ω_5]	([N,d],[50,3])	$D_N \times (Z_5 \times D_{10})$	✓/✓
$\{\star, \frac{\pi}{c}\}$	[1,1,ω_4]	[-1,1,1]	[-1,1,1]	[1,1,ω_4]	([N,d],[96,67])	$D_N \times (SL_3^2 \rtimes Z_4)$	✓/✓*
$\{\star, \frac{\pi}{c}\}$	[1,ω_4,-ω_4]	[-1,1,1]	[-1,1,1]	[1,1,ω_5]	([N,d],[100,6])	$D_N \times (Z_5 \times (Z_5 \rtimes Z_4))$	✓/✓

Table 7.3 – Flavour symmetries controlling $\lambda_{dl}^{[e3X]}$, U_c, and portions of $U_{\mu\tau}$ in SE1. NOTES: $N \in \{28, 30\}$ for all leptoquarks in Pattern A, $N = 14$ for $\Delta_3^{(\mu)}$ in Pattern B, and $N \in \{14, 28\}$ for Δ_1^μ in Pattern B. The corresponding phase alignments are those of $\Delta_3^{(\mu)}$ in Pattern A. Also, $\{c, d\} = \{N/2, 3\}$ for $D_{N=(28,30)}$, and $\{c, d\} = \{N, 1\}$ for $D_{N=14}$. Finally, the ✓* notation indicates that the result does not appear for $N = 28$, for Δ_1^μ in Pattern B.

Performing the SVD decomposition, we find leptoquark mixing matrices of the following forms:

$$\Lambda_l = \begin{pmatrix} 1 & 0 & 0 \\ 0 & 0 & 1 \\ 0 & 1 & 0 \end{pmatrix}, \quad \Lambda_d = \begin{pmatrix} 0 & \frac{x_X}{\sqrt{x_X^2+1}} & \frac{1}{\sqrt{x_X^2+1}} \\ 0 & -\frac{1}{\sqrt{x_X^2+1}\mathrm{sgn}(x_X)} & \frac{1}{\sqrt{1+\frac{1}{x_X^2}}} \\ 1 & 0 & 0 \end{pmatrix}. \tag{7.63}$$

Using our approximations for the CKM and the PMNS matrix one finds that $x_A = x_B = 0$ and that x_C is not defined. The mixing matrices then simplify to

$$\Lambda_l = \begin{pmatrix} 1 & 0 & 0 \\ 0 & 0 & 1 \\ 0 & 1 & 0 \end{pmatrix}, \quad \Lambda_d = \begin{pmatrix} 0 & 0 & 1 \\ 0 & 1 & 0 \\ 1 & 0 & 0 \end{pmatrix}. \tag{7.64}$$

Hence the group scans are only (potentially) sensitive to $\theta_{\mu\tau}$ and θ_C via U_{PMNS} and U_{CKM}.

Forming the leptoflavour RFS generators and closing the groups, one finds the results in Table 7.3. As is clear, only D_{56} is closed when a group is formed according to Eq. (7.51), whereas more diverse structures are permitted when $\mathcal{G}_\mathcal{F} \cong \mathcal{G}_\mathcal{Q} \times \mathcal{G}_\mathcal{F}$, albeit even here only members of the Dihedral series D_N are found for $\mathcal{G}_\mathcal{Q}$. Given that 1) D_N groups represent the symmetries of polygons and 2) we consider the Cabibbo approximation for U_{CKM}, which of course just represents a (discretized) rotation about the angle θ_C in the (1,2) plane, these results are entirely unsurprising — see tables below and the results and discussion in [107, 242]. The results for $\mathcal{G}_\mathcal{L}$ also include dihedrals, in addition to members of other common finite group series like S_N and $\Sigma(2N^2)$. More complicated structures are also found, as can be seen in the last four lines of the table.[13]

From the phenomenological perspective one observes from the leftmost column that no groups are closed that predict specific values of $\theta_{\mu\tau}$, as indicated by the '$\star$' and as is obvious in the phase

[13] Note that SL_3^2 is the Special Linear Group of 2×2 matrices over the finite field of 3 elements.

$e-\mu$ **Patterns and Fermionic Mixing in SE1**							
$\{t_{\theta_{\mu\tau}}, \theta_C\}$	T_l^{ii}	T_d^{ii}	T_u^{ii}	T_ν^{ii}	GAP-ID	$\mathcal{G}_\mathcal{F}$	A/B
$\{1, \frac{\pi}{15}\}$	[1, 1, -1]	[-1, 1, 1]	[-1, 1, 1]	[-1, 1, 1]	[60, 12]	D_{60}	✓/✓
$\{1, \frac{\pi}{14}\}$	[1, 1, -1]	[-1, 1, 1]	[-1, 1, 1]	[-1, 1, 1]	[84, 14]	D_{84}	✓/✓
$\{t_{\theta_{\mu\tau}}, \theta_C\}$	T_l^{ii}	T_d^{ii}	T_u^{ii}	T_ν^{ii}	GAP-ID	$\mathcal{G}_\mathcal{Q} \times \mathcal{G}_\mathcal{L}$	A/B
$\{1, \frac{\pi}{14}\}$	[1, 1, -1]	[-1, 1, 1]	[1, -1, 1]	[-1, 1, 1]	([14,1],[6,1])	$D_{14} \times S_3$	✗/✓
$\{1, \frac{\pi}{14}\}$	[1, 1, -1]	[-1, 1, 1]	[-1, 1, 1]	[-1, 1, 1]	([28,3],[6,1])	$D_{28} \times S_3$	✓/✗
$\{1, \frac{\pi}{15}\}$	[1, 1, -1]	[-1, 1, 1]	[-1, 1, 1]	[-1, 1, 1]	([30,3],[6,1])	$D_{30} \times S_3$	✓/✗
$\{1, \frac{\pi}{14}\}$	[1, 1, -1]	[-1, 1, 1]	[1, -1, -1]	[1, -1, -1]	([28,3],[12,4])	$D_{28} \times D_{12}$	✓⋆/✓⋆

Table 7.4 – Flavour symmetries controlling $\lambda_{dl}^{[e\mu X]}$, U_C, and $U_{\mu\tau}$ in SE1. When a group is found for both Patterns A and B, the phase assignments given are for Pattern A. These results hold for all three leptoquarks, spare the final row, which only appears for Δ_1^μ (hence the ✓⋆).

alignments of T'_ν — in all cases only the third column of $U_{\mu\tau}$ is controlled by the NADS. Given the form of Eq. (7.64) and setting $\beta_\nu = \alpha_\nu$, T'_ν is then represented by

$$T'_\nu = \begin{pmatrix} e^{i\alpha_\nu} & 0 & 0 \\ 0 & \frac{1}{2}\left(e^{i\alpha_\nu} + e^{i\gamma_\nu}\right) & \frac{1}{2}\left(-e^{i\alpha_\nu} + e^{i\gamma_\nu}\right) \\ 0 & \frac{1}{2}\left(-e^{i\alpha_\nu} + e^{i\gamma_\nu}\right) & \frac{1}{2}\left(e^{i\alpha_\nu} + e^{i\gamma_\nu}\right) \end{pmatrix}, \tag{7.65}$$

which is a generalization of the well-known $\mu-\tau$ operator, which clearly knows nothing of $\theta_{\mu\tau}$. The matrix Eq. (7.65) does however, in the absence of an ambiguity along the lines of Eq. (7.37), predict $\theta_{13}^l = 0$ and $\theta_{23}^l = \pi/4$, and this is consistent with the conclusion in [171] that the RFS of isolation patterns in SE1 predict a null leptonic reactor angle. On the other hand the groups of Table 7.3 do know about specific quantizations of θ_C, and one observes that even if free parameters exist in both the up and down sectors (assuming there is no other model-specific mechanism that prohibits them), the alignments for Δ_3 in Pattern A (those shown) are such that at least the (1,1) element of U_c is unaffected. In particular, the D_N groups can predict both values of the Cabibbo angle we allowed for: $\theta_C \in \pi/14, \pi/15$. This small set is due to the tight experimental bounds in Eq. (7.42).

7.4.2 Two-Columned Patterns

We now investigate the two-columned patterns $\lambda_{dl}^{[ll'1X]}$, where $l, l' = e, \mu, \tau$ and $X = A, B$. There are in total six viable patterns given by

$$\lambda_{dl}^{[e\mu 1X]} = \begin{pmatrix} 0 & 0 & 0 \\ x_X^{[e\mu]} & y_X^{[e\mu]} & 0 \\ z^{[e\mu]} & 1 & 0 \end{pmatrix}, \quad \lambda_{dl}^{[e\tau 1X]} = \begin{pmatrix} 0 & 0 & 0 \\ x_X^{[e\tau]} & 0 & y_X^{[e\tau]} \\ z^{[e\tau]} & 0 & 1 \end{pmatrix}, \quad \lambda_{dl}^{[\mu\tau 1X]} = \begin{pmatrix} 0 & 0 & 0 \\ 0 & x_X^{[\mu\tau]} & y_X^{[\mu\tau]} \\ 0 & z^{[\mu\tau]} & 1 \end{pmatrix}, \tag{7.66}$$

where

$$x_X^{[l_i l_j]} = \frac{V_{u_X b}}{V_{u_X s}} \frac{U_{j1}}{U_{i1}}, \quad y_X^{[l_i l_j]} = -\frac{V_{u_X b}}{V_{u_X s}}, \quad z^{[l_i l_j]} = -\frac{U_{j1}}{U_{i1}}. \tag{7.67}$$

Relying on the CKM and PMNS matrix assumptions in Eqs. (7.38)-(7.39), one finds that

$$x_X^{[l_i l_j]} = y_X^{[l_i l_j]} = 0, \quad z^{[e\mu]} = \frac{\tan\theta_{\mu\tau}}{\sqrt{2}}, \quad z^{[e\tau]} = -\frac{\tan\theta_{\mu\tau}}{\sqrt{2}}, \quad z^{[\mu\tau]} = 1. \tag{7.68}$$

$e-\tau$ **Patterns and Fermionic Mixing in SE1**							
$\{t_{\theta_{\mu\tau}}, \theta_C\}$	T_l^{ii}	T_d^{ii}	T_u^{ii}	T_ν^{ii}	GAP-ID	$\mathcal{G}_\mathcal{F}$	A/B
$\{1, \frac{\pi}{15}\}$	[1, -1, 1]	[-1, 1, 1]	[-1, 1, 1]	[-1, 1, 1]	[30,3]	D_{30}	See caption.
$\{1, \frac{\pi}{14}\}$	[1, -1, 1]	[-1, 1, 1]	[1, -1, 1]	[-1, 1, 1]	[42,5]	D_{42}	
$\{1, \frac{\pi}{15}\}$	[1, -1, 1]	[-1, 1, 1]	[1, -1, 1]	[-1, 1, 1]	[60,12]	D_{60}	
$\{1, \frac{\pi}{14}\}$	[1, -1, 1]	[-1, 1, 1]	[-1, 1, 1]	[-1, 1, 1]	[84,14]	D_{84}	
$\{t_{\theta_{\mu\tau}}, \theta_C\}$	T_l^{ii}	T_d^{ii}	T_u^{ii}	T_ν^{ii}	GAP-ID	$\mathcal{G}_\mathcal{Q} \times \mathcal{G}_\mathcal{L}$	A/B
$\{1, \frac{\pi}{14}\}$	[1, -1, 1]	[-1, 1, 1]	[1, -1, 1]	[-1, 1, 1]	([14,1],[6,1])	$D_{14} \times S_3$	✗/✓
$\{1, \frac{\pi}{14}\}$	[1, -1, 1]	[-1, 1, 1]	[-1, 1, 1]	[-1, 1, 1]	([28,3],[6,1])	$D_{28} \times S_3$	✓/✗
$\{1, \frac{\pi}{14}\}$	[1, -1, 1]	[-1, 1, 1]	[1, -1, -1]	[1, -1, -1]	([28,3],[12,4])	$D_{28} \times D_{12}$	✓⋆/✓⋆
$\{1, \frac{\pi}{15}\}$	[1, -1, 1]	[-1, 1, 1]	[-1, 1, 1]	[-1, 1, 1]	([30,3],[6,1])	$D_{30} \times S_3$	✓/✗

Table 7.5 – The same as Table 7.4, but for $\lambda_{dl}^{[e\tau X]}$. For $\mathcal{G}_\mathcal{F}$, D_{30} is only found for Pattern A, and D_{42} is only found for Pattern B. The same is respectively true for D_{84} and D_{60} when considering $\Delta_3^{(\mu)}$, but both are found in both patterns for Δ_1^μ (we show triplet phases). The ✓⋆ notation implies that this group is only found for Δ_1^μ, and the phases correspond to Pattern A.

Performing the SVD decomposition for each pattern, one obtains

$$\Lambda_l = \begin{pmatrix} \frac{z}{\sqrt{1+z^2}} & \frac{1}{\sqrt{1+z^2}} & 0 \\ 0 & 0 & 1 \\ -\frac{1}{z\sqrt{1+1/z^2}} & \frac{1}{\sqrt{1+1/z^2}} & 0 \end{pmatrix}, \qquad \Lambda_d = \begin{pmatrix} 0 & 0 & 1 \\ 0 & 1 & 0 \\ 1 & 0 & 0 \end{pmatrix}, \tag{7.69}$$

$$\Lambda_l = \begin{pmatrix} \frac{z}{\sqrt{1+z^2}} & 0 & \frac{1}{\sqrt{1+z^2}} \\ -\frac{1}{z\sqrt{1+1/z^2}} & 0 & \frac{1}{\sqrt{1+1/z^2}} \\ 0 & 1 & 0 \end{pmatrix}, \qquad \Lambda_d = \begin{pmatrix} 0 & 0 & 1 \\ 0 & 1 & 0 \\ 1 & 0 & 0 \end{pmatrix}, \tag{7.70}$$

$$\Lambda_l = \begin{pmatrix} 0 & \frac{1}{\sqrt{2}} & \frac{1}{\sqrt{2}} \\ 0 & -\frac{1}{\sqrt{2}} & \frac{1}{\sqrt{2}} \\ 1 & 0 & 0 \end{pmatrix}, \qquad \Lambda_d = \begin{pmatrix} 0 & 0 & 1 \\ 0 & 1 & 0 \\ 1 & 0 & 0 \end{pmatrix}. \tag{7.71}$$

We see that, unlike in the isolation pattern case, information about $\theta_{\mu\tau}$ is communicated to the NADS via both U_{PMNS} and Λ_l.

Tables 7.4-7.6 present our results for the $e-\mu$, $e-\tau$, and $\mu-\tau$ patterns, respectively. We again find that only Dihedral groups are closed when $\mathcal{G}_\mathcal{F}$ controls both leptons and quarks simultaneously, but now the NADS does know about both $\theta_{\mu\tau}$ and θ_C. In particular, for the $e-\mu$ and $e-\tau$ patterns we see that D_N can control bi-maximal $U_{\mu\tau}$ and predict $\theta_C \in \{\pi/14, \pi/15\}$. Hexagonal mixing $U_{\mu\tau}$ is also predicted (alongside of the same Cabibbo matrices) for $\lambda_{dl}^{[\mu\tau X]}$. Finally, the same phenomenology is realized when $\mathcal{G}_\mathcal{F} \cong \mathcal{G}_\mathcal{Q} \times \mathcal{G}_\mathcal{L}$ for $\lambda_{dl}^{[e\mu X]}$ and $\lambda_{dl}^{[e\tau X]}$, but one notices that tri-bimaximal $U_{\mu\tau}$ is also realizable alongside of $\lambda_{dl}^{[\mu\tau X]}$, when $\mathcal{G}_\mathcal{L} \cong Z_3 \times SL_3^2$. As with the isolation patterns, D_N, S_3, $\Sigma(32)$, and complicated product groups all appear as leptonic flavour symmetry candidates.

$\mu-\tau$ **Patterns and Fermionic Mixing in SE1**							
$\{t_{\theta_{\mu\tau}}, \theta_C\}$	T_l^{ii}	T_d^{ii}	T_u^{ii}	T_ν^{ii}	GAP-ID	$\mathcal{G}_\mathcal{F}$	A/B
$\{1, \frac{\pi}{14}\}$	[1, -1, -1]	[1, -1, -1]	[1, -1, -1]	[1, -1, -1]	[56,5]	D_{56}	✓/✓
$\{\frac{1}{\sqrt{3}}, \frac{\pi}{15}\}$	[1, -1, -1]	[1, -1, -1]	[1, -1, -1]	[1, -1, -1]	[60,12]	D_{60}	✓/✓
$\{\frac{1}{\sqrt{3}}, \frac{\pi}{14}\}$	[1, -1, -1]	[1, -1, -1]	[1, -1, -1]	[1, -1, -1]	[84,14]	D_{84}	✓/✓
$\{t_{\theta_{\mu\tau}}, \theta_C\}$	T_l^{ii}	T_d^{ii}	T_u^{ii}	T_ν^{ii}	GAP-ID	$\mathcal{G}_\mathcal{Q} \times \mathcal{G}_\mathcal{L}$	A/B
$\{1, \frac{\pi}{c}\}$	[1,-1,-1]	[1,-1,-1]	[-1,1,-1]	[1,-1,-1]	([N,d],[8,3])	$D_N \times D_8$	See caption below.
$\{\frac{1}{\sqrt{3}}, \frac{\pi}{c}\}$	[1,-1,-1]	[1,-1,-1]	[-1,1,-1]	[1,-1,-1]	([N,d],[12,4])	$D_N \times D_{12}$	
$\{1, \frac{\pi}{c}\}$	[-1,1,1]	[-1,1,1]	[1,-1,1]	[ω_3,1,1]	([N,d],[18,3])	$D_N \times (Z_3 \times S_3)$	
$\{1, \frac{\pi}{c}\}$	[1,-1,-1]	[1,-1,-1]	[-1,1,-1]	[ω_4,-1,-1]	([N,d],[32,11])	$D_N \times \Sigma(32)$	
$\{1, \frac{\pi}{c}\}$	[-1,1,1]	[-1,1,1]	[1,-1,1]	[ω_5,1,1]	([N,d],[50,3])	$D_N \times (Z_5 \times D_{10})$	
$\{\frac{1}{\sqrt{2}}, \frac{\pi}{c}\}$	[ω_3,1,1]	[-1,1,1]	[1,-1,1]	[ω_3,1,1]	([N,d],[72,25])	$D_N \times (Z_3 \times SL_3^2)$	
$\{1, \frac{\pi}{c}\}$	[ω_4,1,1]	[-1,1,1]	[1,-1,1]	[ω_4,1,1]	([N,d],[96,67])	$D_N \times (SL_3^2 \rtimes Z_4)$	

Table 7.6 – The same as Table 7.4, but for $\lambda_{dl}^{[\mu\tau X]}$. Here $N \in \{14, 28, 30\}$, with $N = 14$ holding for Pattern B only and $N = 28, 30$ holding only for Pattern A, except when considering Δ_1^μ, which also realizes Pattern B when $N = 28$, when $\mathcal{G}_\mathcal{L}$ is contained in the first five rows of the $\mathcal{G}_\mathcal{Q} \times \mathcal{G}_\mathcal{L}$ results. $\{c, d\} = \{N/2, 3\}$ for $D_{N=(28,30)}$, and $\{c, d\} = \{N, 1\}$ for $D_{N=14}$. The phase alignments in the $\mathcal{G}_\mathcal{F}$ section correspond to Pattern A, while those given for $\mathcal{G}_\mathcal{Q}$ in the $\mathcal{G}_\mathcal{Q} \times \mathcal{G}_\mathcal{L}$ section are for D_{14}.

7.5 Scanning Partially-Reduced Matrices in SE2

The patterns derived in [171] are appealing due to their simplicity and predictive power. However, the assumptions embedded in SE1 are strong, and can be relaxed in explicit models of flavour. Hence in this section we scan over patterns derived in SE2. In the corresponding subsections below we will explore three symmetry-breaking environments that fall under the SE2 umbrella: one where both quarks and leptons are controlled by RFS, and two where *either* quarks or leptons are controlled by RFS. We discuss the allowed matrices for λ_{dl} and the corresponding phase constraints on $T_{d,l}$ following from these assumptions in what follows. As before, we also give the associated mixing matrices $\Lambda_{d,l}$ derived with an SVD technique, before performing the `GAP` scans according to Eqs. (7.53)-(7.56). We also respect the RFS group order constraint in Eq. (7.61), except for in Section 7.5.1 where we limit $2 \leq \mathcal{O}(T_{l,\nu}) \leq 4$, and our tables of results have the same organization as above. This yields 22680 different combinations of generators getting scanned over in Section 7.5.1 for each leptoquark we consider (and in both patterns $\lambda_{dl}^{[e0,\mu 0]}$), and either 6640 or 9960 combinations in Section 7.5.2, depending on whether we discretize $\theta_{\mu\tau}$ according to Eqs. (7.45a) or (7.45b), respectively. For the simplified pattern studied in Section 7.5.3 we only scan over 660 generator combinations.

In addition to these restrictions we further impose that, when scanning through Eqs. (7.54)-(7.56), the NADS we reconstruct knows about $\theta_{\mu\tau}$ and/or θ_C. That is, we demand

$$T_u^{11} \neq T_u^{22} \quad \text{and} \quad T_\nu^{11} \neq T_\nu^{22} \tag{7.72}$$

when studying $\mathcal{G}_\mathcal{F} \cong \mathcal{G}_\mathcal{Q} \times \mathcal{G}_\mathcal{L}$ in Section 7.5.1 and $\mathcal{G}_{\mathcal{L},\mathcal{Q}}$ in Sections 7.5.2-7.5.3.

Electron Isolation and Fermionic Mixing in SE2					
$\{x_e, t_{\theta_{\mu\tau}}, \theta_C\}$	T_l^{ii}	T_u^{ii}	T_ν^{ii}	GAP-ID	$\mathcal{G}_\mathcal{F}$
$\{\frac{1}{2}, 1, \star\}$	[-1,1,-1]	[-1,-1,1]	[1,-1,-1]	[12,4]	D_{12}
$\{1, \star, \star\}$	[-1,1,-1]	[-1,-1,1]	[-1,-1,1]	[24,12]	S_4
$\{1, \star, \star\}$	[-1,ω_4,ω_4]	[-1,-1,1]	[-1,-1,1]	[96,64]	$\Delta(96)$
$\{x_e, t_{\theta_{\mu\tau}}, \theta_C\}$	T_l^{ii}	T_u^{ii}	T_ν^{ii}	GAP-ID	$\mathcal{G}_\mathcal{Q} \times \mathcal{G}_\mathcal{L}$
$\{\frac{1}{M}, 1, \frac{\pi}{c}\}$	[-1,1,-1]	[-1,1,-1]	[1,-1,-1]	([N,d],[6,1])	$D_N \times S_3$
$\{\frac{1}{M}, 1, \frac{\pi}{c}\}$	[-1,1,-1]	[-1,1,-1]	[ω_4,-ω_4,-1]	([N,d],[24,12])	$D_N \times S_4$
$\{\frac{1}{M}, 1, \frac{\pi}{c}\}$	[-1,ω_4,ω_4]	[-1,1,-1]	[1,-1,-1]	([N,d],[32,11])	$D_N \times \Sigma(32)$
$\{\frac{1}{M}, 1, \frac{\pi}{c}\}$	[-1,ω_4,ω_4]	[-1,1,-1]	[1,ω_4,-ω_4]	([N,d],[96,67])	$D_N \times (SL_3^2 \rtimes Z_4)$

Table 7.7 – Flavour symmetries controlling $\lambda_{dl}^{[e0]}$, U_c, and $U_{\mu\tau}$ in SE2. In all cases $T_d = \text{diag}(1,-1,-1)$, and the filtered results we present here hold for all three leptoquarks. The variables $\{c,d\} = \{N/2, 3\}$ for $D_{N=(28,30)}$, and $\{c,d\} = \{N, 1\}$ for $D_{N=14}$. The phase alignments shown are for D_{14} — send $T_u^{ii} \to [1,-1,-1]$ for $D_{28,30}$. $M \in \{1..5\}$.

7.5.1 Quarks and Leptons

If $\mathcal{G}_\mathcal{F} \to \{\mathcal{G}_u, \mathcal{G}_d, \mathcal{G}_l, \mathcal{G}_\nu\}$ we must still satisfy Eq. (7.20), as in SE1. However, the muon isolation pattern is no longer forbidden and so we obtain

$$\lambda_{dl}^{[e0]} = \lambda_{be}\begin{pmatrix} 0 & 0 & 0 \\ x_e & 0 & 0 \\ 1 & 0 & 0 \end{pmatrix}, \quad \lambda_{dl}^{[\mu 0]} = \lambda_{b\mu}\begin{pmatrix} 0 & 0 & 0 \\ 0 & x_\mu & 0 \\ 0 & 1 & 0 \end{pmatrix}, \quad \text{with} \quad x_X = \frac{\lambda_{sX}}{\lambda_{bX}}. \tag{7.73}$$

These patterns respectively correspond to $-\alpha_l = \beta_d = \gamma_d$ and $-\beta_l = \beta_d = \gamma_d$, for the scalar triplet. For the vector triplet and singlet the minus signs do not appear in these equalities (as in Table 7.2). However, we are not subject to any further equalities between the phases of $T_{u,\nu}$, and so our overall generating set is not as constrained as in SE1 — we are still capable of distinguishing three generations of leptons in both the charged and neutrino sectors. Also note that the quark splitting parameters x_X are bound by many experimental constraints — see the discussion in [163, 171, 173]. In our scans we will demand the following:

$$10^{-4} \leq x_X \leq 1\,, \tag{7.74}$$

as this generates a sufficient number of interesting groups. Extending or limiting this range is a trivial matter and can be tuned in response to further experimental analysis.

Continuing, we derive the corresponding $\Lambda_{d,l}$ rotations from Eq. (7.73), where clearly the matrices in Eq. (7.63) hold for the electron isolation pattern $\lambda_{dl}^{[e0]}$ with $x_X \to x_e$. For the muon isolation pattern one obtains

$$\Lambda_l = \begin{pmatrix} 0 & 1 & 0 \\ 0 & 0 & 1 \\ 1 & 0 & 0 \end{pmatrix}, \qquad \Lambda_d = \begin{pmatrix} 0 & \frac{x_\mu}{\sqrt{x_\mu^2+1}} & \frac{1}{\sqrt{x_\mu^2+1}} \\ 0 & -\frac{1}{\sqrt{x_\mu^2+1}\text{sgn}(x_\mu)} & \frac{1}{\sqrt{1+\frac{1}{x_\mu^2}}} \\ 1 & 0 & 0 \end{pmatrix} \tag{7.75}$$

where as expected only Λ_l changes from the electron analogue.

Muon Isolation and Fermionic Mixing in SE2 ($\mathcal{G}_\mathcal{F}$ Case)					
$\{x_\mu, t_{\theta_{\mu\tau}}, \theta_C\}$	T_l^{ii}	T_u^{ii}	T_ν^{ii}	GAP-ID	$\mathcal{G}_\mathcal{F}$
$\{1, \star, \star\}$	[-1,-1,1]	[-1,-1,1]	[-1,-1,1]	[8,3]	D_8
$\{1, 1, \star\}$	[1,-1,-1]	[-1,-1,1]	[1,-1,-1]	[8,3]	D_8
$\{1, \frac{1}{\sqrt{3}}, \star\}$	[1,-1,-1]	[-1,-1,1]	[1,-1,-1]	[12,4]	D_{12}
$\{1, 1, \star\}$	[1,-1,-1]	[-1,-1,1]	[ω_3,ω_3^2,1]	[12,4]	D_{12}
$\{1, \frac{1}{\sqrt{3}}, \star\}$	[1,-1,-1]	[-1,-1,1]	[ω_4,-ω_4,1]	[24,5]	$Z_4 \times S_3$
$\{\frac{1}{3}, \star, \star\}$	[1,-1,-1]	[-1,-1,1]	[-1,-1,1]	[24,6]	D_{24}
$\{1, 1, \star\}$	[-1,-1,1]	[-1,-1,1]	[1,-1,-1]	[24,12]	S_4
$\{1, \star, \frac{\pi}{14}\}$	[1,-1,-1]	[1,-1,-1]	[-1,-1,1]	[28,3]	D_{28}
$\{1, \frac{1}{\sqrt{3}}, \frac{\pi}{15}\}$	[1,-1,-1]	[1,-1,-1]	[-1,1,-1]	[30,3]	D_{30}
$\{1, \star, \star\}$	[-1,-1,1]	[-1,-1,1]	[ω_4,ω_4,-1]	[32,11]	$\Sigma(32)$
$\{1, 1, \star\}$	[1,-1,-1]	[-1,-1,1]	[1,ω_4,-ω_4]	[32,11]	$\Sigma(32)$
$\{1, 1, \star\}$	[1,-1,-1]	[-1,-1,1]	[1,ω_3,ω_3^2]	[36,12]	$Z_6 \times S_3$
$\{1, \frac{1}{\sqrt{3}}, \frac{\pi}{14}\}$	[1,-1,-1]	[-1,1,-1]	[-1,1,-1]	[42,5]	D_{42}
$\{1, \star, \frac{\pi}{14}\}$	[1,-1,-1]	[1,-1,-1]	[ω_4,ω_4,-1]	[56,4]	$Z_4 \times D_{14}$
$\{1, 1, \frac{\pi}{14}\}$	[1,-1,-1]	[1,-1,-1]	[1,-1,-1]	[56,5]	D_{56}
$\{1, 1, \frac{\pi}{14}\}$	[1,-1,-1]	[1,-1,-1]	[ω_4,-ω_4,1]	[56,7]	$(Z_{14} \times Z_2) \rtimes Z_2$
$\{\frac{1}{5}, 1, \star\}$	[1,-1,-1]	[-1,-1,1]	[ω_3,ω_3^2,1]	[60,5]	A_5
$\{\frac{1}{5}, \frac{1}{\sqrt{3}}, \star\}$	[1,-1,-1]	[-1,-1,1]	[-1,1,-1]	[60,5]	A_5
$\{1, \star, \frac{\pi}{15}\}$	[1,-1,-1]	[1,-1,-1]	[-1,-1,1]	[60,12]	D_{60}
$\{1, \frac{1}{\sqrt{3}}, \frac{\pi}{15}\}$	[1,-1,-1]	[1,-1,-1]	[1,-1,-1]	[60,12]	D_{60}
$\{1, \frac{1}{\sqrt{3}}, \frac{\pi}{14}\}$	[1,-1,-1]	[1,-1,-1]	[1,-1,-1]	[84,14]	D_{84}
$\{1, \star, \star\}$	[ω_4,-1,ω_4]	[-1,-1,1]	[ω_4,ω_4,-1]	[96,67]	$SL_3^2 \rtimes Z_4$

Table 7.8 – The same as in Table 7.7 but for the muon isolation pattern. Here we only show reconstructed $\mathcal{G}_\mathcal{F}$, i.e. those groups formed from the closure of all four RFS generators.

Muon Isolation and Fermionic Mixing in SE2 ($\mathcal{G}_\mathcal{Q} \times \mathcal{G}_\mathcal{L}$ Case)					
$\{x_\mu, t_{\theta_{\mu\tau}}, \theta_C\}$	T_l^{ii}	T_u^{ii}	T_ν^{ii}	GAP-ID	$\mathcal{G}_\mathcal{Q} \times \mathcal{G}_\mathcal{L}$
$\{\frac{1}{M}, 1, \frac{\pi}{c}\}$	[1,-1,-1]	[-1,1,-1]	[ω_3,ω_3^2,1]	([N,d],[6,1])	$D_N \times S_3$
$\{\frac{1}{M}, \frac{1}{\sqrt{3}}, \frac{\pi}{c}\}$	[1,-1,-1]	[-1,1,-1]	[-1,1,-1]	([N,d],[6,1])	$D_N \times S_3$
$\{\frac{1}{M}, 1, \frac{\pi}{c}\}$	[1,-1,-1]	[-1,1,-1]	[1,-1,-1]	([N,d],[8,3])	$D_N \times D_8$
$\{\frac{1}{M}, \frac{1}{\sqrt{3}}, \frac{\pi}{c}\}$	[1,-1,-1]	[-1,1,-1]	[1,-1,-1]	([N,d],[12,4])	$D_N \times D_{12}$
$\{\frac{1}{M}, 1, \frac{\pi}{c}\}$	[-1,-1,1]	[-1,1,-1]	[ω_4,-ω_4,1]	([N,d],[24,12])	$D_N \times S_4$
$\{\frac{1}{M}, 1, \frac{\pi}{c}\}$	[1,-1,-1]	[-1,1,-1]	[1,ω_4,-ω_4]	([N,d],[32,11])	$D_N \times \Sigma(32)$

Table 7.9 – The same as in Table 7.8 but for $\mathcal{G}_\mathcal{Q} \times \mathcal{G}_\mathcal{L}$ group structures. $\{c, d\} = \{N/2, 3\}$ for $D_{N=(28,30)}$, and $\{c, d\} = \{N, 1\}$ for $D_{N=14}$. Again, $M \in \{1..5\}$ and the phase alignments shown are for D_{14} — send $T_u^{ii} \to [1, -1, -1]$ for $D_{28,30}$.

Lepton Isolation and Lepton Mixing in SE2					
$\lvert\tan\theta_{\mu\tau}\rvert$	T_l^{ii}	T_ν^{ii}	GAP-ID	$\mathcal{G}_\mathcal{L}$	Electron/Muon
$1/\sqrt{2}$	$[\omega_3, 1, \omega_3^2]$	$[-1, 1, -1]$	$[12, 3]$	A_4	✓/✓
1	$[1, \omega_4, -\omega_4]$	$[1, -1, -1]$	$[24, 12]$	S_4	✓/✗
$1/\sqrt{2}$	$[1, \omega_3, \omega_3^2]$	$[1, -1, -1]$	$[24, 12]$	S_4	✓/✗
$1/\sqrt{2}$	$[\omega_3, 1, \omega_3^2]$	$[\omega_4, -1, \omega_4]$	$[48, 3]$	$\Delta(48)$	✓/✓
1	$[\omega_4, 1, -1]$	$[1, -1, \omega_4]$	$[48, 30]$	$A_4 \rtimes Z_4$	✗/✓
$1/\sqrt{2}$	$[1, \omega_3, \omega_3^2]$	$[\omega_4, -\omega_4, -\omega_4]$	$[48, 30]$	$A_4 \rtimes Z_4$	✓/✗
$1/\sqrt{2}$	$[\omega_3, 1, \omega_3^2]$	$[1, -1, -1]$	$[72, 42]$	$Z_3 \times S_4$	✗/✓
$1/\sqrt{2}$	$[\omega_3, 1, \omega_3^2]$	$[\omega_5, \omega_5^3, \omega_5]$	$[75, 2]$	$\Delta(75)$	✓/✓
$1/\sqrt{2}$	$[\omega_3, 1, \omega_3^2]$	$[1, \omega_3, 1]$	$[81, 7]$	$\Sigma(81)$	✓/✓
$1/\sqrt{2}$	$[1, \omega_3, \omega_3^2]$	$[\omega_4, 1, -\omega_4]$	$[96, 64]$	$\Delta(96)$	✓/✗
1	$[\omega_4, 1, -1]$	$[1, -1, 1]$	$[96, 186]$	$Z_4 \times S_4$	✓/✓

Table 7.10 – Flavour symmetries $\mathcal{G}_\mathcal{L}$ controlling electron and/or muon isolation patterns $\lambda_{dl}^{[e,\mu]}$ alongside of $U_{\mu\tau}$ lepton mixing in SE2. Note that the phase configurations for $T_{l,\nu}$ are not necessarily equivalent between the electron and muon isolation patterns. When both are applicable (two ✓), we show the phase configurations associated to $\lambda_{dl}^{[\mu]}$.

The results of our scans given these inputs are found in Table 7.7-7.9.[14] For the electron isolation patterns in Table 7.7 one notices that no 'four-generator' group $\mathcal{G}_\mathcal{F}$ was found that can simultaneously quantize x_e, $\theta_{\mu\tau}$, and θ_C. However, the cubic group S_4 and the popular $\Delta(96)$ member of the $\Delta(6N^2)$ series appear for the first time. These, along with D_{12}, can predict the leptoquark coupling ratio x_e, and D_{12} can also control bi-maximal mixing. For $\mathcal{G}_\mathcal{F} \cong \mathcal{G}_\mathcal{Q} \times \mathcal{G}_\mathcal{L}$ one sees that all relevant phenomenological parameters are quantized (as per our assumptions) — all allowed values of x_e and θ_C are possible, but only bi-maximal $U_{\mu\tau}$ mixing is found. In particular, we find that any given $\mathcal{G}_\mathcal{Q} \cong D_N$ is capable of controlling any value of x_e at the same value of θ_C, a fact that we have checked explicitly with (non-automated) `GAP` scripts and an analytic, 'by-hand' closure of $D_{14} \cong \{T'_u, T'_d\}$ at differing x_e. As seen below, similar trends appear for other λ_{dl} when considering independent quark symmetries.

The results for muon isolation ($\lambda_{dl}^{[\mu 0]}$) in Tables 7.8-7.9 are even richer. Concentrating on four-generator $\mathcal{G}_\mathcal{F}$ in Table 7.8, we see that Dihedrals are now capable of quantizing all three parameters in our matrices, predicting either bi-maximal or hexagonal $U_{\mu\tau}$ and both $\pi/14$ and $\pi/15$ for θ_C. The product group $(Z_{14} \times Z_2) \rtimes Z_2$ also controls the full parameter space. However, (amongst others) we also notice that the (very small) $D_{8,12}$ groups and the cubic group S_4 can predict a unit x_μ alongside of bi-maximal lepton mixing, and the popular A_5 group of the alternating group series A_N appears for the first time, predicting either bi-maximal or hexagonal mixing simultaneously with $x_\mu = 1/5$. When the group structure is broadened to Table 7.9 we also see that very small groups in both the quark and lepton sectors yield a rich diversity of phenomenological signatures, including all values of x_μ, as in the electron isolation case.

7.5.2 Leptons Only

When $\mathcal{G}_\mathcal{L} \to \{\mathcal{G}_l, \mathcal{G}_\nu\}$ one can simultaneously control λ_{dl} and U_{PMNS}. In this case only T_l is active in λ_{dl}, so satisfying Eq. (7.20) is then possible if one or more phases of T_l are set to zero. Given that we are now only asking $\mathcal{G}_\mathcal{L}$ to control portions of SM mixing, we additionally demand that $\mathcal{G}_l$ distinguishes all three charged leptons. This then requires that only *one* phase be set to zero. Furthermore, satisfying Eq. (7.20) in way that accounts for $R_{K^{(*)}}$ means that only α_l or β_l can be null. We are therefore led to conclude that only electron and muon isolation patterns are allowed in this environment:

$$\lambda_{dl}^{[e]} = \lambda_{be} \begin{pmatrix} y_e & 0 & 0 \\ x_e & 0 & 0 \\ 1 & 0 & 0 \end{pmatrix}, \quad \lambda_{dl}^{[\mu]} = \lambda_{b\mu} \begin{pmatrix} 0 & y_\mu & 0 \\ 0 & x_\mu & 0 \\ 0 & 1 & 0 \end{pmatrix}, \quad \text{with} \quad x_X = \frac{\lambda_{sX}}{\lambda_{bX}}, \; y_X = \frac{\lambda_{dX}}{\lambda_{bX}}, \tag{7.76}$$

which respectively correspond to $\alpha_l = 0$ and $\beta_l = 0$. Note that, unlike in Section 7.5.1, we are no longer forced to set λ_{de} or $\lambda_{d\mu}$ to zero, since we have no quark symmetry/phases to differentiate down quarks. The lack of an active quark symmetry also means that our scan results hold for all leptoquarks under consideration, since the flavour symmetry active in λ_{dl} only differentiates between them through relative signs in the down quark and charged lepton generators, cf. Table 7.2. It also means we only need to derive Λ_l in this scenario, for which we find the pattern in Eq. (7.63) holds for $\lambda_{dl}^{[e]}$ and that in Eq. (7.75) for $\lambda_{dl}^{[\mu]}$. Note that neither x_X nor y_X appears in the Λ_l of Eq. (7.63) or Eq. (7.75), and so the RFS of $\mathcal{G}_\mathcal{L}$ in this scenario can only control the shape of λ_{dl}, but not the specific values of its free couplings.

In addition to insisting that T_l has three eigenvalues, we will also demand that *either* 1) T_ν has three eigenvalues that can distinguish each neutrino species, and therefore controls a Dirac neutrino mass term with an associated (quantized) $U_{\mu\tau}$ mixing matrix predicted at LO or 2) that T_ν has its phases aligned such that a free parameter can be fitted to θ_{13}^l. In the latter case we can claim that realistic three-generation PMNS mixing is achievable alongside of controlling λ_{dl} at LO.

[14] Note that, due to the abundance of viable phase relationships in this symmetry environment, we have further enforced $\det(T_a) = 1$ in this Subsection. This is consistent with the natural expectation that the NADS is a subgroup of a Special Unitary SU(N) group.

$\lambda^{[bs0]}$ **and Quark Mixing in SE2**		
$\{\theta_C\}$	$\{y_b\}$	$\mathcal{G}_\mathcal{Q} \sim D_N$
$\pi/14$	$\{\frac{1}{5}, \frac{1}{4}, \frac{1}{3}, \frac{1}{2}, 1\}$	$N \in 14, 28$
$\pi/15$	$\{\frac{1}{5}, \frac{1}{4}, \frac{1}{3}, \frac{1}{2}, 1\}$	$N \in 30$
T_d^{ii}	[-1, 1, 1]	
T_u^{ii} $(N = 14)$	[1, -1, 1]	
T_u^{ii} $(N = 28)$	[1, -1, -1]	
T_u^{ii} $(N = 30)$	[-1, 1, 1]	

GAP-ID	$\mathcal{G}_\mathcal{Q}$
[14, 1]	D_{14}
[28, 3]	D_{28}
[30, 3]	D_{30}

Table 7.11 – Flavour symmetries $\mathcal{G}_\mathcal{Q}$ controlling the simplified $\lambda^{[bs0]}$ pattern and U_c quark mixing in SE2.

The results of our `GAP` scans are given in Table 7.10, where one observes that a host of NADS have been recovered, including popular groups like A_4, S_4, $\Sigma(81)$, and more members of the $\Delta(3N^2)$ and $\Delta(6N^2)$ series. We see that all of the patterns we uncovered are consistent with Eq. (7.45b), namely the bi-maximal and tri-bimaximal forms of $U_{\mu\tau}$, and we have also given our results for both patterns in Eq. (7.76) in the same table, as many groups were found in common (albeit with slightly different phase configurations). In particular, we recover the A_4 group used in some of the leptoquark models of [173], including the corresponding VEV alignments.[15] Of course, lifting some or all of our constraints, in particular the demand for phase alignments in the (1,3) or (2,3) sectors of T_ν, would yield a longer Table 7.10, as would expanding the allowed parameter space for $\theta_{\mu\tau}$ or RFS generator phases our scans populate matrices with. This latter statement holds for all scans above, as well.

7.5.3 Quarks Only

As a final study we consider $\mathcal{G}_\mathcal{Q} \to \{\mathcal{G}_u, \mathcal{G}_d\}$, which can simultaneously control λ_{dl} and portions of U_{CKM}. Resolving $R_{K^{(*)}}$ requires that entries in at least one column of the s and b-quark rows be nonzero, and distinguishing two of three quark generations then requires that the all entries of the d-quark row be null. Hence the most general matrix allowed for λ_{dl} is given by

$$\lambda_{dl}^{[bs]} = \lambda_{b\tau} \begin{pmatrix} 0 & 0 & 0 \\ x_s & y_s & z_s \\ x_b & y_b & 1 \end{pmatrix}, \quad \text{with} \quad x_X = \frac{\lambda_{Xe}}{\lambda_{b\tau}}, \quad y_X = \frac{\lambda_{X\mu}}{\lambda_{b\tau}}, \quad z_s = \frac{\lambda_{s\tau}}{\lambda_{b\tau}}. \tag{7.77}$$

This is associated to $\alpha_d \neq \beta_d = \gamma_d = 0$, which in principle permits the determination of the Cabibbo angle, as did all of the simplified models of SE1 except λ_{QL}^{e3C}. As in Section 7.5.2, our results hold for all three leptoquarks under consideration.

The general matrix is hard to work with in an SVD analysis, but we can make a simpler

[15] These simple A_4-based models are again similar to the Altarelli-Feruglio construction [113], where the quark sector is mostly unadressed with the fields assigned as singlets of A_4. The lepton doublet is an A_4 triplet and the A_4 breaking is communicated differently by distinct A_4 triplet flavon VEVs. The extension to leptoquark models in [173] has the same flavon VEV that breaks A_4 in the charged lepton sector being used to make the A_4 invariant for the terms with the leptoquarks, and this specific A_4 breaking then leads to lepton isolation patterns for λ_{dl}. Specifically, the charged lepton VEV is $\sim \langle 1, 0, 0 \rangle$, and so the corresponding RFS generator goes as $T_l = \text{diag}\left(1, \omega_3, \omega_3^2\right)$, which we find for the electron isolation case.

ansätz for $\lambda_{dl}^{[bs]}$— which is motivated by simple flavon models — as follows:

$$\lambda_{dl}^{[bs0]} = \lambda_{b\tau} \begin{pmatrix} 0 & 0 & 0 \\ 0 & y_b & y_b \\ 0 & 1 & 1 \end{pmatrix}. \tag{7.78}$$

For the quark splitting parameter we use the bound in Eq. (7.74) with $x_\mu \to y_b$. The corresponding Λ_d is given in Eq. (7.75), with $x_\mu \to y_b$. Unlike in Section 7.5.2, we see that $\mathcal{G}_\mathcal{Q}$ does have control over the values of the particular leptoquark couplings, and not just the overall shape of λ_{dl}.

The corresponding $\mathcal{G}_\mathcal{Q}$ we recover[16] are given in Table 7.11 where we again only find members of the Dihedral series D_N, also associated to the two values of the Cabibbo angle we permit: $\theta_C \in \pi/14, \pi/15$. However, a number of different quantizations for the quark splitting parameter y_b are found, and so $\mathcal{G}_\mathcal{Q}$ can easily predict different coupling patterns for λ_{dl}, and thereby observables like $R_{K^{(*)}}$.

7.6 Summary and Outlook

We have shown how the patterns of couplings derived in the 'simplified models of flavourful leptoquarks' introduced in [171] can be sourced from the breakdown of a non-Abelian discrete family symmetry (NADS) $\mathcal{G}_\mathcal{F}$. The Abelian residual flavour symmetries (RFS) that remain in the mass terms of SM fermions also control the CKM and PMNS mixing matrices, thereby linking the SM flavour problem with potential observations of lepton non-universality in the $b \to sll$ ratio observables $R_{K^{(*)}}$. In addition, we have generalized the predictions of [171] by identifying two classes of simplified models that employ the RFS mechanism: one where RFS act in all couplings sourced by the original SM-invariant leptoquark terms in Eq. (7.3), as in [171], and one where the RFS only controls the λ_{dl} coupling between down quarks and charged leptons. We referred to these as Symmetry Environment 1 (SE1) and 2 (SE2) respectively, with the latter representing a highly natural relaxation of the former that can easily be realized in simple flavon-based models.

Our approach for finding phenomenologically viable NADS follows the strategy outlined in [107, 216], which is automated via scripts written in the `GAP` language for computational finite algebra. Critically, we perform these scans from the bottom-up, meaning that we first specify the subgroup mediating the RFS in different fermion sectors, discretize all available free parameters in a way that respects experimental constraints, and then close parent $\mathcal{G}_\mathcal{F}$ using the generators of said RFS. We must do so in a basis where these generators simultaneously know about all predictions we want to connect to $\mathcal{G}_\mathcal{F}$, and to that end we derived the so-called 'leptoflavour' basis where λ_{dl} is diagonalized and the physical definitions of the CKM and PMNS matrices are respected. Our scripts then find a plethora of finite groups that can yield the desired phenomenology upon symmetry breaking, including members of many group series like D_N, A_N, S_N, $\Delta(3N^2)$, $\Delta(6N^2)$, $\Sigma(3N^2)$ and $\Sigma(3N^3)$ that are popular in the flavoured model-building community. As an important crosscheck, we recover the A_4 tetrahedral symmetry and corresponding flavon VEV alignments used in [173] when we allow for RFS only in the lepton sector, and so our results provide the relevant information necessary to 'reconstruct' complete models of flavour.

However, beyond the imposition of RFS, the approach to studying flavour discussed here and in [171] is model-independent, as the simplified models we define distill important (falsifiable) phenomenology without committing to additional assumptions regarding the dynamics of flavour-symmetry breaking or any associated UV-complete Lagrangian (which may not be falsifiable). Additionally, the ability to structure leptoquark Yukawa couplings, and not just the mixing associated to them, represents a novel and welcome result in comparison to the application of RFS to the SM alone, and may have applications in other BSM constructions (e.g. multi-Higgs-doublet models). Hence, as the experimental status of LFV, B-meson mixing, and B-decay observables like $R_{K^{(*)}}$ and

[16] We only consider the discretization scheme in Eq. (7.45a), given prior results in [107].

the $b \to c l \nu$ ratio observables $R_{D^{(*)}}$ [243–249] evolve, so will the constraints implied on the various leptoquark couplings, and thereby on the symmetries we employ. We will leave the exploration of these and other aspects of our simplified models, including their UV-completions and implications at the LHC, to future work.

Conclusion

As we have discussed in this manuscript, the Standard Model of particle physics is probably not the ultimate theory of Nature, if such a theory exists. However, because of its various successes at low energy, it provides a consistent description of numerous processes and observables. Therefore, it is quite natural to think that the new physics that would solve the different shortcomings of the SM is based on a similar structure, at least if gravity is not included. Many attempts to solve these issues have been investigated in the past few decades.

Throughout this manuscript, we have considered frameworks beyond the standard model, with a specific focus on Supersymmetry. The SUSY framework has been a very popular extension, and still remains a very appealing way out, despite the lack of experimental signatures at the Large Hadron Collider. In absence of any direct experimental signatures for new physics, one may continue to investigate highly theoretically motivated frameworks. At our knowledge, it is not possible to asses that SUSY is ruled out, as it might lies somewhere above the energy scale reached by the current experiments. Another possibility for why SUSY has not been discovered so far, could be to consider SUSY beyond its vanilla realizations, as the non-trivial extended frameworks could make SUSY hard to discover at colliders.

For instance, SUSY BSM extensions, such as the MSSM, describe a non-trivial flavour structure when we consider the most general framework. Going beyond the Minimal Flavour Violation paradigm, one accesses a rich phenomenology and interesting consequences, such for instance weakening the current bounds on the SUSY spectrum. Moreover, the inclusion and interplays of the flavour violating parameters may lead to indirect smoking guns for SUSY. In this manuscript, we have aimed at providing discussions around non-trivial SUSY flavour structures, using motivated frameworks such as the most general MSSM or flavoured $SU(5)$ Grand Unified Theories extensions.

In the first project presented in this manuscript, we have considered different methods to access information about the underlying flavour structure of the MSSM. Based on the assumption of the observation of a squark-like state, we have given a proof of principle that obtaining information on the flavour structure of the SUSY theories is something feasible.

We then considered the highly motivated framework of flavoured SUSY GUT theories, where the non-trivial flavour structure, reduced to a few number of parameters, is a natural consequence. These models, in addition to the usual SUSY-addressed SM shortcomings, solve the gauge unification problem and the SM flavour problem by using flavour symmetries. We investigated constraints on these type of models, basing the analysis on $A_4 \times SU(5)$ inspired models.

However, we should also think of other alternatives to SUSY that could account for other SM prediction deviations. In particular, one potential hint of Lepton Non Universality has been provided by the LHCb measurements of $R_{K^{(*)}}$. In case of R-parity preserving simple SUSY extensions, these anomalous data cannot be accommodated. One of the most attractive solutions is to include leptoquarks to the SM content.

Therefore, in the last chapter, we have left the SUSY framework to investigate leptoquark SM extensions. Remaining in the context of flavour symmetries, we have found that well controlled and predictive leptoquark couplings can emerge from a parent flavour group. The flavour groups found in this analysis, are compatible with the $R_{K^{(*)}}$ LHCb measurements alongside of leading order SM fermionic mixings. Even if the anomalous $R_{K^{(*)}}$ data would disappear after further experimental analyses, we have proposed a new method for scanning over leptoquark BSM extension and our

results would remain appealing for further model building exploration of leptoquarks.

How to go beyond these studies? Several ongoing projects have already started that I wish to mention here. Additional ideas might as well be considered.

Concerning the first project however, we have come to the conclusion that going beyond the analysis presented might be somehow too early, as it already relies on the assumption of the observation of squark at colliders. This analysis is very simplistic, and further improvements may be considered. First of all, we did not analyses in detail the uncertainties associated to the different methods. Moreover, one should also consider investigating further the feasibility of the method by performing a full collider simulation which would tell if the observables that we have discussed are indeed accessible at LHC, but we assume that this would be needed in case of an actual observation of squark. As a second point, the investigation of additional observables should lead to a significant improvement of the efficiency of the method. Additionally, one can consider other machine learning algorithms to improve the performance.

Regarding the phenomenological analysis of flavoured GUT models, we are currently investigating a more complete setup. Following a model based on $S_4 \times SU(5)$, which includes full Yukawa coupling predictions and an implementation of the seesaw mechanism, we are fitting the various order one parameters of the model to the SM experimental measurements like masses and mixing matrices. Furthermore, we will also include all flavour violating decays and dark matter that we have considered in our previous analysis. The goal of the upcoming study is to identify key observables and signatures at colliders for this type of scenarios. A very interesting aspect is that we expect accurate predictions on the neutrino sector, such as the Majorana/Dirac phases that should lead to potential smoking guns for this model.

Finally, the last project on leptoquarks should lead to many different projects, that are currently under discussion. First, a pure phenomenological analysis about the signatures of the very predictive patterns found would be interesting. In my opinion, a way to do so would be to compute the effective flavour violating operators which would be compared then to different experimental limits. Additionally, recasting or designing new analysis at the LHC to investigate these very predictive patterns would lead to a more restrictive parameter space, selecting more efficiently several data-favoured groups. Furthermore, it would be quite interesting to provide a "user guide" of the bottom-up to top-down approach by building several simple models using different flavour groups found in our analysis; specifically if the flavour group has not been considered so far in the literature (for instance the group A_4 has already been used and has been recovered in our scan). Additionally, as a personal interest, I would like to investigate the UV completion of such models.

Appendix A

Pocket formulae for two component notation

In this appendix we wish to collect a few formulas and definitions that can help for computations, specifically for Chapter 2. We define briefly the two component notation and explicit useful formulas and relations.

A.1 Weyl spinors

As already stated in Sec. 1.2, a Dirac fermion ψ_D can be decomposed in two Weyl fermions, which are fundamental representations of $SU(2) \times SU(2)$:

$$\psi_D = (1/2, 0) + (0, 1/2). \tag{A.1}$$

We can construct ξ_A, a two-component left-handed Weyl spinor which transforms as $(1/2, 0)$. The transformation can be written as:

$$\xi_A \to \xi'_A = (S)_A{}^B \xi_B, \tag{A.2}$$

where $(S)_A{}^B$ is a 2×2 matrix, element of $SL(2, C)$. Similarly, one can define a right-handed Weyl spinor $\bar{\chi}_{\dot{A}}$, transforming as $(0, 1/2)$

$$\bar{\chi}_{\dot{A}} \to \bar{\chi}'_{\dot{A}} = \bar{\chi}_{\dot{B}} (S^\dagger)^{\dot{B}}{}_{\dot{A}}. \tag{A.3}$$

We use the convention that left (resp. right) handed spinors carry undotted (resp. dotted) indices, which contract from bottom left to top right (resp. top left to bottom right). Raising and lowering the indices can be achieved using the purely antisymmetric tensors:

$$\xi^A = \epsilon^{AB} \xi_B, \quad \xi_A = \epsilon_{AB} \xi^B, \quad \bar{\chi}^{\dot{A}} = \epsilon^{\dot{A}\dot{B}} \bar{\chi}_{\dot{B}}, \quad \bar{\chi}_{\dot{A}} = \epsilon_{\dot{A}\dot{B}} \bar{\chi}^{\dot{B}}, \tag{A.4}$$

with

$$\epsilon_{AB} = \begin{pmatrix} 0 & 1 \\ -1 & 0 \end{pmatrix}, \quad \epsilon^{AB} = \begin{pmatrix} 0 & -1 \\ 1 & 0 \end{pmatrix}, \quad \epsilon_{\dot{A}\dot{B}} = \begin{pmatrix} 0 & -1 \\ 1 & 0 \end{pmatrix}, \quad \epsilon^{\dot{A}\dot{B}} = \begin{pmatrix} 0 & 1 \\ -1 & 0 \end{pmatrix}. \tag{A.5}$$

We can transform a left handed Weyl spinor into an right handed one (and vice versa) by using the conjugation:

$$\xi_A = \left(\bar{\xi}_{\dot{A}}\right)^\dagger, \quad \bar{\chi}_{\dot{A}} = (\chi_A)^\dagger. \tag{A.6}$$

Let us mention that the charge conjugaison acts as

$$\xi_A = \left(\bar{\xi}^{\dot{A}}\right)^c, \tag{A.7}$$

and similarly for χ.

A.2 Useful formulas

Contractions of Weyl spinors are defined as:

$$\xi\chi = \xi^A \chi_A, \text{ and } \bar{\xi}\bar{\chi} = \bar{\xi}_{\dot{A}} \bar{\chi}^{\dot{A}}. \tag{A.8}$$

We define now two vectors of matrices

$$\sigma^{\mu}_{A\dot{B}} = (1, \vec{\sigma}), \quad \bar{\sigma}^{\mu\dot{A}B} = (1, -\vec{\sigma}), \tag{A.9}$$

where $\vec{\sigma} = (\sigma_1, \sigma_2, \sigma_3)$ and the σ_i are the pauli matrices. Additionally, we introduce

$$\sigma^{\mu\nu} = \frac{1}{4}\left[\sigma^{\mu}, \sigma^{\nu}\right], \quad \bar{\sigma}^{\mu\nu} = \frac{1}{4}\left[\bar{\sigma}^{\mu}, \bar{\sigma}^{\nu}\right]. \tag{A.10}$$

We can note the following properties

$$\bar{\sigma}^{\mu\dot{A}B} = \epsilon^{\dot{A}\dot{C}}\epsilon^{BD}\sigma^{\mu}_{D\dot{C}}, \tag{A.11a}$$

$$\sigma^{\mu}_{A\dot{B}}\sigma_{\mu C\dot{D}} = \epsilon_{AC}\epsilon_{\dot{B}\dot{D}}\bar{\sigma}^{\mu\dot{D}C}, \tag{A.11b}$$

$$\sigma^{\mu}_{A\dot{B}}\bar{\sigma}^{\dot{C}D}_{\mu} = 2\delta^{D}_{A}\delta^{\dot{C}}{}_{\dot{B}} \tag{A.11c}$$

Using all these definitions and relations, one can build out invariant bilinear forms

$$\xi\chi = \xi^{A}\chi_{A}, \tag{A.12a}$$

$$\bar{\chi}\bar{\xi} = (\xi\chi)^{\dagger}, \tag{A.12b}$$

$$\xi\sigma^{\mu}\bar{\chi} = \xi^{A}\sigma_{A\dot{B}}\bar{\chi}^{\dot{B}} = \left(\chi\sigma^{\mu}\bar{\xi}\right)^{\dagger}, \tag{A.12c}$$

$$\bar{\chi}\bar{\sigma}^{\mu}\xi = \bar{\chi}_{\dot{A}}\bar{\sigma}^{\mu\dot{A}B}\xi_{B} = \left(\bar{\xi}\bar{\sigma}^{\mu}\chi\right)^{\dagger}. \tag{A.12d}$$

Finally, one can show the identities:

$$\xi\sigma^{\mu}\bar{\chi} = -\bar{\chi}\bar{\sigma}^{\mu}\xi, \tag{A.13a}$$

$$\xi\sigma^{\mu\nu}\chi = -\chi\sigma^{\mu\nu}\xi, \tag{A.13b}$$

$$\bar{\xi}\bar{\sigma}^{\mu\nu}\bar{\chi} = -\bar{\chi}\bar{\sigma}^{\mu\nu}\bar{\xi}. \tag{A.13c}$$

Appendix B

SPheno, SU(5) and the super-CKM basis

The CKM basis is the one in which the up- and down-type quark Yukawa matrices are diagonal. The Super-CKM basis (SCKM) is obtained analogously, i.e. the squarks undergo the same rotations as their SM partners. This basis is convenient for phenomenological studies, and allows for a consistent expression of flavour violation throughout the literature. The different rotations for the SM quark and lepton fields are:

$$\begin{aligned} u'_L = V_{u_L} u_L\,, \quad u'_R = V_{u_R} u_R\,, \quad d'_L = V_{d_L} d_L\,, \quad d'_R = V_{d_R} d_R\,, \\ e'_L = V_{e_L} e_L\,, \quad e'_R = V_{e_R} e_R\,, \end{aligned} \tag{B.1}$$

where the primed fields are in the flavour basis and the unprimed fields are in the basis of diagonal Yukawa couplings. The misalignment between up- and down-type quarks leads to the usual CKM matrix:

$$V_{\rm CKM} = V_{u_L}^\dagger V_{d_L}. \tag{B.2}$$

In order to account for the change to the SCKM basis, the numerical programme `SPheno` assumes diagonal down-type Yukawa matrices. In this case the CKM matrix is given by:

$$V_{\rm CKM} = V_{u_L}^\dagger \mathbb{1} = V_{u_L}^\dagger. \tag{B.3}$$

In $SU(5)$-like models, the choice of the representations $F = \bar{\mathbf{5}}$ and $T = \mathbf{10}$ forces relationships between Yukawa couplings to hold at the unification scale:

$$y_u = y_u^T \quad \text{and} \quad y_d = y_e^T. \tag{B.4}$$

As a consequence, we have $V_{u_L} = V_{u_R}$ in this case, meaning both lepton and down-type Yukawas are simultaneously diagonal. For consistency, we then have to perform a systematic CKM rotation for all terms involving V_{u_L} and V_{u_R}. The soft-breaking terms of the Lagrangian transform as follows when switching to the SCKM basis:

$$\begin{aligned} \overline{\widetilde{U}'_{L,R}}\, M_T^2\, \widetilde{U}'_{L,R} &= \overline{\widetilde{U}_{L,R}}\, V_{\rm CKM}\, M_T^2\, V_{\rm CKM}^\dagger\, \widetilde{U}_{L,R}\,, \\ \overline{\widetilde{U}'_R}\, A_u \widetilde{U}'_L &= \overline{\widetilde{U}_R}\, V_{\rm CKM}\, A_u\, V_{\rm CKM}^\dagger\, \widetilde{U}_L\,, \\ \overline{\widetilde{D}'_{L,R}}\, M_{T,F}^2\, \widetilde{D}'_{L,R} &= \overline{\widetilde{D}_{L,R}}\, M_{T,F}^2\, \widetilde{D}_{L,R}\,, \\ \overline{\widetilde{D}'_R}\, A_d\, \widetilde{D}'_L &= \overline{\widetilde{D}_R}\, A_d\, \widetilde{D}_L\,, \\ \overline{\widetilde{L}'_L}\, M_{F,T}^2\, \widetilde{L}'_L &= \overline{\widetilde{L}_L}\, M_{F,T}^2\, \widetilde{L}_L\,, \\ \overline{\widetilde{E}'_R}\, M_{F,T}^2\, \widetilde{E}'_R &= \overline{\widetilde{E}_R}\, M_{F,T}^2\, \widetilde{E}_R\,, \\ \overline{\widetilde{E}'_R}\, A_d^T\, \widetilde{L}'_L &= \overline{\widetilde{E}_R}\, A_d^T\, \widetilde{L}_L\,. \end{aligned} \tag{B.5}$$

Consequently, in the SCKM basis, where the down-type Yukawa matrix is diagonal following the `SPheno` requirements and assuming the $SU(5)$ relations, the 6×6 soft mass matrices in the MSSM (once trilinear couplings have been taken into account) are

$$\begin{aligned} M^2_{\widetilde{D}} &= \begin{pmatrix} M_T^2 & \frac{v_d}{\sqrt{2}} A_D^T \\ \frac{v_d}{\sqrt{2}} A_D & M_F^2 \end{pmatrix}, \qquad M^2_{\widetilde{L}} = \begin{pmatrix} M_F^2 & \frac{v_d}{\sqrt{2}} A_D \\ \frac{v_d}{\sqrt{2}} A_D^T & M_T^2 \end{pmatrix}, \\ M^2_{\widetilde{U}} &= \begin{pmatrix} V_{\rm CKM} M_T^2 V_{\rm CKM}^\dagger & \frac{v_u}{\sqrt{2}} V_{\rm CKM} A_U^T V_{\rm CKM}^\dagger \\ \frac{v_u}{\sqrt{2}} V_{\rm CKM} A_U V_{\rm CKM}^\dagger & V_{\rm CKM} M_T^2 V_{\rm CKM}^\dagger \end{pmatrix}, \end{aligned} \tag{B.6}$$

up to the D-terms and SM masses. Since `SPheno` automatically ensures the CKM rotation for the left-left block of M_U^2, we enforce the rotation for the other blocks of the up-type squark mass matrix by hand before running `SPheno`.

Bibliography

[1] S. L. Glashow. "Partial Symmetries of Weak Interactions". *Nucl. Phys.* 22 (1961), pp. 579–588 (cit. on p. 1).

[2] Steven Weinberg. "A Model of Leptons". *Phys. Rev. Lett.* 19 (1967), pp. 1264–1266 (cit. on p. 1).

[3] S. L. Glashow, J. Iliopoulos, and L. Maiani. "Weak Interactions with Lepton-Hadron Symmetry". *Phys. Rev.* D2 (1970), pp. 1285–1292 (cit. on p. 1).

[4] Steven Weinberg. "Effects of a neutral intermediate boson in semileptonic processes". *Phys. Rev.* D5 (1972), pp. 1412–1417 (cit. on p. 1).

[5] D. J. Gross and Frank Wilczek. "Asymptotically Free Gauge Theories - I". *Phys. Rev.* D8 (1973), pp. 3633–3652 (cit. on p. 1).

[6] D. J. Gross and Frank Wilczek. "Asymptotically Free Gauge Theories - II". *Phys. Rev.* D9 (1974), pp. 980–993 (cit. on p. 1).

[7] H. David Politzer. "Asymptotic Freedom: An Approach to Strong Interactions". *Phys. Rept.* 14 (1974), pp. 129–180 (cit. on p. 1).

[8] G. Arnison et al. "Experimental Observation of Isolated Large Transverse Energy Electrons with Associated Missing Energy at $s^{1/2} = 540$-GeV". *Phys. Lett.* B122 (1983). [,611(1983)], pp. 103–116 (cit. on p. 1).

[9] P. Bagnaia et al. "Evidence for $Z^0 \to e^+e^-$ at the CERN anti-p p Collider". *Phys. Lett.* B129 (1983). [,7.69(1983)], pp. 130–140 (cit. on p. 1).

[10] Serguei Chatrchyan et al. "Observation of a new boson at a mass of 125 GeV with the CMS experiment at the LHC". *Phys. Lett.* B716 (2012), pp. 30–61. arXiv: 1207.7235 [hep-ex] (cit. on p. 1).

[11] Georges Aad et al. "Observation of a new particle in the search for the Standard Model Higgs boson with the ATLAS detector at the LHC". *Phys. Lett.* B716 (2012), pp. 1–29. arXiv: 1207.7214 [hep-ex] (cit. on p. 1).

[12] Katherine Garrett and Gintaras Duda. "Dark Matter: A Primer". *Adv. Astron.* 2011 (2011), p. 968283. arXiv: 1006.2483 [hep-ph] (cit. on p. 1).

[13] Laurent Canetti, Marco Drewes, and Mikhail Shaposhnikov. "Matter and Antimatter in the Universe". *New J. Phys.* 14 (2012), p. 095012. arXiv: 1204.4186 [hep-ph] (cit. on p. 1).

[14] Jerome Martin. "Everything You Always Wanted To Know About The Cosmological Constant Problem (But Were Afraid To Ask)". *Comptes Rendus Physique* 13 (2012), pp. 566–665. arXiv: 1205.3365 [astro-ph.CO] (cit. on p. 1).

[15] Michael Dine. "TASI lectures on the strong CP problem". *Flavor physics for the millennium. Proceedings, Theoretical Advanced Study Institute in elementary particle physics, TASI 2000, Boulder, USA, June 4-30, 2000.* 2000, pp. 349–369. arXiv: hep-ph/0011376 [hep-ph] (cit. on p. 1).

[16] Y. Fukuda et al. "Evidence for oscillation of atmospheric neutrinos". *Phys. Rev. Lett.* 81 (1998), pp. 1562–1567. arXiv: hep-ex/9807003 [hep-ex] (cit. on pp. 1, 4).

[17] R. Aaij et al. "Test of lepton universality with $B^0 \to K^{*0}\ell^+\ell^-$ decays". *JHEP* 08 (2017), p. 055. arXiv: 1705.05802 [hep-ex] (cit. on pp. 1, 83, 84).

[18] Roel Aaij et al. "Test of lepton universality using $B^+ \to K^+\ell^+\ell^-$ decays". *Phys. Rev. Lett.* 113 (2014), p. 151601. arXiv: 1406.6482 [hep-ex] (cit. on pp. 1, 83, 84).

[19] R. Aaij et al. "Measurement of the ratio of the $B^0 \to D^{*-}\tau^+\nu_\tau$ and $B^0 \to D^{*-}\mu^+\nu_\mu$ branching fractions using three-prong τ-lepton decays". *Phys. Rev. Lett.* 120.17 (2018), p. 171802. arXiv: 1708.08856 [hep-ex] (cit. on p. 1).

[20] Y. Sato et al. "Measurement of the branching ratio of $\bar{B}^0 \to D^{*+}\tau^-\bar{\nu}_\tau$ relative to $\bar{B}^0 \to D^{*+}\ell^-\bar{\nu}_\ell$ decays with a semileptonic tagging method". *Phys. Rev.* D94.7 (2016), p. 072007. arXiv: 1607.07923 [hep-ex] (cit. on p. 1).

[21] Michael E. Peskin and Daniel V. Schroeder. *An Introduction to quantum field theory*. Reading, USA: Addison-Wesley, 1995 (cit. on pp. 2, 5, 14).

[22] F. Halzen and Alan D. Martin. *QUARKS AND LEPTONS: AN INTRODUCTORY COURSE IN MODERN PARTICLE PHYSICS*. 1984 (cit. on p. 2).

[23] Matthew D. Schwartz. *Quantum Field Theory and the Standard Model*. Cambridge University Press, 2014 (cit. on p. 2).

[24] Palash B. Pal. "Dirac, Majorana and Weyl fermions". *Am. J. Phys.* 79 (2011), pp. 485–498. arXiv: 1006.1718 [hep-ph] (cit. on p. 2).

[25] H. Fritzsch, Murray Gell-Mann, and H. Leutwyler. "Advantages of the Color Octet Gluon Picture". *Phys. Lett.* 47B (1973), pp. 365–368 (cit. on p. 5).

[26] F. Englert and R. Brout. "Broken Symmetry and the Mass of Gauge Vector Mesons". *Phys. Rev. Lett.* 13 (1964). [,157(1964)], pp. 321–323 (cit. on p. 6).

[27] Peter W. Higgs. "Broken Symmetries and the Masses of Gauge Bosons". *Phys. Rev. Lett.* 13 (1964). [,160(1964)], pp. 508–509 (cit. on p. 6).

[28] Christopher T. Hill and Elizabeth H. Simmons. "Strong dynamics and electroweak symmetry breaking". *Phys. Rept.* 381 (2003). [Erratum: Phys. Rept.390,553(2004)], pp. 235–402. arXiv: hep-ph/0203079 [hep-ph] (cit. on p. 6).

[29] Makoto Kobayashi and Toshihide Maskawa. "CP Violation in the Renormalizable Theory of Weak Interaction". *Prog. Theor. Phys.* 49 (1973), pp. 652–657 (cit. on p. 9).

[30] Nicola Cabibbo. "Unitary Symmetry and Leptonic Decays". *Phys. Rev. Lett.* 10 (1963). [,648(1963)], pp. 531–533 (cit. on p. 9).

[31] Oram Gedalia and Gilad Perez. "Flavor Physics". *Physics of the large and the small, TASI 09, proceedings of the Theoretical Advanced Study Institute in Elementary Particle Physics, Boulder, Colorado, USA, 1-26 June 2009*. 2011, pp. 309–382. arXiv: 1005.3106 [hep-ph] (cit. on p. 9).

[32] Lincoln Wolfenstein. "Parametrization of the Kobayashi-Maskawa Matrix". *Phys. Rev. Lett.* 51 (1983), p. 1945 (cit. on p. 9).

[33] Ziro Maki, Masami Nakagawa, and Shoichi Sakata. "Remarks on the unified model of elementary particles". *Prog. Theor. Phys.* 28 (1962). [,34(1962)], pp. 870–880 (cit. on p. 10).

[34] A. D. Sakharov. "Violation of CP Invariance, C asymmetry, and baryon asymmetry of the universe". *Pisma Zh. Eksp. Teor. Fiz.* 5 (1967). [Usp. Fiz. Nauk161,no.5,61(1991)], pp. 32–35 (cit. on p. 10).

[35] Sacha Davidson, Enrico Nardi, and Yosef Nir. "Leptogenesis". *Phys. Rept.* 466 (2008), pp. 105–177. arXiv: 0802.2962 [hep-ph] (cit. on p. 10).

[36] James M. Cline. "Baryogenesis". *Les Houches Summer School - Session 86: Particle Physics and Cosmology: The Fabric of Spacetime Les Houches, France, July 31-August 25, 2006*. 2006. arXiv: hep-ph/0609145 [hep-ph] (cit. on p. 10).

[37] F. Zwicky. "Die Rotverschiebung von extragalaktischen Nebeln". *Helv. Phys. Acta* 6 (1933). [Gen. Rel. Grav.41,207(2009)], pp. 110–127 (cit. on p. 10).

[38] Antonino Del Popolo. "Dark matter and structure formation a review". *Astron. Rep.* 51 (2007), pp. 169–196. arXiv: 0801.1091 [astro-ph] (cit. on p. 10).

[39] B. P. Abbott et al. "Gravitational Waves and Gamma-rays from a Binary Neutron Star Merger: GW170817 and GRB 170817A". *Astrophys. J.* 848.2 (2017), p. L13. arXiv: 1710.05834 [astro-ph.HE] (cit. on p. 10).

[40] K Kovařík. "Hitchhiker's Guide to Renormalization". *Private communication* (2014) (cit. on p. 11).

[41] Ansgar Denner. "Techniques for calculation of electroweak radiative corrections at the one loop level and results for W physics at LEP-200". *Fortsch. Phys.* 41 (1993), pp. 307–420. arXiv: 0709.1075 [hep-ph] (cit. on p. 11).

[42] G. Passarino and M. J. G. Veltman. "One Loop Corrections for e^+e^- Annihilation Into mu^+mu^- in the Weinberg Model". *Nucl. Phys.* B160 (1979), pp. 151–207 (cit. on p. 11).

[43] Peter W. Graham, David E. Kaplan, and Surjeet Rajendran. "Cosmological Relaxation of the Electroweak Scale". *Phys. Rev. Lett.* 115.22 (2015), p. 221801. arXiv: 1504.07551 [hep-ph] (cit. on p. 11).

[44] Roberto Contino. "The Higgs as a Composite Nambu-Goldstone Boson". *Physics of the large and the small, TASI 09, proceedings of the Theoretical Advanced Study Institute in Elementary Particle Physics, Boulder, Colorado, USA, 1-26 June 2009*. 2011, pp. 235–306. arXiv: 1005.4269 [hep-ph] (cit. on p. 11).

[45] Yun-Jie Huo, Tianjun Li, and Dimitri V. Nanopoulos. "Canonical Gauge Coupling Unification in the Standard Model with High-Scale Supersymmetry Breaking". *JHEP* 09 (2011), p. 003. arXiv: 1011.0964 [hep-ph] (cit. on p. 12).

[46] H. Georgi and S. L. Glashow. "Unity of All Elementary Particle Forces". *Phys. Rev. Lett.* 32 (1974), pp. 438–441 (cit. on pp. 12, 56).

[47] K. Abe et al. "Search for proton decay via $p \to e^+\pi^0$ and $p \to \mu^+\pi^0$ in 0.31 megaton.years exposure of the Super-Kamiokande water Cherenkov detector". *Phys. Rev.* D95.1 (2017), p. 012004. arXiv: 1610.03597 [hep-ex] (cit. on p. 12).

[48] M. Drees, R. Godbole, and P. Roy. *Theory and phenomenology of sparticles: An account of four-dimensional N=1 supersymmetry in high energy physics*. 2004 (cit. on pp. 13, 22, 26, 27).

[49] Matteo Bertolini. "Lectures on Supersymmetry". https://people.sissa.it/ bertmat/teaching.htm (2016) (cit. on pp. 13, 17, 22).

[50] Luc Frappat. "Introduction à la supersymétrie". *Private communication* (2015) (cit. on pp. 13, 17, 22).

[51] Sidney R. Coleman and J. Mandula. "All Possible Symmetries of the S Matrix". *Phys. Rev.* 159 (1967), pp. 1251–1256 (cit. on p. 14).

[52] Rudolf Haag, Jan T. Lopuszanski, and Martin Sohnius. "All Possible Generators of Supersymmetries of the s Matrix". *Nucl. Phys.* B88 (1975). [,257(1974)], p. 257 (cit. on p. 14).

[53] Harold Erbin. "Supersymetrie". https://www.lpthe.jussieu.fr/∼erbin/files/classical_susy.pdf (2012) (cit. on p. 16).

[54] Abdus Salam and J. A. Strathdee. "Supergauge Transformations". *Nucl. Phys.* B76 (1974), pp. 477–482 (cit. on p. 17).

[55] J. E. Campbell. "On a Law of Combination of Operators (Second Paper)*". *Proceedings of the London Mathematical Society* s1-29.1 (Nov. 1897), pp. 14–32. eprint: http://oup.prod.sis.lan/plms/article-pdf/s1-29/1/14/4407250/s1-29-1-14.pdf (cit. on p. 18).

[56] F Hausdorff. "Die symbolische Exponentialformel in der Gruppentheorie". *Ber. Verh. Kgl. SÃ¤chs. Ges. Wiss. Leipzig., Math.-phys. Kl.* 58 (1906), pp. 19–48 (cit. on p. 18).

[57] L. Girardello and Marcus T. Grisaru. "Soft Breaking of Supersymmetry". *Nucl. Phys.* B194 (1982), p. 65 (cit. on pp. 25, 26).

[58] John R. Ellis et al. "Supersymmetric Relics from the Big Bang". *Nucl. Phys.* B238 (1984). [,223(1983)], pp. 453–476 (cit. on p. 31).

[59] Gerard Jungman, Marc Kamionkowski, and Kim Griest. "Supersymmetric dark matter". *Phys. Rept.* 267 (1996), pp. 195–373. arXiv: hep-ph/9506380 [hep-ph] (cit. on p. 31).

[60] Riccardo Catena and Laura Covi. "SUSY dark matter(s)". *Eur. Phys. J.* C74 (2014), p. 2703. arXiv: 1310.4776 [hep-ph] (cit. on p. 31).

[61] L. Covi. "Gravitino Dark Matter and the ILC". *Nuovo Cim.* C033N2 (2010), pp. 25–29. arXiv: 1003.3819 [hep-ph] (cit. on p. 31).

[62] Luigi Delle Rose et al. "Sneutrino Dark Matter, Constraints and Perspectives". 2018. arXiv: 1804.07753 [hep-ph] (cit. on p. 31).

[63] B. C. Allanach et al. "SUSY Les Houches Accord 2". *Comput. Phys. Commun.* 180 (2009), pp. 8–25. arXiv: 0801.0045 [hep-ph] (cit. on pp. 32, 67).

[64] Gino Isidori and David M. Straub. "Minimal Flavour Violation and Beyond". *Eur. Phys. J.* C72 (2012), p. 2103. arXiv: 1202.0464 [hep-ph] (cit. on p. 33).

[65] Amit Chakraborty et al. "Flavour-violating decays of mixed top-charm squarks at the LHC". *Eur. Phys. J.* C78.10 (2018), p. 844. arXiv: 1808.07488 [hep-ph] (cit. on pp. 35, 37).

[66] Karen De Causmaecker et al. "General squark flavour mixing: constraints, phenomenology and benchmarks". *JHEP* 11 (2015), p. 125. arXiv: 1509.05414 [hep-ph] (cit. on pp. 35, 37, 44–49, 71).

[67] M. Tanabashi et al. "Review of Particle Physics". *Phys. Rev.* D98.3 (2018), p. 030001 (cit. on pp. 36, 65, 67, 68).

[68] Y. Amhis et al. "Averages of b-hadron, c-hadron, and τ-lepton properties as of summer 2016". *Eur. Phys. J.* C77.12 (2017), p. 895. arXiv: 1612.07233 [hep-ex] (cit. on p. 36).

[69] Luca Di Luzio, Matthew Kirk, and Alexander Lenz. "Updated B_s-mixing constraints on new physics models for $b \to s\ell^+\ell^-$ anomalies". *Phys. Rev.* D97.9 (2018), p. 095035. arXiv: 1712.06572 [hep-ph] (cit. on pp. 36, 67, 68).

[70] Joachim Brod and Martin Gorbahn. "Next-to-Next-to-Leading-Order Charm-Quark Contribution to the CP Violation Parameter ϵ_K and ΔM_K". *Phys. Rev. Lett.* 108 (2012), p. 121801. arXiv: 1108.2036 [hep-ph] (cit. on pp. 36, 68).

[71] Jordan Bernigaud and Björn Herrmann. "First steps towards the reconstruction of the squark flavour structure". *SciPost Phys.* 6 (2019), p. 066. arXiv: 1809.04370 [hep-ph] (cit. on p. 37).

[72] S. Heinemeyer et al. "Electroweak precision observables in the MSSM with nonminimal flavor violation". *Eur. Phys. J.* C37 (2004), pp. 481–493. arXiv: hep-ph/0403228 [hep-ph] (cit. on p. 37).

[73] M. Ciuchini et al. "Soft SUSY breaking grand unification: Leptons versus quarks on the flavor playground". *Nucl. Phys.* B783 (2007), pp. 112–142. arXiv: hep-ph/0702144 [HEP-PH] (cit. on pp. 37, 63, 76, 79).

[74] Giuseppe Bozzi et al. "Squark and gaugino hadroproduction and decays in non-minimal flavour violating supersymmetry". *Nucl. Phys.* B787 (2007), pp. 1–54. arXiv: 0704.1826 [hep-ph] (cit. on pp. 37–40).

[75] F. del Aguila et al. "Collider aspects of flavour physics at high Q". *Eur. Phys. J.* C57 (2008), pp. 183–308. arXiv: 0801.1800 [hep-ph] (cit. on p. 37).

[76] Benjamin Fuks, Björn Herrmann, and Michael Klasen. "Flavour Violation in Gauge-Mediated Supersymmetry Breaking Models: Experimental Constraints and Phenomenology at the LHC". *Nucl. Phys.* B810 (2009), pp. 266–299. arXiv: 0808.1104 [hep-ph] (cit. on p. 37).

[77] Benjamin Fuks, Björn Herrmann, and Michael Klasen. "Phenomenology of anomaly-mediated supersymmetry breaking scenarios with non-minimal flavour violation". *Phys. Rev.* D86 (2012), p. 015002. arXiv: 1112.4838 [hep-ph] (cit. on p. 37).

[78] Bhaskar Dutta and Yukihiro Mimura. "Electron $g-2$ with flavor violation in MSSM". *Phys. Lett.* B790 (2019), pp. 563–567. arXiv: 1811.10209 [hep-ph] (cit. on p. 37).

[79] Björn Herrmann, Michael Klasen, and Quentin Le Boulc'h. "Impact of squark flavour violation on neutralino dark matter". *Phys. Rev.* D84 (2011), p. 095007. arXiv: 1106.6229 [hep-ph] (cit. on p. 37).

[80] Monika Blanke and Simon Kast. "Top-Flavoured Dark Matter in Dark Minimal Flavour Violation". *JHEP* 05 (2017), p. 162. arXiv: 1702.08457 [hep-ph] (cit. on p. 37).

[81] Monika Blanke, Satrajit Das, and Simon Kast. "Flavoured Dark Matter Moving Left". *JHEP* 02 (2018), p. 105. arXiv: 1711.10493 [hep-ph] (cit. on p. 37).

[82] Tobias Hurth and Werner Porod. "Flavour violating squark and gluino decays". *JHEP* 08 (2009), p. 087. arXiv: 0904.4574 [hep-ph] (cit. on p. 37).

[83] A. Bartl et al. "Impact of squark generation mixing on the search for gluinos at LHC". *Phys. Lett.* B679 (2009), pp. 260–266. arXiv: 0905.0132 [hep-ph] (cit. on p. 37).

[84] Matthias Bruhnke, Björn Herrmann, and Werner Porod. "Signatures of bosonic squark decays in non-minimally flavour-violating supersymmetry". *JHEP* 09 (2010), p. 006. arXiv: 1007.2100 [hep-ph] (cit. on p. 37).

[85] A. Bartl et al. "Impact of squark generation mixing on the search for squarks decaying into fermions at LHC". *Phys. Lett.* B698 (2011). [Erratum: Phys. Lett.B700,390(2011)], pp. 380–388. arXiv: 1007.5483 [hep-ph] (cit. on pp. 37, 38).

[86] Monika Blanke et al. "Flavoured Naturalness". *JHEP* 06 (2013), p. 022. arXiv: 1302.7232 [hep-ph] (cit. on p. 37).

[87] A. Bartl et al. "$h^0 \to c\bar{c}$ as a test case for quark flavor violation in the MSSM". *Phys. Rev.* D91.1 (2015), p. 015007. arXiv: 1411.2840 [hep-ph] (cit. on p. 37).

[88] Mihailo Backović, Alberto Mariotti, and Michael Spannowsky. "Signs of Tops from Highly Mixed Stops". *JHEP* 06 (2015), p. 122. arXiv: 1504.00927 [hep-ph] (cit. on p. 37).

[89] M. Arana-Catania, S. Heinemeyer, and M. J. Herrero. "Updated Constraints on General Squark Flavor Mixing". *Phys. Rev.* D90.7 (2014), p. 075003. arXiv: 1405.6960 [hep-ph] (cit. on p. 37).

[90] Kamila Kowalska. "Phenomenology of SUSY with General Flavour Violation". *JHEP* 09 (2014), p. 139. arXiv: 1406.0710 [hep-ph] (cit. on p. 37).

[91] G. Brooijmans et al. "Les Houches 2017: Physics at TeV Colliders New Physics Working Group Report". *Les Houches 2017: Physics at TeV Colliders New Physics Working Group Report*. 2018. arXiv: 1803.10379 [hep-ph] (cit. on p. 37).

[92] E. Boos et al. "Polarization in sfermion decays: Determining tan beta and trilinear couplings". *Eur. Phys. J.* C30 (2003), pp. 395–407. arXiv: hep-ph/0303110 [hep-ph] (cit. on p. 38).

[93] Edmond L. Berger et al. "Measuring Top Quark Polarization in Top Pair plus Missing Energy Events". *Phys. Rev. Lett.* 109 (2012), p. 152004. arXiv: 1207.1101 [hep-ph] (cit. on p. 38).

[94] G. Bélanger et al. "Top Polarization in Stop Production at the LHC". *JHEP* 05 (2013), p. 167. arXiv: 1212.3526 [hep-ph] (cit. on p. 38).

[95] Arun Prasath V, Rohini M. Godbole, and Saurabh D. Rindani. "Longitudinal top polarisation measurement and anomalous Wtb coupling". *Eur. Phys. J.* C75.9 (2015), p. 402. arXiv: 1405.1264 [hep-ph] (cit. on p. 38).

[96] *Toolkit for Multivariate Data Analysis with* ROOT *(*TMVA*)*. https://root.cern/tmva (cit. on p. 44).

[97] Zhi-zhong Xing. "Quark Mass Hierarchy and Flavor Mixing Puzzles". *Int. J. Mod. Phys.* A29 (2014), p. 1430067. arXiv: 1411.2713 [hep-ph] (cit. on p. 52).

[98] Sheldon Stone. "New physics from flavour". *PoS* ICHEP2012 (2013), p. 033. arXiv: 1212.6374 [hep-ph] (cit. on p. 52).

[99] Frank F. Deppisch. "Lepton Flavour Violation and Flavour Symmetries". *Fortsch. Phys.* 61 (2013), pp. 622–644. arXiv: 1206.5212 [hep-ph] (cit. on p. 51).

[100] Guido Altarelli and Ferruccio Feruglio. "Discrete Flavor Symmetries and Models of Neutrino Mixing". *Rev. Mod. Phys.* 82 (2010), pp. 2701–2729. arXiv: 1002.0211 [hep-ph] (cit. on pp. 51, 53, 85).

[101] Jun-Nan Lu and Gui-Jun Ding. "Quark and lepton mixing patterns from a common discrete flavor symmetry with a generalized CP symmetry". *Phys. Rev.* D98.5 (2018), p. 055011. arXiv: 1806.02301 [hep-ph] (cit. on pp. 51, 85, 95).

[102] Luca Merlo. "Phenomenology of Discrete Flavour Symmetries". PhD thesis. Padua U., 2010. arXiv: 1004.2211 [hep-ph] (cit. on p. 51).

[103] Martin Holthausen, Manfred Lindner, and Michael A. Schmidt. "CP and Discrete Flavour Symmetries". *JHEP* 04 (2013), p. 122. arXiv: 1211.6953 [hep-ph] (cit. on p. 51).

[104] S. T. Petcov. "Discrete Flavour Symmetries, Neutrino Mixing and Leptonic CP Violation". *Eur. Phys. J.* C78.9 (2018), p. 709. arXiv: 1711.10806 [hep-ph] (cit. on p. 51).

[105] Alexander Blum and Claudia Hagedorn. "The Cabibbo Angle in a Supersymmetric D(14) Model". *Nucl. Phys.* B821 (2009), pp. 327–353. arXiv: 0902.4885 [hep-ph] (cit. on p. 51).

[106] Francisco J. de Anda and Stephen F. King. "An $S_4 \times SU(5)$ SUSY GUT of flavour in 6d". *JHEP* 07 (2018), p. 057. arXiv: 1803.04978 [hep-ph] (cit. on p. 51).

[107] Ivo de Medeiros Varzielas, Rasmus W. Rasmussen, and Jim Talbert. "Bottom-Up Discrete Symmetries for Cabibbo Mixing". *Int. J. Mod. Phys.* A32.06n07 (2017), p. 1750047. arXiv: 1605.03581 [hep-ph] (cit. on pp. 52, 85, 94–96, 100, 109).

[108] C. D. Froggatt and Holger Bech Nielsen. "Hierarchy of Quark Masses, Cabibbo Angles and CP Violation". *Nucl. Phys.* B147 (1979), pp. 277–298 (cit. on p. 52).

[109] Maria Dimou, Stephen F. King, and Christoph Luhn. "Approaching Minimal Flavour Violation from an $SU(5) \times S_4 \times U(1)$ SUSY GUT". *JHEP* 02 (2016), p. 118. arXiv: 1511.07886 [hep-ph] (cit. on pp. 52, 60, 61, 81).

[110] Iain K. Cooper, Stephen F. King, and Christoph Luhn. "A4xSU(5) SUSY GUT of Flavour with Trimaximal Neutrino Mixing". *JHEP* 06 (2012), p. 130. arXiv: 1203.1324 [hep-ph] (cit. on pp. 52, 64).

[111] Ivo de Medeiros Varzielas and Daniel Pidt. "Towards realistic models of quark masses with geometrical CP violation". *J. Phys.* G41 (2014), p. 025004. arXiv: 1307.0711 [hep-ph] (cit. on p. 53).

[112] Mu-Chun Chen, Jinrui Huang, and William Shepherd. "Dirac Leptogenesis with a Non-anomalous $U(1)'$ Family Symmetry". *JHEP* 11 (2012), p. 059. arXiv: 1111.5018 [hep-ph] (cit. on p. 53).

[113] Guido Altarelli and Ferruccio Feruglio. "Tri-bimaximal neutrino mixing, A(4) and the modular symmetry". *Nucl. Phys.* B741 (2006), pp. 215–235. arXiv: hep-ph/0512103 [hep-ph] (cit. on pp. 53, 55, 87, 89, 94, 108).

[114] Reinier de Adelhart Toorop. "A flavour of family symmetries in a family of flavour models". PhD thesis. Leiden, Netherlands: Leiden U., 2012 (cit. on pp. 53, 54).

[115] P. F. Harrison, D. H. Perkins, and W. G. Scott. "Tri-bimaximal mixing and the neutrino oscillation data". *Phys. Lett.* B530 (2002), p. 167. arXiv: hep-ph/0202074 [hep-ph] (cit. on pp. 53, 87, 95).

[116] Ivan Esteban et al. "Global analysis of three-flavour neutrino oscillations: synergies and tensions in the determination of $\theta_23, \delta_C P$, and the mass ordering". *JHEP* 01 (2019), p. 106. arXiv: 1811.05487 [hep-ph] (cit. on pp. 53, 83).

[117] S. T. Petcov and A. V. Titov. "Assessing the Viability of A_4, S_4 and A_5 Flavour Symmetries for Description of Neutrino Mixing". *Phys. Rev.* D97.11 (2018), p. 115045. arXiv: 1804.00182 [hep-ph] (cit. on p. 53).

[118] Sumit K. Garg. "Consistency of perturbed Tribimaximal, Bimaximal and Democratic mixing with Neutrino mixing data". *Nucl. Phys.* B931 (2018), pp. 469–505. arXiv: 1712.02212 [hep-ph] (cit. on p. 53).

[119] Ugo Amaldi, Wim de Boer, and Hermann Furstenau. "Comparison of grand unified theories with electroweak and strong coupling constants measured at LEP". *Phys. Lett.* B260 (1991), pp. 447–455 (cit. on p. 55).

[120] Wim de Boer and Christian Sander. "Global electroweak fits and gauge coupling unification". *Phys. Lett.* B585 (2004), pp. 276–286. arXiv: hep-ph/0307049 [hep-ph] (cit. on p. 56).

[121] Jakob Schwichtenberg. "Gauge Coupling Unification without Supersymmetry" (2018). arXiv: 1808.10329 [hep-ph] (cit. on p. 56).

[122] Stephen M. Barr. "A New Symmetry Breaking Pattern for SO(10) and Proton Decay". *Phys. Lett.* 112B (1982), pp. 219–222 (cit. on p. 58).

[123] Toru Goto and Takeshi Nihei. "Effect of RRRR dimension five operator on the proton decay in the minimal SU(5) SUGRA GUT model". *Phys. Rev.* D59 (1999), p. 115009. arXiv: hep-ph/9808255 [hep-ph] (cit. on p. 58).

[124] Hitoshi Murayama and Aaron Pierce. "Not even decoupling can save minimal supersymmetric SU(5)". *Phys. Rev.* D65 (2002), p. 055009. arXiv: hep-ph/0108104 [hep-ph] (cit. on p. 58).

[125] Borut Bajc, Pavel Fileviez Perez, and Goran Senjanovic. "Proton decay in minimal supersymmetric SU(5)". *Phys. Rev.* D66 (2002), p. 075005. arXiv: hep-ph/0204311 [hep-ph] (cit. on p. 58).

[126] Howard Georgi and C. Jarlskog. "A New Lepton - Quark Mass Relation in a Unified Theory". *Phys. Lett.* 86B (1979), pp. 297–300 (cit. on p. 59).

[127] Katri Huitu et al. "Implications of different supersymmetry breaking patterns for the spectrum and decay of neutralinos and charginos". *Phys. Rev.* D82 (2010), p. 115003. arXiv: 1006.0661 [hep-ph] (cit. on p. 59).

[128] Achille Corsetti and Pran Nath. "Gaugino mass nonuniversality and dark matter in SUGRA, strings and D-brane models". *Phys. Rev.* D64 (2001), p. 125010. arXiv: hep-ph/0003186 [hep-ph] (cit. on p. 59).

[129] S. F. King, J. P. Roberts, and D. P. Roy. "Natural dark matter in SUSY GUTs with non-universal gaugino masses". *JHEP* 10 (2007), p. 106. arXiv: 0705.4219 [hep-ph] (cit. on p. 59).

[130] Stephen P. Martin. "Non-universal gaugino masses from non-singlet F-terms in non-minimal unified models". *Phys. Rev.* D79 (2009), p. 095019. arXiv: 0903.3568 [hep-ph] (cit. on p. 59).

[131] A. Masiero et al. "Naturally Massless Higgs Doublets in Supersymmetric SU(5)". *Phys. Lett.* 115B (1982), pp. 380–384 (cit. on p. 59).

[132] Steve F. King and Iain N. R. Peddie. "Canonical normalization and Yukawa matrices". *Phys. Lett.* B586 (2004), pp. 83–94. arXiv: hep-ph/0312237 [hep-ph] (cit. on p. 60).

[133] Steve F. King et al. "Kahler corrections and softly broken family symmetries". *JHEP* 07 (2005), p. 049. arXiv: hep-ph/0407012 [hep-ph] (cit. on p. 60).

[134] Stefan Antusch and Christian Hohl. "Predictions from a flavour GUT model combined with a SUSY breaking sector". *JHEP* 10 (2017), p. 155. arXiv: 1706.04274 [hep-ph] (cit. on p. 60).

[135] Jordan Bernigaud et al. "Non-minimal flavour violation in $A_4\times$ SU(5) SUSY GUTs with smuon assisted dark matter". *JHEP* 03 (2019), p. 067. arXiv: 1812.07463 [hep-ph] (cit. on pp. 61, 62).

[136] Alexander S. Belyaev, Steve F. King, and Patrick B. Schaefers. "Muon g-2 and dark matter suggest nonuniversal gaugino masses: $\mathbf{SU(5)} \times \mathbf{A_4}$ case study at the LHC". *Phys. Rev.* D97.11 (2018), p. 115002. arXiv: 1801.00514 [hep-ph] (cit. on pp. 61, 62, 64, 65, 67).

[137] Stefan Antusch, Stephen F. King, and Martin Spinrath. "Spontaneous CP violation in $A_4 \times SU(5)$ with Constrained Sequential Dominance 2". *Phys. Rev.* D87.9 (2013), p. 096018. arXiv: 1301.6764 [hep-ph] (cit. on pp. 61, 64).

[138] Maria Dimou, Stephen F. King, and Christoph Luhn. "Phenomenological implications of an $SU(5)\times S_4\times U(1)$ SUSY GUT of flavor". *Phys. Rev.* D93.7 (2016), p. 075026. arXiv: 1512.09063 [hep-ph] (cit. on p. 61).

[139] Stephen P. Martin. "A Supersymmetry primer" (1997). [Adv. Ser. Direct. High Energy Phys.18,1(1998)], pp. 1–98. arXiv: hep-ph/9709356 [hep-ph] (cit. on p. 63).

[140] Benjamin D. Callen and Raymond R. Volkas. "Large lepton mixing angles from a 4+1-dimensional SU(5) x A(4) domain-wall braneworld model". *Phys. Rev.* D86 (2012), p. 056007. arXiv: 1205.3617 [hep-ph] (cit. on p. 64).

[141] Iain K. Cooper, Stephen F. King, and Christoph Luhn. "SUSY SU(5) with singlet plus adjoint matter and A4 family symmetry". *Phys. Lett.* B690 (2010), pp. 396–402. arXiv: 1004.3243 [hep-ph] (cit. on p. 64).

[142] Fredrik Björkeroth et al. "Towards a complete $A_4\times$ SU(5) SUSY GUT". *JHEP* 06 (2015), p. 141. arXiv: 1503.03306 [hep-ph] (cit. on p. 64).

[143] P. A. R. Ade et al. "Planck 2015 results. XIII. Cosmological parameters". *Astron. Astrophys.* 594 (2016), A13. arXiv: 1502.01589 [astro-ph.CO] (cit. on pp. 65, 68).

[144] Georges Aad et al. "Search for direct production of charginos, neutralinos and sleptons in final states with two leptons and missing transverse momentum in pp collisions at $\sqrt{s} = 8$ TeV with the ATLAS detector". *JHEP* 05 (2014), p. 071. arXiv: 1403.5294 [hep-ex] (cit. on p. 65).

[145] Paolo Gondolo and Graciela Gelmini. "Cosmic abundances of stable particles: Improved analysis". *Nucl. Phys.* B360 (1991), pp. 145–179 (cit. on p. 67).

[146] Werner Porod. "SPheno, a program for calculating supersymmetric spectra, SUSY particle decays and SUSY particle production at e+ e- colliders". *Comput. Phys. Commun.* 153 (2003), pp. 275–315. arXiv: hep-ph/0301101 [hep-ph] (cit. on pp. 67, 68).

[147] W. Porod and F. Staub. "SPheno 3.1: Extensions including flavour, CP-phases and models beyond the MSSM". *Comput. Phys. Commun.* 183 (2012), pp. 2458–2469. arXiv: 1104.1573 [hep-ph] (cit. on pp. 67, 68).

[148] Y. Amhis et al. "Averages of b-hadron, c-hadron, and τ-lepton properties as of summer 2016". *Eur. Phys. J.* C77.12 (2017), p. 895. arXiv: 1612.07233 [hep-ex] (cit. on p. 68).

[149] G. Bélanger et al. "MicrOMEGAs: A Program for calculating the relic density in the MSSM". *Comput. Phys. Commun.* 149 (2002), pp. 103–120. arXiv: hep-ph/0112278 [hep-ph] (cit. on pp. 67, 68).

[150] G. Bélanger et al. "micrOMEGAs: Version 1.3". *Comput. Phys. Commun.* 174 (2006), pp. 577–604. arXiv: hep-ph/0405253 [hep-ph] (cit. on pp. 67, 68).

[151] D. Barducci et al. "Collider limits on new physics within micrOMEGAs 4.3". *Comput. Phys. Commun.* 222 (2018), pp. 327–338. arXiv: 1606.03834 [hep-ph] (cit. on pp. 67, 68).

[152] Florian Staub. "From Superpotential to Model Files for FeynArts and CalcHep/CompHep". *Comput. Phys. Commun.* 181 (2010), pp. 1077–1086. arXiv: 0909.2863 [hep-ph] (cit. on p. 67).

[153] Florian Staub. "Automatic Calculation of supersymmetric Renormalization Group Equations and Self Energies". *Comput. Phys. Commun.* 182 (2011), pp. 808–833. arXiv: 1002.0840 [hep-ph] (cit. on p. 67).

[154] Florian Staub. "SARAH 4 : A tool for (not only SUSY) model builders". *Comput. Phys. Commun.* 185 (2014), pp. 1773–1790. arXiv: 1309.7223 [hep-ph] (cit. on p. 67).

[155] Werner Porod, Florian Staub, and Avelino Vicente. "A Flavor Kit for BSM models". *Eur. Phys. J.* C74.8 (2014), p. 2992. arXiv: 1405.1434 [hep-ph] (cit. on p. 67).

[156] T. Humair. "talk at 2019 Rencontres de Moriond, Electroweak Interactions and Unified Theories, http://moriond.in2p3.fr/2019/EW" () (cit. on pp. 83, 84).

[157] Jordan Bernigaud, Ivo de Medeiros Varzielas, and Jim Talbert. "Finite Family Groups for Fermionic and Leptoquark Mixing Patterns" (2019). arXiv: 1906.11270 [hep-ph] (cit. on p. 83).

[158] Johannes Albrecht. "Lepton Flavour Universality tests with B decays at LHCb". *53rd Rencontres de Moriond on QCD and High Energy Interactions (Moriond QCD 2018) La Thuile, Italy, March 17-24, 2018*. 2018. arXiv: 1805.06243 [hep-ex] (cit. on p. 83).

[159] Gudrun Hiller and Frank Kruger. "More model-independent analysis of $b \to s$ processes". *Phys. Rev.* D69 (2004), p. 074020. arXiv: hep-ph/0310219 [hep-ph] (cit. on p. 84).

[160] Marzia Bordone, Gino Isidori, and Andrea Pattori. "On the Standard Model predictions for R_K and R_{K^*}". *Eur. Phys. J.* C76.8 (2016), p. 440. arXiv: 1605.07633 [hep-ph] (cit. on p. 84).

[161] Roel Aaij et al. "Search for lepton-universality violation in $B^+ \to K^+\ell^+\ell^-$ decays". *Phys. Rev. Lett.* 122.19 (2019), p. 191801. arXiv: 1903.09252 [hep-ex] (cit. on p. 84).

[162] M. Prim. "talk at 2019 Rencontres de Moriond, Electroweak Interactions and Unified Theories, http://moriond.in2p3.fr/2019/EW" () (cit. on p. 84).

[163] Gudrun Hiller and Martin Schmaltz. "R_K and future $b \to s\ell\ell$ physics beyond the standard model opportunities". *Phys. Rev.* D90 (2014), p. 054014. arXiv: 1408.1627 [hep-ph] (cit. on pp. 84, 89, 104).

[164] Bernat Capdevila et al. "Patterns of New Physics in $b \to s\ell^+\ell^-$ transitions in the light of recent data". *JHEP* 01 (2018), p. 093. arXiv: 1704.05340 [hep-ph] (cit. on p. 84).

[165] Wolfgang Altmannshofer, Peter Stangl, and David M. Straub. "Interpreting Hints for Lepton Flavor Universality Violation". *Phys. Rev.* D96.5 (2017), p. 055008. arXiv: 1704.05435 [hep-ph] (cit. on p. 84).

[166] Guido D'Amico et al. "Flavour anomalies after the R_{K^*} measurement". *JHEP* 09 (2017), p. 010. arXiv: 1704.05438 [hep-ph] (cit. on p. 84).

[167] Gudrun Hiller and Ivan Nisandzic. "R_K and R_{K^*} beyond the standard model". *Phys. Rev.* D96.3 (2017), p. 035003. arXiv: 1704.05444 [hep-ph] (cit. on pp. 84, 89).

[168] Marco Ciuchini et al. "On Flavourful Easter eggs for New Physics hunger and Lepton Flavour Universality violation". *Eur. Phys. J.* C77.10 (2017), p. 688. arXiv: 1704.05447 [hep-ph] (cit. on p. 84).

[169] Ashutosh Kumar Alok et al. "New Physics in $b \to s\mu^+\mu^-$ after the Measurement of R_{K^*}". *Phys. Rev.* D96.9 (2017), p. 095009. arXiv: 1704.07397 [hep-ph] (cit. on p. 84).

[170] Marco Ciuchini et al. "New Physics in $b \to s\ell^+\ell^-$ confronts new data on Lepton Universality" (2019). arXiv: 1903.09632 [hep-ph] (cit. on p. 84).

[171] Ivo de Medeiros Varzielas and Jim Talbert. "Simplified Models of Flavourful Leptoquarks". *Eur. Phys. J.* C79.6 (2019), p. 536. arXiv: 1901.10484 [hep-ph] (cit. on pp. 84, 85, 87–90, 96, 99, 101, 103, 104, 109).

[172] Ben Gripaios, Marco Nardecchia, and S. A. Renner. "Composite leptoquarks and anomalies in B-meson decays". *JHEP* 05 (2015), p. 006. arXiv: 1412.1791 [hep-ph] (cit. on p. 84).

[173] Ivo de Medeiros Varzielas and Gudrun Hiller. "Clues for flavor from rare lepton and quark decays". *JHEP* 06 (2015), p. 072. arXiv: 1503.01084 [hep-ph] (cit. on pp. 84, 88, 89, 104, 108, 109).

[174] Ben Gripaios, M. Nardecchia, and S. A. Renner. "Linear flavour violation and anomalies in B physics". *JHEP* 06 (2016), p. 083. arXiv: 1509.05020 [hep-ph] (cit. on p. 84).

[175] Martin Bauer and Matthias Neubert. "Minimal Leptoquark Explanation for the $R_{D^{(*)}}$, R_K , and $(g-2)_g$ Anomalies". *Phys. Rev. Lett.* 116.14 (2016), p. 141802. arXiv: 1511.01900 [hep-ph] (cit. on p. 84).

[176] Pere Arnan et al. "Loop effects of heavy new scalars and fermions in $b \to s\mu^+\mu^-$". *JHEP* 04 (2017), p. 043. arXiv: 1608.07832 [hep-ph] (cit. on p. 84).

[177] Gudrun Hiller, Dennis Loose, and Kay Schönwald. "Leptoquark Flavor Patterns & B Decay Anomalies". *JHEP* 12 (2016), p. 027. arXiv: 1609.08895 [hep-ph] (cit. on p. 84).

[178] Andreas Crivellin et al. "Lepton Flavor Non-Universality in B decays from Dynamical Yukawas". *Phys. Lett.* B766 (2017), pp. 77–85. arXiv: 1611.02703 [hep-ph] (cit. on p. 84).

[179] Andreas Crivellin, Dario Muller, and Toshihiko Ota. "Simultaneous explanation of $R(D^{(*)})$ and $b \to s\mu^+\mu^-$:the last scalar leptoquarks standing". *JHEP* 09 (2017), p. 040. arXiv: 1703.09226 [hep-ph] (cit. on p. 84).

[180] Rodrigo Alonso et al. "Anomaly-free local horizontal symmetry and anomaly-full rare B-decays". *Phys. Rev.* D96.7 (2017), p. 071701. arXiv: 1704.08158 [hep-ph] (cit. on p. 84).

[181] Cesar Bonilla et al. "$U(1)_{B_3-3L_\mu}$ gauge symmetry as a simple description of $b \to s$ anomalies". *Phys. Rev.* D98.9 (2018), p. 095002. arXiv: 1705.00915 [hep-ph] (cit. on p. 84).

[182] Stephen F. King. "Flavourful Z$'$ models for $R_{K^{(*)}}$". *JHEP* 08 (2017), p. 019. arXiv: 1706.06100 [hep-ph] (cit. on p. 84).

[183] Daniel Aloni et al. "Testing minimal flavor violation in leptoquark models of the $R_{K^{(*)}}$ anomaly". *JHEP* 11 (2017), p. 109. arXiv: 1708.06161 [hep-ph] (cit. on p. 84).

[184] Nima Assad, Bartosz Fornal, and Benjamin Grinstein. "Baryon Number and Lepton Universality Violation in Leptoquark and Diquark Models". *Phys. Lett.* B777 (2018), pp. 324–331. arXiv: 1708.06350 [hep-ph] (cit. on p. 84).

[185] Lorenzo Calibbi, Andreas Crivellin, and Tianjun Li. "Model of vector leptoquarks in view of the B-physics anomalies". *Phys. Rev.* D98.11 (2018), p. 115002. arXiv: 1709.00692 [hep-ph] (cit. on p. 84).

[186] Ivo de Medeiros Varzielas and Stephen F. King. "$R_{K^{(*)}}$ with leptoquarks and the origin of Yukawa couplings". *JHEP* 11 (2018), p. 100. arXiv: 1807.06023 [hep-ph] (cit. on p. 84).

[187] B. Grinstein, S. Pokorski, and G. G. Ross. "Lepton non-universality in B decays and fermion mass structure". *JHEP* 12 (2018), p. 079. arXiv: 1809.01766 [hep-ph] (cit. on p. 84).

[188] Bartosz Fornal, Sri Aditya Gadam, and Benjamin Grinstein. "Left-Right SU(4) Vector Leptoquark Model for Flavor Anomalies". *Phys. Rev.* D99.5 (2019), p. 055025. arXiv: 1812.01603 [hep-ph] (cit. on p. 84).

[189] B. C. Allanach et al. "Hadron collider sensitivity to fat flavourful Z′s for $R_{K^{(*)}}$". *JHEP* 03 (2019), p. 137. arXiv: 1810.02166 [hep-ph] (cit. on p. 84).

[190] Ivo De Medeiros Varzielas and Stephen F. King. "Origin of Yukawa couplings for Higgs bosons and leptoquarks". *Phys. Rev.* D99.9 (2019), p. 095029. arXiv: 1902.09266 [hep-ph] (cit. on p. 84).

[191] B. C. Allanach, J. M. Butterworth, and Tyler Corbett. "Collider Constraints on Z' Models for Neutral Current $B-$Anomalies" (2019). arXiv: 1904.10954 [hep-ph] (cit. on p. 84).

[192] Marzia Bordone et al. "A three-site gauge model for flavor hierarchies and flavor anomalies". *Phys. Lett.* B779 (2018), pp. 317–323. arXiv: 1712.01368 [hep-ph] (cit. on p. 84).

[193] Marzia Bordone et al. "Low-energy signatures of the PS^3 model: from B-physics anomalies to LFV". *JHEP* 10 (2018), p. 148. arXiv: 1805.09328 [hep-ph] (cit. on p. 84).

[194] Claudia Cornella, Javier Fuentes-Martin, and Gino Isidori. "Revisiting the vector leptoquark explanation of the B-physics anomalies" (2019). arXiv: 1903.11517 [hep-ph] (cit. on p. 84).

[195] Alakabha Datta, Divya Sachdeva, and John Waite. "A unified explanation of $b \to s\mu^+\mu^-$ anomalies, neutrino masses and $B \to \pi K$ puzzle" (2019). arXiv: 1905.04046 [hep-ph] (cit. on p. 84).

[196] A. Angelescu et al. "Closing the window on single leptoquark solutions to the B-physics anomalies". *JHEP* 10 (2018), p. 183. arXiv: 1808.08179 [hep-ph] (cit. on p. 84).

[197] Damir Bečirević et al. "Scalar leptoquarks from grand unified theories to accommodate the B-physics anomalies". *Phys. Rev.* D98.5 (2018), p. 055003. arXiv: 1806.05689 [hep-ph] (cit. on p. 84).

[198] Monika Blanke and Andreas Crivellin. "B Meson Anomalies in a Pati-Salam Model within the Randall-Sundrum Background". *Phys. Rev. Lett.* 121.1 (2018), p. 011801. arXiv: 1801.07256 [hep-ph] (cit. on p. 84).

[199] I. Doršner et al. "Physics of leptoquarks in precision experiments and at particle colliders". *Phys. Rept.* 641 (2016), pp. 1–68. arXiv: 1603.04993 [hep-ph] (cit. on pp. 84, 87).

[200] Gudrun Hiller, Dennis Loose, and Ivan Nišandžić. "Flavorful leptoquarks at hadron colliders". *Phys. Rev.* D97.7 (2018), p. 075004. arXiv: 1801.09399 [hep-ph] (cit. on pp. 84, 89).

[201] Bastian Diaz, Martin Schmaltz, and Yi-Ming Zhong. "The leptoquark Hunter's guide: Pair production". *JHEP* 10 (2017), p. 097. arXiv: 1706.05033 [hep-ph] (cit. on p. 84).

[202] Martin Schmaltz and Yi-Ming Zhong. "The leptoquark Hunter's guide: large coupling". *JHEP* 01 (2019), p. 132. arXiv: 1810.10017 [hep-ph] (cit. on p. 84).

[203] Michael J. Baker et al. "High- p_T signatures in vector–leptoquark models". *Eur. Phys. J.* C79.4 (2019), p. 334. arXiv: 1901.10480 [hep-ph] (cit. on p. 84).

[204] C. S. Lam. "Symmetry of Lepton Mixing". *Phys. Lett.* B656 (2007), pp. 193–198. arXiv: 0708.3665 [hep-ph] (cit. on pp. 85, 93, 95).

[205] D. Hernandez and A. Yu. Smirnov. "Lepton mixing and discrete symmetries". *Phys. Rev.* D86 (2012), p. 053014. arXiv: 1204.0445 [hep-ph] (cit. on pp. 85, 95).

[206] Reinier de Adelhart Toorop, Ferruccio Feruglio, and Claudia Hagedorn. "Finite Modular Groups and Lepton Mixing". *Nucl. Phys.* B858 (2012), pp. 437–467. arXiv: 1112.1340 [hep-ph] (cit. on pp. 85, 95).

[207] C. S. Lam. "Finite Symmetry of Leptonic Mass Matrices". *Phys. Rev.* D87.1 (2013), p. 013001. arXiv: 1208.5527 [hep-ph] (cit. on pp. 85, 95).

[208] Martin Holthausen, Kher Sham Lim, and Manfred Lindner. "Lepton Mixing Patterns from a Scan of Finite Discrete Groups". *Phys. Lett.* B721 (2013), pp. 61–67. arXiv: 1212.2411 [hep-ph] (cit. on pp. 85, 95).

[209] Martin Holthausen and Kher Sham Lim. "Quark and Leptonic Mixing Patterns from the Breakdown of a Common Discrete Flavor Symmetry". *Phys. Rev.* D88 (2013), p. 033018. arXiv: 1306.4356 [hep-ph] (cit. on pp. 85, 95).

[210] Stephen F. King, Thomas Neder, and Alexander J. Stuart. "Lepton mixing predictions from $\Delta(6n^2)$ family Symmetry". *Phys. Lett.* B726 (2013), pp. 312–315. arXiv: 1305.3200 [hep-ph] (cit. on pp. 85, 95).

[211] Luis Lavoura and Patrick Otto Ludl. "Residual $\mathbb{Z}_2 \times \mathbb{Z}_2$ symmetries and lepton mixing". *Phys. Lett.* B731 (2014), pp. 331–336. arXiv: 1401.5036 [hep-ph] (cit. on pp. 85, 95).

[212] Renato M. Fonseca and Walter Grimus. "Classification of lepton mixing matrices from finite residual symmetries". *JHEP* 09 (2014), p. 033. arXiv: 1405.3678 [hep-ph] (cit. on pp. 85, 95).

[213] Bo Hu. "Lepton Mixing, Residual Symmetries, and Trigonometric Diophantine Equations". *Phys. Rev.* D90.7 (2014), p. 073012. arXiv: 1407.4722 [hep-ph] (cit. on pp. 85, 95).

[214] Anjan S. Joshipura and Ketan M. Patel. "A massless neutrino and lepton mixing patterns from finite discrete subgroups of U(3)". *JHEP* 04 (2014), p. 009. arXiv: 1401.6397 [hep-ph] (cit. on pp. 85, 95).

[215] Anjan S. Joshipura and Ketan M. Patel. "Discrete flavor symmetries for degenerate solar neutrino pair and their predictions". *Phys. Rev.* D90.3 (2014), p. 036005. arXiv: 1405.6106 [hep-ph] (cit. on pp. 85, 95).

[216] Jim Talbert. "[Re]constructing Finite Flavour Groups: Horizontal Symmetry Scans from the Bottom-Up". *JHEP* 12 (2014), p. 058. arXiv: 1409.7310 [hep-ph] (cit. on pp. 85, 94–96, 109).

[217] Chang-Yuan Yao and Gui-Jun Ding. "Lepton and Quark Mixing Patterns from Finite Flavor Symmetries". *Phys. Rev.* D92.9 (2015), p. 096010. arXiv: 1505.03798 [hep-ph] (cit. on pp. 85, 95).

[218] Stephen F. King and Patrick Otto Ludl. "Direct and Semi-Direct Approaches to Lepton Mixing with a Massless Neutrino". *JHEP* 06 (2016), p. 147. arXiv: 1605.01683 [hep-ph] (cit. on pp. 85, 95).

[219] Chang-Yuan Yao and Gui-Jun Ding. "CP Symmetry and Lepton Mixing from a Scan of Finite Discrete Groups". *Phys. Rev.* D94.7 (2016), p. 073006. arXiv: 1606.05610 [hep-ph] (cit. on pp. 85, 95).

[220] Jun-Nan Lu and Gui-Jun Ding. "Alternative Schemes of Predicting Lepton Mixing Parameters from Discrete Flavor and CP Symmetry". *Phys. Rev.* D95.1 (2017), p. 015012. arXiv: 1610.05682 [hep-ph] (cit. on pp. 85, 95).

[221] Cai-Chang Li, Jun-Nan Lu, and Gui-Jun Ding. "Toward a unified interpretation of quark and lepton mixing from flavor and CP symmetries". *JHEP* 02 (2018), p. 038. arXiv: 1706.04576 [hep-ph] (cit. on pp. 85, 95).

[222] Claudia Hagedorn and Johannes König. "Lepton and Quark Mixing from Stepwise Breaking of Flavor and CP" (2018). arXiv: 1811.07750 [hep-ph] (cit. on pp. 85, 95).

[223] Jun-Nan Lu and Gui-Jun Ding. "Dihedral flavor group as the key to understand quark and lepton flavor mixing". *JHEP* 03 (2019), p. 056. arXiv: 1901.07414 [hep-ph] (cit. on pp. 85, 95).

[224] Shao-Feng Ge, Duane A. Dicus, and Wayne W. Repko. "Z_2 Symmetry Prediction for the Leptonic Dirac CP Phase". *Phys. Lett.* B702 (2011), pp. 220–223. arXiv: 1104.0602 [hep-ph] (cit. on p. 85).

[225] Shao-Feng Ge, Duane A. Dicus, and Wayne W. Repko. "Residual Symmetries for Neutrino Mixing with a Large θ_{13} and Nearly Maximal δ_D". *Phys. Rev. Lett.* 108 (2012), p. 041801. arXiv: 1108.0964 [hep-ph] (cit. on p. 85).

[226] Stephen F. King and Christoph Luhn. "Neutrino Mass and Mixing with Discrete Symmetry". *Rept. Prog. Phys.* 76 (2013), p. 056201. arXiv: 1301.1340 [hep-ph] (cit. on pp. 85, 87).

[227] Walter Grimus and Patrick Otto Ludl. "Finite flavour groups of fermions". *J. Phys.* A45 (2012), p. 233001. arXiv: 1110.6376 [hep-ph] (cit. on p. 85).

[228] Martin Schœnert et al. " GAP – Groups, Algorithms, and Programming – version 3 release 4 patchlevel 4"" (1997) (cit. on pp. 85, 94).

[229] The GAP Group. "GAP – Groups, Algorithms, and Programming, Version 4.10.1, https://www.gap-system.org" (2019) (cit. on pp. 85, 94).

[230] P. Minkowski. "$\mu \to e\gamma$ at a Rate of One Out of 10^9 Muon Decays?" *Phys. Lett.* **67B** *(1977) 421* (1977) (cit. on p. 86).

[231] Ivo de Medeiros Varzielas, Graham G. Ross, and Jim Talbert. "A Unified Model of Quarks and Leptons with a Universal Texture Zero". *JHEP* 03 (2018), p. 007. arXiv: 1710.01741 [hep-ph] (cit. on pp. 87, 95).

[232] Sacha Davidson, David C. Bailey, and Bruce A. Campbell. "Model independent constraints on leptoquarks from rare processes". *Z. Phys.* C61 (1994), pp. 613–644. arXiv: hep-ph/9309310 [hep-ph] (cit. on p. 89).

[233] Aseshkrishna Datta, Fu-Sin Ling, and Pierre Ramond. "Correlated hierarchy, Dirac masses and large mixing angles". *Nucl. Phys.* B671 (2003), pp. 383–400. arXiv: hep-ph/0306002 [hep-ph] (cit. on p. 95).

[234] Adisorn Adulpravitchai, Alexander Blum, and Werner Rodejohann. "Golden Ratio Prediction for Solar Neutrino Mixing". *New J. Phys.* 11 (2009), p. 063026. arXiv: 0903.0531 [hep-ph] (cit. on p. 95).

[235] M. Fukugita, M. Tanimoto, and T. Yanagida. "Atmospheric neutrino oscillation and a phenomenological lepton mass matrix". *Phys. Rev.* D57 (1998), pp. 4429–4432. arXiv: hep-ph/9709388 [hep-ph] (cit. on p. 95).

[236] Carlo Giunti. "Current status of neutrino masses and mixings" (2002). [Nucl. Phys. Proc. Suppl.117,24(2003)], pp. 24–28. arXiv: hep-ph/0209103 [hep-ph] (cit. on p. 95).

[237] Carl H. Albright, Alexander Dueck, and Werner Rodejohann. "Possible Alternatives to Tribimaximal Mixing". *Eur. Phys. J.* C70 (2010), pp. 1099–1110. arXiv: 1004.2798 [hep-ph] (cit. on p. 95).

[238] M. Olechowski and S. Pokorski. "Heavy top quark and scale dependence of quark mixing". *Phys. Lett. B* 257 (1991) (cit. on p. 96).

[239] Graham Ross and Mario Serna. "Unification and fermion mass structure". *Phys. Lett.* B664 (2008), pp. 97–102. arXiv: 0704.1248 [hep-ph] (cit. on p. 96).

[240] S. H. Chiu and T. K. Kuo. "Renormalization of the quark mass matrix". *Phys. Rev.* D93.9 (2016), p. 093006. arXiv: 1603.04568 [hep-ph] (cit. on p. 96).

[241] Hajime Ishimori et al. "Non-Abelian Discrete Symmetries in Particle Physics". *Prog. Theor. Phys. Suppl.* 183 (2010), pp. 1–163. arXiv: 1003.3552 [hep-th] (cit. on p. 98).

[242] A. Blum, C. Hagedorn, and M. Lindner. "Fermion Masses and Mixings from Dihedral Flavor Symmetries with Preserved Subgroups". *Phys. Rev.* D77 (2008), p. 076004. arXiv: 0709.3450 [hep-ph] (cit. on p. 100).

[243] J. P. Lees et al. "Evidence for an excess of $\bar{B} \to D^{(*)}\tau^-\bar{\nu}_\tau$ decays". *Phys. Rev. Lett.* 109 (2012), p. 101802. arXiv: 1205.5442 [hep-ex] (cit. on p. 110).

[244] J. P. Lees et al. "Measurement of an Excess of $\bar{B} \to D^{(*)}\tau^-\bar{\nu}_\tau$ Decays and Implications for Charged Higgs Bosons". *Phys. Rev.* D88.7 (2013), p. 072012. arXiv: 1303.0571 [hep-ex] (cit. on p. 110).

[245] M. Huschle et al. "Measurement of the branching ratio of $\bar{B} \to D^{(*)}\tau^-\bar{\nu}_\tau$ relative to $\bar{B} \to D^{(*)}\ell^-\bar{\nu}_\ell$ decays with hadronic tagging at Belle". *Phys. Rev.* D92.7 (2015), p. 072014. arXiv: 1507.03233 [hep-ex] (cit. on p. 110).

[246] Roel Aaij et al. "Measurement of the ratio of branching fractions $\mathcal{B}(\bar{B}^0 \to D^{*+}\tau^-\bar{\nu}_\tau)/\mathcal{B}(\bar{B}^0 \to D^{*+}\mu^-\bar{\nu}_\mu)$". *Phys. Rev. Lett.* 115.11 (2015). [Erratum: Phys. Rev. Lett.115,no.15,159901(2015)], p. 111803. arXiv: 1506.08614 [hep-ex] (cit. on p. 110).

[247] S. Hirose et al. "Measurement of the τ lepton polarization and $R(D^*)$ in the decay $\bar{B} \to D^*\tau^-\bar{\nu}_\tau$". *Phys. Rev. Lett.* 118.21 (2017), p. 211801. arXiv: 1612.00529 [hep-ex] (cit. on p. 110).

[248] R. Aaij et al. "Test of Lepton Flavor Universality by the measurement of the $B^0 \to D^{*-}\tau^+\nu_\tau$ branching fraction using three-prong τ decays". *Phys. Rev.* D97.7 (2018), p. 072013. arXiv: 1711.02505 [hep-ex] (cit. on p. 110).

[249] G. Caria. "talk at 2019 Rencontres de Moriond, Electroweak Interactions and Unified Theories, http://moriond.in2p3.fr/2019/EW" (2019) (cit. on p. 110).